

Universiteit
Leiden
The Netherlands

Anthracycline biosynthesis in Streptomyces: engineering, resistance and antimicrobial activity

Hulst, M.B.

Citation

Hulst, M. B. (2024, June 20). *Anthracycline biosynthesis in Streptomyces: engineering, resistance and antimicrobial activity*. Retrieved from https://hdl.handle.net/1887/3764194

Version:	Publisher's Version
License:	Licence agreement concerning inclusion of doctoral thesis in the Institutional Repository of the University of Leiden
Downloaded from:	https://hdl.handle.net/1887/3764194

Note: To cite this publication please use the final published version (if applicable).

Anthracycline biosynthesis in *Streptomyces*: engineering, resistance and antimicrobial activity

Mandy B. Hulst

Cover illustration: Naomi Hulst
Layout and design: Hans Schaapherder, persoonlijkproefschrift.nl
Printed by: Ridderprint, ridderprint.nl

Copyright © 2024, Mandy B. Hulst

All rights reserved. No part of this thesis may be reproduced, distributed, sorted in a retrieval system, or transmitted in any form or by any means without prior permission of the author or, where applicable, the publisher holding the copyright on the published articles.

Anthracycline biosynthesis in *Streptomyces*: engineering, resistance and antimicrobial activity

Proefschrift

ter verkrijging van
de graad van doctor aan de Universiteit Leiden,
op gezag van rector magnificus prof.dr.ir. H. Bijl,
volgens besluit van het college voor promoties
te verdedigen op donderdag 20 juni 2024
klokke 10:00 uur

door

Mandy B. Hulst

geboren te Rotterdam, Nederland
in 1994

Promotoren:

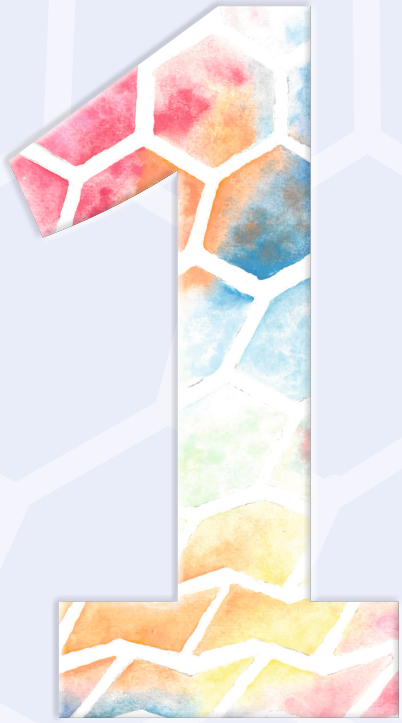
Prof.dr. G.P. van Wezel
Prof.dr. J.J.C. Neefjes

Promotiecommissie:

Prof.dr. A.H. Meijer
Prof.dr. N.I. Martin
Prof.dr. J. den Hertog
Prof.dr. J.T. Pronk (Delft University of Technology)
Dr. E. Nybo (Ferris State University)

Contents

Chapter 1	Thesis outline	7
Chapter 2	Anthracyclines: biosynthesis, engineering and clinical applications	11
Chapter 3	Metabolic engineering of *Streptomyces peucetius* for biosynthesis of *N*,*N*-dimethylated anthracyclines	47
Chapter 4	Cryptic transporter genes that confer resistance to anthracyclines in *Streptomyces*	81
Chapter 5	*N*,*N*-dimethylated anthracyclines with improved antibiotic activity	125
Chapter 6	Integrated proteomics and metabolomics analysis of small-scale *Streptomyces peucetius* cultures	143
Chapter 7	General discussion	160
	Nederlandse samenvatting	166
	References	172
	Curriculum vitae	190
	Publications	192



Thesis outline

Actinobacteria are a diverse phylum of Gram-positive bacteria with a multicellular lifestyle[1]. These bacteria are well known for the production of bioactive natural products, many of which have applications in the fields of human, animal and plant health[2–4]. The genes involved in the production of these bioactive metabolites are typically clustered on the genome in so-called biosynthetic gene clusters (BGCs). The production of bioactive metabolites is strictly regulated by a complex network of cluster-situated and global regulators[5,6]. Additionally, BGCs often harbour resistance genes to counteract the toxicity of their cognate products[7].

Subject of this thesis are the anthracyclines, glycosylated aromatic polyketides produced by Actinobacteria. The most renowned anthracyclines are daunorubicin and doxorubicin, natural products that are produced by *Streptomyces peucetius*[8–10]. Although these compounds were initially discovered by their antibiotic activity, their potent anticancer activity led to their development as anticancer drugs. Despite their remarkable efficacy against acute leukaemia and various solid tumours[11,12], their application is limited by severe side effects, such as cardiotoxicity, therapy-related tumours and infertility[13]. Notably, the toxicity of anthracyclines also prevented their application as antibiotics. **Chapter 2** provides a review of recent developments in anthracycline research. In this review, we discuss: (1) the biological role of anthracyclines in producer strains; (2) clinical applications and limitations of anthracyclines as anticancer drugs; (3) new insights into anthracycline biosynthesis; (4) newly discovered anthracyclines via genome mining, metabolic engineering, and combinatorial biosynthesis; and (5) strategies for improved production levels of anthracyclines.

The mode-of-action of anthracyclines involves interaction with DNA, resulting in DNA double-strand breaks via the trapping and poisoning of topoisomerase II onto the DNA, and chromatin damage via the eviction of histones at defined sites in the genome[14,15]. Anthracycline-induced cardiotoxicity results from the combination of both activities, while compounds inducing only chromatin damage maintain anticancer efficacy with limited side effects[14,16]. Importantly, *N,N*-dimethylation of the amino sugar moiety of doxorubicin resulted the absence of DNA damaging activity, while showing increased anticancer activity[16]. Consequently, *N,N*-dimethyldoxorubicin (DMdoxo) was proposed as a promising alternative to doxorubicin with potentially prolonged treatment options. Subsequently, a comprehensive evaluation of a structurally diverse library of anthracyclines revealed that the presence of a tertiary amine on the first sugar moiety generally results in the loss of DNA-damaging activity while exhibiting improved cytotoxicity[17–19].

For the evaluation of anticancer properties, DMdoxo was synthesised through organic chemistry[16]. Although naturally occurring DMdoxo has never been reported, the *N,N*-dimethylated amino sugar is found in other anthracycline biosynthetic pathways. In **Chapter 3**, we describe the engineering of the doxorubicin biosynthetic pathway in *S. peucetius* for the biosynthesis of *N,N*-dimethylated anthracyclines. Through the introduction of enzymes from the *Streptomyces galilaeus* aclarubicin pathway and the *Streptomyces purpurascens* rhodomycin pathway, we achieved the biosynthesis of *N,N*-dimethyldaunorubicin. However, two factors limited the product yield of the engineered strain: (1) our results suggest that the P450 monooxygenase DoxA is

inhibited by the *N,N*-dimethyl moiety of the unnatural substrates; and (2) *N,N*-dimethylated anthracyclines proved to exert a stronger cytotoxic effect on *S. peucetius* compared to the natural variants, resulting in product toxicity.

The susceptibility of *S. peucetius* to *N,N*-dimethylated anthracyclines evoked our interest in exploring anthracycline resistance mechanisms in actinomycetes. In **Chapter 4**, we investigated anthracycline resistance within our laboratory's actinomycete collection. Additionally, we performed adaptive laboratory evolution experiments of selected streptomycetes with the toxic compound DMdoxo. The results indicate that DMdoxo exerts higher antibacterial activity than doxorubicin, and that challenge with DMdoxo induces the activation of cryptic resistance export systems in strains that do not produce anthracyclines themselves.

The severe side effects associated with anthracyclines prevented their development as antibiotics. Nevertheless, detoxified anthracyclines with limited side effects may offer a potential therapeutic window for their use as antibiotics. In **Chapter 5**, we evaluated the antimicrobial activity of a library of 35 structurally diverse anthracyclines[17–19] against ESKAPE pathogens. Compounds with potent cytotoxic activity against human cancer cell lines also exhibited strong antimicrobial activity, particularly against Gram-positive bacteria, including methicillin-resistant *Staphylococcus aureus* (MRSA). Generally, *N,N*-dimethylated anthracyclines showed increased antimicrobial activity.

Actinobacteria continue to be an important source of natural products with medicinal properties[2–4]. For the discovery of new compounds and the development of efficient producer strains, high-throughput multi-omics analysis in a useful tool. In **Chapter 6**, we developed an integrated quantitative proteomics and metabolomics workflow for small-scale *Streptomyces* cultures. The workflow provided good quality data from a technical perspective, although biological reproducibility should be optimised in future work.

Finally, the main findings of this work are summarised and discussed in **Chapter 7**.



Anthracyclines: biosynthesis, engineering and clinical applications

Mandy B. Hulst*, Thadee Grocholski*, Jacques J.C. Neefjes, Gilles P. van Wezel† and Mikko Metsä-Ketelä†

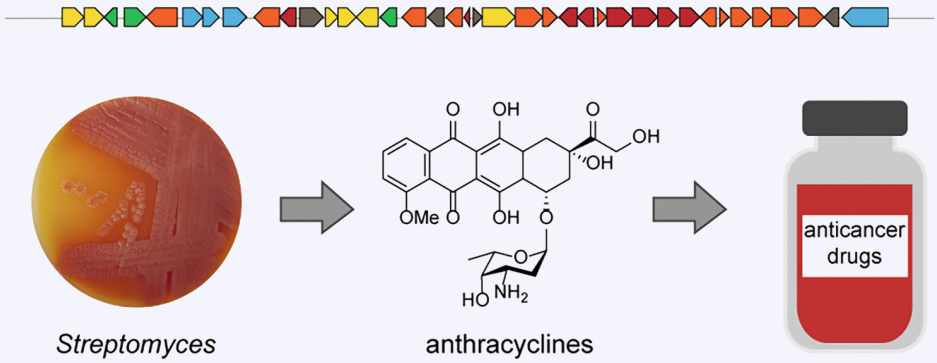
* These authors contributed equally.
† Corresponding authors.

Nat. Prod. Rep. 2022; **39**, 814–841.

Abstract

Covering: January 1995 to June 2021

Anthracyclines are glycosylated microbial natural products that harbor potent antiproliferative activities. Doxorubicin has been widely used as an anticancer agent in the clinic for several decades, but its use is restricted due to severe side effects such as cardiotoxicity. Recent studies into the mode-of-action of anthracyclines have revealed that effective cardiotoxicity-free anthracyclines can be generated by focusing on histone eviction activity, instead of canonical topoisomerase II poisoning leading to double-strand breaks in DNA. These developments have coincided with an increased understanding of the biosynthesis of anthracyclines, which has allowed generation of novel compound libraries by metabolic engineering and combinatorial biosynthesis. Coupled to the continued discovery of new congeners from rare Actinobacteria, a better understanding of the biology of *Streptomyces* and improved production methodologies, the stage is set for the development of novel anthracyclines that can finally surpass doxorubicin at the forefront of cancer chemotherapy.



Introduction

Natural products derived from the secondary metabolism of bacteria and fungi are an important source of antibiotics and other drugs. About 70% of the approved drugs are natural products or derived from a natural product[20]. The majority of the bioactive secondary metabolites are produced by Actinobacteria and especially by members of the genus *Streptomyces*[2,4,21,22]. There are many classes of secondary metabolites, and these compounds may have a range of bioactivities, including antibacterial, anticancer, antifungal, antiviral, anthelmintic, herbicidal, or immunosuppressive activity[3,20]. The compounds can be divided into different structural families, with polyketides, non-ribosomal peptides, ribosomally synthesized post-translationally modified peptides (RiPPs), terpenoids, and alkaloids as major examples.

Subject of this review are the anthracyclines, which are aromatic type II polyketides assembled by sequential condensation of acyl-CoA units. Aromatic polyketides are classified based on the carbon scaffold as anthracyclines, angucyclines, aureolic acids, tetracyclines, tetracenomycins, pentangular polyphenols, and benzoisochromanequinones[23]. The polyphenolic aglycone units are typically decorated by a number of tailoring reactions such as methylation, amination, oxidation and glycosylation to generate further structural diversity[24]. The best-known aromatic polyketides are the tetracyclines, which are active against a wide range of both Gram-positive and Gram-negative bacteria. Chlortetracycline or aureomycin was isolated from *Streptomyces aureofaciens* in 1947[25]. Tetracyclines are protein synthesis inhibitors that target the bacterial ribosome[26,27]. The first anthracyclines that were discovered were the rhodomycins (e.g. rhodomycin B, **1**) (Figure 1), which displayed strong antibiotic activity against *Staphylococcus aureus*[28]. However, the anthracyclines are particularly known for their potent anticancer activity[11,29]. Brockmann later defined anthracyclines as "yellow-red or red, optically active dyes" that consist of a linear tetracyclic 7,8,9,10-tetrahydro-5,12-naphtacenoquinone scaffold, which is decorated with one or more sugar moieties[30].

The best-known anthracyclines are daunorubicin (**2**) and doxorubicin (**3**) (Figure 1). In the early 1960s, **2** was isolated from *Streptomyces peucetius*[9,10]. The molecule demonstrated exceptionally strong activity against acute leukemia[12]. Random mutagenesis of the daunorubicin producing strain resulted in the even more potent derivative **3**[8]. Despite serious dose-limiting adverse effects, the two anthracyclines continue to be used in first-line chemotherapy for the treatment of solid and hematological tumors[31]. More anthracyclines were isolated from *Streptomyces* species in the following years, including nogalamycin (**4**) from *Streptomyces nogalater*[32], aclacinomycin A (**5**) from *Streptomyces galilaeus*[33], and steffimycin B (**6**) from *Streptomyces steffisburgensis*[34] (Figure 1). The structurally unique **4** demonstrated high activity against Gram-positive bacteria and several cancer lines, but severe toxicity prevented its progress in clinical trials[35]. The anthracycline **5** demonstrated potent antileukemia activity and low cardiotoxicity and is currently prescribed exclusively in Japan and China[13]. Many attempts, particularly in the 1980s, were made to expand the chemical space of existing anthracyclines by semi-synthesis in search for analogues with reduced cardiotoxicity[36]. Notably, these failed to yield clinically relevant derivatives with increased activity spectrum and reduced cardiotoxicity[13].

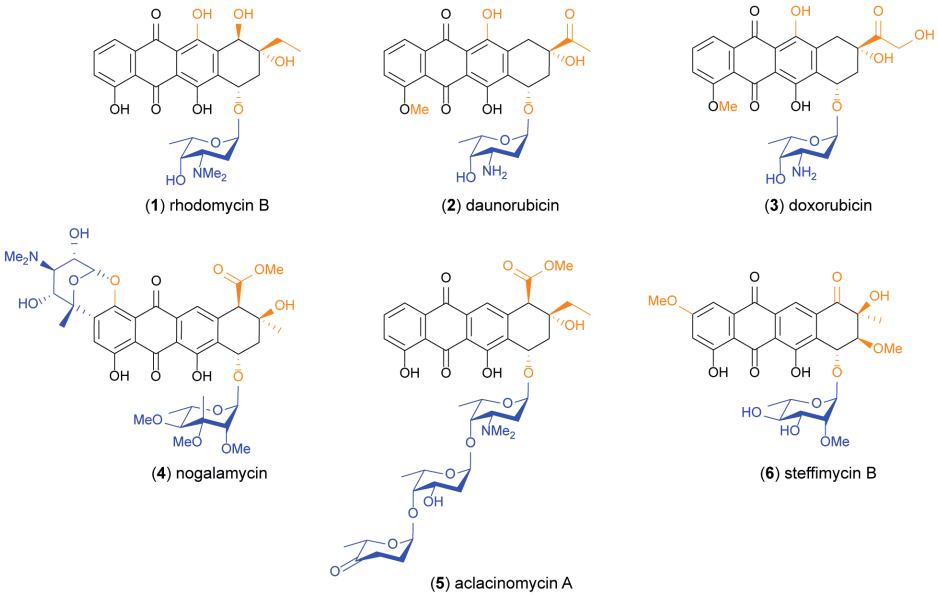


Figure 1. Chemical structures of classical anthracyclines. Structures of rhodomycin B (**1**), daunorubicin (**2**), doxorubicin (**3**), nogalamycin (**4**), aclacinomycin A (**5**) and steffimycin B (**6**), which are produced by *S. purpurascens*, *S. peucetius* (both **2** and **3**), *S. nogalater, S. galilaeus* and *S. steffisburgensis*, respectively. The common linear tetracyclic 7,8,9,10-tetrahydro-5,12-naphtacenoquinone scaffold is present in all structures. The chemical diversity of these compounds occurs either from their tailoring enzymes (orange) or their sugar moieties (blue).

Recent new insights into the mechanism of action and biosynthetic pathways of anthracyclines suggest that it is finally feasible to find "a better doxorubicin"[13]. The aim of this review is to provide a comprehensive overview of the current literature on biosynthesis, mode-of-action and medical application of anthracyclines, and provide pointers towards further exploration of the chemical space of these important tetracyclic polyketides. First, we will discuss the production of anthracyclines by Actinobacteria and their biological role. Second, we will review the application of anthracyclines as anticancer compounds. Third, recent advances in the understanding of the biosynthetic pathways of anthracyclines will be discussed. Finally, we evaluate approaches that may be employed to find new anthracyclines as well as strategies to optimize the production of anthracyclines by genetic engineering and optimization of the fermentation process.

Actinobacteria as anthracycline producers

Biology and secondary metabolism of Actinobacteria

Actinobacteria are a diverse phylum of Gram-positive bacteria with high G+C DNA content, which are widely distributed in both aquatic and terrestrial ecosystems[37]. The bacteria have a multicellular lifestyle[38]. The best characterized genus of Actinobacteria is *Streptomyces*. The

bacteria play a key ecological role in their environment due to their ability to break down a wide range of macromolecules and scavenge nutrients. Streptomycetes are mycelial organisms that reproduce by sporulation, with a lifecycle that is similar to that of filamentous fungi[38]. A single uninucleoid spore germinates and then grows out by a combination of hyphal tip extension and branching into a complex mycelial network of large multinucleoid cells[39,40]. During this process, enzymes are released extracellularly to break down natural polymers in the environment to provide nutrients for the vegetative mycelium[41]. When conditions become limiting, a complex regulatory network initiates the production of aerial hyphae. The nutrients required for this process are supplied by autolytical degradation of the old vegetative mycelium, also known as substrate mycelium[42,43]. This involves a process of programmed cell death (PCD), which is a hallmark of all multicellular bacteria[38]. Eventually, the reproductive aerial hyphae differentiate into chains of uninucleoid spores, which are dispersed into the environment in search of new nutrients[44].

This process of morphological differentiation is closely connected to chemical differentiation, namely the onset of secondary metabolism and antibiotic production, which correlates temporally with development[5,6,45]. The genes involved in the production of secondary metabolites are typically clustered on the genome in so-called biosynthetic gene clusters (BGCs). Whole genome sequencing revealed that streptomycetes generally contain a multitude of BGCs, and far more than originally anticipated[46]. However, many compounds originating from these BGCs have escaped screening, because the BGCs may be poorly expressed under laboratory conditions, or because the production levels of the metabolites are too low to detect[47]. The environmental cues that activate the expression of many BGCs in their natural environment are likely missing in the laboratory[48–51]. Such 'cryptic' BGCs potentially specify a rich variety of bioactive molecules and are thus attractive targets for new studies. Developments in bioinformatics, genetic and analytical tools may lead to the discovery of new natural products[48,49,52].

Most antibiotics are produced by filamentous microorganisms. A likely explanation is that antibiotics play a role in their defense to protect the biochemical building blocks that are released by the autolytic degradation of their mycelium in a nutrient-deprived environment, which will attract motile competitors[21,38,53]. Anthracyclines generally display antibiotic activity against Gram-positive bacteria, although synergistic effects together with the antibiotic rifampicin have also been observed against Gram-negative bacteria[54]. Moreover, as anthracyclines intercalate into DNA, they are effective antiproliferative agents against eukaryotic cell lines. Recently, the DNA-targeting activity of anticancer compounds was also shown to limit infection by DNA phages, which may have been an evolutionary driver for streptomycetes to produce anthracyclines[55]. Interestingly, anticancer compounds may play an important physiological role in the bacterial life cycle that is complementary to that of antibiotics, by actually driving the PCD process. The accumulation of DNA damaging compounds right at the onset of development may promote PCD by destroying a network of cells within the substrate mycelium, thus accelerating the provision of nutrients to feed the build-up of the aerial mycelium[56,57]. Besides a role in chemical warfare, secondary metabolites

may play a role in interspecies and intraspecies communication[58]. These diverse roles of secondary metabolites have provided a significant selective advantage for the producing organisms and have promoted the evolution of the tremendous chemodiversity of microbial natural products[59,60].

Self-resistance to anthracyclines

Anticancer agents that affect DNA structure and/or inhibit DNA functions are also cytotoxic to their producers[57]. Therefore, the production of these compounds is tightly regulated and usually coincides with expression of resistance genes[4,7]. Different self-resistance mechanisms against anticancer compounds include efflux, sequestration, modification, self-sacrifice, and metabolic dormancy[57].

Anthracyclines are usually exported by ABC-transporters in the producer strains of *Streptomyces*. This limits the toxicity for the producer strains, analogous as human or mouse tumor cells can protect themselves (through overexpression of ABC transporter MDR1 (ABCB1))[61]. As additional protection mechanism some anthracycline BGCs encode UvrA-like proteins that are involved in the nucleotide excision repair of DNA (Figure 2). The daunorubicin BGC includes four genes involved in self-resistance[62,63]. The first genes, *drrA* and *drrB*, encode an ABC transporter that supports the efflux of **2** and **3**[64,65]. Directly downstream of these genes lies *drrD*, which is involved in self-resistance as well. A *drrD* deletion mutant showed reduced self-resistance, but the mechanism has not yet been elucidated[66]. The gene product of *drrC* is homologous to UvrA-like proteins and is involved in the recognition and repair of DNA damage[67–69]. Recently, another mechanism of self-resistance was identified in *S. peucetius*. A yet unidentified secreted protein binds to extracellular **2**, thereby controlling extracellular drug concentrations and preventing uptake by the bacterium[70]. The resistance and biosynthetic genes are regulated by a cascade of pathway-specific regulators. The mechanism is similar to the regulation of the undecylprodigiosin cluster of the model organism *Streptomyces coelicolor*, which we will discuss first.

Transcriptional control of biosynthetic gene clusters

Much of our knowledge on antibiotic production and regulation originates from the model organism *S. coelicolor*[71]. Before the publication of its complete genome sequence, which was the first *Streptomyces* genome to be published[46], it was recognized that this strain produces the blue-pigmented actinorhodin (Act), the red-pigmented undecylprodigiosin (Red), the calcium-dependent antibiotic (CDA), and the plasmid-encoded methylenomycin (Mmy)[72,73]. The gene clusters of the genome-encoded antibiotics are controlled by the cluster-situated regulators (CSRs) ActII-ORF4, RedD and CdaR, respectively, which all belong to the family of *Streptomyces* antibiotic regulatory proteins (SARPs)[74]. The genes for these pivotal regulators are all subject to translational control by the BldA tRNA, which is required for the translation of the rare UUA codon for leucine. This tRNA is also required for the proper translation of many developmental genes and is therefore a key 'regulator' in the control of development and antibiotic production[75,76].

The production of secondary metabolites by *Streptomyces* is tightly regulated *via* a complex network of signaling cascades and feedback loops, which involves both translational and transcriptional regulation[5,6]. The most abundant pleotropic regulators in *Streptomyces* are two-component systems, which allow for a rapid response to altering environments. The pleotropic regulators can act directly by binding to cluster-situated regulators (CSRs) or indirectly by influencing other regulatory pathways. Subsequently, the CSR—or a hierarchical cascade of CSRs within the BGC – modulates the expression of the genes in the BGC[45].

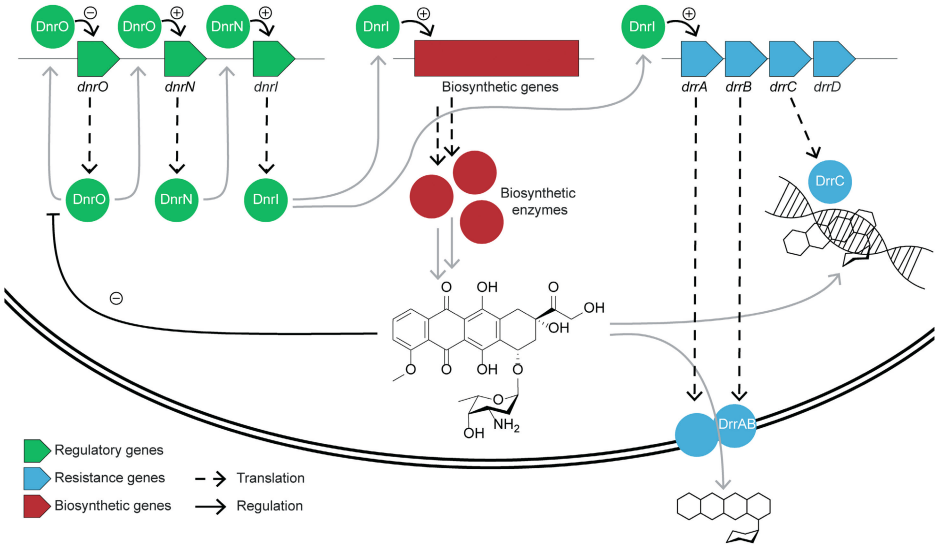


Figure 2. Regulation of the daunorubicin biosynthetic gene cluster and resistance mechanisms. The doxorubicin BGC is regulated by a cascade of three regulators (green). *DnrI* directly controls the expression of the biosynthetic (red) and resistance (blue) genes by binding to the promoter regions within the cluster. *DnrN* is also a DNA-binding protein that binds to the *dnrI* promoter to activate transcription. *DnrO* activates the transcription of *dnrN* and represses its own transcription. The glycosylated products of the biosynthetic pathway inhibit the binding of *dnrO* to the *dnrO* promoter, which leads to the activation of *dnrN* and hence *dnrI*. The cluster has four resistance genes (blue) that are activated by DnrI. The two first genes, *drrA* and *drrB*, together encode an ABC transporter that supports the efflux of daunorubicin (**2**) and doxorubicin (**3**). The gene product of *drrC* is homologous to UvrA-like proteins and is involved in the recognition and repair of DNA damage caused by the products of the pathway. The precise function of *drrD* has not been elucidated. The biosynthetic genes are visualized as a single box and include around 30 genes that together encode the minimal PKS for the tetracyclic skeleton, the post-PKS tailoring enzymes, and those for glycosylation.

The regulation of the BGC for Red is one of the best studied examples and may partly serve as an example for the regulation of the daunorubicin BGC. The production of Red is under positive control of the CSR RedD[77,78]. The transcription of *redD* is in turn regulated by RedZ, which is a pseudo-response regulatory protein[79]. The regulation of the daunorubicin BGC (Figure 2) is similar to that of the Red BGC, whereby *dnrI* and *dnrN* are homologues of *redD* and *redZ*, respectively. DnrI directly controls the transcription of the biosynthetic and resistance genes by binding to the promoter regions within the cluster[80]. DnrN is also a DNA-binding protein that binds to the

dnrI promoter to activate transcription[81]. However, regulation of the daunorubicin BGC is a three-tier transcriptional activator system, and also involves the TetR-family transcriptional regulator *dnrO*, which activates the transcription of *dnrN*[82]. *DnrO* also represses its own transcription.

Interestingly, anticancer compounds may play a direct role in the transcriptional control of their BGCs by virtue of their DNA-intercalating activities. Jadomycin is an angucycline-type polyketide with anticancer activity and is produced by *Streptomyces venezuelae* ISP5230. The jadomycin BGC encodes five regulators (JadR1-R2 and JadW1-W3)[83,84]. JadR1 is the pathway-specific activator of jadomycin biosynthesis and indispensable for its production[85]. The DNA binding activity of the atypical response regulators JadR1 (OmpR family) and RedZ (NadR family) is controlled by the intracellular concentration of jadomycin and Red, respectively. The compounds bind to these transcription factors to inhibit transcription[86]. Similarly, in *S. peucetius*, drug-mediated control is mediated *via* inhibition of the DNA binding capacity of *dnrO* by **2**[82]. In fact, all of the glycosylated products in the pathway inhibit the DNA–*dnrO* binding and *dnrO* expression is increased, which leads to the activation of *dnrN* and hence *dnrI* (Figure 2). Thus, the transcriptional activation of the enzymes required for antibiotic production go hand-in-hand with the activation of the resistance machinery.

Understanding of the regulatory networks that control the anthracycline production, and of the mechanisms that provide self-resistance, is of critical importance for the development of successful metabolic engineering and strain engineering approaches. Understanding of regulation will allow for increased production levels and understanding of resistance mechanisms will facilitate engineering strategies to reduce toxicity issues.

Anthracyclines as anticancer drugs

Many anthracyclines, including **2**, were originally isolated as potential new antibiotics[10]. However, the observation of the antiproliferative activity *in vitro* and in mice initiated the development of **2** as an anticancer drug. The success of the molecule in the clinic led to the generation of hundreds of anthracycline analogues by modified bacteria and half-chemistry[15]. Currently, six different semi-synthetic variants of **2** (Figure 1) are used in the clinic in cancer treatment: **3** (Figure 1), epirubicin (**7**), idarubicin (**8**), pirarubicin (**9**) and valrubicin (**10**) (Figure 3, Table 1)[87]. In addition, the totally synthetic amrubicin (**11**), which contains a minimalistic version of the daunosamine sugar, is used in lung cancer chemotherapy in Japan (Figure 3, Table 1)[88]. These anthracycline drugs are a cornerstone in oncology treatments and more than one million cancer patients are treated with these drugs annually.

While these drugs are effective in the treatment of a series of solid and blood cancer types, their application is limited by life-threatening toxicity, especially cardiotoxicity. Cardiotoxicity resulting in heart failure may be acute, but in general is increasing with accumulated dose. For these reasons, anthracycline application is usually limited to six courses, because further

accumulation of the drugs is considered an unacceptable risk of heart failure. Juvenile cancer patients may get higher doses (because 'their heart can handle it'), while senior patients (usually over 70–75 years) and people with a poor heart function are excluded from anthracycline-based therapy[15]. Since cancer is often a disease of elderly people, a major patient group is excluded from this often effective treatment or simply treated at a non-effective low dose. Many young cancer survivors suffer heart problems later in life due to the cardiotoxic effects of anthracyclines. Interestingly, the triglycosylated **5**, which is the only anthracycline used in the clinic that is not based on **2**, is not significantly cardiotoxic in animal models, but is mainly used in the treatment of hematological malignancies such as acute myeloid leukemia (AML)[89–91]. **11** is also a variant with limited cardiotoxicity and is used in Japan for the treatment of lung cancer. Most tumor types are treated with anthracycline variants that show dose-dependent cardiotoxicity that limits treatment. In fact, cancer treatment is limited by the risk of cardiotoxicity rather than by the anticancer activity.

Table 1. Activity of classical and semi-synthetic anthracyclines. The application of anthracyclines as anticancer drugs is limited by their severe side effects, including cardiotoxicity resulting in heart failure. Anthracyclines may have two activities: poisoning of topoisomerase II resulting in DNA breaks, and the eviction of histones from the DNA resulting in the loss of epigenetic information. Not all anthracyclines have been tested for their activities and side effects. Notably, cardiotoxicity does not occur for anthracyclines that exhibit either DNA breaks or histone eviction activity (**5**, **11** and **12**).

Name	Cytotoxicity	Cardiotoxicity	DNA breaks	Histone eviction
Rhodomycin B (**1**)	+	?	?	?
Daunorubicin (**2**)	+	+	+	+
Doxorubicin (**3**)	+	+	+	+
Nogalamycin (**4**)	+	+	+*	?
Aclacinomycin A (**5**)	+	-	-	+
Steffimycin B (**6**)	+	?	?	?
Epirubicin (**7**)	+	+	+	+
Idarubicin (**8**)	+	+	+	+
Pirarubicin (**9**)	+	+	+	?
Valrubicin (**10**)	+	+	+	?
Amrubicin (**11**)	+	-	+	-
N,*N*-dimethyldoxorubicin (**12**)	+	-	-	+

* Topoisomerase I poison.

An antibiotic turned into an anticancer drug

Modern anticancer drugs are designed to inhibit proteins typically involved in the epigenetic code, DNA repair, apoptosis, or epigenetics. Anthracyclines were identified in screens for compounds that inhibit cell growth under tissue culture conditions. They would not easily have been identified in more target-directed screens, as is the standard in these times. Anthracyclines consist of a tetracyclic aglycone associated to an amino sugar. The tetracyclic moiety ensures intercalation into the DNA double helix, while the amino sugar positions into

the DNA minor groove (Figure 4A)[92]. This results in the poisoning of the enzyme topo-isomerase II (Topo II) and traps this enzyme on the DNA[93]. The function of Topo II is to alter the topology of DNA and relax supercoiled DNA by cutting the DNA double helix and passing it through the enzyme for re-ligation[94]. The molecular interaction of anthracyclines with Topo II is unclear, but another intercalating agent etoposide has been shown to stabilize the cleavage complex of Topo II, which prevents re-ligation and leads to DNA double-strand breaks (Figure 4B)[95]. The treatment of patients with anthracyclines results in cells containing many DNA breaks[15]. DNA breaks—if not swiftly repaired—will activate ATM1 and TP53 to initiate apoptosis. The cellular response to DNA breaks can easily be detected by probing Western blots for histone H2AX phosphorylated by ATM1 (also called γH2AX). DNA breaks can be directly detected by constant field electrophoresis[16]. Since fast-growing cells (like cancer cells) are more sensitive to the effects of DNA breaks, they die more efficiently thus providing a therapeutic window for Topo II poisons. However, other fast-growing cells such as hair cells and immune cells are also affected, which explains some of the direct reversible side effects of these drugs.

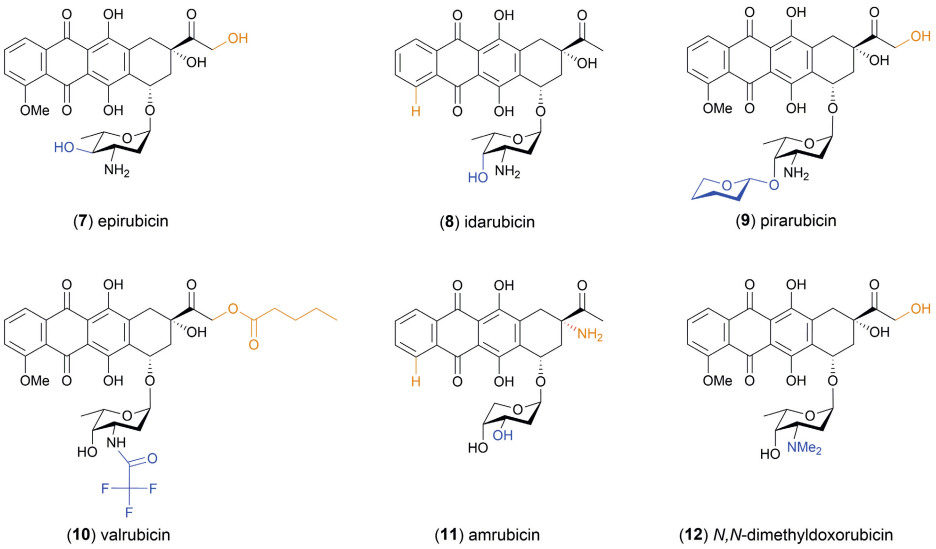


Figure 3. Chemical structures of semi-synthetic anthracyclines as anticancer drugs. Semi-synthetic anthracyclines epirubicin (**7**), idarubicin (**8**), pirarubicin (**9**) and valrubicin (**10**) are in clinical use. The fully synthetic amrubicin (**11**) is also used in anticancer chemotherapy. *N*,*N*-dimethyldoxorubicin (**12**) is a promising drug under development. The chemical differences in the aglycone (orange) or the sugar moiety (blue) are highlighted.

The mechanism of action of **5** is, however, an interesting exception. This drug does not cause any DNA breaks because it traps and poisons Topo II at an earlier step in the DNA break-and-repair cycle before the DNA break is initiated. Yet, this drug is highly effective in the treatment of AML tumors[14,96]. Further studies revealed a new activity of anthracycline drugs: the removal of nucleosomes from defined areas in the genome as detected by life imaging of photoactivate PAGFP-histones, magnetic tweezers on chromatin and FAIR-Seq (Figure 4C)[97]. Histones are the

major proteins of chromatin and facilitate packaging of DNA within cells[14,16,97]. Post-translational modifications of histone tails are important determinants for compactization of chromatin and regulation of gene expression, and mark the epigenetic code. Since histones released from DNA are degraded and replaced by nascent histones, the anthracyclines are effectively altering the epigenetic code and could thus be considered epigenetic drugs as well with specificity for the regions where histone eviction occurs[15].

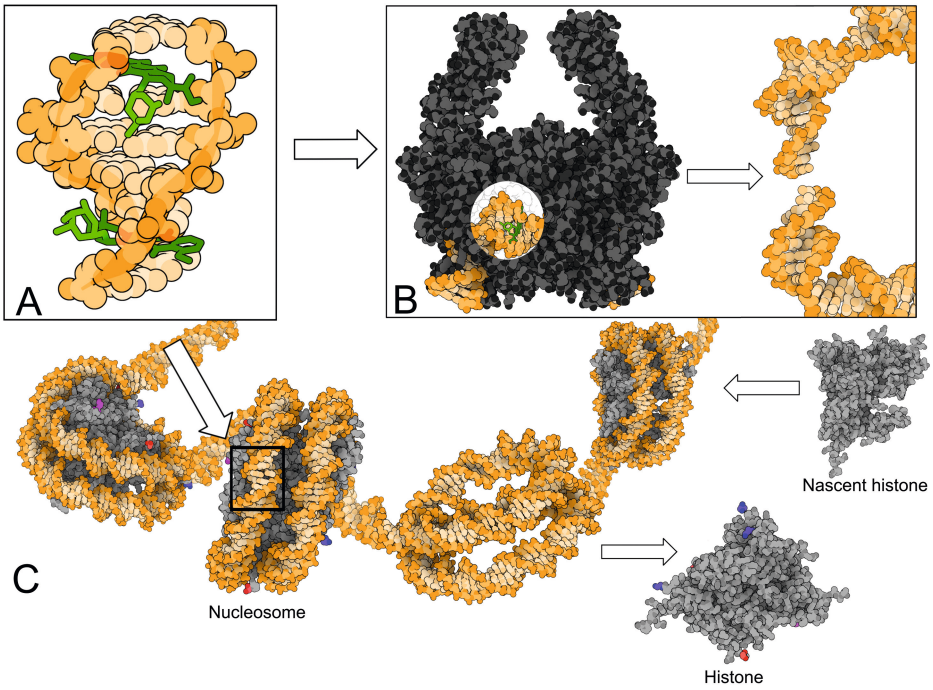


Figure 4. Mechanism of action of anthracyclines. (A) The doxorubicin (**3**) aglycone (dark green) intercalates into the DNA double helix (orange), while the amino sugar (light green) is positioned in the DNA minor groove. **(B)** The anthracycline–DNA complex poisons topoisomerase II (black) so that the enzyme is trapped on the DNA. In case of **3** (green), the poisoning leads to DNA double-strand breaks, whereas other anthracyclines such as **5** and **12** do not induce DNA breaks. **(C)** Anthracyclines act as epigenetic drugs *via* release of histones from the nucleosome. Histones (grey) are commonly modified by methylation (red), acetylation (purple), ubiquitination (blue) or phosphorylation (not shown). Histone eviction alters the accessibility of DNA and influences gene transcription. The introduction of nascent histones (grey) leads to loss of epigenetic information encoded in the histone tails.

The question then is which of these activities is more important for the anticancer effects of anthracyclines. Structure/function relationships revealed that **11** (where the amino group is located on the tetracyclic aglycone instead of the sugar moiety) showed only DNA break activity, while semi-synthetic *N*,*N*-dimethyldoxorubicin (**12**) (Figure 3, Table 1) solely displayed nucleosome eviction activity[16]. Recent studies have shown that **12** has high cytotoxic activity similar to **3**, which is in contrast to **11** that has only mild cytotoxicity. This suggests that histone eviction could be the most relevant bioactivity in anthracycline chemotherapy[15,16,89–91].

While anthracycline drugs have been used in the clinic for almost 50 years for the treatment of cancer patients, the molecular basis of the anticancer effects is only partially understood. For example, why nucleosome eviction causes cytotoxicity is unclear, as is the reason for the relative tumor selectivity of these drugs.

The side effects

The major and treatment-limiting side effect of anthracyclines is accumulated cardiotoxicity. In other words, the treatment is not halted because of the failure to eliminate cancer cells, but due to the side effects. In the 1980s, scientists of the National Cancer Institute performed an extensive synthesis of analogues of **3** with the aim to identify compounds lacking the cardiotoxic side effects[98]. And failed. Later studies revealed that **7** and other newer anthracyclines are somewhat less cardiotoxic. This variant was tested in mice, rats, and rabbits, but was not further developed for unknown reasons. Out of all of the doxorubicin derivatives in clinical use, only **11** can be considered significantly less cardiotoxic[99], but the compound has minor effects on tumors and is difficult to obtain. For these reasons, **11** is hardly used in cancer therapy.

Both **5** and **12** have a *N*,*N*-dimethyl group on the sugar moiety and both fail to induce DNA breaks, but still promote nucleosome eviction. Both compounds trap Topo II on DNA but poison the enzyme before the DNA breaks are made. The reduced (cardio)toxic effects of cancer treatment with **5** have been observed by oncologists, but never systematically studied. Since the prospects of AML patients are very poor, cardiotoxicity is possibly a minor issue in the treatment of these patients and therefore largely ignored. When tested in mice as well as human cardiomyocyte microcultures, **5** and **12** did not show any cardiotoxicity[16,18]. However, as mentioned above, **11**—the anthracycline drug that only induces DNA breaks—also lacks cardiotoxicity. This suggests that cardiotoxicity of **2**, **3**, **7** and **8** is caused by the combination of the nucleosome eviction and DNA breaks, whereas drugs with one of the two activities do not induce cardiotoxicity[16,18]. Consequently, chemical separation of these activities may lead to drug variants lacking cardiotoxic activity.

Anthracyclines have additional activities that have been considered to be the source of cardiotoxicity. Especially the formation of reactive oxygen species (ROS) has gained wide attention[100]. Anthracyclines may poison Topo IIβ in mitochondria, which affects transcription and mitochondria replication and results in the induction of ROS. Since heart muscle cells have many mitochondria for the production of ATP, cardiomyocytes may be particularly hit by anthracyclines. For these reason, ROS inhibitors have been generated that, however, have only limited effects on the cardiotoxicity of anthracyclines[101]. Besides that, **12** is equally efficient in producing radicals as **3**, but is not cardiotoxic. This suggests that radical formation is not directly related to cardiotoxicity.

Anthracyclines are not only toxic to the heart. As can be expected, they eliminate not only fast-growing tumor cells, but also immune cells, often resulting in reversible neutropenia. This implies that patients are initially more susceptible for infections after treatment with these drugs.

These drugs also affect spermatogenesis (albeit this was not observed for **5** in mice)[102]. Sperm cells from juvenile cancer patients are often isolated and stored for future family planning.

All anthracyclines used in the clinic except **5** induce DNA breaks. Consequently, errors can be introduced in the subsequent DNA repair process. A critical step in DNA repair is the phosphorylation of histone H2AX by ATM kinases. Because histone H2AX is also removed by anthracyclines, DNA repair is strongly attenuated when compared to Topo II poisons that do not evict histones (such as etoposide), which may further increase the error rate of DNA repair[14]. In almost one percent of patients treated with **2** or **3**, so-called treatment induced tumors emerge, usually an Acute Myeloid Leukemia (AML) or Acute Lymphocytic Leukemia (ALL) within two years after completion of the anticancer treatment[103]. Anthracycline variants lacking DNA break activity will not induce these 'secondary tumors', as shown for **5** in TP53 heterozygous mice[16]. Anthracycline variants *N*,*N*-dimethylated amino sugar all showed a loss in DNA break inducing activity, while retaining histone eviction and cytotoxicity[18,19]. Rhodomycin B could also be a member of this subgroup of anthracyclines, acting mainly *via* histone eviction.

The anthracyclines used in the clinic are effective as anticancer drugs for a variety of tumor types. The drugs also have major side effects of which cardiotoxicity is most acute and treatment limiting. Controlling the side effects of **5** and **12** would strongly improve the application of this cornerstone in cancer treatment.

Biosynthesis

The biosynthesis of anthracyclines in Actinobacteria can be divided into two stages, where conserved biosynthetic pathways are utilized for formation of the anthracyclinone carbon scaffold, followed by generation of structural diversity in later stages in so-called tailoring steps[104]. Particularly significant are glycosylation steps, where anthracyclinones are decorated with diverse carbohydrate moieties originating from D-glucose-6-phosphate[105]. Other important tailoring steps include methylations and various redox reactions, which further modify the metabolites. Anthracyclines are thus formed by complex multi-enzyme pathways, which explain that they cannot easily be made by full chemistry.

Biosynthesis of anthracycline aglycones *via* canonical polyketide pathways

The formation of anthracyclines has been intensely investigated due to their medical importance and most biosynthetic steps have been elucidated at the molecular level. Anthracyclines belong to type II polyketides and thus share common ancestry for carbon chain formation with bacterial fatty acid synthase machineries[106]. The starter unit may be either acetyl-CoA or propionyl-CoA, where the latter is generated by dedicated cluster-situated acyltransferases and propionyl-CoA synthases[107–109]. Nine rounds of iterative Claisen condensations with malonyl-CoA by the so-called minimal polyketide synthase (minPKS) leads to formation of the initial anthracycline decaketide (Figure 5A)[110–112].

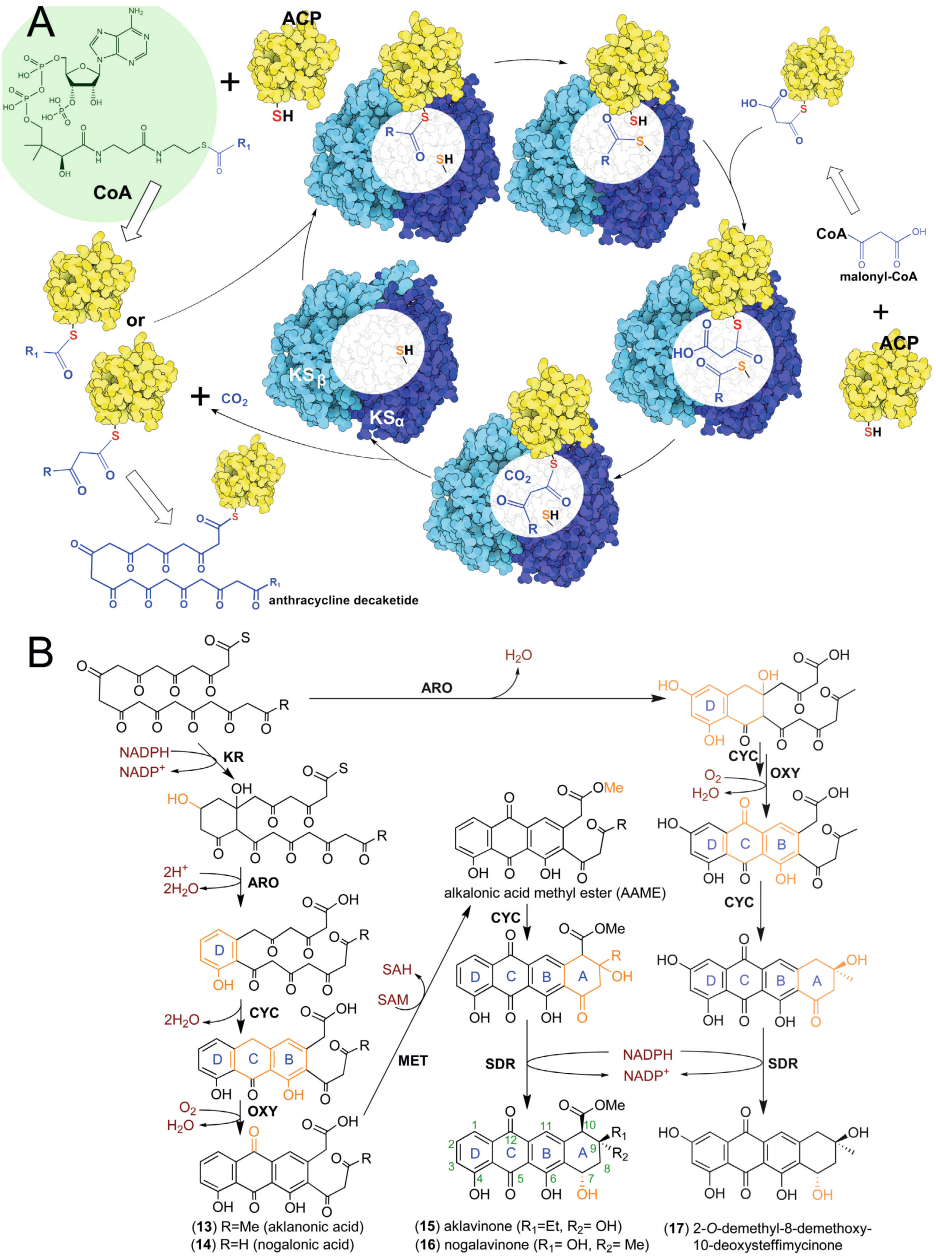


Figure 5. Biosynthesis of anthracycline aglycones. (A) The biosynthesis of type II polyketides, including anthracyclines, involves an iterative cycle of reactions involving three proteins that form the minimal polyketide synthase (minPKS). The acyl carrier protein (ACP; in yellow) contains a phosphopantetheine prosthetic group derived from CoA onto which the polyketide is assembled. The ketosynthase (KS) consists of two subunits, namely the catalytic KS_{α} (dark blue) and chain length determinant KS_{β} (light blue). Polyketide biosynthesis starts with coupling of an acetyl or propionyl (R_1) unit to the ACP. During the catalytic cycle, the growing polyketide is transferred from the ACP to an active site cysteine of KS_{α}.

After initial transfer to the KS_α, the ACP also supplies the ketosynthase with malonyl units. Incorporation of each malonyl unit in a Claisen condensation reaction catalyzed by KS_β extends the polyketide by two carbons. The polyketide is simultaneously transferred back to the ACP. Nine extension rounds are required for formation of the anthracycline decaketide structure. **(B)** After formation of the anthracycline decaketide, the polyketide undergoes a series of subsequent reactions catalyzed by ketoreductases (KR), aromatases (ARO), cyclases (CYC), oxygenases (OXY), methyltransferases (MET) as well as short-chain dehydrogenase/reductases (SDR), leading to the stable aglycone intermediates (**15**, **16**, **17**). Depending on the cyclase that performs closure of the A-ring, the stereochemistry of C*9* may differ, such as *9R** for (**15**) and *9S** for (**16**). Steffimycin biosynthesis branches off at an earlier stage and includes unique features such as an unusual 2-hydroxyl group due to lack of a KR enzyme and decarboxylative cyclization of the A-ring. The relevant positions of reaction products in each step are illustrated in orange.

The minPKS is composed of a heterodimeric ketosynthase (KS_α/KS_β) responsible for the chain elongation reactions and an acyl carrier protein (ACP), where the highly reactive poly-β-keto intermediate is covalently tethered[113,114].

Experiments on the daunorubicin and nogalamycin pathways have clarified how the first stable intermediates, aklanonic acid (**13**) and nogalonic acid (**14**), respectively, are folded in a controlled manner (Figure 5B)[111,115]. The process is initiated by 9-ketoreduction (KR) and aromatization (ARO) of the D-ring, which is followed by cyclization of C- and B-rings by a dedicated cyclase (CYC)[116,117]. The precise timing for release of the polyketide from the carrier protein is unknown, but the quinone forming 12-oxygenases (OXY) are able to utilize substrates that are not bound to ACP[118–120]. Next, the terminal carboxyl group is *O*-methylated by *S*-adenosyl-L-methionine (SAM)-dependent methyltransferases (MET), an essential step for cyclization of the A-ring (Figure 5B)[121]. Closure of the fourth ring occurs *via* Aldol condensation and these cyclases (CYC) determine the *9R* or *9S* stereochemistry of anthracyclines[115,122,123]. The final step in the biosynthesis of the key intermediates aklavinone (**15**) and nogalavinone (**16**) is ketoreduction by short-chain dehydrogenase/reductases (SDR) that retain exclusively the *7S* stereochemistry (Figure 5B)[117,124].

Deviation from this classical biosynthetic model transpires on the steffimycin-subclass of anthracyclines, where the lack of a 9-ketoreductase on the pathway leads to the archetypical 2-hydroxyl group[125]. Additionally, the fourth ring cyclase StfX, which is unrelated to SnoaL and AknH, acts on an ACP bound thioester and catalyzes decarboxylative cyclization to form 2-*O*-demethyl-8-demethoxy-10-deoxysteffimycinone (**17**) (Figure 5B)[126].

Biosynthesis of diverse carbohydrates

Anthracyclines contain a broad selection of 6-deoxysugar units that are typically associated with microbial natural products[127,128]. These include many 2,6-dideoxy- and 2,3,6-trideoxysugars[105], but the two most common substrates used in glycosylation of the 7-position are the amino sugars TDP-L-daunosamine (**18**)[129] and TDP-L-rhodosamine (**19**)[130], which have been enzymatically synthesized using proteins from the nogalamycin pathway (Figure 6)[131]. Rare carbohydrates attached to anthracyclines include brasiliose[132], L-decilonitrose[133], a γ-branched octose[134], and the 4-ketosugars cinerulose and L-aculose[130].

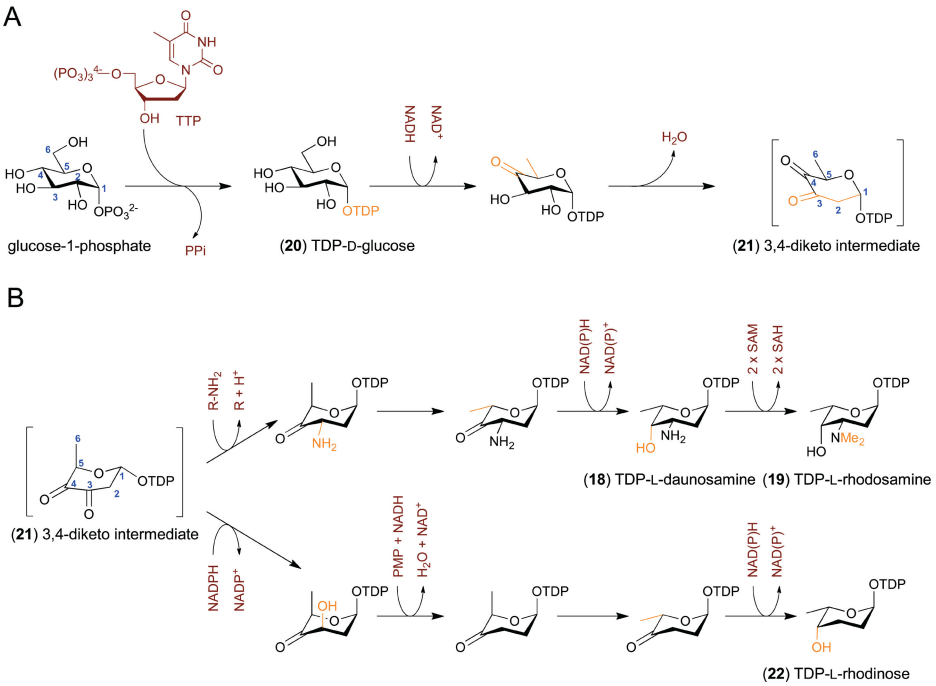


Figure 6. Biosynthesis of diverse carbohydrates. (A) The biosynthesis of 6-deoxysugars starts with the attachment of thymidine monophosphate to glucose-1-phosphate resulting in TDP-D-glucose (**20**). This is followed by two consecutive dehydration reactions by SDR enzymes resulting the formation of a common unstable 3,4-diketo intermediate (**21**). **(B)** The biosynthesis of amino and deoxysugars branch off from the intermediate **21**. On pathways towards amino sugars (**18**, **19**), the pyridoxal-5'-phosphate dependent enzymes (PLP) catalyze a 3-transamination reaction followed by a 5-epimerization reaction. Subsequently, **18** is formed through a NADPH stereospecific 4-ketoreductase. A SAM-dependent *N*-dimethylation of **18** leads to **19**. In contrast, the biosynthesis of 2,3,6-trideoxysugars such as **22** proceeds *via* 3-ketoreduction and removal of the 3-hydroxyl group. Subsequent 5-epimerization and 4-ketoreduction finalize formation of **22**.

In general, the early biosynthetic steps for all 6-deoxysugars are conserved and also found in primary metabolic pathways such as cell-wall synthesis[127]. The first step is the attachment of thymidine monophosphate to glucose-1-phosphate to generate TDP-D-glucose (**20**) with concomitant loss of pyrophosphate by nucleotidyltransferases (Figure 6)[135,136]. Two consecutive dehydration reactions, 4,6-dehydration by SDR enzymes[137], and 2,3-dehydration by Nudix hydrolase superfamily proteins[138], lead to formation of an unstable 3,4-diketo intermediate (**21**). Activation of the TDP-carbohydrate in such a manner allows diverse modification reactions to occur and leads to branching of the biosynthetic pathways towards their end products (Figure 6)[128].

On pathways leading to amino sugars, the next step is 3-transamination by pyridoxal-5'-phosphate (PLP) dependent enzymes using amino acid nitrogen group donors (Figure 6)[139]. The importance of the 4-keto group is further highlighted in the 5-epimerization reaction[140], which is facilitated by an enolate anion intermediate at C4[104]. Formation of **18** is completed

through stereospecific 4-ketoreduction using NADPH as the reducing agent, while biosynthesis of **19** continues through SAM-dependent *N*-dimethylation (Figure 6)[131].

In turn, TDP-L-rhodinose (**22**) can be considered an example of a typical anthracycline 2,3,6-trideoxysugar (Figure 6). The biosynthesis continues from the common 3,4-diketo intermediate through 3-ketoreduction. Subsequent removal of the 3-hydroxyl groups is mechanistically challenging due to the proximity of the 4-keto group[141] and requires enzymes containing an [2S–2Fe] iron sulfur cluster, a pyridoxamine-5'-phosphate cofactor and external electron donors such as ferredoxin/ferredoxin reductase[142]. Similarly to amino sugar biosynthesis, the final steps include 5-epimerization and 4-ketoreduction[104].

Glycosylation of anthracyclines

The carbohydrate units are transferred to aglycones by glycosyl transferases (GTs) that typically belong to the B family (GT-B)[143]. The structure of the L-rhodosamine transferase SnogD[144] responsible for 1-*O*-glycosylation on the nogalamycin pathway has demonstrated how the two Rossman fold domains, one for the aglycone acceptor and one for the sugar donor, provide a framework for transfer of diverse carbohydrates to a variety of positions in anthracyclinones[141,143].

In all known instances, the glycosylation at either the 7-position[131,145–147] or the 10-position[145,148] requires an additional P450-enzyme to increase the activity of the *bona fide* GT. The likely role of this P450-enzyme is to act as an allosteric activator[147], a proposal that has been supported by the crystallization of the α2β2 heterodimeric complex from the erythromycin pathway[149]. Strong non-covalent interactions between the partners have been proposed to induce conformational shifts both in the N-terminal aglycone acceptor and C-terminal sugar donor domains of the GTs to aid catalysis[149].

Other tailoring reactions

Modification of the anthracyclinone core in late stage tailoring steps is critical for the chemical diversity of these natural products. The doxorubicin pathway harbors the flavin adenine dinucleotide (FAD) dependent mono-oxygenase *dnrF* which catalyzes a 11-hydroxylation reaction (Figure 7)[150]. The biosynthesis continues through 15-demethylation by the *dnrP* esterase[151,152] and classical 4-*O*-methylation by *dnrK*[121] to generate 13-deoxydaunorubicin (**23**). The heme-containing cytochrome P450-protein DoxA drives the three consecutive 13- and 14-hydroxylation reactions that define the doxorubicin-subclass of anthracyclines (Figure 7)[153]. The daunomycin BGC also encodes additional enzymes that are responsible for formation of baumycin acetals (**24**), which are formed *via* oxidative carbon–carbon bond cleavage of a second nitrososugar (Figure 7)[154].

Rhodomycin biosynthesis proceeds similarly to daunorubicin with homologous proteins for 11-hydroxylation by RdmE[155,156] and 15-demethylation by RdmC[157,158]. The subsequent 10-hydroxylation step is catalyzed by SAM-dependent methyltransferase-like RdmB[158,159], which is interestingly homologous to *dnrK*, to complete formation of **1** (Figure 7).

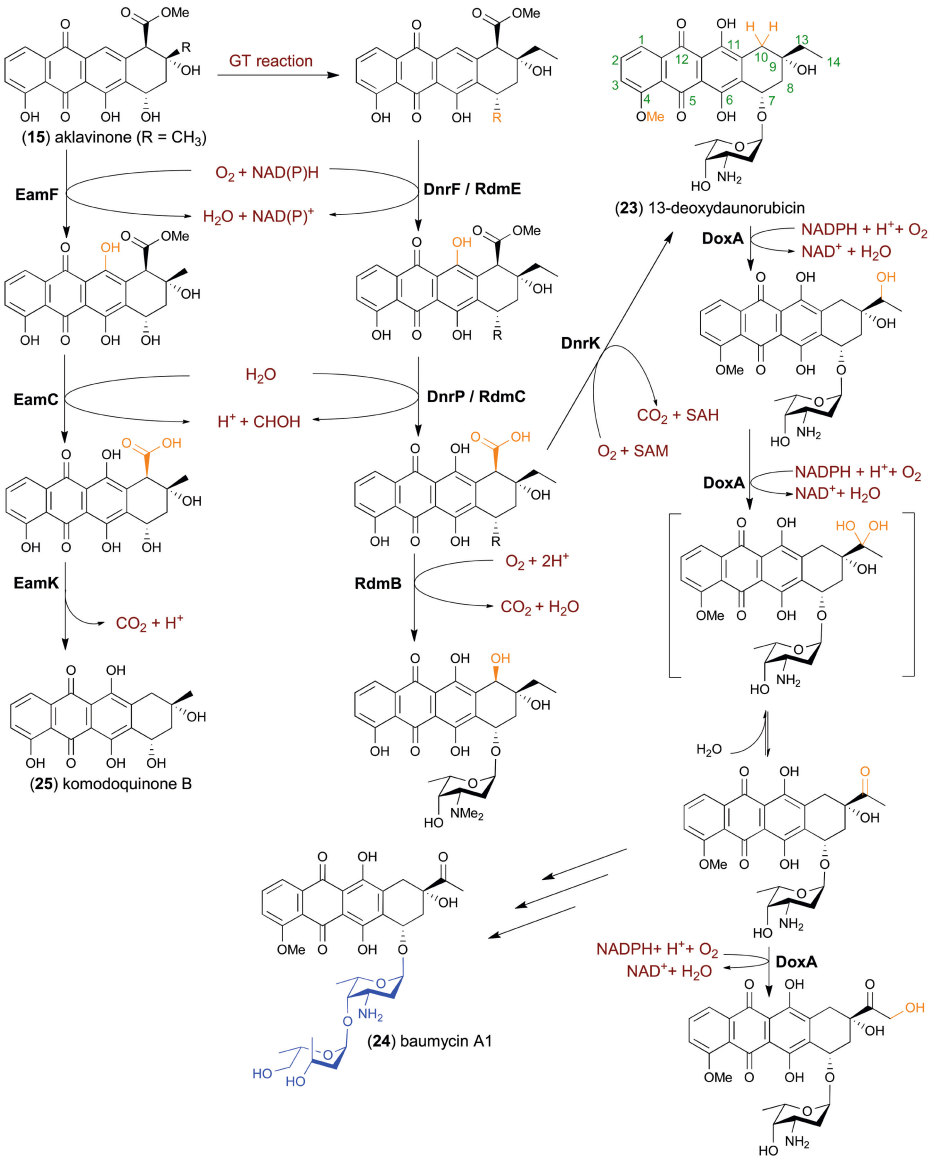


Figure 7. Chemical diversification of rhodomycin, doxorubicin and komodoquinone by tailoring enzymes. Various enzymes introduce chemical diversity (in orange) in the anthracycline backbone in the biosynthesis of **1**, **3** and **25**. All of these pathways share FAD dependent C-11 hydroxylases (DnrF/RdmE/EamF) and C-15 methylesterases (DnrP/RdmC/EamC). The next enzymes on the pathways are SAM-dependent methyltransferase-like proteins (DnrK/RdmB/EamK), which catalyze distinct chemistry. DnrK catalyzes C4-*O*-methylation with C-10 decarboxylated moonlighting activity, RdmB catalyzes C-10 hydroxylation, and EamK catalyzes solely C-10 decarboxylation. The biosynthesis of **3** continues through the action of the heme-dependent cytochrome P450 enzyme DoxA, which catalyzes three successive hydroxylation reactions. The daunomycin BGC also encodes additional enzymes that are responsible for formation of higher glycosides such as baumycin A1 (**24**).

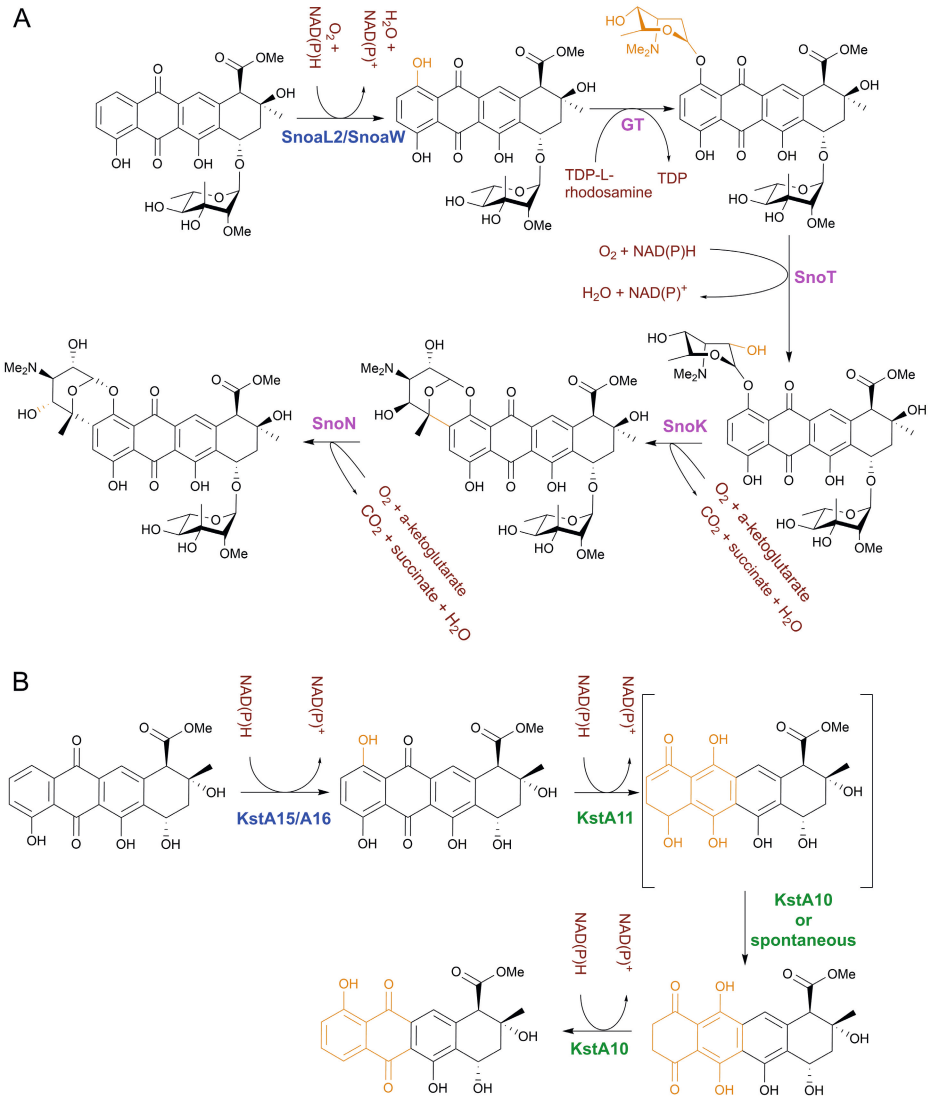


Figure 8. Parallels between tailoring steps in nogalamycin and kosinostatin biosynthesis. (A) The biosynthesis of **4** involves several atypical proteins. Formation of the archetypical epoxyoxocin ring system is initiated by the two-component 1-hydroxylase system SnoaW and SnoaL2. Attachment of the L-rhodosamine sugar is catalyzed by the SnogD glycosyltransferase. The reaction product is 2"-hydroxylated by the Rieske enzyme SnoT. The dual linkage of the amino sugar is completed by SnoK, a non-heme iron and α-ketoglutarate dependent enzyme. The final 4"-epimerization is catalyzed by SnoN. **(B)** The pathway towards **26** also includes a two component 1-hydroxylase system KstA15 and KstA16. In order to remove the 4-hydroxy group, KstA11 catalyzes an asymmetric dearomatization that allows 4-ketoreduction and 3,4-dehydration by KstA10.

Insertion of a single amino acid to *dnrK* suffices to convert 4-*O*-methylation activity to 10-hydroxylation[160], which demonstrates how small changes in biosynthetic enzymes allow the generation of structural diversity in microbial natural products[59]. This is further illustrated by an example from the komodoquinone B (**25**) pathway, where another SAM-dependent methyltransferase-like protein, EamK, catalyzes 10-decarboxylation (Figure 7)[151].

The late stages in the biosynthesis of **4** involve several atypical proteins (Figure 8A). Formation of this nogalamycin-subtype defining epoxyoxocin ring system is initiated by a two-component 1-hydroxylase system[161] that is composed of the SDR enzyme SnoaW and SnoaL2, which is related to polyketide cyclases such as SnoaL[123,162]. A similar system exists on the kosinostatin pathway, where the recruitment of two additional Rossmann-fold proteins KstA10 and KstA11 complete regioisomerization of the phenolic hydroxyl group (Figure 8B)[163]. In nogalamycin biosynthesis, the Rieske enzyme SnoT performs 2"-hydroxylation of the L-nogalamine sugar using a [2S–2Fe] iron sulfur cluster after the second glycosylation event[164]. The dual attachment of the amino sugar is completed by the non-heme iron and α-ketoglutarate dependent SnoK (Figure 8A)[165]. The final step in the biosynthesis of nogalamycin is 4"-epimerization to generate the L-nogalamine carbohydrate by SnoN (Figure 8A), which surprisingly shares significant sequence similarity with SnoK despite the difference in enzymatic activity[165,166].

Other unique post-PKS tailoring steps include oxidation and methylation reactions by P450 and SAM-dependent proteins, respectively, on the steffimycin pathway[125]. An atypical oxidoreductase AknOx catalyzes two subsequent oxidations of the terminal L-rhodosamine sugar to L-aculose supported by a bicovalently bound FAD on the aclacinomycin pathway[167]. Finally, kosinostatin harbors a bicovalently attached pyrrolopyrrole moiety, which is formed in a multi-enzyme cascade including non-ribosomal peptide assembly steps[134].

Discovery

Naturally occurring anthracyclines

The distribution of different classes of microbial natural products is uneven, with some compounds highly specific and only produced by a small number of species, whereas others appear to be 'household' compounds that are produced by almost all species[168]. Examples of household compounds are two compounds produced by nearly all streptomycetes, namely the siderophore desferrioxamine that is required for iron acquisition[169] and the volatile organic compound geosmin, which lends the typical earthy smell to soil[170]. Streptothricin and streptomycin are examples of ubiquitous antibiotics, and during screening at Eli Lilly these compounds were detected in 10% and 1% of the extracts of the *Streptomyces* cultures, respectively, while daptomycin was found in only about 1 in 10^7 extracts[171]. The distribution of genes for biosynthesis of anticancer compounds is similarly uneven[168]. For example, the BGC specifying the macrolide FD-891 is present in almost all publicly available *Streptomyces* genomes[168], which may be due to the fact that apart from cytotoxic activity, FD-891 also acts as a plant

phytotoxin. The distribution of anthracycline BGCs seems to be moderate, with doxorubicin and aclacinomycin pathways identified in 37 and 32 out of 1110 genomes, respectively, while nogalamycin BGC was found only in two genomes[168].

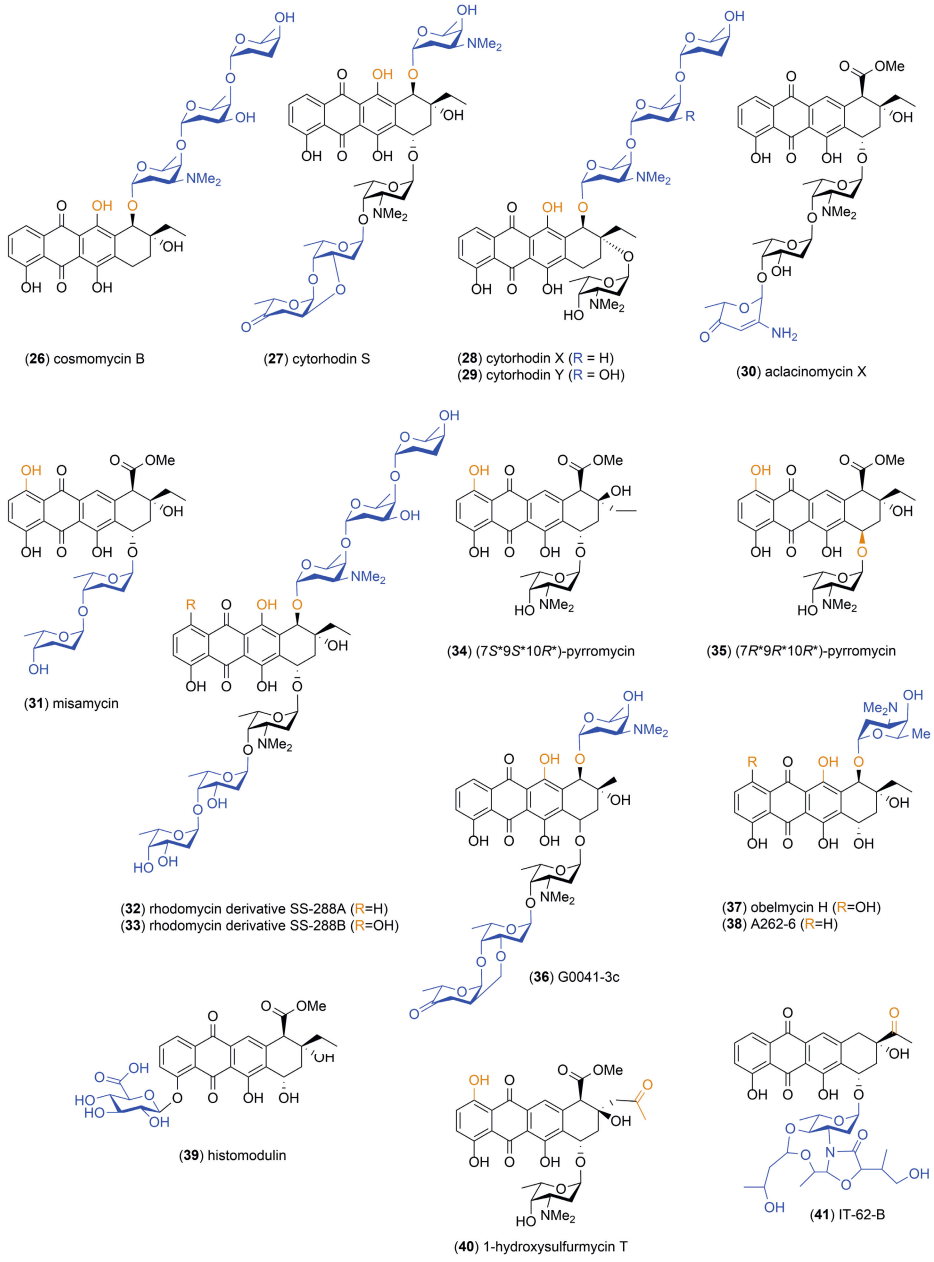


Figure 9. Structures of recently discovered anthracyclines based on the aclacinomycin scaffold. Differences in glycosylation and tailoring are colored in blue and orange, respectively.

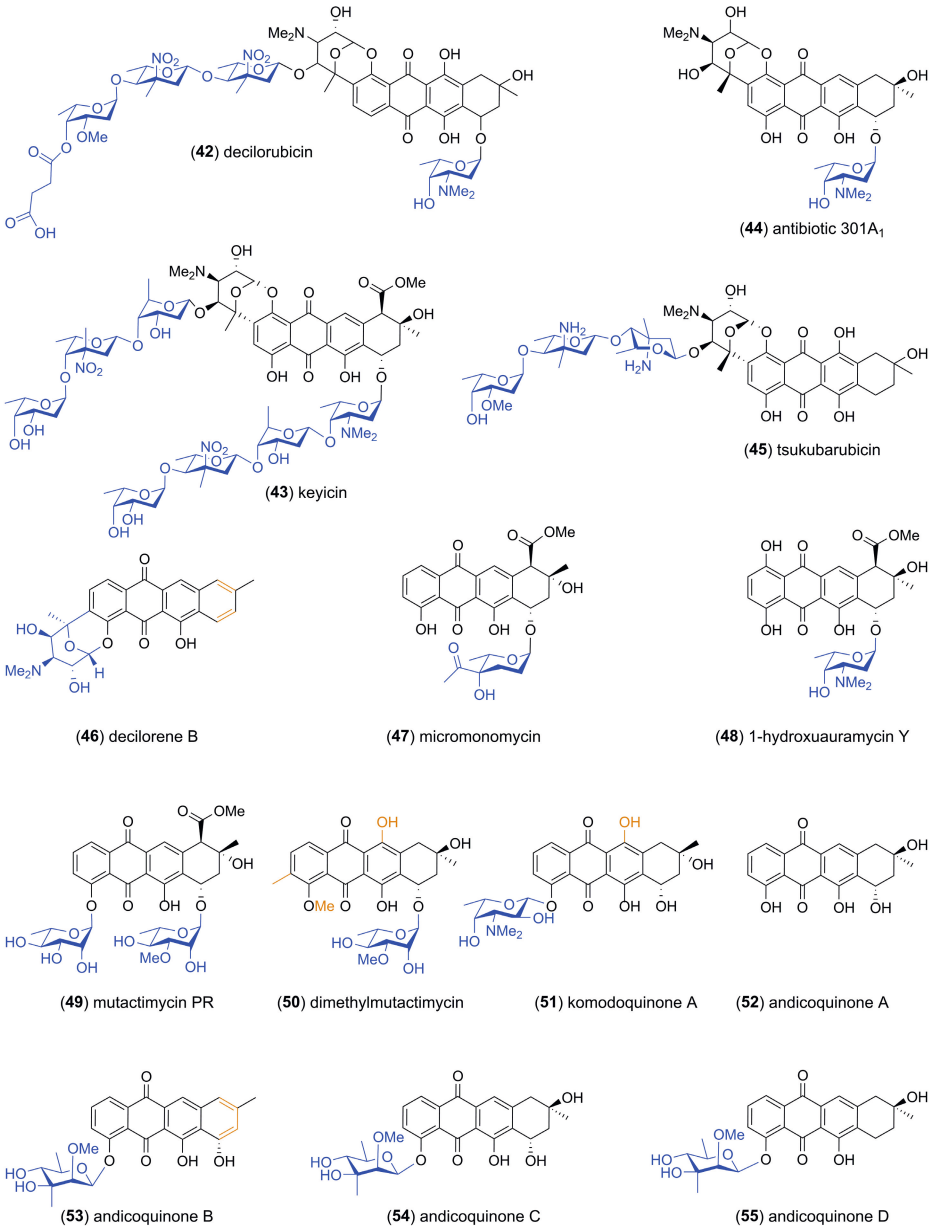


Figure 10. Structures of nogalamycin-type anthracyclines with epoxyoxocin ring systems. Differences in glycosylation and tailoring are colored in blue and orange, respectively. C9 carbon stereochemistry for **42** and **45** was not reported.

Despite the infrequent occurrence of anthracycline BGCs, the medical importance of these compounds has led to the isolation of more than 500 naturally occurring anthracyclines to date[172,173]. The majority of anthracyclines have been discovered from terrestrial *Streptomyces*

species, but the number of compounds obtained from marine and rare Actinobacteria have significantly increased in recent years due to increased bioprospecting of exotic locations. A comprehensive survey of all anthracyclines is beyond the scope of this review, and we will rather focus on compounds isolated during the 'genomics era' in the last 25 years.

Several anthracyclines related to the classical compounds such as **1**, **5**, cosmomycin B (**26**), cytorhodins (**27–29**) (Figure 9), but which harbor differences in the glycosylation and tailoring patterns have been reported. These include aclacinomycin X (**30**)[174], misamycin (**31**)[175], rhodomycin derivatives SS-288A (**32**) and SS-288B (**33**)[176], and two pyrromycins (**34**, **35**) (Figure 9)[177]. G0041-3c (**36**) contains an additional carbohydrate at C10[178], while obelmycin H (**37**) and its congener A262-6 (**38**) are glycosylated only at this position[179]. In turn, histomodulin (**39**) is a rhodomycin derivative containing a glucopyranuronosyl unit at C4[180]. Two doxorubicin-type anthracyclines with a C13 carbonyl group, 1-hydroxysulfurmycin (**40**)[177] and IT-62-B (**41**)[181] have been identified (Figure 9). All these metabolites have been isolated either from terrestrial, marine-derived, or endophytic *Streptomyces* sp.

A few novel nogalamycin-type anthracyclines with the archetypical epoxyoxocin ring system have also been identified. These include derivatives of classical decilorubicin (**42**)[182] such as keyicin (**43**)[133] and antibiotic 301A$_1$ (**44**) (Figure 10), which surprisingly displayed synergistic effects with other antibiotics against Gram-negative *E. coli*[54]. Tsukubarubicin (**45**) lacks carbohydrate units at C7, but contains unusual avidinosamine sugar units appended to the dually attached rhodosamine (Figure 10)[183]. Decilorene B (**46**) harbors the epoxyoxocin ring system in a different regiochemistry appended at C4[184]. Other acetate primed anthracyclines include micromonomycin (**47**), which contains a 2,3,6-trideoxy sugar with an unusual acyl substitution at C4'[185], and 1-hydroxyauramycin Y (**48**) (Figure 10)[177]. In addition, anthracyclines such as mutactimycin PR (**49**)[186], demethyl mutactimycin (**50**)[187], komodoquinone A (**51**)[188] and andicoquinones A–D (**52**–**55**)[184] have been isolated (Figure 10). Noteworthy, several of these anthracyclines contain a more uncommon 4-*O*-glycosylation pattern.

In recent years, several steffimycin-type metabolites have been discovered. These include 11-hydroxy-steffimycin (**56**)[189], steffimycin E (**57**)[190] and the more unusual steffimycin F (**58**)[191], which contains a benzyl group appended to the quinone ring (Figure 11). Novel aranciamycins I (**59**) and J (**60**) have been obtained from a marine-derived *Streptomyces*[192], while aranciamycin anhydride (**62**) was discovered from a strain isolated from the rhizosphere of Norway spruce (Figure 11)[193]. Tetracenoquinocin (**63**), with a fully aromatic A-ring, and 5-iminoaranciamycin (**64**) have been isolated from a sponge-associated streptomycete (Figure 11)[194]. *Amycolatopsis* sp. was found to produce mutactimycin E (**65**), with an atypical C3 methyl group[195]. Nocardicyclins A–B (**66**, **67**) isolated from *Nocardia pseudobrasiliensis*[196] and arimetamycins A–C (**68**–**70**) obtained *via* metagenomics approaches[132] harbor rare brasiliose sugar moieties (Figure 11).

Anthracycline scaffolds with atypical modifications have also been isolated in recent years. A novel cyano-substituted anthracycline (**71**)[197] and a fully aromatized anthracycline that is

O-glycosylated at C4 (**72**)[198] has been characterized from terrestrial *Streptomyces* sp. (Figure 12). Kosinostatin (**73**), a stereoisomer of the classical isoquinocycline B (**74**), contains an unusual pyrrolopyrrole unit[199,200]. In addition, several non-glycosylated kosinostatin/isoquinocycline B pathway intermediates (**75**–**80**) have been isolated from cultures of *Micromonospora* sp. (Figure 12)[199–201].

Finally, numerous new anthracycline aglycones without appended carbohydrates have been characterized recently. Aranciamycin K (**81**) from a marine-derived *Streptomyces* sp.[202] and four anthracyclinones (**82**–**85**) from *Micromonospora* sp.[203] originate from a longer four-carbon butyryl-CoA starter unit (Figure 13). Boshramycinones A–B (**86**, **87**)[204], SS-228*R* (**88**) and related sharkquinone (**89**)[205] from marine-derived streptomycetes harbor fully aromatic A-rings.

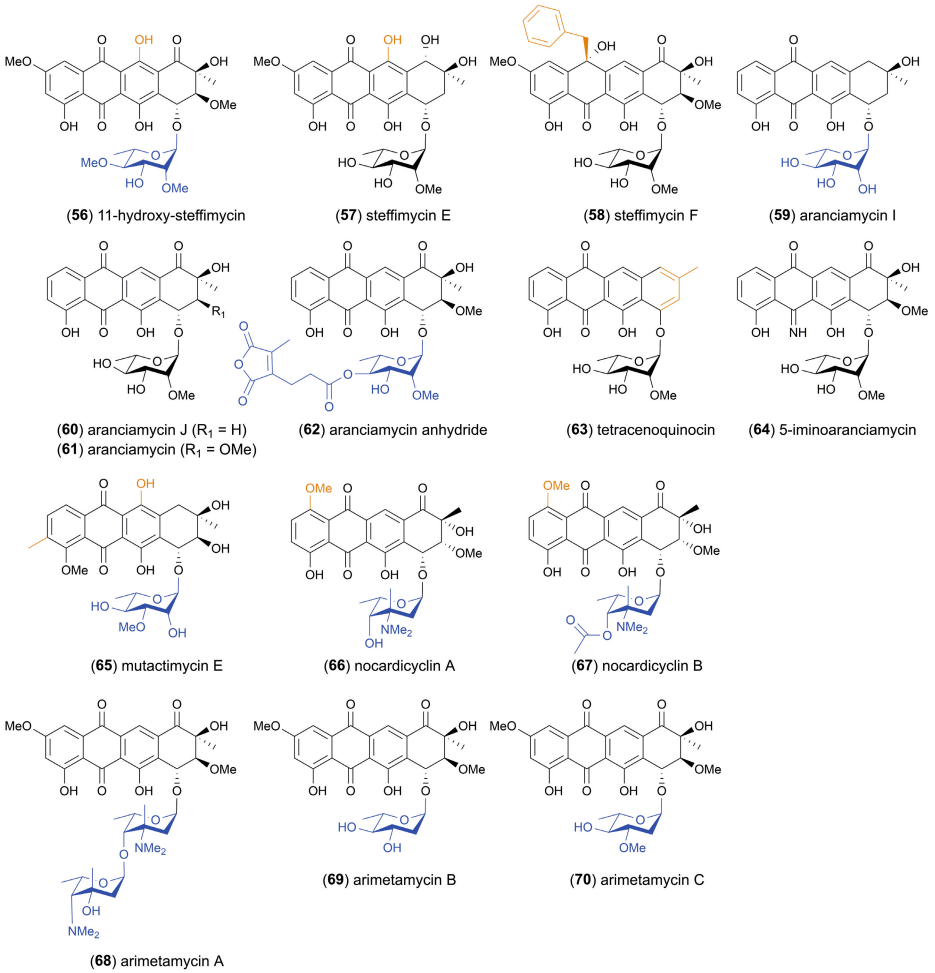


Figure 11. Structures of steffimycin-type anthracyclines. Differences in glycosylation and tailoring are colored in blue and orange, respectively.

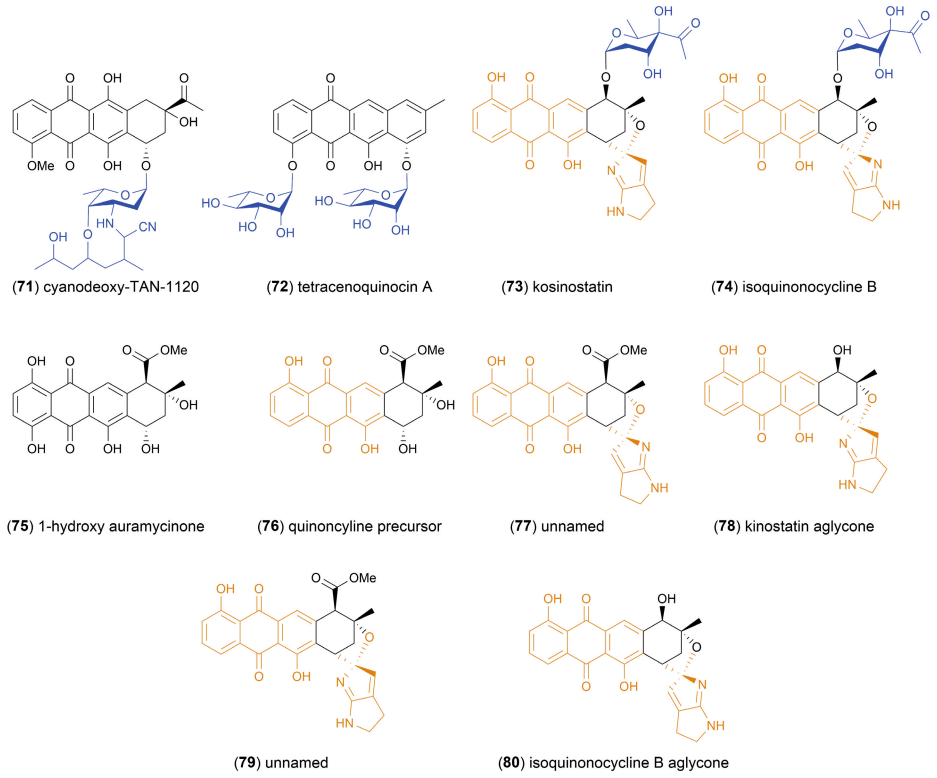


Figure 12. Anthracycline scaffolds with atypical modifications. Differences in glycosylation and tailoring are colored in blue and orange, respectively.

These anthracyclinones are derived from an acetyl-CoA starter unit, as is the related boshramycinone C (**90**) (Figure 13)[204]. The rare actinomycete *Nonomuraea rhodomycinica* NR4-ASC07 was found to produce 3-hydroxy substituted anthracyclinones (**91**)[206], while 2-chloro substituted celastramycin B (**92**) was identified from an endophytic *Streptomyces*[207]. Resomycins A–C (**93**–**95**), with modifications in the A-ring, have been isolated from a chartreusin producing terrestrial *Streptomyces* (Figure 13)[208].

Anthracycline biosynthetic gene clusters

To date 13 BGCs that have been experimentally verified to be involved in anthracycline biosynthesis. The medical importance of **5**[109,209] and **2**[110,210] is reflected in the fact that two BGCs for each have been identified from different *Streptomyces* strains, whereas single BGCs have been confirmed for rhodomycin (**1**)[156], nogalamycin (**4**)[112], cosmomycin (**26**)[148], cytorhodin (**27**)[145], kosinostatin (**73**)[134], aranciamycin (**59**)[211], arimetamycin (**68**)[132], keyicin (**43**)[133], tsukubarubicin (**45**)[183], komodoquinone (**25**)[151], and steffimycin (**6**)[125] pathways (Figure 14).

The majority of BGCs share homologous genes for the assembly of the aglycone units, with the exception of steffimycin, aranciamycin and arimetamycin BGCs, where the biosynthesis proceeds

via a decarboxylative cyclization mechanism[126]. The steffimycin and aranciamycin clusters are exceptional also in the sense that they do not encode any deoxysugar biosynthesis genes and the TDP-L-rhamnose building block has been proposed to be acquired from cell wall metabolism[125,148]. Genes required for formation of amino sugars are widely spread, and include TDP-L-daunosamine, TDP-L-rhodosamine and TDP-brasiliose in the case or arimetamycin[132]. It is noteworthy that also the komodoquinone BGCs harbors deoxysugar biosynthesis genes even though the strain only produced the aglycone komodoquinone B (**25**)[151]. However, glycosylated komodoquinone A (**51**) with a L-rhodosamine moiety has been isolated from another *Streptomyces* strain[188].

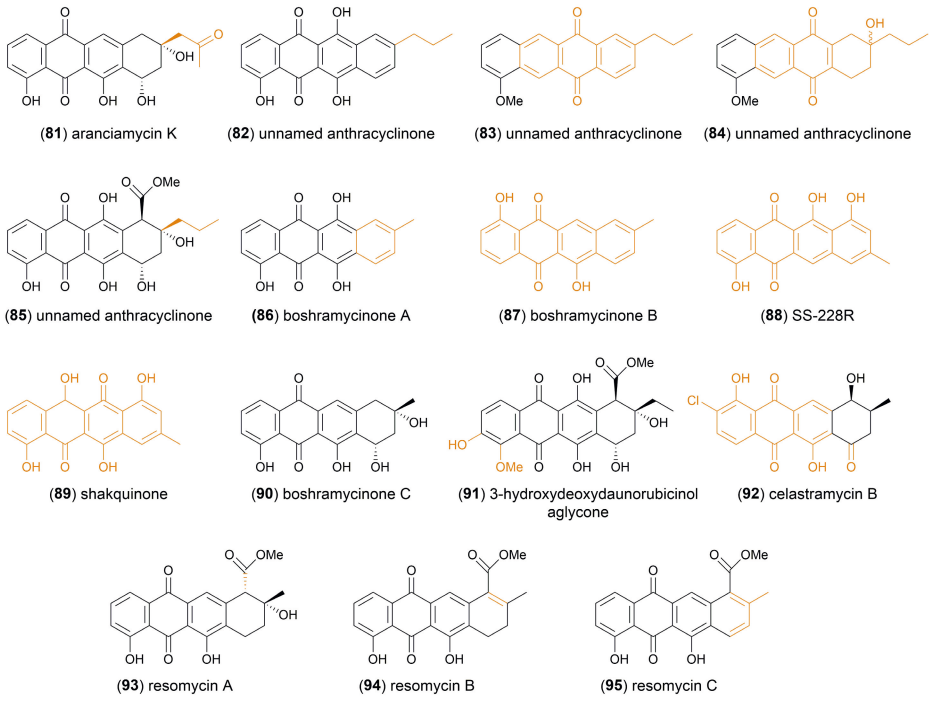


Figure 13. Recently discovered novel anthracyclinones. Unusual features are colored in orange.

The key differences in the BGCs are related to the number of glycosyl transferases, gene sets for the biosynthesis of diverse deoxysugars and the arsenal of tailoring genes present. Different combinations of these elements allow the rationalization for the diversification of anthracyclines. The aclacinomycin BGC does not contain any tailoring genes that modify the aglycone and therefore **5** can be considered as an ancient anthracycline. A noteworthy feature is that some of the more complex pathways appear to have been built on top of ancestral core pathways. For instance, the genomic organization of the arimetamycin BGC suggests that a TDP-brasiliose gene cassette may have merged with an ancestral steffimycin BGC in response to multidrug resistance efflux pumps that recognize the parental compound[132]. Further examples include expansion of the presumably parental nogalamycin and aclacinomycin BGCs through the inclusion of additional glycosyltransferases on the keyicin/tsukubarubicin and cosmomycin/cytorhodin pathways, respectively.

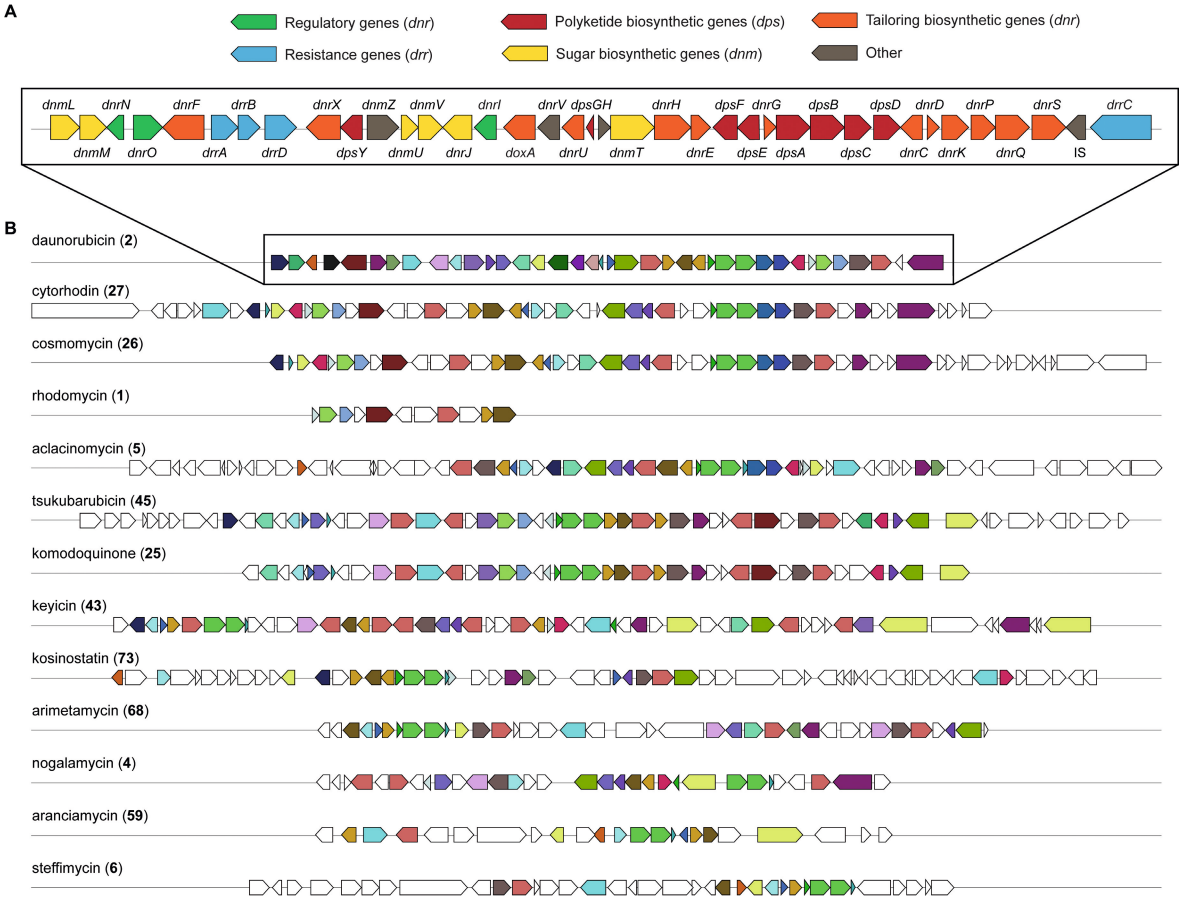


Figure 14. Currently known anthracycline biosynthetic gene clusters. (A) Schematic representation of the daunorubicin BGC. The color scheme represents the global gene function, classified as regulatory genes (green), resistance genes (blue), polyketide biosynthetic genes (red), sugar biosynthetic genes (yellow), tailoring genes (orange), or other (grey). **(B)** Gene cluster homology search of the daunorubicin BGC against twelve other experimentally verified anthracycline BGCs using MultiGeneBlast (v1.1.13) with default parameters[212]. The daunorubicin BGC is visualized in a color scheme that represents homology between genes of different clusters. For most BGCs the total extent of the clusters is unclear. Note that the aranciamycin and steffimycin BGCs lack sugar biosynthesis genes. The rhodomycin BGC has been sequenced only partially.

Genome mining strategies for discovery of novel BGGs

Actinobacteria harbor numerous cryptic or silent BGCs and activation of these pathways has become an increasingly important tool in the discovery of novel secondary metabolites.[40] The correct bioinformatic identification of anthracycline metabolic pathways is an essential prerequisite and few strategies, each with its own benefits and caveats, are available.

Identification of the full complement of cyclase genes is probably the most robust method to classify aromatic polyketides[213], but this is still relatively time consuming and manual curation of sequences is required. However, the fourth ring cyclases such as SnoaL[123] and AknH[122] appear to be highly specific for anthracyclines and can be used as a guide to drive the genome mining efforts. The added benefit is that phylogenetic analysis of the cyclase sequences allows prediction of the stereochemical configuration at C9. The limitation of the method is that steffimycin-type compounds are not detected as they harbor fourth ring cyclases such as StfX[197] that do not share sequence similarities to the canonical anthracycline cyclases.

Another approach is to focus on phylogenetic analysis of ketosynthase sequences, which reflect structures of the end products[214]. The analysis is complicated by the fact that anthracyclines appear to form several distinct clades[215]. Ketosynthase sequence analysis was utilized in the discovery of the arimetamycin pathway from a metagenomics eDNA library[132].

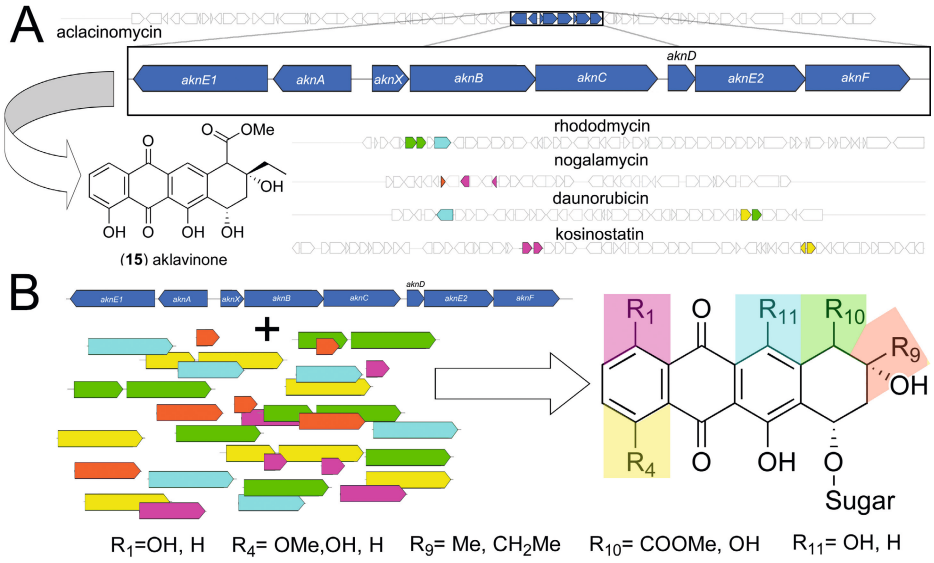


Figure 15. Generation of hybrid anthracyclines in *S. galilaeus* producing aclacinomycins. (A) The aclacinomycin BGC results in the formation of aklavinone (**15**). This aglycone is not modified by native tailoring enzymes, and therefore cloning of tailoring genes from the rhodomycin, nogalamycin, daunorubicin and kosinostatin pathways has led to formation of novel hybrid compounds. **(B)** Libraries of anthracyclines have been generated through modification of the aglycone at R_1 (magenta), R_4 (yellow), R_9 (orange), R_{10} (green), and R_{11} (cyan).

Metabolic engineering and combinatorial biosynthesis

Anthracycline pathways appear to be particularly amenable for pathway engineering efforts to further increase chemical diversity. The metabolic engineering efforts have focused particularly on expression of tailoring genes from related pathways[216] and glycodiversification[105].

S. galilaeus producing **5** and other aclacinomycins has been an ideal host for the generation of hybrid anthracyclines, since the aclacinomycin BGC does not harbor any native aglycone modification genes[216]. This has allowed modification of substituents at R_1, R_4, R_9, R_{10} and R_{11} of the aklavinone aglycone by cloning different combinations of tailoring genes from the rhodomycin[217,218], nogalamycin[115,219,220], daunorubicin[221–223] and kosinostatin[224] pathways (Figure 15). The efficacy of such pathway engineering experiments was demonstrated by expression of the minPKS from the nogalamycin pathway together with the 10-methylesterase, 10-hydroxylase and 11-hydroxylase from the rhodomycin pathway in a *S. galilaeus* mutant HO75, which produces a mixture of differently glycosylated aclacinomycins due to a defective dTDP-hexose-3-dehydratase[225], that resulted in the production of a library of 60 anthracyclines[226]. Hybrid anthracyclines have also been generated by incorporating additional foreign genes to the daunorubicin[219], epelmycin[223] and steffimycin[227] pathways.

Modification of the carbohydrate units of anthracyclines affects the bioactivity of the compounds and therefore the engineering of deoxysugar pathways has generated wide interest. The pioneering example is the production of biosynthetic **7** in *S. peucetius*, which was achieved through inactivation of the natural TDP-4'-keto-2,3,6-trideoxyhexulose reductase gene *dnmV* and expression of 4-ketoreductases with opposite stereoselectivity[228].

The success of these approaches relies on the ability of the glycosyltransferases to recognize and append unnatural TDP-carbohydrates to anthracyclinones. The L-rhamnose glycosyltransferases StfG and AraGT from the steffimycin and aranciamycin pathways appear to be particularly promiscuous towards foreign TDP-carbohydrates. Expression of the aranciamycin BGC in two heterologous hosts led to the isolation of eight differently glycosylated derivatives (Figure 16)[213,229]. In turn, co-expression of the steffimycin BGC together with gene cassettes for synthesis of various TDP-carbohydrates in *S. albus* led to the formation of twelve derivatives (Figure 16)[230].

The heterologous host *S. venezuelae* has also been engineered to produce numerous TDP-carbohydrates and to express the two-component aclacinomycin *aknS* and *aknT* glycosyltransferase system[231]. Bioconversion experiments with extracellularly provided ε-rhodomycinone led to attachment of TDP-L-daunosamine, TDP-L-rhodosamine, TDP-L-ristosamine, TDP-L-vancosamine, TDP-D-digitoxose, TDP-L-digitoxose and TDP-L-rhamnose to the aglycone, and demonstrated the substrate flexibility of glycosyltransferases with the formation of twenty anthracyclines (Figure 17)[231]. The method was expanded to a one-pot combinatorial biosynthesis system, where distinct anthracyclinones and carbohydrates are produced in separate *Streptomyces* strains, but glycosylated anthracyclines are obtained upon co-cultivation. The experiments led to formation of 16 anthracyclines, including seven novel metabolites (Figure 17)[232].

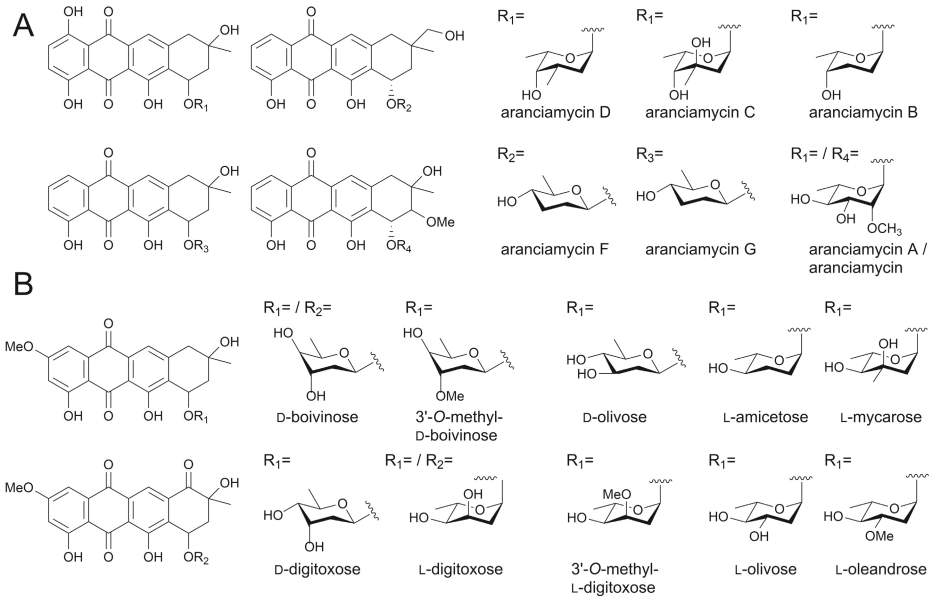


Figure 16. Combinatorial biosynthesis of aranciamycin and steffimycin in heterologous hosts. **(A)** Aranciamycin analogs have been generated by expression of the aranciamycin BGC from *S. echinatus* in *S. albus*, *S. fradiae* Tü2717, *S. fradiae* A0, and *S. diastatochromogenes* Tü6028. Novel glycosides are formed due to the availability of different TDP-carbohydrates in the heterologous hosts and the promiscuity of the glycosyltransferases. **(B)** Heterologous expression of the steffimycin BGC together with various TDP-carbohydrate pathways in *S. albus* led to the generation of twelve glycosylated derivatives of steffimycin.

Another means for generating novel anthracyclinones has been the assembly of polyketide biosynthesis genes in a heterologous host. A number of *Streptomyces* strains have been optimized for the production of heterologous metabolites[233,234]. An example is *S. coelicolor* M1152, which was obtained by deletion of the four main antibiotics clusters and ribosome engineering[235]. *S. venezuelae* is especially well-suited for the heterologous expression of polyketides due to the presence of a large number of innate phosphopantetheinyl transferase genes, which are required for the activity of the PKS machinery[236]. The anthracyclines aklavinone and ε-rhodomycinone have been produced in this host[232]. In addition, **15** and auravinone, which is identical to **16** except for opposite stereochemistry at C9, have been produced in *S. lividans* TK24 and *S. coelicolor* CH999 through assembly of biosynthetic genes from three different anthracycline pathways[109,117].

Improved production of anthracyclines

The secondary metabolites produced by streptomycetes are generally produced in low concentrations (μg·L^{-1} to mg·L^{-1}). *Streptomyces peucetius* ATCC 27952 produces about 1–20 mg·L^{-1} of **3** in production media[63,237]. However, the production titers need to be much higher for industrial-scale production (g·L^{-1}). Traditionally, strains with improved productivity were

obtained by random mutagenesis and screening, also called classical strain improvement[236]. This method has significant drawbacks as it is time-consuming and there is a risk of accumulation of unwanted mutations that affect other properties of the strain[238]. Developments in the fields of genetic engineering and systems biology have resulted in rational strain improvement methods[239,240]. These approaches focus on modification of regulatory networks, increasing precursor availability, increasing expression of rate-limiting biosynthetic enzymes, deleting genes for competing pathways, increasing product tolerance, combinatorial biosynthesis, and heterologous hosts.

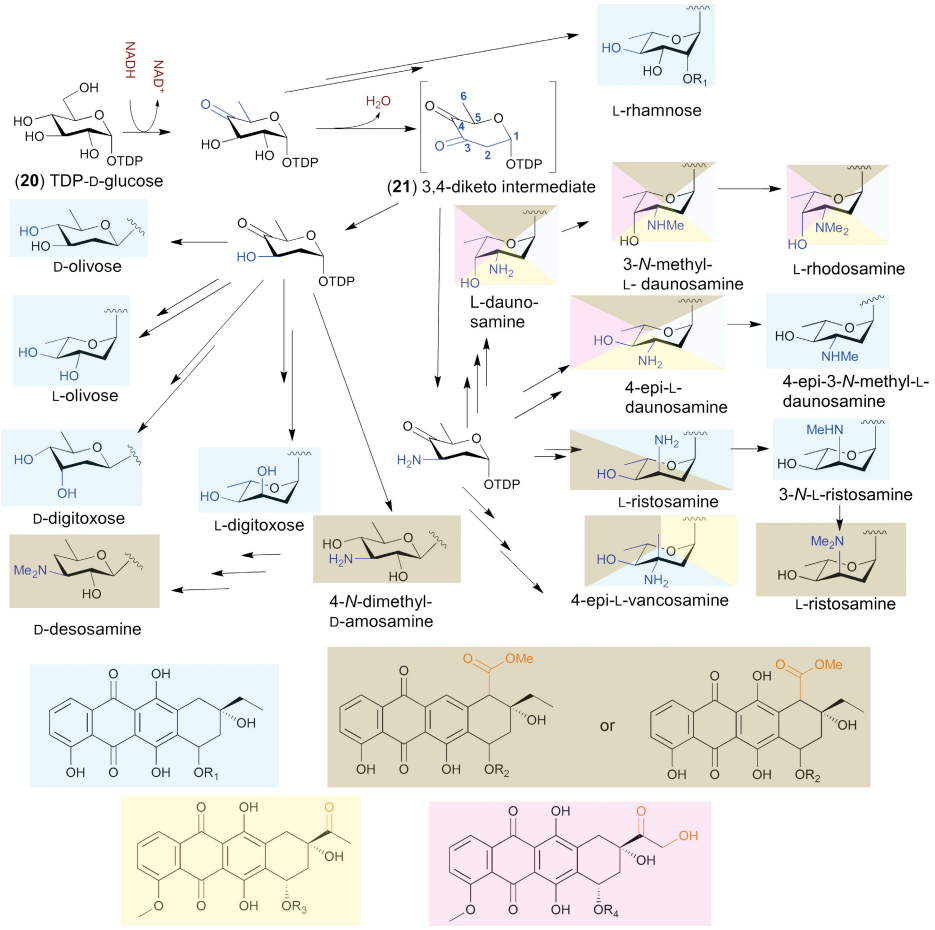


Figure 17. Production of differently glycosylated novel rhodomycins and daunorubicins in *S. venezuelae*. A series of plasmids encoding TDP-carbohydrate pathways (highlighted in cyan, yellow, or magenta) were assembled in *S. venezuelae*. Novel glycosylated anthracyclines were generated by feeding ε-rhodomycinone to the cultures for bioconversion reactions or by co-cultivation (highlighted in brown) with engineered *S. venezuelae* strains expressing core anthracycline pathways. Incorporation of the glycoside to the aglycone was possible due to the promiscuity of the AknS/AknT glycosyltransferase.

Engineering regulatory networks

The production of secondary metabolites is tightly regulated by global and pathway-specific control. Pathway-specific regulators may be positive or negative regulators and are typically regulated by environmental sensors and global regulators. The regulatory network is a key target for strain improvement, for example by overexpression of positive regulators and deletion of negative regulators.

The doxorubicin BGC contains a negative regulator (*dnrO*), and two positive regulators (*dnrN* and *dnrI*) (Figure 2)[82]. Overexpression of *dnrN* and *dnrI* in *S. peucetius* ATCC 29050 resulted in a two-fold (about 200 mg·mL^{-1}) overproduction of **2**[241]. Overexpression of the global regulatory gene *afsR* in *S. peucetius* ATCC 27950 resulted in 4-fold (about 80 mg·mL^{-1}) overproduction of **3**[242]. Overexpression of *dnrN* and *dnrI* under the *ermE** promoter in combination with *afsR* and SAM synthase genes to improve co-substrate availability resulted in up to 4.3-fold (about 7.5 mg·mL^{-1}) overproduction[65]. Other global regulatory proteins that have been targeted to increase the production of **3** are *wblA*[243] and *doxR*[244].

Metabolic engineering for yield improvement

The building blocks of secondary metabolites originate from primary metabolism[238]. The aglycone backbone of anthracyclines is typically constructed from acetyl-CoA or propionyl-CoA and is extended with several units of malonyl-CoA. The sugar moieties generally originate from glucose-6-phosphate. Hence, the anthracycline precursors are generated in glycolysis, the tricarboxylic acid cycle, and the pentose-phosphate pathway. The production of anthracyclines may be improved by increasing the availability of these precursors. Acetyl-CoA carboxylase (Aac) catalyzes the conversion of acetyl-CoA to malonyl-CoA. The biosynthesis of glucose-6-phosphate depends on the activity of phosphoglucomutase (Pgm). Overexpression of *acc* and *pgm* resulted in increased production of anthracycline(-like) compounds[245,246]. The production of **4** by *S. nogalater* NRRL3035, **6** by *S. steffisburgensis* NRRL 3193, and elloramycin by *Streptomyces olivaceus* Tü2353 was increased 1.5 to 2-fold[246]. The availability of acetyl-CoA depends on the triacylglycerol pool. The acetyl-CoA synthase is responsible for the activation of fatty acids with coenzyme A (CoA). Inducible expression of the *S. coelicolor* acetyl-CoA synthase SCO6196 resulted in increased production of actinorhodin (1.9-fold; 216.1 mg·L^{-1}), jadomycin B (1.7-fold; 133.0 mg·L^{-1}), oxytetracycline (4.7-fold; 4.54 g·L^{-1}), and avermectin B_{1a} (0.5-fold; 9.31 g·L^{-1}) in respectively, *Streptomyces coelicolor* M145, *Streptomyces venezuelae* ISP5230, *Streptomyces rimosus* M4018, and *Streptomyces avermitilis* A56[247]. This strategy has not yet been applied for the production of anthracyclines. However, overexpression of two genes involved in CoA biosynthesis (*coaA* and *coaE*) resulted in 2.1-fold (3.34 mg·mL^{-1}) increased production of **3** in *S. peucetius* ATCC 27952[248]. Precursor supply of polyketides has recently been reviewed elsewhere[249].

The overexpression of biosynthetic genes has also been widely applied to improve production levels, with a special focus on rate-limiting enzymes. Heterologous enzymes from the sugar pathway of *S. venezuelae* ATCC 15439 were expressed in *S. peucetius* ATCC 27952, which

resulted in an increased production of **3** by 2.6-fold (about 3.5 mg·mL^{-1})[237]. The activity of the glycosyltransferase DnrS is rate-limiting, resulting in an accumulation of ε-rhodomycin. Combined overexpression of the *S. venezuelae* sugar genes and the native glycosyltransferase pair (*dnrS*/*dnrQ*) resulted in 5.6-fold (about 9.5 mg·mL^{-1}) increased production[237]. The final enzyme in the doxorubicin pathway (DoxA) is responsible for the last three steps towards **3**. Especially the last step from **2** to **3** is 170-fold less efficient than the previous step in the pathway[153]. Overexpression of *doxA* is not sufficient to significantly improve production of **3**, which is still an interesting target for engineering[250].

Another strategy may be to express multiple copies of the BGC. During classical strain improvement, amplification of BGCs has been reported as a cause for yield improvement, for example for penicillin[251] and kanamycin[252] production. Currently, several methods like the TAR system, the IR system and the BAC system are available for the cloning of entire BGCs, which can be used for heterologous expression or duplication of the BGC in the native host[253].

Secondary metabolites are often toxic to their producers. Consequently, increasing product tolerance by overexpression of resistance genes is another widely applied strategy. The DNA damaging activity of anthracyclines may also affect the producing strain. Therefore, the BGCs generally include exporters and DNA repair mechanisms. Overexpression of the doxorubicin resistance genes *drrA* and *drrB* (Figure 2) in *S. peucetius* ATCC 27952 resulted in a 2.2-fold (about 3 mg·mL^{-1}) increased production of **3**, and overexpression of *drrC* (Figure 2) in a 5.1-fold (about 7.0 mg·mL^{-1}) increase[254]. In addition, improved resistance enhances the stability of the production strain, which is an important consideration for industrial production.

Another approach for improving production is the inactivation of competing pathways. Two examples can be taken from the doxorubicin pathway. First, the availability of the sugar moiety daunosamine can be increased by inactivation of the rhamnose pathway that competes for intermediates. Inactivation of the final enzyme in the biosynthetic pathway of rhamnose (RmdD) may result in an increased daunosamine availability, which could result in increased production of **3**[65,255]. Besides that, the production levels of **2** and **3** are decreased due their conversion into baumycin-like higher glycosides. The enzymes responsible for these conversions are *dnrH*, *dnrU*, and *dnrX*. Deletion of *dnrH* resulted in increased production of **2** in *S. peucetius* ATCC 27952 of 8.5-fold (about 15 mg·mL^{-1}). Deletion of *dnrH* and *dnrX* resulted in a 3-fold (14 mg·mL^{-1}) increased production of **2**[256,257].

Fermentation and media

The production of secondary metabolites is linked to changes in the environment, and therefore optimizing media and fermentation methods is crucial to increase production levels. Carbon catabolite repression plays a role in most streptomycetes, resulting in reduced production of secondary metabolites in the presence of a high concentration of carbon source, mainly glucose[258]. However, high growth rates are often obtained with glucose as carbon source. Consequently, medium design is always a trade-off between growth rates and production

rates[238]. The production of **3** is reduced in high glucose conditions[259], and high levels of inorganic phosphate also repress production of anthracyclines by *S. peucetius*[260]. Phosphate levels dictate the transition from primary to secondary metabolism[261]. Recently, the production of **3** was improved to 1.1 $g \cdot L^{-1}$ by a combination of classical strain improvement and medium optimization[262].

Perspectives

Back in 1992, Weiss wondered whether 'We will ever find a better doxorubicin' after the generation of hundreds of semi-synthetic derivatives that did not significantly improve the outcome of anticancer chemotherapy or limit the side effects[13]. Yet, recent studies with these old drugs using new technologies have identified unrecognized activities that are unique to anthracycline drugs: nucleosome eviction. The complex bioactivities of anthracyclines suggest that additional relevant activities may be uncovered in the future. While the anticancer activities of anthracyclines can sometimes be improved as exemplified by the recently discovered semi-synthetic utorubicin[263], the major limitation in the use of these drugs are the toxic side effects. The strongly reduced toxicity profile of **12**, without compromising anticancer efficacy, shows that overcoming toxicity issues is possible. Further points of interest are modifications affecting tissue distribution and/or reducing the removal of drugs from cells by ABC transporters such as MDR1, which may contribute to better anthracycline drugs.

These developments have coincided with an increased understanding of how *Streptomyces* bacteria are able to produce numerous anthracyclines with relative ease. The accumulation of next-generation sequencing data and modern synthetic biology techniques will offer unprecedented possibilities for manipulation of anthracycline biosynthetic pathways to further increase the chemical diversity within this family of compounds. Discovery of novel anthracyclines continues to thrive also by traditional means, by focusing on culture extracts from isolates of rare Actinobacteria.

One critical issue for future development of anthracycline drugs is the need for coordination between natural product discovery and bioactivity profiling. Most of the anthracyclines described in this review have never been tested, for instance, towards histone eviction activity or cardiotoxicity. The primary reason is the shift in anthracycline research back to academia due to current lack of interest from pharmaceutical companies. An international multidisciplinary community effort to routinely screen all newly discovered compounds for bioactivities beyond basic cytotoxicity parameters is gravely needed. If successful, the combination of metabolic engineering, semi-synthesis and modern bioactivity profiling will allow re-evaluation of the chemical space around anthracyclines and discovery of improved drugs. For these reasons, the future of anthracycline drugs looks bright and, yes, we believe that a better doxorubicin can indeed be found.



Metabolic engineering of *Streptomyces peucetius* for biosynthesis of *N,N*-dimethylated anthracyclines

Mandy B. Hulst, Le Zhang, Helga U. van der Heul, Chao Du, Somayah S. Elsayed, Arina Koroleva, Thadee Grocholski, Dennis P.A. Wander, Mikko Metsä-Ketelä, Jacques J.C. Neefjes and Gilles P. van Wezel

Front. Bioeng. Biotechnol. 2024; **12**, 1363803.

Abstract

Daunorubicin and doxorubicin, two anthracycline polyketides produced by *Streptomyces peucetius*, are potent anticancer agents that are widely used in chemotherapy, despite severe side effects. Recent advances have highlighted the potential of producing improved derivatives with reduced side effects by incorporating L-rhodosamine, the *N,N*-dimethyl analogue of the native amino sugar moiety. In this study, we aimed to produce *N,N*-dimethylated anthracyclines by engineering the doxorubicin biosynthetic pathway in the industrial *S. peucetius* strain G001. To achieve this, we introduced genes from the aclarubicin biosynthetic pathway encoding the sugar *N*-methyltransferases AclP and AknX2. Furthermore, the native gene for glycosyltransferase DnrS was replaced with genes encoding the aclarubicin glycosyltransferases AknS and AknT. Additionally, the gene for methylesterase RdmC from the rhodomycin biosynthetic pathway was introduced. A new host was engineered successfully, whereby genes from the aclarubicin pathway were introduced and expressed. LC-MS/MS analysis of the engineered strains showed that dimethylated sugars were efficiently produced, and that these were incorporated into the anthracycline biosynthetic pathway to produce the novel dimethylated anthracycline *N,N*-dimethyldaunorubicin. Further downstream tailoring steps catalysed by the cytochrome P450 monooxygenase DoxA exhibited limited efficacy with *N,N*-dimethylated substrates. This resulted in only low production levels of *N,N*-dimethyldaunorubicin and no *N,N*-dimethyldoxorubicin, most likely due to the low affinity of DoxA for dimethylated substrates. *S. peucetius* G001 was engineered such as to produce *N,N*-dimethylated sugars, which were incorporated into the biosynthetic pathway. This allowed the successful production of *N,N*-dimethyldaunorubicin, an anticancer drug with reduced cytotoxicity. DoxA is the key enzyme that determines the efficiency of the biosynthesis of *N,N*-dimethylated anthracyclines, and engineering of this enzyme will be a major step forwards toward the efficient production of more *N,N*-dimethylated anthracyclines, including *N,N*-dimethyldoxorubicin. This study provides valuable insights into the biosynthesis of clinically relevant daunorubicin derivatives, highlighting the importance of combinatorial biosynthesis.

Introduction

The secondary metabolic pathways of bacteria and fungi yield valuable natural products that serve as an important source of antibiotics and other drugs. Actinobacteria, especially members of the *Streptomyces* genus, stand out as prolific producers of these bioactive secondary metabolites[3,21]. These compounds exhibit a broad range of bioactivities, including antibacterial, anticancer, antifungal, antiviral, anthelmintic, herbicidal, and immunosuppressive effects[4,20]. Natural products can be categorised into distinct structural families based on their biosynthetic origin, such as polyketides, non-ribosomal peptides, ribosomally synthesised post-translationally modified peptides (RiPPs), terpenoids, and alkaloids. The wide range of bioactivities and structural variations highlights the importance of natural products for drug development[20].

Polyketides are a diverse class of natural products renowned for their remarkable structural complexity[23]. The polyketide backbone is assembled through the iterative condensation of acyl-CoA units, a process catalysed by the polyketide synthase (PKS) enzyme complexes[264]. Type I polyketides are synthesised by large multimodular enzyme sets, while type II polyketides are synthesised by the iterative action of a single enzyme set[265]. The polyketide scaffold is diversified by modifications introduced via tailoring reactions such as methylation, amination, oxidation, and glycosylation, resulting in a broad range of structures and biological activities[24]. Anthracyclines are glycoside antibiotics whose aglycones are called anthracyclinones[30]. They are aromatic type II polyketides that feature a linear tetracyclic 7,8,9,10-tetrahydro-5,12-naphthacenequinone scaffold and are decorated with one or more sugar moieties anthracyclinones[30]. Anthracyclines are especially renowned for their potent anticancer activities[266]. The best-known members of this group, daunorubicin (**5**) and doxorubicin (**6**), are natural products of *Streptomyces peucetius* var. *caesius*[8–10]. Daunorubicin (**5**) and doxorubicin (**6**) are glycosides of the amino sugar L-daunosamine (highlighted in orange in Figure 1A). These compounds have demonstrated exceptional efficacy against acute leukaemia and various types of solid tumours[11,12]. Despite their clinical successes, the application of the drugs is limited by serious side effects, such as cardiotoxicity, therapy-related tumours and infertility[13].

Anthracyclines have long been recognised as topoisomerase II inhibitors that induce DNA double-strand breaks[92]. However, a secondary effect of anthracyclines was recently discovered: the eviction of histones, which results in chromatin damage[14,15]. Notably, anthracyclines that trigger both, DNA double-strand breaks and histone eviction, are associated with cardiotoxicity, one of the major side effects of anthracycline drugs[14,16]. A screening of chemically synthesised doxorubicin derivatives resulted in a set of compounds with improved activities compared to doxorubicin[16–19]. Particularly, *N,N*-dimethylation of the amino sugar moiety results in the loss of DNA damage activity. *N,N*-dimethyldaunorubicin (**11**, Figure 1A) and *N,N*-dimethyldoxorubicin (**12**, Figure 1A) exhibit histone eviction activity without causing DNA damage, making them promising alternatives for anticancer treatment with reduced risk of cardiotoxicity[16–19].

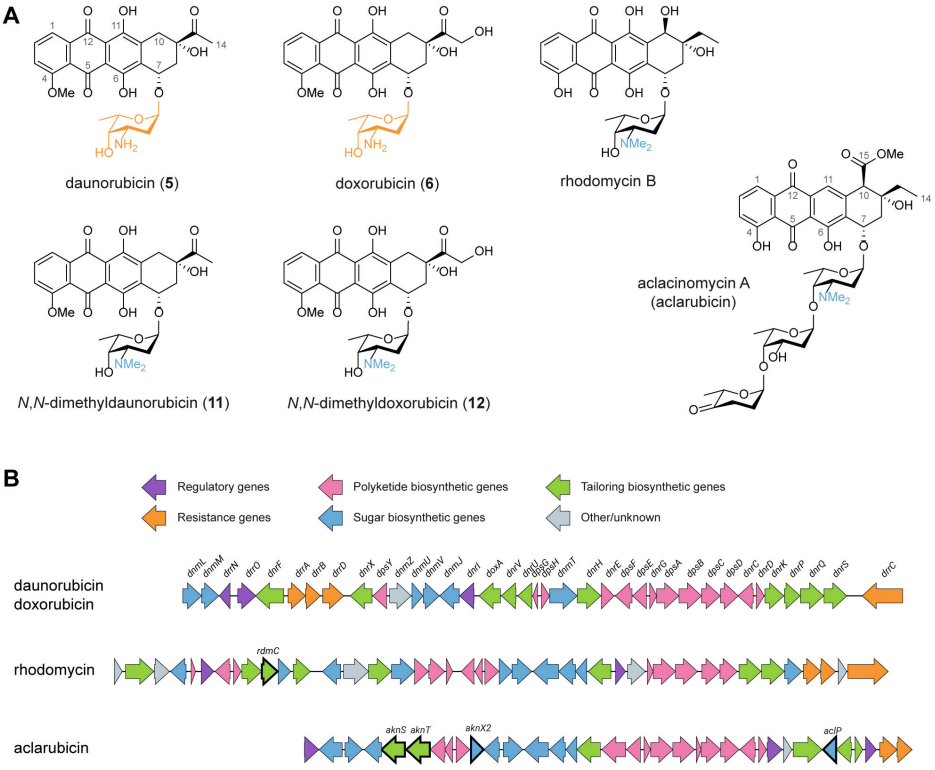


Figure 1. Chemical structures and BGCs of anthracyclines described in this work. (A) Chemical structures of daunorubicin, doxorubicin, *N*,*N*-dimethyldaunorubicin (**11**), *N*,*N*-dimethyldoxorubicin (**12**), rhodomycin B and aclacinomycin A (aclarubicin). **(B)** The BGCs of daunorubicin/doxorubicin, rhodomycin and aclarubicin were aligned and visualised using clinker[290]. To achieve biosynthesis of *N*,*N*-dimethyldaunorubicin (**11**) and *N*,*N*-dimethyldoxorubicin (**12**), several genes from the rhodomycin and aclarubicin BGCs were introduced to *S. peucetius*, as highlighted in bold.

To achieve a sustainable and efficient production process for *N*,*N*-dimethyldaunorubicin (**11**) and *N*,*N*-dimethyldoxorubicin (**12**), biosynthesis presents a compelling alternative to chemical synthesis. Therefore, the aim of this work is to establish a biosynthetic production pathway for *N*,*N*-dimethyldaunorubicin (**11**) and *N*,*N*-dimethyldoxorubicin (**12**) in *S. peucetius*. Although *N*,*N*-dimethylated daunorubicin or doxorubicin have never been isolated from natural sources, the *N*,*N*-dimethylated amino sugar L-rhodosamine commonly occurs in natural anthracyclines, such as aclacinomycins (Figure 1A), rhodomycins (Figure 1A), cosmomycins, and cytorhodins[104]. Therefore, the doxorubicin biosynthetic pathway could potentially be modified for production of *N*,*N*-dimethyldaunorubicin (**11**) and *N*,*N*-dimethyldoxorubicin (**12**) by heterologous expression of genes from other anthracycline biosynthetic gene clusters (BGCs, Figure 1B).

Anthracycline biosynthetic pathways are generally divided into three stages: (amino) sugar biosynthesis, polyketide biosynthesis to generate the aglycone, followed by several tailoring steps of the aglycone including glycosylation[104]. Heterologous expression of genes from various

anthracycline BGCs has previously been applied successfully as strategy for the biosynthesis of new anthracyclines[105,266]. For the biosynthesis of *N,N*-dimethylated daunorubicin and doxorubicin, the native doxorubicin biosynthetic pathway should be modified in three steps: (Step 1) *N,N*-dimethylation of TDP-L-daunosamine to TDP-L-rhodosamine, (Step 2) glycosylation of the anthracyclinone ε-rhodomycinone with L-rhodosamine instead of L-daunosamine, and (Step 3) further tailoring steps to achieve full conversion of the aglycone toward *N,N*-dimethyldoxorubicin (**12**) (Figure 2).

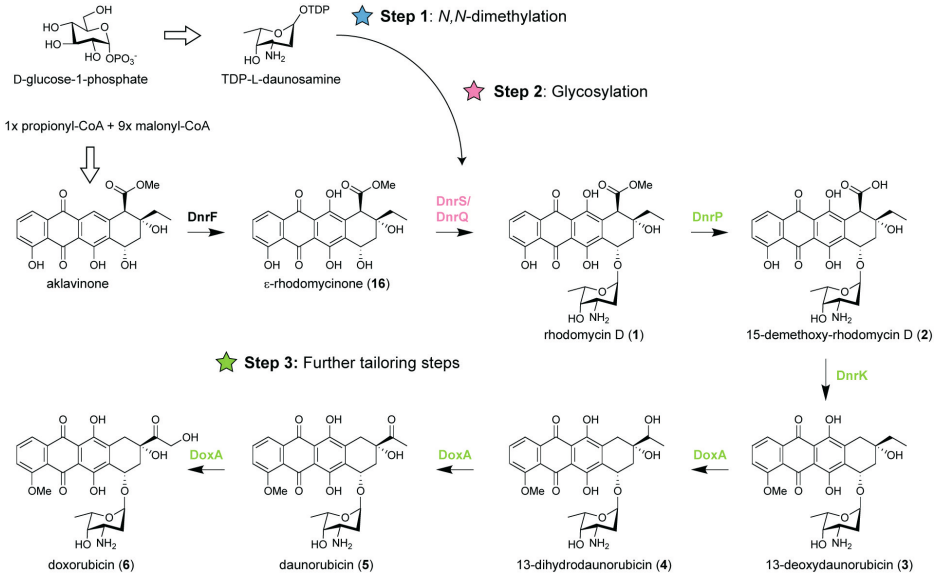


Figure 2. Biosynthetic pathway of doxorubicin and modifications required for biosynthesis of *N,N*-dimethylated daunorubicin and doxorubicin. Doxorubicin biosynthesis occurs in three stages: biosynthesis of TDP-L-daunosamine from D-glucose-1-phosphate, biosynthesis of ε-rhodomycinone (**16**) from one propionyl-CoA and nine malonyl-CoA units, followed by tailoring steps of the aglycone. For biosynthesis of *N,N*-dimethylated daunorubicin and doxorubicin, the pathway should be modified in three steps: (1) *N,N*-dimethylation of TDP-L-daunosamine to TDP-L-rhodosamine, (2) glycosylation of ε-rhodomycinone (**16**) with L-rhodosamine instead of L-daunosamine, and (3) the further tailoring steps should be performed when L-rhodosamine is attached.

For Step 1, a methyltransferase could be introduced to catalyse the conversion of TDP-L-daunosamine to TDP-L-rhodosamine. The enzymatic synthesis of TDP-L-rhodosamine occurs via an *S*-adenosyl-L-methionine (SAM)-dependent *N*-methyltransferase[131]. The aclarubicin biosynthetic pathway of *Streptomyces galilaeus* contains the AclP and AknX2 *N*-methyltransferases[130], which are both required for *N,N*-dimethylation of TDP-L-daunosamine[231]. For Step 2, a glycosyltransferase is required to attach rhodosamine to ε-rhodomycinone. Glycosyltransferases are well-described as promiscuous enzymes that can accept a wide range of substrates[105]. The native glycosyltransferase DnrS may be able to glycosylate with rhodosamine but may also favour daunosamine. Alternatively, glycosyltransferases of the aclarubicin and rhodomycin biosynthetic pathway could be heterologously expressed. The final challenge (Step 3) involves

further tailoring reactions catalysed by the 15-methyleserase DnrP, 4-*O*-methyltransferase DnrK, and cytochrome P450 monooxygenase DoxA[267]. An alternative for DnrP may be found in the rhodomycin pathway of *Streptomyces purpurascens*. RdmC is a homologue of DnrP that natively accepts ε-rhodomycin T (**7**) as substrate, which harbours the *N,N*-dimethylated amino sugar moiety[160]. The following enzyme DnrK catalyses 4-*O*-methylation as well as moonlighting activity 10-decarboxylation, which is a unique feature among the characterised anthracycline methyltransferases[121,160]. The final enzyme DoxA is also unique to the doxorubicin pathway, where the conversion from daunorubicin (**5**) to doxorubicin (**6**) is notably inefficient[153,254].

To achieve optimal production results, an industrial *S. peucetius* strain optimised for doxorubicin production was used as background strain. G001 is an industrial strain derived from *S. peucetius* by *N*-methyl-*N'*-nitro-*N*-nitrosoguanidine (NTG) mutagenesis[268]. Compared to wild-type *S. peucetius*, the industrial strain produces more than hundred times more daunorubicin (**5**) and doxorubicin (**6**), which makes it an appropriate choice as parental strain for the engineering efforts. Here we present the outcomes of the genetic engineering strategies applied to biosynthetically produce *N,N*-dimethyldaunorubicin (**11**) and *N,N*-dimethyldoxorubicin (**12**). The results indicate that *N,N*-dimethyldaunorubicin (**11**) can be produced by combinatorial biosynthesis. However, further optimisation of DoxA is crucial to enhance the production titres of *N,N*-dimethyldaunorubicin (**11**) and achieve biosynthesis of *N,N*-dimethyldoxorubicin (**12**).

Results

Attachment of L-rhodosamine to ε-rhodomycinone via heterologous expression of aclarubicin sugar *N*-methyltransferases and glycosyltransferases

The first challenge in the biosynthetic production of *N,N*-dimethyldaunorubicin (**11**) and *N,N*-dimethyldoxorubicin (**12**) is to provide the *N,N*-dimethylated amino sugar L-rhodosamine that cannot be naturally biosynthesised by *S. peucetius*. L-Rhodosamine occurs in various natural anthracyclines, such as aclarubicin and rhodomycin B (Figure 1A). The aclarubicin biosynthetic pathway of *S. galilaeus* features two *N*-methyltransferases, AclP and AknX2, which can catalyse the conversion of the activated amino sugar TDP-L-daunosamine to TDP-L-rhodosamine (Step 1, Figure 3C). Additionally, the aclarubicin biosynthetic pathway contains the glycosyltransferase/auxiliary protein pair AknS and AknT, which normally catalyse the glycosylation of aklavinone with rhodosamine to yield aclacinomycin T (**14**). However, the doxorubicin biosynthetic pathway differs from the aclarubicin pathway by the presence of DnrF, which catalyses the 11-hydroxylation of aklavinone to ε-rhodomycinone (**16**) before glycosylation (Figure 3C). If AknS/AknT would be able to glycosylate ε-rhodomycinone (**16**) with rhodosamine, it would result in the production of ε-rhodomycin T (**7**) (Step 2).

The construct pRDS[231] harbours the methyltransferase genes *aclP* and *aknX2* and the glycosyltransferase genes *aknS* and *aknT* from *S. galilaeus,* and genes for the biosynthesis of

TDP-L-rhodosamine from *S. peucetius* and *Streptomyces venezuelae*. This construct is a derivative of pWHM3[269], an unstable multicopy vector that harbours a thiostrepton cassette (Supplementary Figure S1). pRDS was introduced into G001 via protoplast transformation, resulting in strain MAG301. The recombinant strain harbours all the genes for the enzymes required for both Step 1 and Step 2 (Figure 3A). To evaluate the effect of introducing pRDS on the metabolite profile, both G001 and MAG301 were cultivated in E1 medium[270] with added HP20 resin.

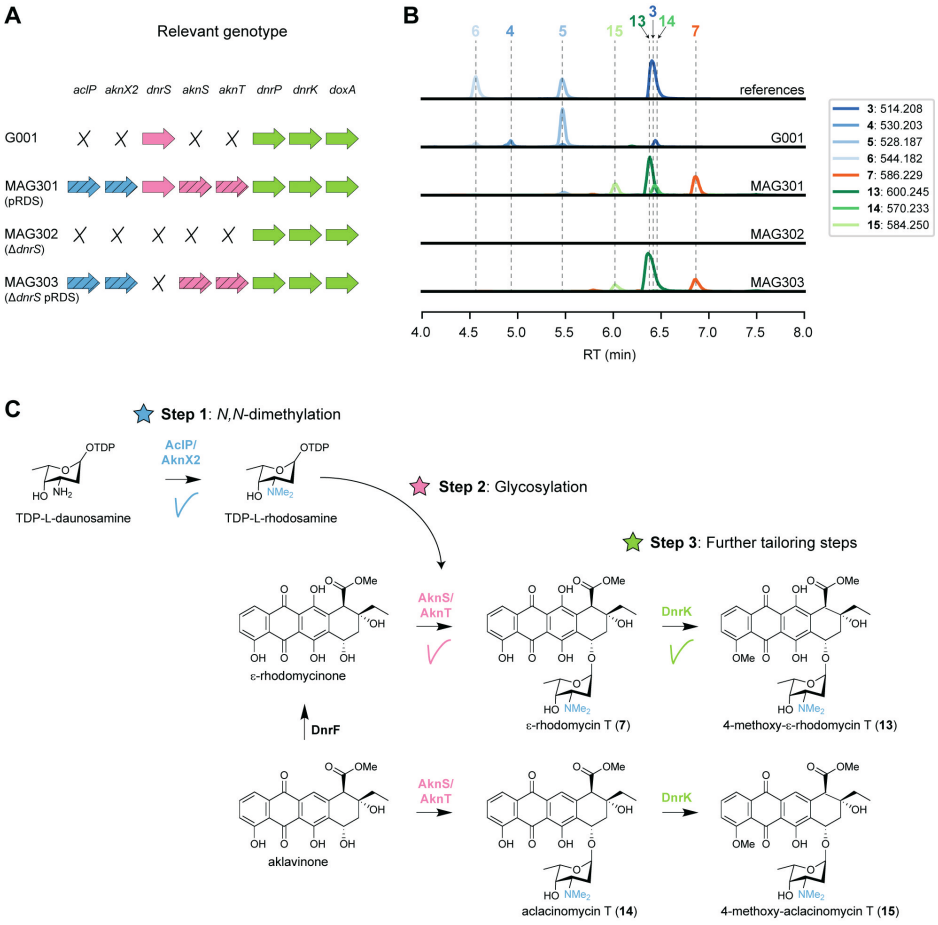


Figure 3. Expression of aclarubicin methyltransferases and glycosyltransferases genes in G001 results in the attachment of L-rhodosamine to ε-rhodomycinone. (A) Schematic representation of the relevant genotype of the strains used in this experiment, with heterologous genes indicated by a diagonal striped pattern. **(B)** LC-MS analysis of crude extracts of G001, MAG301, MAG302 and MAG303 cultivated in E1 medium. Extracted ion chromatograms showing the mass peaks $[M+H]^+$ of compounds **3**–**7** and **13**–**15**. **(C)** Schematic representation of the engineered doxorubicin pathway. Introduction of the *N*-methyltransferases (*aclP/aknX2*) and glycosyl transferases (*aknS/aknT*) genes from the aclarubicin BGC resulted in incorporation of L-rhodosamine onto ε-rhodomycinone (**16**), forming ε-rhodomycin T (**7**). ε-Rhodomycin T (**7**) was converted to 4-methoxy-ε-rhodomycin T (**13**) by DnrK. Additionally, a minor mass peak of daunorubicin (**5**) was detected in MAG301, which was completely abolished in MAG303 where the native glycosyltransferase gene *dnrS* was deleted.

The resin binds the anthracyclines, thereby preventing product inhibition and toxicity. After 4 days of incubation at 30 °C, metabolites were extracted using acetone, dried, re-dissolved in 80% acetonitrile and analysed using liquid chromatography-mass spectrometry (LC-MS). The LC-MS data were processed using MZmine, resulting in a list containing all the mass features and their peak areas detected in each crude extract. In cases where reference compounds were unavailable, annotation was based on the predicted *m/z* values of the $[M+H]^+$ adduct ions and expected fragmentation patterns (Supplementary Table S3).

The LC-MS chromatograms of G001 and MAG301 (G001 pRDS) exhibited distinctly different mass peaks (Figure 3B). The main peak observed in the chromatogram of G001 corresponded to daunorubicin (**5**), and a smaller peak was annotated as doxorubicin (**6**). Furthermore, minor peaks were annotated as the precursors 13-deoxydaunorubicin (**3**) and 13-dihydrodaunorubicin (**4**), respectively (Figure 3B). The introduction of pRDS to G001 (MAG301) resulted in a shift in the metabolite profile (Figure 3B). The main mass peaks detected in the LC-MS chromatogram of MAG301 were annotated as to ε-rhodomycin T (**7**) and 4-methoxy-ε-rhodomycin T (**13**). These results indicate that ε-rhodomycinone (**16**) was successfully glycosylated with rhodosamine, yielding ε-rhodomycin T (**7**) (Figure 3C). The main peak corresponding to 4-methoxy-ε-rhodomycin T (**13**) indicated that 4-*O*-methylation activity was successful, but 10-decarboxylation and the final hydroxylation steps were unsuccessful. In the native doxorubicin pathway, DnrP catalyses 15-methylesterase activity of rhodomycin D (**1**), and subsequently DnrK catalyses 10-decarboxylation. The accumulation of 4-methoxy-ε-rhodomycin T (**13**) in the engineered pathway suggested that DnrP cannot catalyse 15-methylesterase activity of ε-rhodomycin T (**7**) or 4-methoxy-ε-rhodomycin T (**13**).

Furthermore, minor peaks were observed in the chromatogram of MAG301, which were annotated as aclacinomycin T (**14**) and 4-methoxy-aclacinomycin T (**15**), respectively (Figure 3C). The presence of these compounds suggests that 11-hydroxylation of aklavinone to ε-rhodomycinone (**16**) by DnrF was not complete. All in all, the expression of sugar *N*-methyltransferases and glycosyltransferases of the aclarubicin biosynthetic pathway resulted in the incorporation of rhodosamine onto ε-rhodomycinone (**16**) (Figure 3C). However, optimisation of the further tailoring reactions toward *N,N*-dimethyldoxorubicin (**12**) are required.

Deletion of the native glycosyltransferase gene *dnrS*

The chromatogram of MAG301 also contained a minor mass peak that corresponds to daunorubicin (**5**), indicating partial glycosylation of ε-rhodomycinone (**16**) with daunosamine rather than with rhodosamine (Figure 3B). The native doxorubicin glycosyltransferase DnrS may prefer TDP-L-daunosamine over TDP-L-rhodosamine, which could explain the observed by-products. To address this hypothesis, the native glycosyltransferase gene *dnrS* within the doxorubicin BGC was deleted (Figure 3A).

A deletion mutant of *dnrS* was created using a method published previously[271], which is based on the unstable multicopy plasmid pWHM3[269]. A knock-out construct was generated

that harbours the about 1 kb regions upstream and downstream of *dnrS* interspaced by the apramycin resistance gene *aacC4* flanked by *loxP* recognition sites (pGWS1431, Supplementary Figure S1). The knock-out construct was introduced to G001 via protoplast transformation. The presence of the *loxP* recognition sites allowed the efficient removal of the apramycin resistance cassette by introduction of the pUWLCRE construct for expression of the Cre recombinase[272]. Consequently, we obtained a mutant where the entire coding region of *dnrS* was deleted, which is designated MAG302 (Figure 3A).

MAG302 (G001 Δ*dnrS*) was cultivated in E1 medium, and the metabolite profile was analysed in a similar manner as described above. As expected, no glycosylated anthracyclinones could be detected in the LC-MS chromatogram of MAG302 (Figure 3B). The main peak in the chromatogram of MAG302 corresponded to ε-rhodomycinone (**16**) (Supplementary Figure S3). Subsequently, pRDS was introduced into MAG302 via protoplast transformation to generate MAG303 (Figure 3A). In contrast to MAG301, MAG303 harbours only the aclarubicin glycosyltransferases, but not the doxorubicin glycosyltransferase. MAG303 (G001 Δ*dnrS* pRDS) was cultivated in E1 medium, and the metabolite profile was analysed in a similar manner as described above. Notably, the production of daunorubicin (**5**) was completely abolished in MAG303 (Figure 3B). When solely aclarubicin glycosyltransferases are present, ε-rhodomycinone (**16**) undergoes glycosylation exclusively with rhodosamine instead of daunosamine. These results indicate that the deletion of *dnrS* successfully directed the pathway toward glycosylation with rhodosamine.

Heterologous expression of *rdmC* enables *N,N*-dimethyldaunorubicin biosynthesis

After successful sugar *N*-methylation (Step 1) and glycosylation (Step 2), the next bottleneck in the *N,N*-dimethyldoxorubicin biosynthetic pathway lies in the downstream tailoring reactions (Step 3). The production of 4-methoxy-ε-rhodomycin T (**13**) indicated that DnrP could not catalyse 15-methylesterase activity of *N,N*-dimethylated substrates. Consequently, we searched for an alternative enzyme with 15-methylesterase activity of ε-rhodomycin T (**7**).

In *S. purpurascens*, the rhodomycin biosynthetic pathway harbours the enzyme RdmC, a homologue of DnrP, which accepts ε-rhodomycin T (**7**) as substrate[160]. The coding region of *rdmC* was positioned behind the constitutive *ermE** promoter[273], and cloned into the integrative vector pSET152[274], resulting in pGWS1432 (Supplementary Figure S1). The construct was introduced to MAG303 via conjugation, resulting in strain MAG304. The resulting strain harbours the methyltransferases and glycosyltransferases genes from the aclarubicin BGC (on pRDS), the methylesterase gene *rdmC* from the rhodomycin BGC (on pGWS1432), and a deletion of the native glycosyltransferase (*dnrS*) (Figure 4A). MAG304 (G001 Δ*dnrS* pRDS +*rdmC*) was cultivated in E1 medium, and the metabolite profile was analysed in a similar manner as described above. The main peak observed in the chromatogram of MAG304 was annotated as *N,N*-dimethyl-13-deoxydaunorubicin (**9**), and a smaller peak as *N,N*-dimethyl-13-dihydrodaunorubicin (**10**). Remarkably, a minor peak was annotated as *N,N*-dimethyldaunorubicin (**11**), which is one of the targeted products (Figure 4B). Additionally, the production of ε-rhodomycin T (**7**), 4-methoxy-

ε-rhodomycin T (**13**), aclacinomycin T (**14**) and 4-methoxy-aclacinomycin T (**15**) was abolished (Figure 4B). The metabolite profile of MAG304 indicated successful replacement of DnrP by RdmC. The 15-methylesterase activity of RdmC is essential for the 10-decarboxylation moonlighting activity of DnrK, thus enabling the production of *N,N*-dimethyl-13-deoxydaunorubicin (**9**). The final three steps from *N,N*-dimethyl-13-deoxydaunorubicin (**9**) to *N,N*-dimethyldoxorubicin (**12**) are catalysed by the cytochrome P450 monooxygenase DoxA (Figure 4C). For G001, the main peak in the chromatogram corresponds to daunorubicin (**5**), which indicates that the final 14-hydroxylation step toward doxorubicin (**6**) is inefficient, while the two 13-hydroxylation steps catalysed by DoxA exhibit high efficiency. In contrast, for MAG304, the main peak corresponds to *N,N*-dimethyl-13-deoxydaunorubicin (**9**), indicating that all steps catalysed by DoxA are inefficient when the compounds are *N,N*-dimethylated.

Taken together, introduction of *rdmC* into the engineered G001 strain proved to be a successful strategy to achieve 10-decarboxylation of ε-rhodomycin T (**7**). Combined activity of RdmC and DnrK resulted in the production of *N,N*-dimethyldaunorubicin (**11**). The accumulation of the precursor *N,N*-dimethyl-13-deoxydaunorubicin (**9**) indicates that the next bottleneck in the engineered pathway is the final enzyme DoxA.

To enable further genetic engineering, the genes located on pRDS and pGWS1432 were combined on a single integrative vector. For this, the coding region of *rdmC* with an engineered R15 ribosomal binding site[275] and L3S1P47 terminator[276] was amplified by PCR. The *aclP* coding region was amplified by PCR from pRDS. The two fragments were introduced into EcoRI-digested pSET152[274]. The entire DNA fragment containing *aknT-aknS-desIII-desIV-dpsG-dpsH-dnmT-dnmZ-dnmU* was excised from pRDS and cloned into *aclP-rdmC*::pSET152 to generate pGWS1433-v1. Illumina sequencing of pRDS indicated the presence of an EcoRI site in the intergenic region between *aclP* and *aknX2* (Supplementary Figure S1). Consequently, our cloning strategy resulting in the loss of a fragment of 70 bp from the construct, which we then re-introduced. For this, the *dnmU-dnmV-dnmJ-aknX2* region was amplified from pRDS, including the missing sequence at the end of *aknX2*. The *aclP-rdmC* region was amplified by PCR from pGWS1433-v1. The two fragments were cloned into BamHI-linearised pGWS1433-v1 via Gibson assembly[277], resulting in pGWS1433 (Supplementary Figure S1). The correct sequence of the whole construct was confirmed by Sanger sequencing. The resulting construct was introduced to MAG302 (G001 Δ*dnrS*) via conjugation to generate MAG305 (Figure 4A). MAG304 and MAG305 harbour the same heterologous genes. However, in the case of MAG305, all the heterologous genes are located on pSET152, whereas in the case of MAG304 all heterologous genes are located on pRDS, except for *rdmC* which is located on pSET152.

MAG305 was cultivated in E1 medium, and the metabolite profile was analysed and annotated in a similar manner as described above. Similar as for MAG304, the main peak in the chromatogram of MAG305 corresponded to *N,N*-dimethyl-13-deoxydaunorubicin (**9**), while *N,N*-dimethyldoxorubicin (**12**) could not be detected (Figure 4B), indicating that this strain could be use for further engineering.

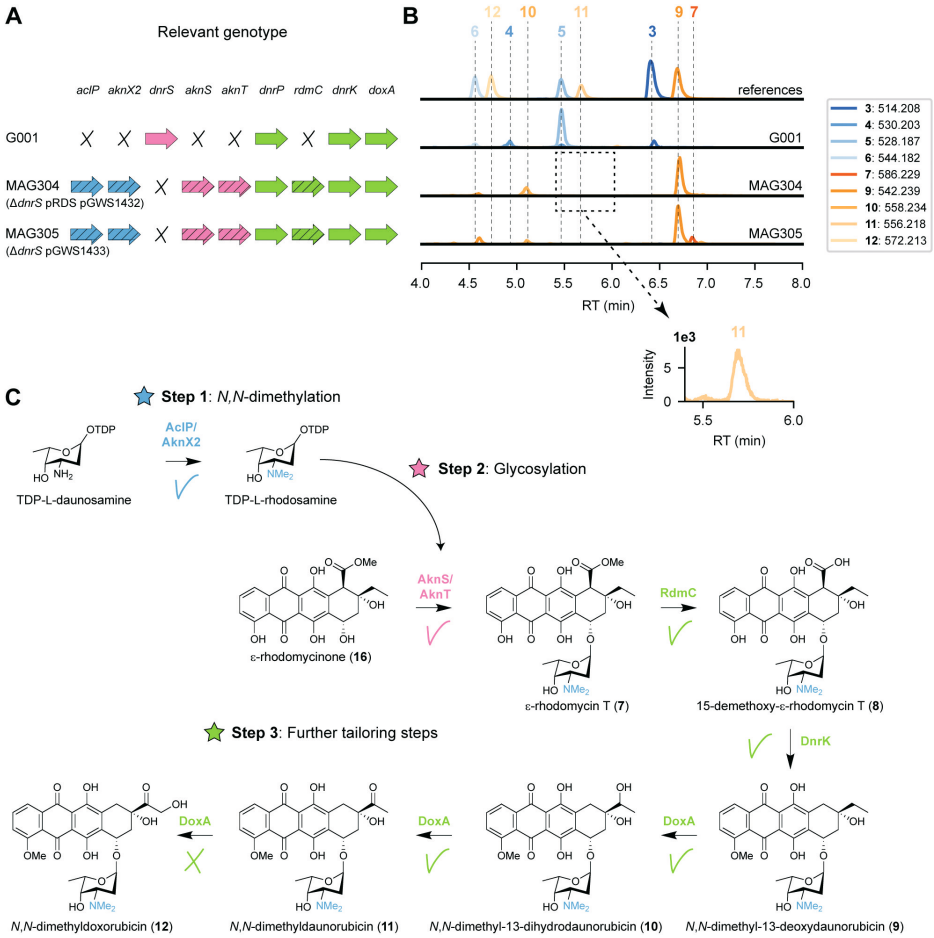


Figure 4. Expression of rhodomycin methylesterase gene in G001 results in the production of *N,N*-dimethyldaunorubicin. (A) Schematic representation of the relevant genotype of the strains used in this experiment, with heterologous genes indicated by a diagonal striped pattern. **(B)** LC-MS analysis of crude extracts of G001, MAG304 and MAG305 cultivated in E1 medium. Extracted ion chromatograms showing the mass peaks $[M+H]^+$ of compounds **3**–**7** and **9**–**12**. **(C)** Schematic representation of the proposed biosynthetic pathway for *N,N*-dimethyldoxorubicin (**12**). Introduction of the 15-methylesterase gene *rdmC* from the rhodomycin BGC resulted in the production of *N,N*-dimethyl-13-deoxydaunorubicin (**9**) and *N,N*-dimethyl-13-dihydrodaunorubicin (**10**). A minor peak was detected for *N,N*-dimethyldaunorubicin (**11**), but *N,N*-dimethyldoxorubicin (**12**) could not be detected.

DoxA is the bottleneck for biosynthesis of *N,N*-dimethyldoxorubicin

Heterologous expression of enzymes from the aclarubicin and rhodomycin pathways to G001 resulted in the biosynthesis of *N,N*-dimethyldaunorubicin (**11**). The results indicated that the bottleneck in the engineered biosynthetic pathway are the final three tailoring steps catalysed by DoxA. It is worth noting that the final 14-hydroxylation step catalysed by DoxA is notably inefficient in the doxorubicin biosynthetic pathway[254]. In fact, enzyme kinetic experiments

revealed that the catalytic constant V_{max} is 520-fold lower for the conversion of daunorubicin (**5**) to doxorubicin (**6**) compared to the preceding step[153].

Abundance of DoxA

Quantitative proteomics was performed to analyse the abundance of DoxA in the engineered strain MAG304. The strain was cultivated in E1 medium, and biomass was collected after 2, 3 and 4 days (*n*=3). In all samples, at least one peptide was detected that could be connected to DoxA. The abundance of all proteins was quantified via LFQ analysis, which provides a normalised concentration based on the presence of at least two peptide sequences for each protein. In 4 days-old-cultures only one peptide could be connected to DoxA, which is below the threshold. In the samples from 2 and 3 days-old-cultures, the abundance of DoxA was higher than 30% and 29% of other detected proteins (*n*=3), respectively (Figure 5A). The results suggest that the abundance of DoxA is not likely the limiting factor for its activity (see Discussion).

Heterologous expression of *doxA*

DoxA catalyses multi-step oxidation reactions on different carbon atoms (Figure 2). The oxidation reactions catalysed by DoxA are a unique feature of the doxorubicin pathway that is not found for other anthracyclines. To our knowledge, no DoxA homologue is known to accept *N,N*-dimethylated substrates. However, it may be possible to find an alternative DoxA enzyme with improved activity. All known members of the DoxA family originate from daunorubicin or doxorubicin producers, namely *S. peucetius* ATCC 27952, *S. peucetius* ATCC 29050, *Streptomyces* sp. C5 and *Streptomyces coeruleorubidus*. A BLASTP search with *S. peucetius* DoxA also indicated that the genome of *S. bellus* also encodes a closely related DoxA enzyme (Supplementary Figure S4). The DoxA enzymes of *S. peucetius* ATCC 27952 and ATCC 29050 are identical. The DoxA enzymes of *Streptomyces* sp. C5, *S. coeruleorubidus* and *S. bellus* share 95.0%, 99.3% and 99.3% identity with *S. peucetius* DoxA, respectively. We decided to express the *S. bellus* and *S. coeruleorubidus doxA* genes each individually in the engineered strain MAG304.

The coding sequences of *S. peucetius*, *S. bellus* and *S. coeruleorubidus doxA* were codon-optimised based on the native codon preference of *Streptomyces coelicolor*. To optimise expression of the *doxA* genes, the respective coding sequences were positioned behind the strong *gapdh* promoter P7[275] and the helicase ribosomal binding site R9 from bacteriophage φC31[275], while the *aph* terminator[278] was positioned behind the genes. The DNA fragments were synthesised and cloned into pMS82[279] using EcoRV to generate pGWS1434 (*doxA*-1 of *S. peucetius*), pGWS1435 (*doxA*-2 of *S. bellus*), and pGWS1436 (*doxA*-3 of *S. coeruleorubidus*). The constructs (Supplementary Figure S1) were conjugated into MAG304 to generate MAG306 (*doxA*-1), MAG307 (*doxA*-2) and MAG308 (*doxA*-3).

The strains were cultivated in E1 medium, and the metabolite profile was analysed and annotated in a similar manner as described above. For all strains, the main peak in the chromatograms corresponded to *N,N*-dimethyl-13-deoxydaunorubicin (**9**), while *N,N*-dimethyldoxorubicin (**12**)

could not be detected (Figure 5B). The expression of heterologous and codon-optimised *doxA* genes did not affect the metabolite profile of the engineered strain. The results suggest that the alternative DoxA enzymes have similar activity as *S. peucetius* DoxA.

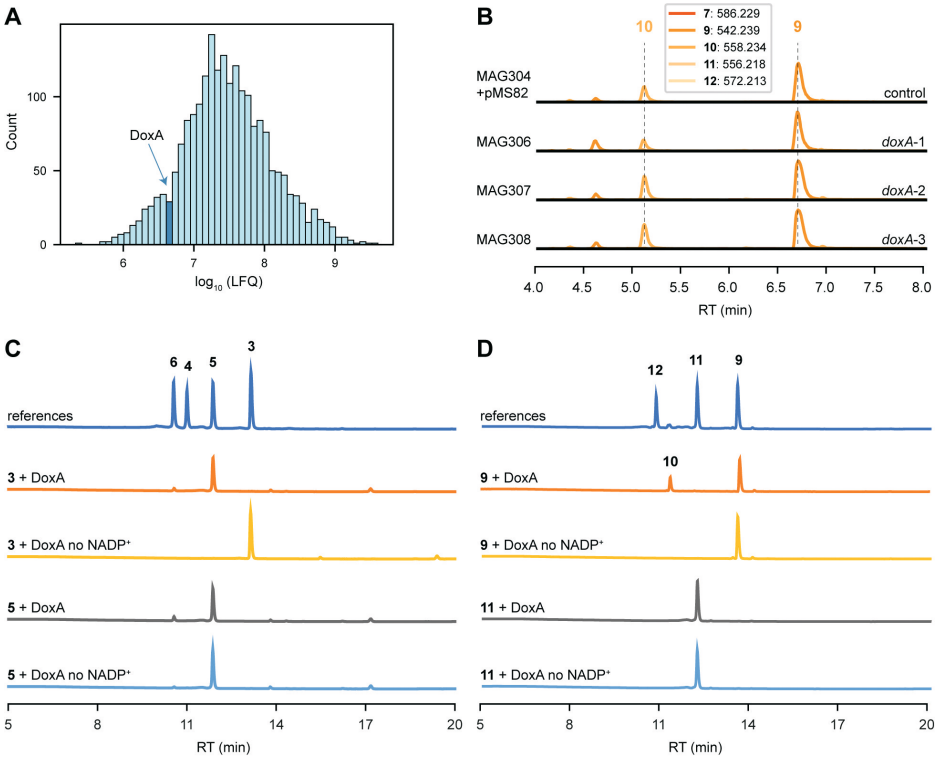


Figure 5. DoxA is the bottleneck for biosynthesis of *N,N*-dimethyldoxorubicin. (A) MS-based quantitative proteomics analysis of MAG304 cultivated in E1 medium for 3 days. Histogram showing distribution of the relative intensity level (log_{10} LFQ) of all detected proteins (n=3). The bar that includes the abundance of DoxA is highlighted. **(B)** LC-MS analysis of crude extracts of MAG304 pMS82, MAG306 (*doxA*-1), MAG307 (*doxA*-2) and MAG308 (*doxA*-3) cultivated in E1 medium. Extracted ion chromatograms showing the mass peaks $[M+H]^+$ of compounds **7**–**12**. For all strains, the main peak corresponded to *N,N*-dimethyl-13-deoxydaunorubicin (**9**), and *N,N*-dimethyldoxorubicin (**12**) could not be detected. **(C)** HPLC analysis of DoxA enzymatic assays. UV-Vis chromatogram traces were recorded at 490 nm. A reaction mixture without the addition of $NADP^+$ was used as the negative control. The activity of DoxA with the natural substrates 13-deoxydaunorubicin (**3**) and daunorubicin (**5**). **(D)** The activity of DoxA with *N,N*-dimethyl substrates *N,N*-dimethyl-13-deoxydaunorubicin (**9**) and *N,N*-dimethyldaunorubicin (**11**).

Enzymatic assays with DoxA

To evaluate the ability of DoxA to catalyse oxidation reactions on different substrates, *in vitro* enzyme activity was tested using the natural substrates 13-deoxydaunorubicin (**3**) and daunorubicin (**5**), and their *N,N*-dimethylated derivatives. HPLC analysis of the reaction products revealed that DoxA effectively converted 13-deoxydaunorubicin (**3**) to both daunorubicin (**5**) and doxorubicin (**6**), with daunorubicin (**5**) being the predominant product. The reaction with

daunorubicin (**5**) only resulted in a minor conversion to doxorubicin (**6**) (Figure 5C). These results are consistent with *in vivo* findings, where cultivation of G001 primarily yields daunorubicin (**5**) with minor amounts of doxorubicin (**6**).

In contrast, when *N,N*-dimethyl-13-deoxydaunorubicin (**9**) was utilised as substrate, DoxA exclusively catalysed the reaction toward *N,N*-dimethyl-13-dihydrodaunorubicin (**10**), and the conversion was found to be incomplete (Figure 5D). DoxA did not exhibit catalytic activity toward *N,N*-dimethyldaunorubicin (**11**) (Figure 5D). LC-MS analysis of the reaction product confirmed that no *N,N*-dimethyldoxorubicin (**12**) could be detected (Supplementary Figure S22). These results also align with *in vivo* findings, where engineered G001 strains, such as MAG304, accumulate *N,N*-dimethyl-13-deoxydaunorubicin (**9**) and *N,N*-dimethyl-13-dihydrodaunorubicin (**10**) with trace amounts of *N,N*-dimethyldaunorubicin (**11**). The results suggest that the activity of DoxA with *N,N*-dimethylated substrates likely represents a limiting factor in the biosynthesis of *N,N*-dimethylated anthracyclines (see Discussion).

N,N-dimethyldoxorubicin is toxic to the producer strain

During the construction of the engineered G001 strains, we noticed that the development of the strains was blocked, most likely caused by the production of cytotoxic anthracyclines. On SFM agar plates, G001 and MAG301 (G001 pRDS) exhibited a distinctive 'bald' phenotype, characterised by the absence of aerial hyphae and spores (Figure 6A). Notably, the deletion of the glycosyltransferase gene *dnrS* (MAG302) led to in the production of white aerial hyphae. However, upon introduction of the aclarubicin glycosyltransferase and methyltransferase genes (MAG303) the strain reverted to the 'bald' phenotype without aerial hyphae production. The introduction of the methylesterase gene *rdmC* (MAG304) further crippled the strain, evident by the reduction in colony size. We hypothesised that product toxicity could inhibit the development of the strains and consequently impact productivity. Therefore, we conducted a microbial inhibition assay involving doxorubicin, *N,N*-dimethyldoxorubicin (**12**) and two precursors.

To investigate the resistance of G001, 5 µL of mycelium stock was spotted at a concentration of $1.0 \cdot 10^4$ CFU per spot on SFM agar plates with increasing concentration of 13-deoxydaunorubicin (**3**), doxorubicin (**6**), *N,N*-dimethyl-13-deoxydaunorubicin (**9**) or *N,N*-dimethyldoxorubicin (**12**). After 3 days of incubation at 30 °C, growth was examined visually. Surprisingly, G001 exhibited no growth at 5 $\mu g \cdot mL^{-1}$ *N,N*-dimethyldoxorubicin (**12**), whereas its growth was uninhibited at 25 $\mu g \cdot mL^{-1}$ doxorubicin (Supplementary Figure S5). Furthermore, the main product of the engineered strain MAG304, *N,N*-dimethyl-13-deoxydaunorubicin (**9**), inhibited the growth of G001 at a concentration of 10 $\mu g \cdot mL^{-1}$, whereas no growth inhibition was observed when exposed to 25 $\mu g \cdot mL^{-1}$ 13-deoxydaunorubicin (**3**). These results suggest that the toxicity of the produced compounds may inhibit the biosynthesis of *N,N*-dimethylated anthracyclines.

The doxorubicin BGC harbours several resistance genes, including the ABC-transporter genes *drrA* and *drrB*. Overexpression of these transporter genes may alleviate the toxicity associated with *N,N*-dimethylated anthracyclines. The coding region of *drrA-drrB* was positioned downstream

of the constitutive *ermE** promoter[273], and cloned into the multicopy vector pWHM3-oriT to generate pGWS1437 (Supplementary Figure S1). pWHM3-oriT is a derivative of pWHM3[269] that harbours *oriT* to allow for its conjugative transfer[280]. Subsequently, pGWS1437 was introduced to MAG305 (G001 Δ*dnrS* pGWS1433), via conjugation, resulting in strain MAG309.

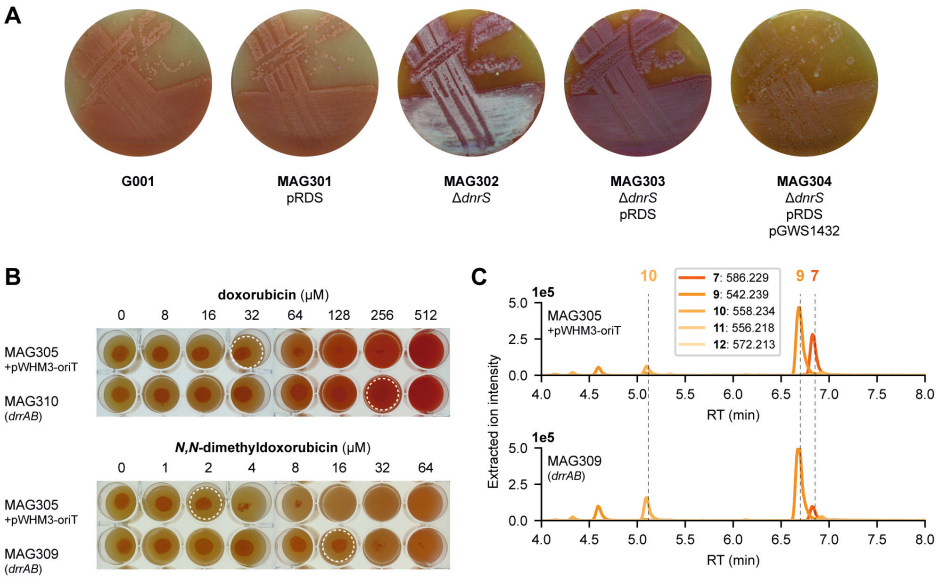


Figure 6. Toxicity of *N,N*-dimethyldoxorubicin. (A) G001, MAG301, MAG302, MAG303 and MAG304 were streaked on SFM agar plates (supplemented with 20 μg·mL^{-1} thiostrepton for strains harbouring pRDS). The development is blocked by the production of anthracyclines. MAG304 exhibited the most pronounced inhibition of development. In contrast, deletion of the glycosyltransferase gene *dnrS* in MAG302 stimulated development. **(B)** MAG305 pWHM3-oriT and MAG309 (*drrAB*) were spotted on SFM agar plates supplemented with increasing concentrations of doxorubicin (**6**) or *N,N*-dimethyldoxorubicin (**12**). For each strain, 5 μL of spore or mycelium stock was spotted at a concentration of 1.0·10^4 CFU per spot and the plates were incubated at 30 °C for 4 days. Dashed circles indicate the highest concentration that does not inhibit growth. For MAG305, the inhibitory concentration of *N,N*-dimethyldoxorubicin (**12**) is 16-fold lower than that of doxorubicin (**6**). Overexpression of *drrAB* increased resistance to both compounds eight-fold. **(C)** LC-MS analysis of crude extracts of MAG305 pWHM3-oriT and MAG309 (*drrAB*) cultivated in E1 medium. Extracted ion chromatograms showing the mass peaks [M+H]$^+$ of compounds **7**–**12**. Overexpression of *drrAB* resulted in a 3.7-fold increased production of *N,N*-dimethyldaunorubicin (**11**).

To investigate the resistance of MAG305 pWHM3-oriT and MAG309 (*drrAB*), 5 μL of mycelium stock was spotted at a concentration of 1.0·10^4 CFU per spot on SFM agar plates with increasing concentration of doxorubicin (**6**) or *N,N*-dimethyldoxorubicin (**12**). After 4 days of incubation at 30 °C, growth was examined visually. For MAG305, the inhibitory concentration of *N,N*-dimethyldoxorubicin was 16-fold lower than that of doxorubicin. Overexpression of the *drrAB* genes in MAG309 resulted in an eight-fold increase in resistance to both doxorubicin (32 to 256 μM) and *N,N*-dimethyldoxorubicin (2 to 16 μM) (Figure 6B). Although the resistance of MAG309 to *N,N*-dimethyldoxorubicin (16 μM) remained two-fold lower than that of the control strain to doxorubicin (32 μM), this enhanced resistance may increase *N,N*-dimethylated anthracycline

production. MAG305 pWHM3-oriT and MAG309 (*drrAB*) were cultivated in E1 medium, and the metabolite profile was analysed and annotated in a similar manner as described above. In both strains, the main peak in the chromatogram corresponded to *N,N*-dimethyl-13-deoxydaunorubicin (**9**), and *N,N*-dimethyldoxorubicin (**12**) could not be detected (Figure 6C). However, overexpression of *drrAB* resulted in a relative increase of 2.1-fold, 4.9-fold and 3.7-fold in the production of *N,N*-dimethyl-13-deoxydaunorubicin (**9**), *N,N*-dimethyl-13-dihydrodaunorubicin (**10**) and *N,N*-dimethyldaunorubicin (**11**), respectively (n=3). Additionally, the peak area of ε-rhodomycin T (**7**) was 1.3-fold decreased. These results indicate that the overexpression of *drrAB* pushed the reaction more toward *N,N*-dimethyldaunorubicin (**11**). However, it is important to note that the tailoring reactions catalysed by DoxA require optimisation for efficient biosynthesis of *N,N*-dimethyldaunorubicin (**11**) and *N,N*-dimethyldoxorubicin (**12**).

Discussion

The aim of this study was the biosynthesis of the two anthracyclines *N,N*-dimethyldaunorubicin (**11**) and *N,N*-dimethyldoxorubicin (**12**), because of their significant therapeutic potential[16,17]. To achieve this goal, a combinatorial engineering approach was adopted, involving the introduction of genes from the aclarubicin and rhodomycin BGCs into the industrial doxorubicin overproducer G001. This strategy successfully led to the biosynthesis of *N,N*-dimethyldaunorubicin (**11**). However, it resulted in low yields of *N,N*-dimethyldaunorubicin (**11**) with no detection of its downstream derivative *N,N*-dimethyldoxorubicin (**12**). Subsequent attempts to optimise the final tailoring reactions catalysed by the cytochrome P450 monooxygenase DoxA proved challenging.

Firstly, we introduced the genes encoding the sugar *N*-methyltransferases AclP and AknX2 and the glycosyltransferases AknS and AknT from the aclarubicin biosynthetic pathway into G001 using the multicopy plasmid pRDS[231]. Introduction of pRDS into G001 led to the successful incorporation of L-rhodosamine onto ε-rhodomycinone (**16**) (Figure 3). Subsequent deletion of the native glycosyltransferase gene *dnrS* abolished production of daunorubicin (**5**), a by-product in this context (Figure 3). Analysis of the produced metabolites revealed that the 15-methylesterase activity, catalysed by DnrP in the native doxorubicin pathway, did not occur in the engineered strain (Figure 3). Instead, ε-rhodomycin T (**7**) was directly 4-*O*-methylated by the moonlighting activity of DnrK[160], yielding 4-methoxy-ε-rhodomycin T (**13**). Furthermore, incomplete 11-hydroxylation activity by DnrF resulted in the by-products aclacinomycin T (**14**) and 4-*O*-methyl-aclacinomytin T (**15**).

Subsequently, we introduced the gene encoding the DnrP homolog RdmC from the rhodomycin biosynthetic pathway into the engineered strain. RdmC catalyses the conversion of ε-rhodomycin T (**7**) into 15-demethyl-ε-rhodomycin T (**8**) in the rhodomycin pathway[160]. Introduction of *rdmC* to the engineered strain resulted in the desired 15-demethylation activity, and subsequent 4-*O*-methylation and 10-carboxylation by DnrK (Figure 4). Notably, this resulted in the production of the targeted compounds, *N,N*-dimethyldaunorubicin (**11**). While the engineered strain

produced *N,N*-dimethyldaunorubicin (**11**), it was in limited quantities, and the final step toward *N,N*-dimethyldoxorubicin (**12**) was not achieved.

In the native doxorubicin pathway, the multistep conversion of 13-deoxydaunorubicin (**3**) to doxorubicin (**6**) is catalysed by DoxA. Notably, the conversion from daunorubicin (**5**) to doxorubicin (**6**) is more than 100-fold less efficient compared to the previous two steps[153]. Given the inherent inefficiency of the 14-hydroxylation, even with the natural substrate, it is not surprising that the corresponding 14-hydroxylation of the unnatural substrate *N,N*-dimethyldaunorubicin (**11**) is challenging. However, the accumulation of *N,N*-dimethyl-13-deoxydaunorubicin (**9**) and *N,N*-dimethyl-13-dihydrodaunorubicin (**10**) in the engineered strain is unexpected considering that the conversion to daunorubicin (**5**) is complete in the parental strain. Consequently, DoxA constitutes a potential bottleneck in the proposed biosynthetic pathway.

We confirmed that DoxA was expressed in significant quantities in the engineered strain. Quantitative proteomics demonstrated the abundance of DoxA in the engineered strain MAG304, suggesting that the protein level of DoxA is not a limiting factor (Figure 5A). In contrast to the previous engineering steps, no heterologous DoxA enzyme is known to accept *N,N*-dimethylated substrates. In fact, the DoxA enzyme is unique to the doxorubicin biosynthetic pathway. Nevertheless, we decided to express the genes encoding close DoxA homologs from *S. bellus* and *S. coeruleorubidus* in the engineered strain. Unsurprisingly, this effort did not result in improved productivity (Figure 5B).

To confirm that the activity of DoxA is a key bottleneck in the production of *N,N*-dimethylated anthracyclines, we conducted enzymatic assays of DoxA with both natural and *N,N*-dimethylated substrates. The reaction products indicated that while DoxA efficiently converts the natural substrate 13-deoxydaunorubicin (**3**) to daunorubicin (**5**), the conversion of *N,N*-dimethyl-13-deoxydaunorubicin (**9**) is very inefficient (Figure 5C and D). Moreover, DoxA could not convert *N,N*-dimethyldaunorubicin (**11**) to *N,N*-dimethyldoxorubicin (**12**) (Supplementary Figure S22). Taken together, these findings suggest that DoxA is inhibited by the *N,N*-dimethyl moiety of the unnatural substrates. Further studies should be conducted to confirm this hypothesis. Rational engineering of DoxA may be required to optimise the activity to identify mutant DoxA variants with enhanced enzymatic activity for conversion of *N,N*-dimethylated substrates.

This study also highlighted the inherent challenge of cytotoxicity associated with anthracycline production in the producer strain. *N,N*-dimethylated anthracyclines proved to assert a stronger cytotoxic effect than the natural variants (Supplementary Figure S5). Overexpression of *drrAB* in the engineered strain resulted in an eight-fold increase in resistance to both doxorubicin (**6**) and *N,N*-dimethyldoxorubicin (**12**) (Figure 6). This improved resistance pushed the pathway more toward *N,N*-dimethyldaunorubicin (**11**), although the productivity was still low (Figure 6).

The efficient production of *N,N*-dimethyl-13-deoxydaunorubicin (**9**) by MAG304 provides a promising outlook for biosynthesis of *N,N*-dimethylated anthracyclines. Further strain

development in terms of DoxA activity and improved resistance could provide sufficient productivity. In industry, doxorubicin is mainly produced semi-synthetically from daunorubicin (Lown, 1993). Similarly, it would be possible to produce *N,N*-dimethyldoxorubicin semi-synthetically if sufficient productivity of *N,N*-dimethyldaunorubicin is achieved.

N,N-dimethylated anthracyclines represent promising alternatives for conventional anticancer drugs, offering reduced cardiotoxic risks[14–16]. This study demonstrates the potential for biosynthesis of *N,N*-dimethylated anthracyclines via combinatorial biosynthesis. While we successfully produced *N,N*-dimethyldaunorubicin (**11**), future work should focus on optimising the cytochrome P450 monooxygenase DoxA, responsible for the final three oxidation reactions in the engineered pathway.

Materials and Methods

Bacterial strains and growth conditions

The bacterial strains used in this work are listed in Table 1. *E. coli* strains JM109[281], and ET12567/pUZ8002[282] were used for routine cloning and for conjugation or isolation of non-methylated DNA, respectively. *E. coli* strains were cultivated at 37 °C on Luria-Bertani (LB) agar plates or in LB medium supplemented with the appropriate antibiotics.

Table 1. Strains used in this study.

Strain	Description	References
E. coli JM109	For routine plasmid maintenance and cloning	[281]
E. coli ET12567/pUZ8002	Methylation-deficient strain for isolation of non-methylated DNA and conjugating plasmids into *Streptomyces*	[282]
E. coli TOP10	For protein expression	Invitrogen
S. peucetius var. *caesius* ATCC 27952	Derived from *Streptomyces peucetius* ATCC 29050, producer of daunorubicin and doxorubicin	ATCC[8]
S. peucetius G001	Derived from ATCC 27952 by NTG mutagenesis; increased production of daunorubicin	[268]
MAG301	G001 + pRDS	This work
MAG302	G001 Δ*dnrS*	This work
MAG303	G001 Δ*dnrS* + pRDS	This work
MAG304	G001 Δ*dnrS* + pRDS + pGWS1432	This work
MAG305	G001 Δ*dnrS* + pGWS1433	This work
MAG306	G001 Δ*dnrS* + pRDS + pGWS1432 + pGWS1434	This work
MAG307	G001 Δ*dnrS* + pRDS + pGWS1432 + pGWS1435	This work
MAG308	G001 Δ*dnrS* + pRDS + pGWS1432 + pGWS1436	This work
MAG309	G001 Δ*dnrS* + pGWS1433 + pGWS1437	This work

Table 2. Origin and function of genes and enzymes used in this study.

Gene	Enzyme	Size (nt/aa)	Origin	CDS	Catalytic function
aknX2	AknX2	717/238	*S. galilaeus*	CP966_RS29165	*N*-methyltransferase
aclP	AclP	732/243	*S. galilaeus*	CP966_RS29066	*N*-methyltransferase
dnrS	DnrS	1296/431	*S. peucetius*	CGZ69_RS24500	Glycosyltransferase
dnrQ	DnrQ	1317/438	*S. peucetius*	CGZ69_RS24505	Glycosyltransferase auxiliary protein
aknS	AknS	1332/443	*S. galilaeus*	CP966_RS29040	Glycosyltransferase
aknT	AknT	1332/443	*S. galilaeus*	CP966_RS29045	Glycosyltransferase auxiliary protein
dnrP	DnrP	885/294	*S. peucetius*	CGZ69_RS24510	15-Methylesterase
rdmC	RdmC	894/297	*S. purpurascens*	LYO46_16725	15-Methylesterase
dnrK	DnrK	1071/356	*S. peucetius*	CGZ69_RS24515	4-*O*-methyltransferase (10-decarboxylase moonlighting activity)
doxA	DoxA	1248/415	*S. peucetius*	CGZ69_RS24600	Cytochrome P450 monooxygenase
*doxA-1**	DoxA-1	1248/415	*S. peucetius*	CGZ69_RS24600	Cytochrome P450 monooxygenase
*doxA-2**	DoxA-2	1248/415	*S. bellus*	GCM10010244_ 64990	Cytochrome P450 monooxygenase
*doxA-3**	DoxA-3	1248/415	*S. coeruleorubidus*	CP976_32970	Cytochrome P450 monooxygenase
drrA	DrrA	993/330	*S. peucetius*	CGZ69_RS24655	ABC-family transporter (ATP-binding subunit)
drrB	DrrB	852/283	*S. peucetius*	CGZ69_RS24650	ABC-family transporter (permease subunit)

* Genes were codon-optimised based on the codon usage of *S. coelicolor*.

All media and routine *Streptomyces* techniques have been described previously[1]. *S. peucetius* G001[268] was used as parental strain. Soy flour mannitol (SFM) agar plates were used to grow *Streptomyces* for phenotypical characterisation. Tryptone soy broth (TSB) was used for liquid cultivation of *Streptomyces* strains. The growth media were supplemented with 20 μg·mL^{-1} thiostrepton when required. Cultures were grown in a total volume of 20 mL of liquid medium in 100 mL Erlenmeyer flasks equipped with metal coils. Shake flasks were incubated in an orbital shaker with a 2-inch orbit at 200 rpm at 30 °C. Due to poor sporulation of *S. peucetius* strains, mycelium stocks were prepared as an alternative to spore stocks. Strains were cultivated in TSB medium for 2 days, the biomass was washed with 10.3% (w/v) sucrose, resuspended in 20% (w/v) glycerol, and stored at –80 °C.

Plasmids and strains generated in this study

All plasmids described in this work are listed in Supplementary Table S1 and primers in Supplementary Table S2. Plasmid maps were generated using SnapGene 6.0 (Supplementary Figure S1).

Construct for gene disruption of *dnrS*

The strategy for creating deletion mutants is based on the unstable multicopy vector pWHM3[269], as described previously[271]. Briefly, a knock-out construct was generated containing an apramycin resistance cassette that is flanked by the upstream and downstream region of the targeted gene. The about 1 kb upstream and downstream regions of *dnrS* (Table 2) were amplified from *S. peucetius* ATCC 27952 genomic DNA using primers MH301/MH302 and MH303/MH304. The DNA fragments were subsequently cloned into pWHM3 using EcoRI/HindIII. The apramycin resistance gene *aacC4* flanked by two *loxP* recognition sites was cloned in-between the flanking regions of *dnrS* using an engineered XbaI restriction site. The resulting knock-out construct, designated as pGWS1431 (Supplementary Figure S1), was verified using Sanger sequencing. Subsequently, the construct was introduced to G001 via protoplast transformation[1]. The desired double-crossover mutant was selected by resistance against apramycin (50 μg·mL^{-1}) and sensitivity to thiostrepton (20 μg·mL^{-1}). The presence of the *loxP* recognition sites allowed the efficient removal of the apramycin resistance cassette from the chromosome following the introduction of pUWLCRE that expresses the Cre recombinase[272]. The successful deletion of *dnrS* and removal of the apramycin resistance cassette was confirmed by gel electrophoresis of the PCR product of primers MH305/MH306. A distinct band was observed at the expected size of 489 (Supplementary Figure S2).

Constructs for expression of biosynthetic genes

For the expression of biosynthetic genes, the integrative vector pSET152[274], the integrative vector pMS82[279], and the multicopy vector pWHM3-oriT[280] were employed. pSET152 and pMS82 integrate into the attachment sites within the *Streptomyces* genome for bacteriophages φC31 and φBT1, respectively. The vectors harbour the apramycin and hygromycin resistance cassettes, respectively. pWHM3-oriT[280] is a derivative of pWHM3[269] that harbours *oriT* to allow for its conjugative transfer and a thiostrepton resistance cassette.

To generate a construct for expression of *rdmC* from *S. purpurascens* ATCC 25489 (Table 2), the coding sequence (+0/+944, relative to the start codon of *rdmC*, amplified by primers MH307/MH308 from pBAD/HisB-rdmC[160]) under control of the constitutive *ermE** promoter[273] was cloned into pSET152[274] using EcoRI/XbaI (pGWS1432, Supplementary Figure S1).

The expression cassette of pRDS[231] was cloned into pSET152[274] along with *rdmC* to generate a construct for expression of the sugar biosynthesis genes and tailoring genes for *N,N*-dimethyldoxorubicin (**12**) biosynthesis. In this construct, the capsid ribosomal binding site R15 from bacteriophage φC31[275], the coding region of *rdmC*, and the L3S1P47 terminator[276] were cloned downstream the *aclP* gene in the pRDS expression cassette. The ribosomal binding site R15 was introduced to *rdmC* via primers MH309/MH310 (amplified from pGWS1432). The pUCK_L3S1P47 vector that harbours the L3S1P47 terminator was linearised by primers MH311/MH312. The two fragments were used to generate R15-*rdmC*-L3S1P47::pUCK via Gibson assembly[277]. Subsequently, the R15-*rdmC*-L3S1P47 region was amplified by primers MH313/MH314. The coding sequence of *aclP* and its upstream region containing an EcoRI restriction site was amplified by primers MH315/HH316 from pRDS. The two fragments were cloned into EcoRI/BamHI linearised pSET152 vector via Gibson assembly[277] (*aclP*-R15-*rdmC*-L3S1P47::pSET152). The expression cassette of pRDS minus *aclP* was excised from the pRDS expression vector using EcoRI and cloned into the EcoRI linearised *aclP*-R15-*rdmC*-L3S1P47::pSET152, resulting in pGWS1433-v1. The correct orientation of the fragment was verified by Sanger sequencing using the M13_R primer.

Illumina sequencing of pRDS indicated the presence of an unanticipated EcoRI site in the intergenic region between *aclP* and *aknX2*. Consequently, the 70 bp sequence between the EcoRI site within the coding region of *aknX2* and the EcoRI site in the intergenic region between *aclP* and *aknX2* is missing in pGWS1433-v1. The missing sequence was introduced to the construct via Gibson assembly[277]. The *dnmU-dnmV-dnmJ-aknX2* region was amplified from pRDS by primers MH319/MH320, including the missing sequence at the end of *aknX2*. The *aclP-rdmC* region was amplified from pGWS1433-v1 by primers MH317/MH318. The two fragments were cloned into BamHI linearised pGWS1433-v1 via Gibson assembly[277], resulting in pGWS1433 (Supplementary Figure S1). The introduction of the 70 bp sequence was confirmed by Sanger sequencing using the M13_R primer.

Three constructs were designed for the expression of *doxA* from *S. peucetius*, and two heterologous *doxA* genes from *S. bellus* and *S. coeruleorubidus*, respectively (Table 2). The DoxA enzymes of both strains have 99.3% sequence identity with *S. peucetius* DoxA. The genes were codon optimised based on the native codon preference of *S. coelicolor* using GenSmart Design (GenScript Biotech Crop, NJ, USA). The coding sequences were flanked by the *gapdh* promoter P7 from *Tsukamurella paurometabola*[275] with the helicase ribosomal binding site R9 from bacteriophage φC31[275] and the *aph* terminator[278]. The DNA fragments were synthesised by BaseGene (Leiden) and provided in pUC19 flanked by EcoRV sites. The fragments were cloned into pMS82[279] using EcoRV to generate pGWS1434 (*doxA*-1 of *S. peucetius*), pGWS1435 (*doxA*-2

of *S. bellus*), and pGWS1436 (*doxA*-3 of *S. coeruleorubidus*). The orientation of the fragments was determined by Sanger sequencing using the M13_R primer (Supplementary Figure S1).

To generate a construct for expression of *drrA* and *drrB* from *S. peucetius* ATCC 27952 (Table 2), the coding sequence of *drrAB* (+0/+1897 relative to the start codon of *drrA*, amplified by primers MH321/MH322) under control of the constitutive *ermE** promoter[273] was cloned into pWHM3-oriT using EcoRI/XbaI (pGWS1437, Supplementary Figure S1).

Metabolomics

Metabolite extraction

S. peucetius strains were cultivated in E1 medium[270], to which 5% (w/v) Diaion HP20 (Resindion SRL) was added prior to autoclaving. A 25 µL aliquot of mycelium stock was inoculated into 25 mL E1 medium in 100 mL Erlenmeyer flasks without metal coil. The cultures were incubated in a rotary shaker at 30 °C for 4 days. Following fermentation, both resin and biomass were collected by vacuum filtration, washed with distilled water, and extracted three times with 25 mL acetone by overnight soaking. The acetone extracts were evaporated under a nitrogen flow at 40 °C, and subsequently re-dissolved in 80% acetonitrile to obtain a final concentration of 1 mg·mL^{-1} crude extract for LC-MS/MS analysis.

LC-MS analysis

LC-MS/MS acquisition was performed using a Shimadzu Nexera X2 UHPLC system, with attached photodiode array detector (PDA), coupled to a Shimadzu 9030 QTOF mass spectrometer (MS), equipped with a standard electrospray ionisation (ESI) source unit, in which a calibrant delivery system (CDS) was installed. A total of 2 µL were injected into a Waters Acquity HSS C_{18} column (1.8 µm, 100 Å, 2.1 × 100 mm). The column was maintained at 30 °C, and run at a flow rate of 0.5 mL·min^{-1}, using 0.1% formic acid in H_2O as solvent A, and 0.1% formic acid in acetonitrile as solvent B. A gradient was employed for chromatographic separation starting at 15% B for 1 min, then 15–60% B for 9 min, 60–100% B for 1 min, and finally held at 100% B for 3 min. The column was re-equilibrated to 5% B for 3 min before the next run was started. The PDA acquisition was performed in the range 200–600 nm, at 4.2 Hz, with 1.2 nm slit width. The flow cell was maintained at 40 °C.

All samples were analysed in positive polarity, using data dependent acquisition mode. In this regard, full scan MS spectra (*m/z* 100–2000, scan rate 20 Hz, ID disabled) were followed by three data dependent MS/MS spectra (*m/z* 100–2000, scan rate 20 Hz, ID disabled) for the three most intense ions per scan. The ions were selected when they reach an intensity threshold of 1500, isolated at the tuning file Q1 resolution, fragmented using collision induced dissociation at fixed collision energy of 20 eV, and excluded for 0.01 s before being re-selected for fragmentation. The parameters used for the ESI source were: interface voltage 4 kV, interface temperature 300 °C, nebulising gas flow 3 L·min^{-1}, and drying gas flow 10 L·min^{-1}.

Annotation of mass features in LC/MS data

Raw data obtained from LC-MS analysis were converted to mzXML centroid files using Shimadzu LabSolutions Postrun analysis. The files were imported into MZmine 2.53[283] for data processing. Extracted ion chromatograms were generated with an *m/z* tolerance set to 0.002 *m/z* or 10.0 ppm.

For statistical analysis, LC-MS data were processed as described previously[284]. Briefly, mass ion peaks were detected (positive polarity, mass detector: centroid) and their chromatograms were built using ADAP chromatogram builder[285] (minimum group size in number of scans: 10; group intensity threshold: 200). The detected peaks were smoothed (filter width: 9), and the chromatograms were deconvoluted (algorithm: local minimum search; chromatographic threshold: 85%; search minimum in RT range: 0.05; minimum relative height: 1%; minimum ratio of peak top/edge: 2; peak duration: 0.03–2.00 min). The detected peaks were deisotoped (monotonic shape; maximum charge: 2; representative isotope: most intense). The peak list was exported as a comma-separated file. Data of three independent replicates were used to calculate the change in the mass peak areas of the different metabolites across the different tested strains.

LC-MS data used to identify compounds **1**–**16** in the extracts of the tested strains is provided in Supplementary Table S3 and Supplementary Figures S6–S18. Compounds **3**[17], **5** (Sanofi BV), **6** (Accord Healthcare Limited), **9**[17], **11**[17] and **12**[16] were annotated by matching the retention time, HRMS and HRMS/MS spectra to reference compounds. Compounds **4**, **7**, **10**, **13**–**16** were annotated based on their calculated exact mass and expected MS/MS spectra. Compounds **1**, **2**, **8** and **12** could not be detected in the crude extracts of the engineered strains.

Proteomics

MAG304 was cultivated in E1 medium. Biomass was harvested after 2, 3 or 4 days of incubation (n=3), snap-frozen in liquid nitrogen and stored at –80 °C until analysis. The frozen biomass was lysed using a Bioruptor Plus (Diagenode SA) and proteins were extracted using lysis buffer [4% SDS, 100 mM Tris-HCl (pH 7.6), 50 mM EDTA]. Sample preparation for LC-MS/MS measurement was performed as described previously[286]. Briefly, total protein was precipitated using the chloroform-methanol method[287] and dissolved in 0.1% RapiGest SF surfactant (Waters Crop.) at 95 °C. The protein concentration was determined using the BCA method. Protein samples were reduced by adding 5 mM dithiothreitol (DTT) and incubated in the dark at 60 °C for 30 min, followed by thiol group protection using 21.6 mM iodoacetamide and incubation in the dark at room temperature for 30 min. Subsequently, 0.1 µg of trypsin (recombinant, proteomics grade, Roche) per 10 µg of protein was added, and samples were digested overnight at 37 °C. After digestion, trifluoroacetic acid was added to a concentration of 0.5%. The samples were incubated at 37 °C for 30 min, followed by centrifugation to degrade and remove the RapiGest SF. The resulting peptide solution, containing 6 µg of peptides, was cleaned and desalted using StageTips[288]. Briefly, 6 µg of peptides was loaded on a conditioned StageTip with two 1 mm diameter C_{18} disks (Empore, product number 2215), washed twice using a 0.5% formic acid solution, and eluted with elution solution (80% acetonitrile and 0.5% formic acid). Acetonitrile

was evaporated using a SpeedVac. The final peptide concentration was adjusted to 40 ng·µL^{-1} using sample solution (3% acetonitrile and 0.5% formic acid) for analysis.

Quantitative proteomics was performed as described previously[286]. Briefly, the desalted peptide solution was separated using an UltiMate 3000 RSLCnano system (Thermo Scientific) set in a trap-elute configuration, coupled with a QExactive HF mass spectrometer (Thermo Scientific). The liquid chromatography system used a Waters nanoEase M/Z Symmetry C_{18} trap column (5 µm, 100 Å, 180 µm × 20 mm) for peptide loading and retention, and a Waters nanoEase M/Z HSS T3 C_{18} analytical column (1.8 µm, 100 Å, 75 µm × 250 mm) for peptide separation. The mass spectrometer was operated in positive mode with data-dependent acquisition. Raw LC-MS/MS files were analysed using MaxQuant software v2.2.0.0[289] using the label-free quantification (LFQ) method.

Bioinformatics

The BGCs of doxorubicin/daunorubicin, aclarubicin and rhodomycin were visualised using clinker[290]. DoxA homologs were identified using NCBI BLASTP search (http://blast.ncbi.nlm.nih.gov). Alignment of the obtained protein sequences was performed using Cluster Omega 1.2.4[291].

Enzymatic assays

Enzymatic activity assays were conducted as described elsewhere in detail[292].The DoxA, DnrV, FDX4 and SFR proteins were produced as N-terminally 6×His-tagged recombinant proteins in *E. coli* TOP10 and purified by affinity chromatography using TALON Superflow resin (GE Healthcare). Proteins were concentrated using Amicon Ultra-4 10K centrifugal filters (Merck Millipore) and stored at –20°C in 40% glycerol. The proteins were analysed for purity and molecular weight using SDS-PAGE. Enzymatic activity measurements were carried out at room temperature overnight. Then, reactions were extracted with 4:1 mixture of chloroform and methanol. The extracts were evaporated using a vacuum concentrator and dissolved in methanol for HPLC analysis. HPLC analysis was performed using a Shimadzu Nexera X3 system with a PDA detector and a Phenomenex Kinetex C_{18} column (2.6 µM, 100 Å, 4.6 × 100 mm). The column was run at a flow rate of 0.5 mL·min^{-1}, using 0.1% formic acid, 15% acetonitrile and 85% H_2O as solvent A, and 100% acetonitrile as solvent B. A gradient was employed starting at 100% A for 2 min, then 0–60% B for 18 min, 100% B for 4 min, and finally 100% A for 5 min. The absorbance of the samples was recorded at 490 nm. The reaction products were annotated by comparison to reference compounds for compounds **3**[17], **5** (Sanofi BV), **6** (Accord Healthcare Limited), **9**[17], **11**[17] and **12**[16]. For enzymatic assays with compounds **9**[17] and **11**[17], high resolution electrospray ionisation mass spectra were recorded on a Waters Acquity RDa detector using a Waters XBridge BEH C_{18} column (5 µm, 130 Å, 4.6 × 30 mm). The column was run at a flow rate of 0.8 mL·min^{-1}, using 0.1% formic acid in H_2O as solvent A, and 0.1% formic acid in acetonitrile as solvent B. A gradient was employed starting at 2–100% B for 132 s, then 100% B for 18 s, 100–2% B for 18 s, and finally 2% B for 12 s. The reaction products were annotated by comparison to reference compounds for compounds **11**[17] (Supplementary

Figure S19) and **12**[16] (Supplementary Figure S20). Compound **10** was annotated based on calculated exact mass (Supplementary Figure S21).

Microbial inhibition assays

To investigate the resistance of *S. peucetius* to anthracyclines, 5 µL of mycelium stock was spotted at a concentration of $1.0 \cdot 10^4$ colony forming units (CFU) per spot on SFM agar plates supplemented with increasing concentrations of compounds **3**[17], **6** (Accord Healthcare Limited), **9**[17] and **12**[16]. After 3 or 4 days of incubation at 30 °C, growth was examined visually.

Availability of data

Supplementary Figures S6–S22 are available online in the Supplementary Material on the journal's website: https://www.frontiersin.org/articles/10.3389/fbioe.2024.1363803/full#supplementary-material

Table S1. Plasmids used in this study.

Plasmid	Description	References
pWHM3	*E. coli*/*Streptomyces* shuttle vector, high copy number in *E. coli*, Amp^R, Thio^R	269
pWHM3-oriT	pWHM3-derivative harbouring *oriT* site for conjugative transfer in the NdeI site, Amp^R, Thio^R	280
pSET152	*E. coli*/*Streptomyces* shuttle vector, harbouring *attP* site and integrase for phage φC31 for stable integration into the chromosomal *attB* site of *Streptomyces*, Apra^R	274
pMS82	*E. coli*/*Streptomyces* shuttle vector, harbouring *attP* site and integrase for phage φBT1 for stable integration into the chromosomal *attB* site of *Streptomyces*, Hyg^R	279
pUWLCRE	Cre recombinase expression construct, Amp^R, Thio^R	272
pRDS	pWHM3-derivative with aclarubicin, doxorubicin and rhodomycin biosynthetic genes, Amp^R, Thio^R	231
pBAD/HisB	*E. coli* construct for protein expression with His-tag, Amp^R	Invitrogen
pBAD/HisB-rdmC	pBAD/HisB-derivative with *rdmC* from *S. purpurascens* ATCC 25489, Amp^R	160
pBAD/HisB-doxA	pBAD/HisB-derivative with *doxA* from *S. peucetius* ATCC 27952, Amp^R	292
pBAD/HisB-dnrV	pBAD/HisB-derivative with *dnrV* from *S. peucetius* ATCC 27952, Amp^R	292
pBAD/HisB-fdx4	pBAD/HisB-derivative with *fdx4* from *S. peucetius* ATCC 27952, Amp^R	292
pBAD/HisB-sfr	pBAD/HisB-derivative with spinach ferredoxin reductase gene *sfr*, Amp^R	292
pUCK_L3S1P47	pUCK-derivative with the synthetic L3S1P47 terminator, Kan^R	276
pGWS1431	pWHM3-derivative with the flanking regions of *S. peucetius dnrS* interspersed with the Apra^R-*loxP* cassette, Amp^R, Thio^R, Apra^R	This work
pGWS1432	pSET152-derivative with the coding region of *S. purpurascens rdmC* under control of the *ermE** promoter, Apra^R	This work
pGWS1433	pSET152-derivative with the expression cassette of pRDS and coding region of *rdmC* under control of the R15 RBS and L3S1P47 terminator, Apra^R	This work
pGWS1434	pMS82-derivative with codon optimised *S. peucetius doxA* under control of the P7 promoter, R9 RBS and *aph* terminator, Hyg^R	This work
pGWS1435	pMS82-derivative with codon optimised *S. bellus doxA* under control of the P7 promoter, R9 RBS and *aph* terminator, Hyg^R	This work
pGWS1436	pMS82-derivative with codon optimised *S. coeruleorubidus doxA* under control of the P7 promoter, R9 RBS and *aph* terminator, Hyg^R	This work
pGWS1437	pWHM3-oriT-derivative with the coding region of *S. peucetius drrAB* under control of the *ermE** promoter, Amp^R, Thio^R	This work

Table S2. Primers used in this study.

Primer	Sequence (5' to 3')*
MH301	GATC**AAGCTT**CCCGCAGGAGCACGTTCTCG
MH302	GATCGAAGTTATCGCGCATC**TCTAGA**ACCCTCCCTGGGTCACTTCTG
MH303	GATCGAAGTTATCCATCACC**TCTAGA**TGGAGTACGGCCAGGTAGAG
MH304	GATC**GAATTC**ATCGTCATCGAGCACAATC
MH305	CCCGGTTTCACGCACATGGC
MH306	GTCCCGGCAGATCAGCGTGG
MH307	GATCGAATTC**CATATG**ATGTCCGAACGCATCGTGCCGAG
MH308	GATC**TCTAGA**CAGCCAAGCTTCATCGTCTC
MH309	ATGTTCTTTCCTGCGTTATCTCTAAGTAAGGAGTGTCCATATGTCCGAACGCATCGTGCCGAGCG
MH310	GGGAGGCCTTTTTTCGAAAATCAGGCCGCCGAGCGGGTGT
MH311	ACACCCGCTCGGCGGCCTGATTTTCGAAAAAAGGCCTCCCAAATC
MH312	ATGGACACTCCTTACTTAGAGATAACGCAGGAAAGAACATGTGAGCAAAAGGCC
MH313	AGCCGGCCGCGCGGGACTGATCTAAGTAAGGAGTGTCCATATG
MH314	ACGGCCAGTGCCAAGCTTGGGCTGCAGGTCGACTCTAGAGGGATCCTTTTGTTGCTATAAAAAAAGGCCCC
MH315	ATAACAATTTCACACAGGAAACAGCTATGACATGATTACGGAATTCCTGGAGGACGGACC
MH316	ATGGACACTCCTTACTTAGATCAGTCCCGCGCGGCCGGCTGCG
MH317	GGCGGGCGACGCGGGACCGG
MH318	GAATTCAACGGAACAGCCGGCGTCGGTGAACGCGG
MH319	CCGGCTGTTCCGTTGAATTCCTGGAGGACGGACCCACCGGCCGCG
MH320	GTGCCAAGCTTGGGCTGCAGGTCGACTCTAGAGGGATCC
MH321	GATCGAATTC**CATATG**AACACGCAGCCGACACG
MH322	GATCAAGCTT**TCTAGA**CTCACACCCCCTCAACGACG
M13_R	AGCGGATAACAATTTCACACAGG

* Restriction sites used for cloning are presented in boldface: GAATTC, EcoRI; CATATG, NdeI; AAGCTT, HindIII; TCTAGA, XbaI; GGATCC, BamHI; GGTACC, KpnI.

Table S3. LC-MS data used to identify compounds 1–16 in the extracts of the tested strains.

#	Name	Chemical formula	Calculated *m/z*, adduct ion	Observed *m/z*	RT (min)	Source
1	rhodomycin D	$C_{28}H_{31}NO_{11}$	558.1975, $[M+H]^+$	N.D.	N.D.	N.D.
2	15-demethoxy-rhodomycin D	$C_{27}H_{29}NO_{11}$	544.1819, $[M+H]^+$	N.D.	N.D.	N.D.
3	13-deoxy-daunorubicin	$C_{27}H_{31}NO_9$	514.2077, $[M+H]^+$; 367.1182, $[M+H\text{-sugar-}H_2O]^+$	514.2071; 367.1174	6.4	reference compound[17]
4	13-dihydro-daunorubicin	$C_{27}H_{31}NO_{10}$	530.2026, $[M+H]^+$; 383.1131, $[M+H\text{-sugar}]^+$	530.2017; 383.1126	4.9	crude extract G001
5	daunorubicin	$C_{27}H_{29}NO_{10}$	528.1870, $[M+H]^+$; 363.0868, $[M+H\text{-sugar-}H_2O]^+$	528.1862; 363.0864	5.5	Sanofi BV
6	doxorubicin	$C_{27}H_{29}NO_{11}$	544.1819, $[M+H]^+$; 379.0818, $[M+H\text{-sugar-}H_2O]^+$	544.1816; 379.0812	4.6	Accord Healthcare Limited
7	ε-rhodomycin T	$C_{30}H_{35}NO_{11}$	586.2288, $[M+H]^+$; 393.0974, $[M+H\text{-sugar-}H_2O]^+$	586.2285; 393.0970	6.9	crude extract MAG301
8	15-demethoxy-ε-rhodomycin T	$C_{29}H_{33}NO_{11}$	572.2132, $[M+H]^+$	N.D.	N.D.	N.D.
9	*N*,*N*-dimethyl-13-deoxydaunorubicin	$C_{29}H_{35}NO_9$	542.2390, $[M+H]^+$; 349.1076, $[M+H\text{-sugar-}H_2O]^+$	542.2385; 349.1071	6.7	reference compound[17]
10	*N*,*N*-dimethyl-13-dihydrodaunorubicin	$C_{29}H_{35}NO_{10}$	558.2339, $[M+H]^+$; 383.1131, $[M+H\text{-sugar}]^+$	558.2333; 383.1124	5.1	crude extract MAG304
11	*N*,*N*-dimethyl-daunorubicin	$C_{29}H_{33}NO_{10}$	556.2183, $[M+H]^+$; 363.0868, $[M+H\text{-sugar-}H_2O]^+$	556.2177; 363.0861	5.7	reference compound[17]
12	*N*,*N*-dimethyl-doxorubicin	$C_{29}H_{33}NO_{11}$	572.2132, $[M+H]^+$; 379.0818, $[M+H\text{-sugar-}H_2O]^+$	N.D.	4.7	reference compound[16]
13	4-methoxy-ε-rhodomycin T	$C_{31}H_{37}NO_{11}$	600.2445, $[M+H]^+$; 407.1131, $[M+H\text{-sugar-}H_2O]^+$	600.2441; 407.1127	6.4	crude extract MAG301
14	aclacinomycin T	$C_{30}H_{35}NO_{10}$	570.2339, $[M+H]^+$; 377.1025, $[M+H\text{-sugar-}H_2O]^+$	570.2334; 377.1021	6.4	crude extract MAG301
15	4-methoxy-aclacinomycin T	$C_{31}H_{37}NO_{10}$	584.2496, $[M+H]^+$; 391.1182, $[M+H\text{-sugar-}H_2O]^+$	584.2492; 391.1174	6.0	crude extract MAG301
16	ε-rhodomycinone	$C_{22}H_{20}O_9$	451.1005, $[M+Na]^+$; 361.0712, $[M+H\text{-}2H_2O\text{-}2CH_3OH]^+$	451.1006; 361.0707	9.5	crude extract G001



Figure S1. *[continued on next page].*

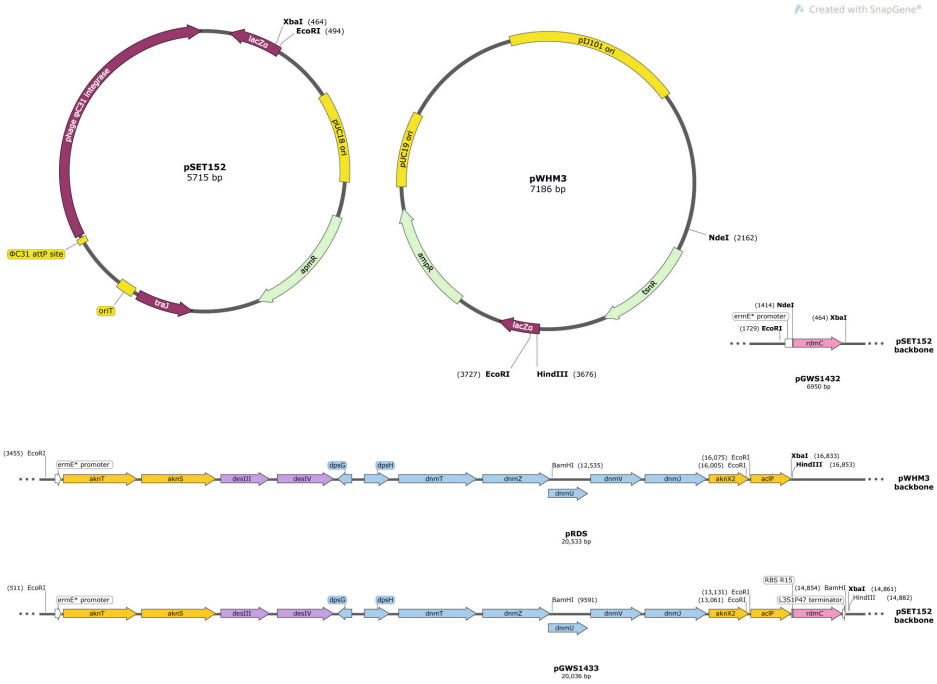


Figure S1. Plasmid maps of constructs used in this study. Restriction sites used for cloning are indicated. Resistance cassettes are abbreviated as: *ampR*, ampicillin; *apmR*, apramycin; *hygR*, hygromycin; *tsnR*, thiostrepton. Biosynthetic genes are coloured by source organism: *S. peucetius*, pink; *S. galilaeus*, blue; *S. venezuelae*, purple; *S. purpurascens*, green; other, orange. Plasmid maps were generated using SnapGene 6.0.

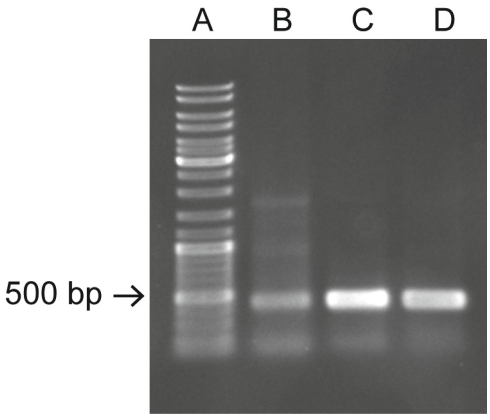


Figure S2. PCR analysis confirms the successful deletion of *dnrS* in G001. Gel electrophoresis of PCR products of primers MH305 and MH306 on genomic DNA of three clones of G001 Δ*dnrS*. The amplification of the target DNA fragment of 489 bp confirms the successful knock out of *dnrS* in all three clones. G001 Δ*dnrS* clone 2 was selected. Lane A: GeneRuler DNA Ladder Mix. Lane B–D: G001 Δ*dnrS* clone 1–3, respectively.

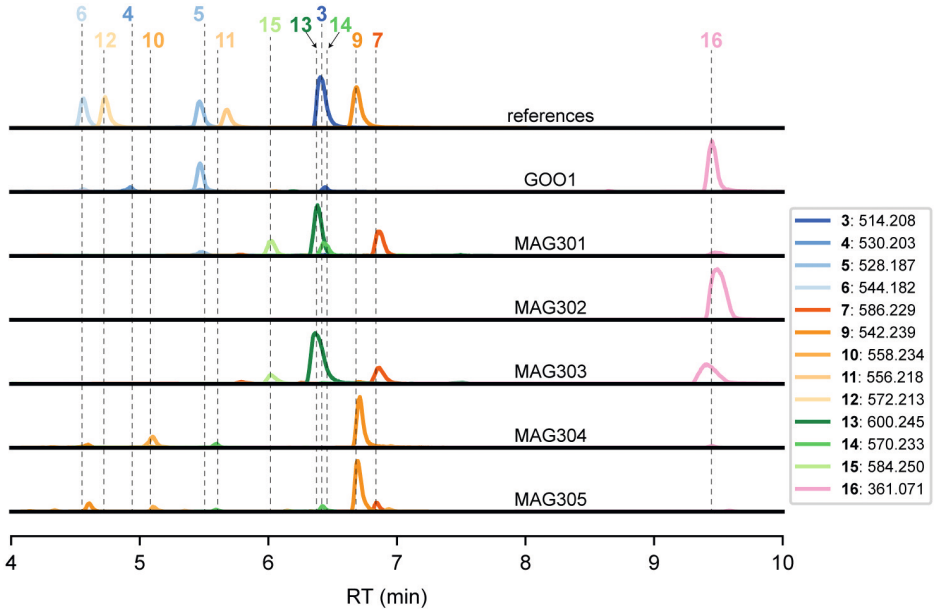


Figure S3. Analysis of engineered strains by LC-MS/MS. LC-MS analysis of crude extracts of G001 and engineered strains MAG301 (G001 pRDS), MAG302 (G001 Δ*dnrS*), MAG303 (G001 Δ*dnrS* pRDS), MAG304 (G001 Δ*dnrS* pRDS pGWS1432) and MAG305 (G001 Δ*dnrS* pGWS1433) cultivated in E1 medium with added HP20 resin. Extracted ion chromatograms showing the mass peaks $[M+H]^+$ of compounds **3**–**7** and **9**–**15**, and the mass peaks $[M+H-2H_2O-2CH_3OH]^+$ of compound **16**.

```
Q59971.1          MSGEAPRVAVDPFSCPMMTMQRKPEVHDAFREAGPVVEVNAPAGGPAWVITDDALAREVL   60
WP_167537468.1    -------------------MQRKPEVHDAFREAGPVVEVNAPAGGPAWVITDDALAREVL   41
ATW50545.1        MSGEAPRVAVDPFACPMMTMQRKPEVHDAFREAGPVVEVNAPAGGPAWVITDDALAREVL   60
Q9ZAU3.1          -------MAVDPFACPMMTMQRKPEVHDAFREAGPVVEVNAPAGGPAWVITDDALAREVL   53
WP_274819524.1    -------------------MQRKPEVHDAFREAGPVVEVNAPAGGPAWVITDDALAREVL   41
WP_193507397.1    -------------------MQRKPEVHDAFREAGPVVEVNAPAGGPAWVITDDALAREVL   41
                                     ************************************

Q59971.1          ADPRFVKDPDLAPTAWRGVDDGLDIPVPELRPFTLIAVDGEDHRRLRRIHAPAFNPRRLA   120
WP_167537468.1    ADPRFVKDPDLAPAAWRGVDDGLDIPVPELRPFTLIAVDGEAHRRLRRIHAPAFNPRRLA   101
ATW50545.1        ADPRFVKDPDLAPAAWRGVDDGLDIPVPELRPFTLIAVDGEAHRRLRRIHAPAFNPRRLA   120
Q9ZAU3.1          ADPRFVKDPDLAPAAWRGVDDGLDIPVPELRPFTLIAVDGEAHRRLRRIHAPAFNPRRLA   113
WP_274819524.1    ADPRFVKDPDLAPAAWRGVDDGLDIPVPELRPFTLIAVDGEAHRRLRRIHAPAFNPRRLA   101
WP_193507397.1    ADPRFVKDPDLAPAAWRGVDDGLDIPVPELRPFTLIAVDGEAHRRLRRIHAPAFNPRRLA   101
                  ************:*************************** ******************

Q59971.1          ERTDRIAAIADRLLTELADSSDRSGEPAELIGGFAYHFPLLVICELLGVPVTDPAMAREA   180
WP_167537468.1    ERTDRIAAIAGRLLTELADASGRSGKPAELIGGFAYHFPLLVICELLGVPVTDPAMAREA   161
ATW50545.1        ERTDRIAAIAGRLLTELADASGRSGKPAELIGGFAYHFPLLVICELLGVPVTDPAMAREA   180
Q9ZAU3.1          ERTDRIAAIAGRLLTELADASGRSGKPAELIGGFAYHFPLLVICELLGVPVTDPAMAREA   173
WP_274819524.1    ERTDRIAAIAGRLLTELADASGRSGKPAELIGGFAYHFPLLVICELLGVPVTDPAMAREA   161
WP_193507397.1    ERTDRIAAIAGRLLTELADTSGRSGKPAELIGGFAYHFPLLVICELLGVPVTDPAMAREA   161
                  **********.********:*.***:**********************************

Q59971.1          VGVLKALGLGGPQSAGGDGTDPAGDVPDTSALESLLLEAVHAARRKDTRTMTRVLYERAQ   240
WP_167537468.1    VSVLKALGLGGPQSGGGDGTDPAGDMPDTSALESLLLEAVHSARRNDTPTMTRVLYERAQ   221
ATW50545.1        VSVLKALGLGGPQSGGGDGTDPAGGVPDTSALESLLLEAVHSARRNDTPTMTRVLYERAQ   240
Q9ZAU3.1          VSVLKALGLGGPQSGGGDGTDPAGGVPDTSALESLLLEAVHSARRNDTPTMTRVLYERAQ   233
WP_274819524.1    VSVLKALGLGGPQSGGGDGTDPAGGVPDTSALESLLLEAVHSARRNDTRTMTRVLYERAQ   221
WP_193507397.1    VSVLKALGLGGPQSGGGDGTDPAGGVPDTSALESLLLEAVHSARRNDTPTMTRVLYERAQ   221
                  *.************.*********.:***************:***:** ************

Q59971.1          AEFGSVSDDQLVYMITGLIFAGHDTTGSFLGFLLAEVLAGRLAADADGDAISRFVEEALR   300
WP_167537468.1    AEFGSVSDDQLVYMITGLIFAGHDTTGSFLGFLLAEVLAGRLAADADEDAVSRFVEEALR   281
ATW50545.1        AEFGSVSDDQLVYMITGLIFAGHDTTGSFLGFLLAEVLAGRLAADADEDAVSRFVEEALR   300
Q9ZAU3.1          AEFGSVSDDQLVYMITGLIFAGHDTTGSFLGFLLAEVLAGRLAADADEDAVSRFVEEALR   293
WP_274819524.1    AEFGSVSDDQLVYMITGLIFAGHDTTGSFLGFLLAEVLAGRLAADADEDAVSRFVEEALR   281
WP_193507397.1    AEFGSVSDDQLVYMITGLIFAGHDTTGSFLGFLLAEVLAGRLAADADEDAVSRFVEEALR   281
                  ********************************************** **:*********

Q59971.1          HHPPVPYTLWRFAATEVVIRGVRLPRGAPVLVDIEGTNTDGRHHDAPHAFHPDRPSRRRL   360
WP_167537468.1    YHPPVPYTLWRFAATEVTIGGVRLPRGAPVLVDIEGTNTDGRHHDAPHAFHPDRPSWRRL   341
ATW50545.1        YHPPVPYTLWRFAATEVTIGGVRLPRGAPVLVDIEGTNTDGRHHDAPHAFHPDRPSWRRL   360
Q9ZAU3.1          YHPPVPYTLWRFAATEVTIGGVRLPRGAPVLVDIEGTNTDGRHHDAPHAFHPDRPSWRRL   353
WP_274819524.1    YHPPVPYTLWRFAATEVTIGGVRLPRGAPVLVDIEGTNTDGRHHDAPHAFHPDRPSWRRL   341
WP_193507397.1    YHPPVPYTLWRFAATEVTIGGVRLPRGAPVLVDIEGTNTDGRHHDDPHAFHPDRPSWRRL   341
                  :****************.* ************************ ********** ***

Q59971.1          TFGDGPHYCIGEQLAQLESRTMIGVLRSRFPQARLAVPYEELRWCRKGAQTARLTDLPVW   420
WP_167537468.1    TFGDGPHYCIGEQLAQLESRTMIGVLRSRFPEARLAVPYDELRWSRKGAQTARLTELPVW   401
ATW50545.1        TFGDGPHYCIGEQLAQLESRTMIGVLRSRFPEARLAVPYDELRWCRKGAQTARLTELPVW   420
Q9ZAU3.1          TFGDGPHYCIGEQLAQLESRTMIGVLRSRFPEARLAVPYDELRWCRKGAQTARLTELPVW   413
WP_274819524.1    TFGDGPHYCIGEQLAQLESRTMIGVLRSRFPEARLAVPYDELRWSRKGAQTARLTELPVW   401
WP_193507397.1    TFGDGPHYCIGEQLAQLESRTMIGVLRSRFPEARLAVPYDELRWSRKGAQTARLTELPVW   401
                  ********************************:*******:****.**********:****

Q59971.1          LR          422   Streptomyces sp. C5
WP_167537468.1    LR          403   S. coeruleorubidus ATCC 13740
ATW50545.1        LR          422   S. peucetius var. caesius ATCC 27952
Q9ZAU3.1          LR          415   S. peucetius ATCC 29050
WP_274819524.1    LR          403   S. coeruleorubidus DM
WP_193507397.1    LR          403   S. bellus
                  **
```

Figure S4. Sequence alignment of DoxA with closest homologs found by an NCBI BLASTP search. Protein sequences that share ›95% identity with *S. peucetius* var. *caesius* ATCC 27952 DoxA (ATW50545.1) were aligned using Clustal Omega 1.2.4.

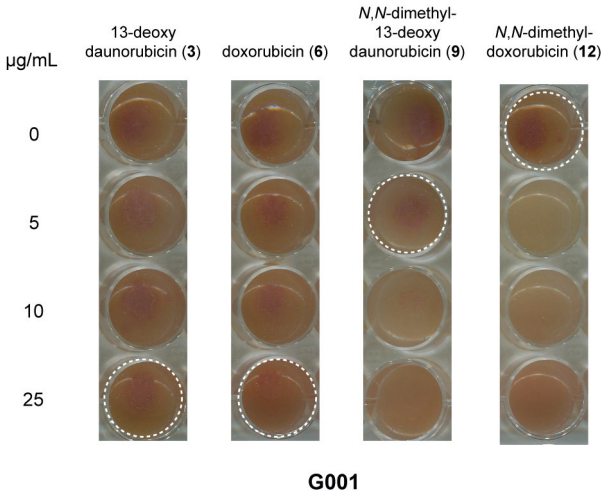


Figure S5. Toxicity of *N,N*-dimethyldoxorubicin. G001 was spotted on SFM agar plates supplemented with increasing concentrations of 13-deoxydaunorubicin (**3**), doxorubicin (**6**), *N,N*-dimethyl-13-deoxydaunorubicin (**9**) and *N,N*-dimethyldoxorubicin (**12**) and incubated at 30 °C for 3 days. The highest concentration that supported growth is indicated by a white dashed circle.



Cryptic transporter genes that confer resistance to anthracyclines in *Streptomyces*

Mandy B. Hulst, Le Zhang, Chao Du, Hannah E. Augustijn, Thadee Grocholski, Dennis P.A. Wander, Mikko Metsä-Ketelä, Jacques J.C. Neefjes and Gilles P. van Wezel

Abstract

Doxorubicin (Doxo) is a potent anticancer drug produced by *Streptomyces peucetius*, but its clinical application is limited by severe dose-dependent side effects. *N*,*N*-dimethyldoxorubicin (DMdoxo) has emerged as a promising alternative, exhibiting comparable efficacy but with reduced side effects. However, biosynthesis of DMdoxo is challenging due to its intrinsic toxicity to the producer strain. Here we show that DMdoxo exerts higher antibacterial activity than Doxo itself, and that challenge with DMdoxo induces the activation of cryptic resistance export systems in streptomycetes unable to produce anthracyclines. Evolution of *Streptomyces lividans* TK24 for DMdoxo-resistant variants resulted in the emergence of spontaneous mutants. Transcriptome analysis of mutants with enhanced resistance revealed elevated expression of two gene pairs, *cdtAB* and *sclAB*, which both encode ATP-binding cassette transporters. Introduction of either transporter pair under the control of the constitutive *ermE** promoter conferred more than eight-fold increase in resistance in the parental strain to both Doxo and DMdoxo. Phylogenetic analysis of 629 genomes of Streptomycetaceae indicated that 12% of the genomes encode at least one transporter, suggesting a widespread resistance mechanism against anthracyclines. Thus, our study identified two cryptic transporters that are activated in response to anthracyclines, providing resistance to these compounds.

Introduction

Doxorubicin (Doxo), an anthracycline polyketide originally discovered in extracts of *Streptomyces peucetius* var. *caesius*, is a potent anticancer drug[11]. However, its clinical application is limited by significant side effects, including cardiotoxicity, therapy-related tumours, and infertility[13]. To address these limitations, extensive research efforts have been dedicated to the synthesis of Doxo derivatives through both biosynthesis and organic synthesis approaches. Among these alternative compounds, *N*,*N*-dimethyldoxorubicin (DMdoxo) has emerged as a promising candidate as it has lost most toxicities without loss in anticancer activities[16].

Anthracyclines are glycoside antibiotics with aglycones that are called anthracyclinones[30]. These compounds are categorised as aromatic type II polyketides, characterised by a linear tetracyclic structure with a 7,8,9,10-tetrahydro-5,12-naphthacenequinone scaffold, and are decorated with one or more sugar moieties. Anthracyclines exert their anticancer activities through DNA interaction, which results in two distinct effects: DNA damage, via the trapping and poisoning of topoisomerase II onto the DNA resulting in DNA double-strand breaks, and chromatin damage, involving the eviction of histones at defined sites in the genome[14,15]. Anthracyclines inducing both DNA double-strand breaks and histone eviction have been associated with cardiotoxicity, a major side effect of anthracycline drugs. In contrast, histone eviction activity alone is associated with limited side effects. *N*,*N*-dimethylation of Doxo resulted in the loss of DNA damage activity, while maintaining histone eviction activity with no loss in cytotoxicity[16]. Given that toxicity currently limits the treatment of cancer patients, this positions DMdoxo as a promising candidate for an improved anticancer drug that may even be used in a more chronic manner in cancer treatment.

Despite their efficacy as anticancer compounds, the DNA intercalating activity of anthracyclines evokes self-toxicity in the producer strain. Consequently, anthracycline-producing *Streptomyces* strains have evolved self-resistance mechanisms[266]. These mechanisms are encoded within the anthracycline biosynthetic gene clusters (BGCs) and play a crucial role in protecting the producer strains. Various self-resistance mechanisms against anticancer compounds encompass efflux, sequestration, modification, self-sacrifice, and metabolic dormancy[57]. Anthracycline BGCs typically harbour genes encoding ATP-binding cassette (ABC) transporters that facilitate the efflux of the produced compounds[266]. The daunorubicin BGC of *S. peucetius* comprises four genes involved in self-resistance. Among these, *drrA* and *drrB* encode an ABC transporter facilitating the efflux of daunorubicin and Doxo[64]. DrrC is homologous to UvrA-like proteins and is involved in recognising and repairing DNA damage[68]. The fourth gene, *drrD*, has also been implicated in resistance, although the exact mechanism remains unknown[66].

In principle, the biosynthesis of DMdoxo can be achieved by combining enzymes from the biosynthetic pathways of Doxo, aclacinomycin, and rhodomycin. However, despite the expression of all the necessary enzymes in an engineered *S. peucetius* strain, the crude extracts did not yield detectable levels of DMdoxo[293]. A key bottleneck may be the significant toxicity of

DMdoxo to the engineered strain, as it was 16-fold more toxic compared to Doxo. This finding suggests that it is imperative to develop a DMdoxo-resistant host to achieve biosynthesis of DMdoxo and evoked our interest in exploring anthracycline resistance mechanisms of actinomycetes. Actinomycetes are typically found in complex environments with diverse microbial communities, where they must protect their habitat from competitors[21,51]. They employ secondary metabolites for both communication and defence. Anthracyclines may also play a role in this complex ecological system. Consequently, it is plausible that other actinomycetes have evolved resistance mechanisms to mitigate the toxic effects of anthracyclines.

The primary goal of this study was to explore and uncover anthracycline resistance mechanisms in actinomycetes. We observed a relatively high frequency of Doxo resistance within our laboratory's actinomycete collection, while resistance to DMdoxo was far less common. The toxicity of DMdoxo explains why it is difficult or impossible to identify streptomycetes naturally producing this compound. Subsequently, we demonstrated that anthracycline resistance can be activated in strains that do not produce anthracyclines through adaptive laboratory evolution with DMdoxo. Through reverse engineering, we identified two cryptic transporters that confer resistance to both Doxo and DMdoxo. Finally, phylogenetic analysis revealed that the presence of homologs of the two transporters is relatively common and not correlated to the presence of anthracycline BGCs.

Results

Antimicrobial activity of doxorubicin and *N,N*-dimethyldoxorubicin

The anthracycline *N,N*-dimethyldoxorubicin (DMdoxo) is a promising effective anticancer compound with reduced side effects compared to doxorubicin (Doxo). However, biosynthesis efforts for DMdoxo face challenges due to the inherent sensitivity of *S. peucetius* to DMdoxo[293]. These results prompted us to explore anthracycline resistance mechanisms of actinomycetes. To assess the tolerance of *Streptomyces* species to Doxo and DMdoxo, we tested a panel of six strains, each known to produce different classes of aromatic polyketides. The panel consisted of *S. peucetius*, *Streptomyces galilaeus*, *Streptomyces venezuelae*, *Streptomyces rimosus*, *Streptomyces coelicolor* M145 and *Streptomyces lividans* TK24. *S. galilaeus* produces aclacinomycins, which are anthracyclines that are closely related to Doxo. *S. venezuelae* produces jadomycins, which belong to the angucyclines. Angucyclines are polyketides with a non-linear tetracyclic aglycone. *S. rimosus* produces the polyketide tetracycline. Furthermore, the panel included the model strains *S. coelicolor* M145 and *S. lividans* TK24 that are derivatives of the model strains *S. coelicolor* A3(2) and *S. lividans* 1326, which lack their genomic plasmids.

Each strain was spotted at a concentration of $1.0 \cdot 10^4$ CFU per spot onto SFM agar plates with increasing Doxo or DMdoxo concentrations. *S. venezuelae* and *S. rimosus* demonstrated surprisingly high resistance levels to Doxo and were able to grow in the presence of 256 µM or 512 µM Doxo, respectively (Figure 1). This finding is particularly striking when considering that

64 µM Doxo severely inhibited the growth of the model Doxo producer *S. peucetius*. Additionally, *S. coelicolor* M145 and *S. lividans* TK24 also demonstrated relatively high resistance, with growth at 32 µM or 64 µM Doxo, respectively. Interestingly, all of the strains were much more sensitive to DMdoxo than to Doxo, failing to grow at concentrations higher than 2 µM or 4 µM DMdoxo (Figure 1).

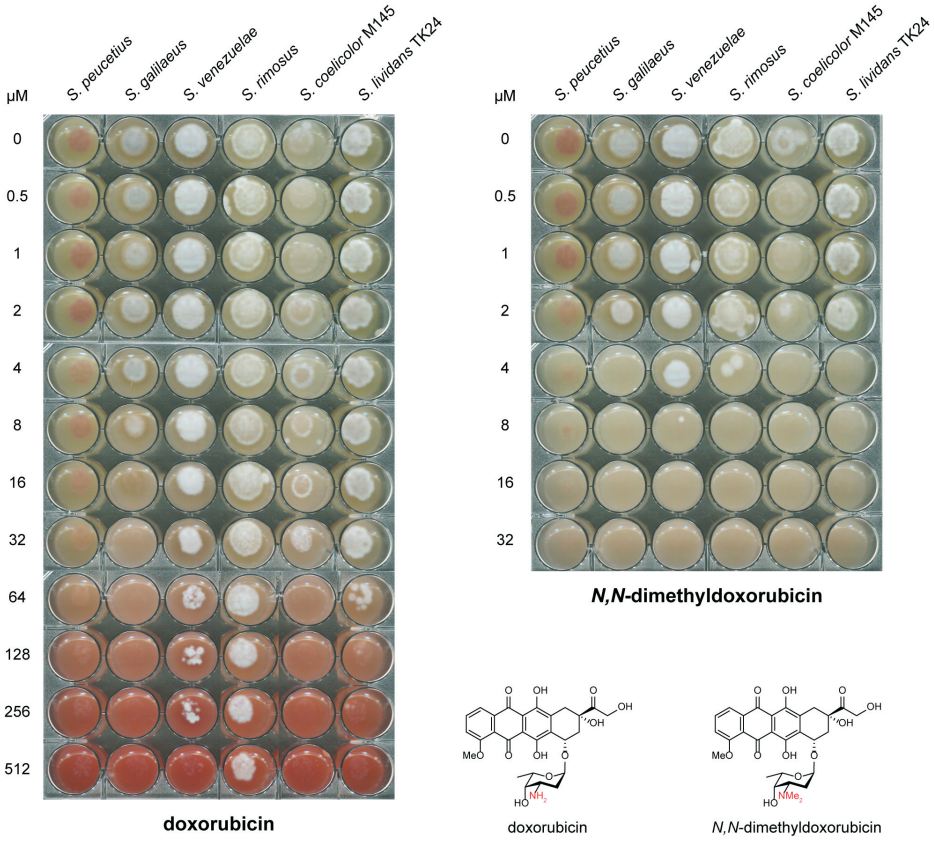


Figure 1. Sensitivity of selected *Streptomyces* strains against Doxo and DMdoxo. Anthracycline producers *S. peucetius* (produces Doxo) and *S. galilaeus* (produces aclarubicin), angucycline producer *S. venezuelae* (produces jadomycin), tetracycline producer *S. rimosus* and the model strains *S. coelicolor* M145 and *S. lividans* TK24 were spotted on SFM agar plates with 0.5 to 512 µM Doxo or 0.5 to 32 µM DMdoxo (both compounds are visible as red pigments). For each strain, 5 µL was spotted at a concentration of $1.0 \cdot 10^4$ CFU per spot and the plates were incubated at 30 °C for 4 days. All tested strains exhibited higher resistance to Doxo than to its close derivative DMdoxo.

To comprehensively evaluate resistance to Doxo and DMdoxo, we screened our in-house MBT collection, consisting of actinomycetes isolated from soil originating from the Himalaya mountain range in Nepal and the Qinling Mountains in China[294], Dutch dune soil, isolates from a wastewater treatment plant[295] and sponge-associated isolates[296]. Approximately 350 strains were spotted at high density onto SFM agar plates with 50 $\mu g \cdot mL^{-1}$ (i.e. 92 µM) Doxo

or 25 μg·mL^{-1} (i.e. 44 μM) DMdoxo. The strains exhibited large variation in their growth when exposed to the two compounds. About 40% of the strains demonstrated resistance to 50 μg·mL^{-1} (i.e. 92 μM) Doxo. About 31% of the strains demonstrated inhibited growth, while about 9% of the strains grew well and developed aerial hyphae or spores. In contrast, only six strains demonstrated growth in the presence of 25 μg·mL^{-1} (i.e. 44 μM) DMdoxo.

To illustrate the difference in toxicity of Doxo and DMdoxo, a subset of 72 representative strains is shown in Figure 2A. Each strain was spotted at high density onto SFM agar plates supplemented with 25 μM Doxo or DMdoxo. This revealed striking differences between colonies grown on Doxo or DMdoxo, showing that resistance to Doxo is relatively common, while resistance to DMdoxo is a rare phenomenon among actinomycetes. For example, when grown on Doxo, strains HP5 ("1" in Figure 2A), HP40 ("2") and Hm84 ("3") showed inhibition of development, slightly reduced growth, and normal growth, respectively, while the strains could not or hardly grow on DMdoxo. Six strains were selected that demonstrated growth at the high concentration of 25 μg·mL^{-1} (i.e. 44 μM) DMdoxo and studied in more detail. These strains were spotted at high density on SFM agar plates with increasing Doxo or DMdoxo concentrations. All strains demonstrated resistance to 200 μM Doxo, with a phenotype comparable to the control plate without Doxo (Figure 2B). Among these, *Streptomyces* sp. Els4, *Streptomyces* sp. Hm84 and *Streptomyces* sp. MBT74 demonstrated the highest resistance to DMdoxo and were able to grow in the presence of 200, 100 and 80 μM DMdoxo, respectively. However, growth and development were significantly inhibited by DMdoxo at the given concentrations, evident from the absence of aerial hyphae and spore formation. Els4, Hm84 and MBT74 showed normal growth and development at DMdoxo concentrations up to 80, 20 and 40 μM, respectively (Figure 2B).

Considering their high tolerance to Doxo and DMdoxo, the genomes of Els4, Hm84 and MBT74 were analysed in more detail. The whole genome sequences of Els4 and Hm84 were determined using Illumina sequencing, while the genome sequence of MBT74 was already available[294]. Draft genomes were assembled for Els4 and Hm84 resulting in 164 and 163 contigs, respectively (Supplementary Table S5). The genomes were analysed for the presence of putative biosynthetic gene clusters (BGCs) using antiSMASH 7.0[297], which were annotated using the MiBIG database[298]. We were particularly interested in the presence of anthracycline BGCs or other polyketide type II BGCs that may harbour resistance genes. Analysis of the Els4 genome predicted the presence of 38 putative BGCs (Supplementary Table S6), of which BGC2 showed very high similarity to the BGC for the angucycline warkmycin (MIBiG cluster BGC0001438, 97% similarity[299]). AntiSMASH predicted 21 putative BGCs in the genome of MBT74 (Supplementary Table S7), but no BGCs were detected for type II polyketides other than the BGC for the biosynthesis of a spore pigment. The Hm84 genome contained 37 putative BGCs (Supplementary Table S8), of which BGC37 showed high similarity with the BGC for the angucycline jadomycin (MIBiG cluster BGC000234, 85% similarity).

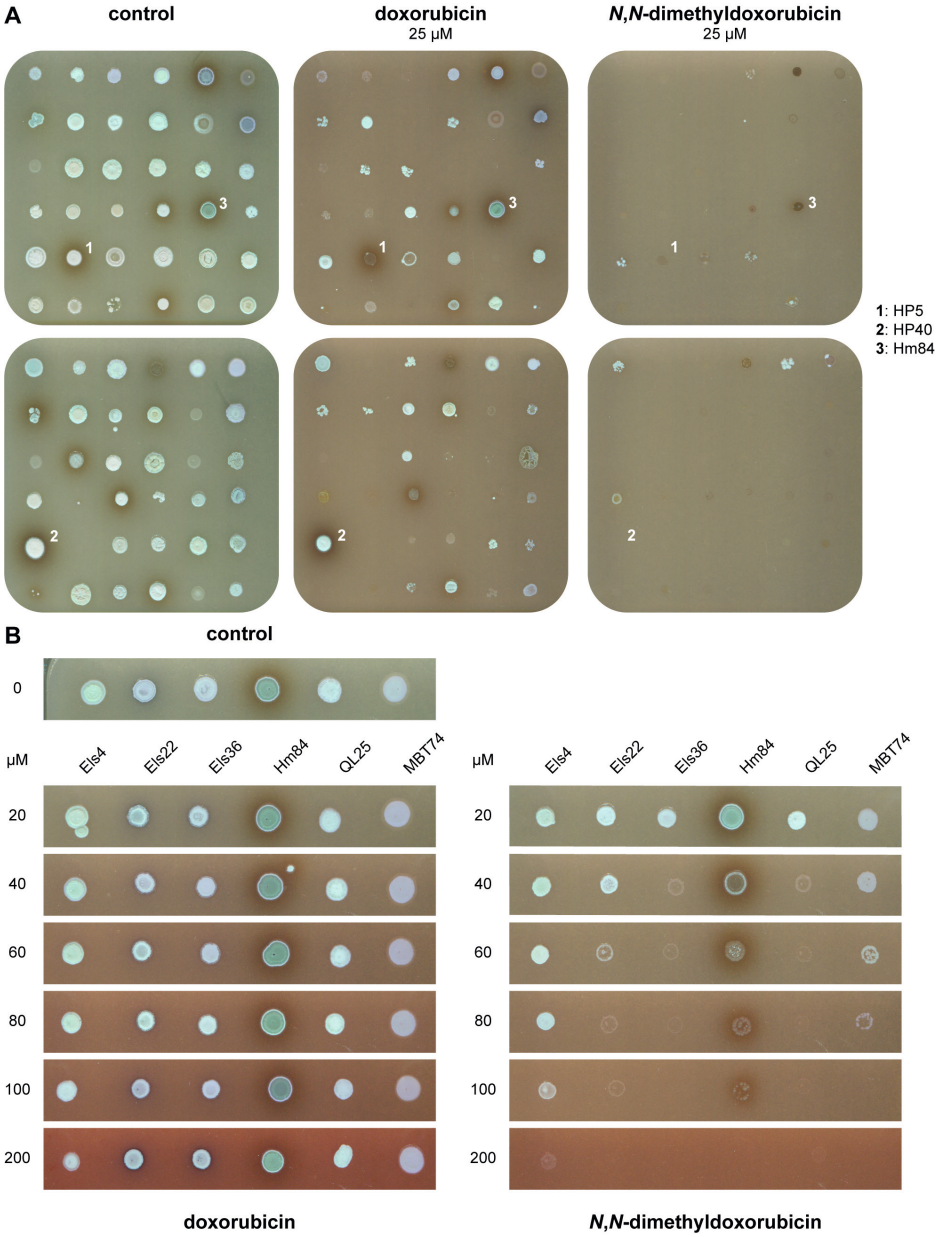


Figure 2. Resistance of wild-type actinomycetes against Doxo and DMdoxo. (A) A subset of 72 representative strains of our in-house collection of actinomycetes was spotted on SFM agar plates with 25 µM Doxo or DMdoxo. For each strain, 2 µL of highly concentrated spore or mycelial stock was spotted, and the plates were incubated at 30 °C for 3 days. Resistance to Doxo is more commonly observed than resistance to DMdoxo. *Streptomyces* sp. HP5, *Streptomyces* sp. HP40 and *Streptomyces* sp. Hm84 are indicated by 1, 2 and 3, respectively. **(B)** Six strains that displayed strong resistance to DMdoxo were spotted on SFM agar plates with 20 to 200 µM Doxo or DMdoxo. For each strain, 2 µL of highly concentrated or mycelial stock was spotted, and the plates were incubated at 30 °C for 3 days.

Both *S. venezuelae* and Hm84 harbour a jadomycin BGC and demonstrated relatively high resistance to Doxo. To test whether the presence of the jadomycin BGC may confer resistance to DMdoxo, the entire BGC was deleted from the genome of *S. venezuelae* as described[271]. The method makes use of the unstable multicopy vector pWHM3-oriT[280], which is a derivative of pWHM3[269] that harbours *oriT* to allow for its conjugative transfer. Approximately 1.5 kb regions flanking the jadomycin BGC (upstream of *jadR3* and downstream of *jadR**)[300] were amplified from genomic DNA using PCR, and the apramycin resistance gene *aacC4* was then cloned in between. The resulting knock-out construct (pGWS1447) was introduced into *S. venezuelae* via conjugation, and mutants were obtained by selecting for apramycin resistance and loss of thiostrepton resistance used for vector selection. Thus, we obtained a mutant where the entire BGC of jadomycin was replaced by the apramycin cassette, which is designated MAG409. Wild-type *S. venezuelae* and its mutant derivative MAG409 were spotted on SFM agar plates with increasing Doxo concentrations. Deletion of the jadomycin BGC did not affect the resistance of *S. venezuelae* to Doxo (Supplementary Figure S2).

Adaptive laboratory evolution generates anthracycline-resistant mutants

To activate cryptic anthracycline resistance mechanisms, we employed an adaptive laboratory evolution approach with a panel of streptomycetes. We hypothesised that anthracycline resistance mechanisms may be inactive under standard conditions and may be activated under evolutionary pressure. For this experiment, the panel of strains was comprised of *S. peucetius*, *S. galilaeus*, *S. coelicolor* A3(2), *S. lividans* TK24, *Streptomyces showdoensis* and *Streptomyces curacoi*. As discussed above, *S. peucetius* is a producer of Doxo, *S. galilaeus* is a producer of aclarubicin, *S. coelicolor* A3(2) is a wild-type model strain and *S. lividans* TK24 is a variant of wild-type strain *S. lividans* 1326 without genomic plasmids. *S. curacoi* and *S. showdoensis* were included to ensure a diverse panel of strains.

Evolution was achieved through serial propagation of batch cultures in TSB medium with progressively increasing DMdoxo concentrations (Figure 3A). In between transfers, strains were selected based on improved resistance as monitored by growth on SFM agar plates supplemented with different DMdoxo concentrations. The experiments were concluded once the strains demonstrated growth in TSB medium supplemented with 100 $\mu g \cdot mL^{-1}$ (i.e. 175 µM) DMdoxo, typically accomplished within ten transfers. Spore or mycelial stocks were prepared, and the evolved strains were labelled by adding "-Evo". To study the phenotypes of the parental and evolved strains and their levels of resistance, they were grown on SFM agar. Evolved isolates of both *S. coelicolor* and *S. galilaeus* displayed obvious developmental defects, manifested as a so-called "bald" (non-sporulating) phenotype, characterised by the absence of white aerial hyphae or grey spores (Figure 3B). In terms of their resistance, the parental strains were susceptible to 20 µM DMdoxo, except for *S. curacoi*, which could grow up to 40 µM DMdoxo (Supplementary Figure S3). *S. curacoi* also exhibited high levels of resistance to Doxo and could grow even in the presence of 200 µM Doxo. Among the evolved strains, TK24-EvoA1, *S. coelicolor*-Evo and *S. showdoensis*-Evo exhibited high levels of resistance, being able to grow in the presence of 200 µM Doxo or DMdoxo (Figure 3C). We decided to continue with TK24-EvoA1

for further investigation. *S. showdoensis*-Evo and *S. coelicolor*-Evo were excluded from further analysis, for reasons of lack of genetic tractability and lack of development, respectively.

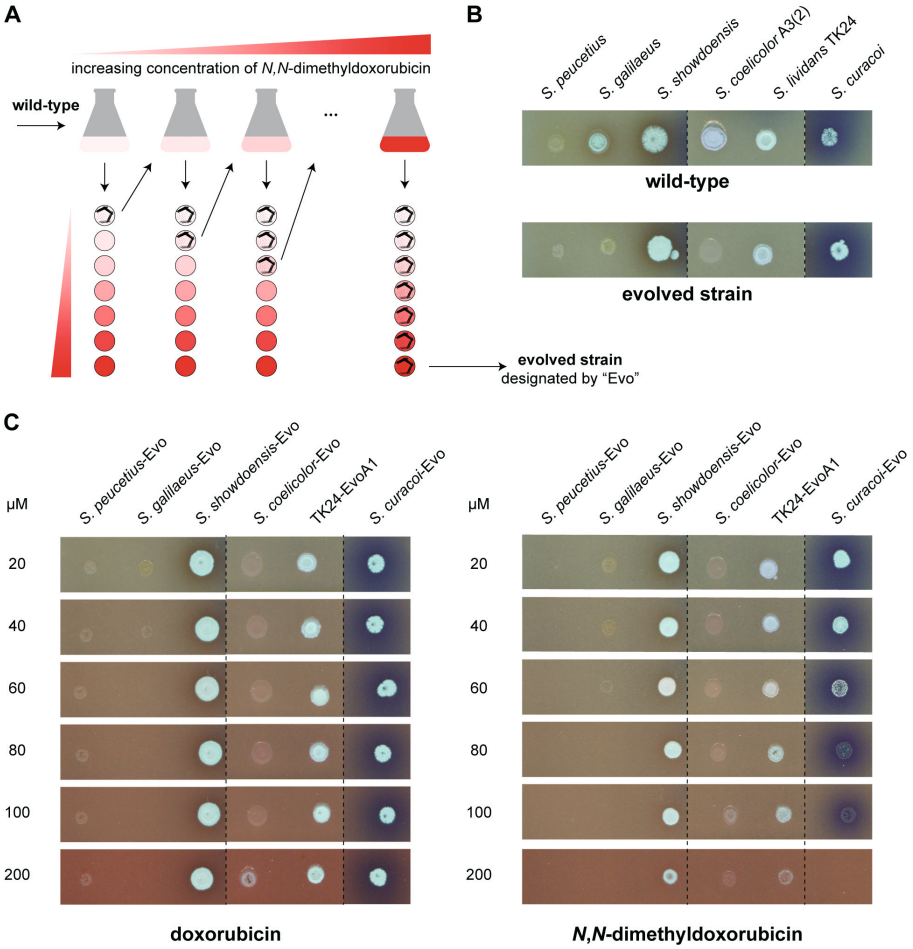


Figure 3. Adaptive laboratory evolution to obtain DMdoxo-resistant derivatives induces anthracycline resistance in various *Streptomyces* species. (A) Schematic representation of the adaptive laboratory evolution experiment with increasing DMdoxo concentrations. Wild-type strains were inoculated in TSB medium with sub-inhibitory levels of DMdoxo. Once the cultures reached stationary growth, they were streaked onto SFM agar plates with increasing DMdoxo concentrations. Biomass from the highest concentration that supported growth was then used to inoculate fresh TSB medium with the corresponding DMdoxo concentration. This process was repeated until a concentration of 100 μg·mL^{-1} (i.e. 175 μM) DMdoxo was achieved. **(B)** The parental and evolved strains of *S. peucetius*, *S. galilaeus*, *S. showdoensis*, *S. coelicolor* A3(2), *S. lividans* TK24 and *S. curacoi* were spotted on SFM agar plates. For each strain, 2 μL of highly concentrated spore or mycelial stock was spotted, and the plates were incubated at 30 °C for 3 days. Evolved isolates of *S. galilaeus* and *S. coelicolor* exhibited a 'bald' phenotype. **(C)** The parental and evolved strains were spotted on SFM agar plates with 20 to 200 μM Doxo or DMdoxo concentrations. For each strain, 2 μL of highly concentrated spore or mycelial stock was spotted, and the plates were incubated at 30 °C for 3 days. Evolved isolates of *S. showdoensis*, *S. coelicolor* and *S. lividans* TK24 exhibited the highest level of resistance to DMdoxo.

Whole-genome sequencing followed by Illumina paired-end sequencing was performed on TK24-EvoA1 to identify genomic variants that emerged during the evolution of TK24 (genome accession of the parental strain is NZ_CP009124.1). Genomic variant detection was performed using *breseq* v.0.38.1[301]. Mutations in pseudogene regions and silent mutations in coding regions were disregarded. Following these filtering steps, only three mutations were identified in TK24-EvoA1 (Table 1).

Table 1. Genomic variants identified in TK24 isolates from evolution experiments with DMdoxo.

Position*	Locus tag*	Variants	Annotation	Description	Isolate+
Genomic variants detected in evolution line A					
4,570,869	SLIV_RS 20695	substitution G→A	R71Q CGG→CAG	putative PadR-family transcriptional regulator (*cdtR*)	A1
4,571,366	SLIV_RS 20700	substitution C→A	intergenic 27	daunorubicin resistance protein DrrA-family ABC transporter ATPbinding subunit (*cdtA*)	A1
5,118,539	SLIV_RS 22890	insertion $C_{5\to6}$	frameshift 453/1482 nt	putative polysaccharide synthase (*matA*)	A1
Genomic variants detected in evolution line B					
1,743,319	SLIV_RS 07645	substitution G→A	P350S CCG→TCG	putative secreted hydrolase	B2–4
3,728,105	SLIV_RS 16660	substitution C→T	intergenic 11	daunorubicin resistance protein DrrA-family ABC transporter ATPbinding subunit (*sclA*)	B3
3,728,109	SLIV_RS 16660	substitution C→T	intergenic 15	daunorubicin resistance protein DrrA-family ABC transporter ATPbinding subunit (*sclA*)	B1
3,728,134	SLIV_RS 16660	substitution G→C	intergenic 40	daunorubicin resistance protein DrrA-family ABC transporter ATPbinding subunit (*sclA*)	B3
4,693,120	SLIV_RS 21250	insertion $C_{8\to9}$	intergenic 74	porphobilinogen synthase (*hemB*)	B4
5,121,114	SLIV_RS 22895	substitution C→A	A516D GCC→GAC	putative polysaccharide synthase (*matB*)	B1–4
7,392,037	SLIV_RS 33230	substitution A→C	V61G GTC→GGC	lipoprotein	B1
7,548,390	SLIV_RS 34020	substitution A→C	V92G GTG→GGG	nitroreductase-family deazaflavindependent oxidoreductase	B1

* The nucleotide positions and locus tags refer to the published reference genome of *S. lividans* TK24 (accession NZ_CP009124.1). Only non-silent mutations in coding sequences and mutations in intergenic sequences are shown.

+ The notation refers to the annotation of TK24-Evo strains as specified in Supplementary Table S1.

The three mutations were: (1) a single nucleotide permutation (SNP) within the coding region of transcriptional regulatory gene SLIV_RS20695; (2) a SNP in the upstream region of the adjacent gene SLIV_RS20700, which encodes an ABC transporter subunit with homology to the DrrAB transporter in the daunorubicin BGC; and (3) a frameshift mutation in the *matA* gene that is required for the production of the extracellular polysaccharide poly-β-*N*-acetylglucosamine (PNAG)[302].

S. lividans harbours a cryptic transporter that confers resistance to anthracyclines

Since two of the three mutations mapped to the same transporter locus, these were considered as primary candidates to confer anthracycline resistance in TK24-EvoA1. The transporter locus consists of a regulatory gene and two genes that encode a putative ABC transporter pair with high homology to the DrrAB transporter in the daunorubicin BGC. SLIV_RS20700 is homologous to DrrA, featuring a sequence identity of 51% with a coverage of 95% (Table 2). SLIV_RS20705 is homologous to DrrB, featuring a sequence identity of 36% with a coverage of 85% (Table 2). A putative *padR*-family transcriptional regulatory gene (SLIV_RS20695) is located immediately downstream of the transporter genes. Analysis of the TK24 genome using antiSMASH 7.0[297] indicated that the transporter genes are not part of a BGC. The genes for the putative regulator and two transporter subunits were designated *cdtR, cdtA* and *cdtB*, respectively, for **c**ryptic **d**oxorubicin **t**ransporter (Supplementary Table S4). The first mutation in TK24-EvoA1 is located in the upstream region of *cdtA*, and the second mutation is located in the coding region of *cdtR* (Table 1).

Table 2. Homology comparison between ABC transporters DrrAB, CdtAB and SclAB.

Protein pair	Identity (%)	Coverage (%)
DrrA/CdtA	51.4%	95%
DrrA/SclA	51.1%	92%
CdtA/SclA	63.0%	95%
DrrB/CdtB	35.5%	85%
DrrB/SclB	32.4%	71%
CdtB/SclB	44.1%	98%

Based on the enhanced resistance, we hypothesised that the mutations in TK24-EvoA1 led to upregulation of the transporter genes, and to enhanced export of anthracyclines. To test this hypothesis, transcriptome analysis was performed with TK24 and TK24-EvoA1. For this, TK24 and its derivative TK24-EvoA1 were grown on MM agar plates and mycelium was harvested after 24 h and 64 h (n=3). From these samples, RNA was isolated and prepared for RNA sequencing (RNAseq) analysis (see Materials & Methods for details). The data were normalised using DESeq2 v.1.34.0[303], and a Volcano plot was generated to evaluate the differentially expressed genes in TK24-EvoA1 (Figure 4A). Importantly, and in line with our hypothesis, the *cdtAB* transporter genes were significantly upregulated in the evolved strain (Figure 4B). Surprisingly, another transporter gene pair was also highly overexpressed in TK24-EvoA1 (this is worked out further below).

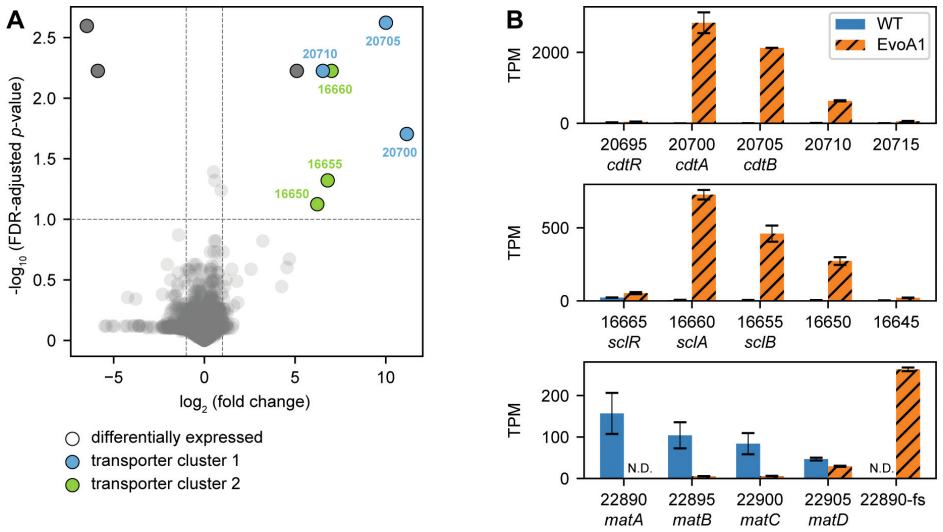


Figure 4. Changes in global gene expression in evolved strain *S. lividans* TK24-EvoA1. (A) Volcano plot of transcriptome data of TK24-EvoA1 and its parental strain grown on MM agar plates for 64 h (n=3). Genes with an FDR-adjusted p-value ‹0.1 and fold change ›2 are outlined with a black stroke. Positive $\log_2$ fold change values represent overexpression in the evolved strain. Two transporter loci exhibited significant overexpression in the evolved strain: SLIV_RS20700–20710 (highlighted in blue) and SLIV_RS16665–16650 (highlighted in green). **(B)** Bar plots of gene expression of the *cdt* locus (SLIV_RS20695–20715), the *scl* locus (SLIV_RS16665–16645), and the *mat* locus (SLIV_RS22890–22905). The bars represent the mean TPM values, and error bars indicate standard deviation (two-sample t-test, p‹0.01 for all depicted genes; N.D, not detected). Locus tags (SLIV_RS) are provided for reference (accession NZ_CP009124.1). 22890-fs indicates the *matA-matB* fusion transcript resulting from a frameshift in *matA* in TK24-EvoA1.

To investigate the role of *cdtR*, *cdtA* and *cdtB* in anthracycline resistance, we constructed deletion mutants and overexpression strains, as described below. Each strain was spotted at a concentration of $1.0 \cdot 10^4$ CFU onto SFM agar plates with increasing Doxo or DMdoxo concentrations. We aimed to constitutively express the transporter genes in TK24 to investigate whether this leads to increased resistance to Doxo and DMdoxo. To achieve this, the gene pair *cdtA-cdtB* was positioned behind the strong and constitutive *ermE** promoter[273] in the integrative vector pSET152[274]. Subsequently, the construct (pGWS1441) was introduced into TK24 via conjugation, resulting in strain MAG401 (Figure 5A). In line with the concept that the transporter may be involved in anthracycline resistance, constitutive expression of *cdtAB* in TK24 resulted in a more than eight-fold increased resistance to both Doxo (from 4 to ›64 µM) and DMdoxo (from ‹1 to 8 µM) (Figure 5C). These results show that the CdtAB transporter is involved in anthracycline resistance. However, it is important to note that the evolved strain TK24-EvoA1 exhibited resistance to more than 64 µM DMdoxo, whereas the expression construct with *cdtAB* increased DMdoxo resistance to only 8 µM. These results suggest that the transporter may not be the only resistance mechanism activated in TK24-EvoA1.

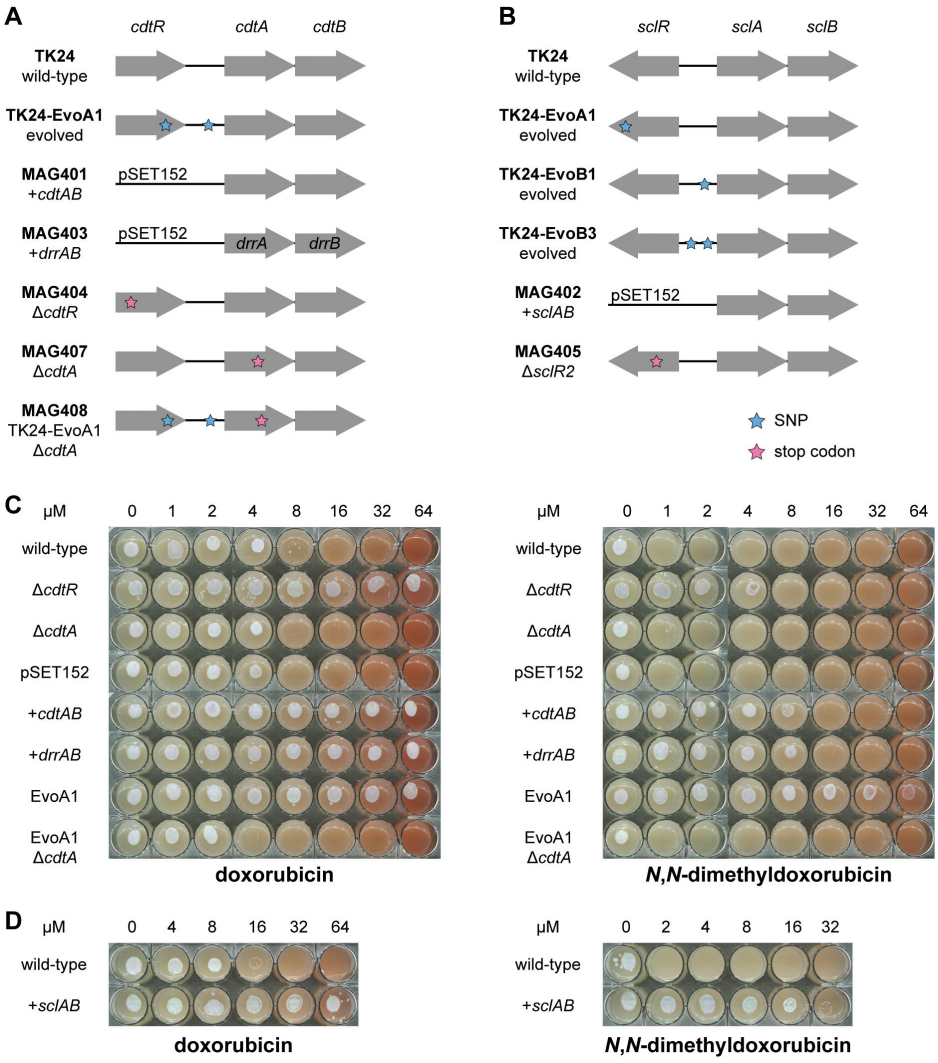


Figure 5. Activation of cryptic transporter loci *cdt* or *scl* in *S. lividans* TK24 confers resistance to Doxo and DMdoxo. Schematic representation of the strains used in this experiment related to **(A)** the *cdt* transporter locus and **(B)** the *scl* transporter locus. **(C)** S. lividans TK24 and its derivatives MAG404 (Δ*cdtR*), MAG407 (Δ*cdtA*), TK24 pSET152, MAG401 (*ermE**p-*cdtAB*), MAG403 (*ermE**p-*drrAB*), TK24-EvoA1 and MAG408 (TK24-EvoA1 Δ*cdtA*) were spotted on SFM agar plates supplemented with 1 to 64 μM Doxo or DMdoxo. For each strain, 5 μL of spore stock was spotted at a concentration of $1.0 \cdot 10^4$ CFU per spot and the plates were incubated at 30 °C for 3 days. Expression of *cdtAB* under the control of the *ermE** promoter in TK24 conferred resistance to ›64 μM Doxo and 8 μM DMdoxo. Inactivation of *cdtA* in TK24-EvoA1 rendered the strain susceptible to Doxo and DMdoxo. **(D)** TK24 and MAG402 (*ermE**p-*sclAB*) were spotted on SFM agar plates supplemented with Doxo (4–64 μM) or DMdoxo (2–32 μM). Expression of *sclAB* under the control of the *ermE** promoter in TK24 conferred resistance to ›64 μM Doxo and 16 μM DMdoxo.

Subsequently, we compared the level of resistance conferred by CdtAB of *S. lividans* with that of the Doxo transporter DrrAB originating from *S. peucetius*. To ensure maximum comparability, a similar expression construct was generated for the expression of the Doxo transporter genes *drrA-drrB* as was used for expression of the native *S. lividans* transporters genes. The construct (pGWS1443) was introduced into TK24 via conjugation, resulting in strain MAG403 (Figure 5A). Interestingly, introducing the expression constructs with *cdtAB* or *drrAB* in TK24 had the same effect. In both cases, resistance to both Doxo and DMdoxo was increased by more than eight-fold (Figure 5C).

Downstream of *cdtAB* lies *cdtR*, which encodes a putative PadR-family regulator. The gene was mutated in the evolution experiments whereas the expression of *cdtAB* was strongly upregulated. This suggests a model wherein CdtR act as a repressor of the transporter genes; if this is indeed the case, inactivation of *cdtR* in TK24 should result in upregulation of the transporter genes, leading to increased resistance. To verify that such is indeed the case, we inactivated *cdtR* via introduction of a stop codon at nucleotide position 40 (Q14*), using the CRISPR cytidine deaminase-based base editing system (CRISPR-cBEST)[304]. To do so, a *cdtR*-targeting spacer was introduced into CRISPR-cBEST construct pGWS1384. Subsequently, the resulting construct (pGWS1444) was introduced into TK24 via conjugation, resulting in strain MAG404 (Figure 5A). The successful introduction of the stop codon was confirmed by Sanger sequencing. Consistent with our hypothesis, the inactivation of *cdtR* in parental strain TK24 also resulted in increased resistance to both Doxo (from 4 µM to ›64 µM) and DMdoxo (from ‹1 µM to 4 µM) (Figure 5C). To further assess the role of the CdtAB transporter in the observed enhanced anthracycline resistance of TK24-EvoA1, we disrupted the transporter gene *cdtA* by introducing a stop codon at nucleotide position 526 (W178*). Therefore, a *cdtA*-targeting spacer was introduced into pGWS1384. Subsequently, the construct (pGWS1445) was used to create a stop codon in *cdtA* in TK24-EvoA1, resulting in strain MAG408 (Figure 5A). The inactivation of *cdtA* in the evolved strain resulted in strongly reduced resistance to both Doxo (from ›64 µM to 2 µM) and DMdoxo (from 64 µM to ‹1 µM) (Figure 5C). Similarly, *cdtA* was disrupted in TK24 (generating strain MAG407), but as expected this did not alter the already low resistance to Doxo or DMdoxo (Figure 5C).

Repeated evolution experiment reveals mutations in a second transporter locus

SNP analysis of TK24-EvoA1 revealed mutations that led to the activation of the transporter gene pair *cdtAB*. However, transcriptome data showed that a second transporter gene pair was also upregulated in the Doxo resistant mutant (Figure 4). This second transporter locus consists of a regulatory gene (*sclR*) and two genes (*sclAB*) that encode another ABC transporter pair with high homology to the DrrAB transporter in the daunorubicin BGC (Supplementary Table S4)[305]. SclA (SLIV_RS16660) is homologous to DrrA with an aa sequence identity of 51% with a coverage of 92% (Table 2). SclB (SLIV_RS16655) is homologous to DrrB, featuring an aa sequence identity of 32% with a coverage of 71% (Table 2). A *tetR*-family transcriptional regulatory gene (*sclR*, SLIV_RS16665) is located downstream of these transporter genes. Prior

research in *S. coelicolor* demonstrated that SCO4358 (an ortholog of SclR) acts as a repressor of SCO4359–4360 (encoding a SclAB ortholog), while the transporter acts as a multidrug transporter[305]. Interestingly, deletion of *sclR* in *S. coelicolor* resulted in about two-fold enhanced resistance to daunorubicin[305]. We were therefore curious if SclAB was also involved in the Doxo and DMdoxo resistance of TK24-EvoA1.

Upon further investigation of this genomic region in TK24-EvoA1, a partial mutation was identified in *sclR* resulting in an amino acid change (L242R). The mutation was detected in 41% of the Illumina reads. Sanger sequencing of PCR products of 15 single colonies indicated that the mutation was present in three out of 15 colonies. Interestingly, when we repeated the evolution experiment and performed SNP analysis on four additional anthracycline-resistant mutants (TK24-EvoB1-B4), we also identified mutations in the *scl* transporter locus. In TK24 evolution line B, three distinct mutations were located in the promoter region of *sclA*, of which one mutation occurred in TK24-EvoB1 and two mutations in TK24-EvoB3 (Table 1).

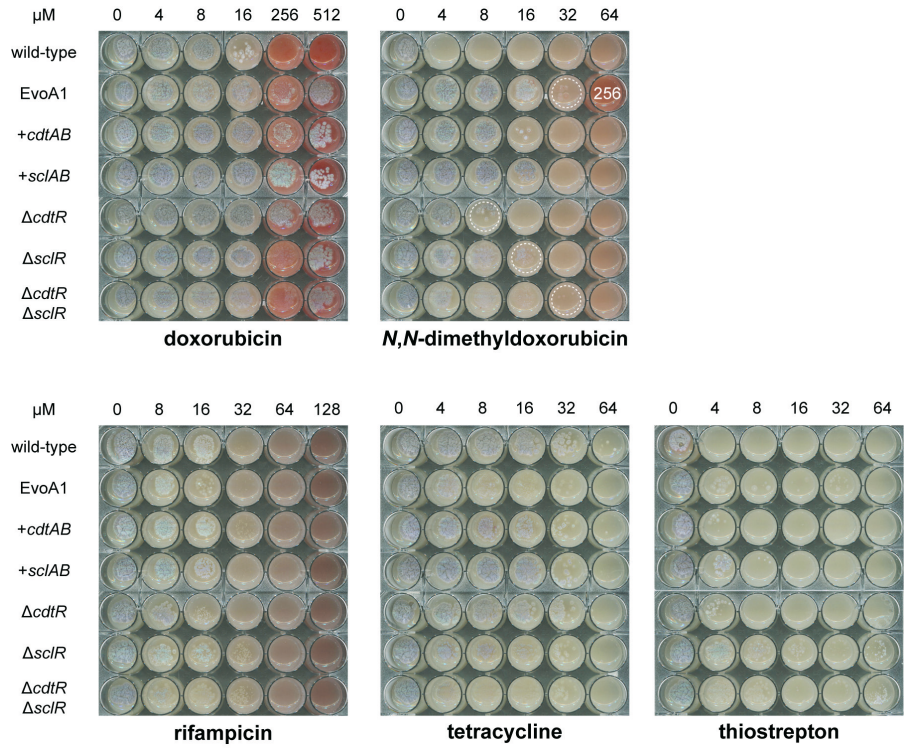


Figure 6. Role of CdtAB and SclAB transporters in resistance against different antibiotics. *S. lividans* TK24 and its derivatives MAG401 (*ermE**p-*cdtAB*), MAG402 (*ermE**p-*sclAB*), MAG404 (Δ*cdtR*), MAG405 (Δ*sclR*) and MAG406 (Δ*cdtR*Δ*sclR*) were spotted onto SFM agar plates supplemented with Doxo (4–512 μM), DMdoxo (4–64 μM), rifampicin (8–64 μM), tetracycline (4–64 μM) or thiostrepton (8–64 μM). For each strain, 5 μL of spore stock was spotted at a concentration of $1.0 \cdot 10^4$ CFU per spot and the plates were incubated at 30 °C for 6 days. Dashed circles indicate the highest concentration that allows growth. In one well, a final concentration of 256 μM DMdoxo was added, which is indicated.

The other two isolates from this evolution line did not have mutations in either the *scl* or *cdt* locus. We constructed an overexpression strain to study the effect of the SclAB transporter on Doxo and DMdoxo resistance. The gene pair *sclA-sclB* was positioned behind the strong and constitutive *ermE** promoter in the integrative vector pSET152. The construct (pGWS1442) was then introduced into TK24 via conjugation, resulting in strain MAG402 (Figure 5B). The recombinant strain showed enhanced resistance to both Doxo (from 8 to ›64 µM) and DMdoxo (from ‹2 to 16 µM) (Figure 5D). This indicates that the SclAB transporter can provide strong resistance to Doxo and DMdoxo.

Taken together, these data suggests that both transporter pairs CdtAB and SclAB can provide significant resistance to anthracyclines. While expression of either *cdtAB* or *sclAB* under the control of the *ermE** promoter resulted in increased Doxo and DMdoxo resistance, it was insufficient to reach the same levels of resistance as the evolved strain TK24-EvoA1. To test whether the co-expression of both transporters further increased resistance, a derivative of TK24 was created wherein both *cdtR* and *sclR* were inactivated. Using the same strategy as for the other mutants, strain TK24 Δ*cdtR*Δ*sclR* was created and designated MAG406. We also created the single mutant TK24 Δ*sclR* as control, which was designated MAG405. The Doxo and DMdoxo resistance of the single and double mutants was evaluated. All mutants were resistant to at least 512 µM Doxo (Figure 6). However, a difference between the two transporters could be observed with DMdoxo. Strains expressing *cdtAB* could grow with up to 8 µM DMdoxo, whereas the strains expressing *cdtAB* could grow with two-fold more DMdoxo (Figure 6). Interestingly, the double mutant of *cdtR* and *sclR* could grow with up to 32 µM DMdoxo, similar as the evolved strain TK24-EvoA1 (Figure 6).

CdtAB and SclAB exhibit specificity for anthracyclines

Transporters CdtAB and SclAB both provided significant resistance to anthracyclines. To investigate the specificity of the two cryptic transporters, the resistance to other classes of antibiotics was also evaluated. Antibiotics that were tested were rifampicin, tetracycline and thiostrepton, besides Doxo and DMdoxo. Tetracycline is a tetracyclic aromatic polyketide that is structurally related to Doxo, and which like Doxo is a DNA-targeting antibiotic. Rifampicin targets RNA polymerase, whereas thiostrepton is an oligopeptide that targets the ribosome. We tested the panel of antibiotics against *S. lividans* TK24, and its derivatives TK24-EvoA1, MAG401 (*ermE**p-*cdtAB*), MAG402 (*ermE**p-*sclAB*), MAG404 (Δ*cdtR*), MAG405 (Δ*sclR*) and MAG406 (Δ*cdtR*Δ*sclR*). The evolved strain TK24-EvoA1 did not exhibit increased resistance to rifampicin or tetracycline as compared to the parental strain (Figure 6). The mutant strains exhibited various levels of resistance to rifampicin and tetracycline, but never more than a two-fold difference as compared to the parental strain (Figure 6). More variety in resistance to thiostrepton was observed. Strains expressing *sclAB* (MAG402, MAG405 and MAG406) showed higher resistance to thiostrepton than the parental strain. However, growth and development of the mutants was inhibited at the low concentration of 4 µM thiostrepton, whereas the mutant strains grew at very high concentrations of Doxo (up to 512 µM).

N,N-dimethyldoxorubicin resistant mutants also harbour SNPs in the *mat* locus

In TK24 evolution line A only three mutations were found, two SNPs in the *cdt* locus and a frameshift mutation in *matA* (SLIV_RS22890). The frameshift mutation within the coding region of *matA* in TK24-EvoA1 resulted in an in-frame fusion of *matA* and *matB* (Table 1, Figure 4). Importantly, we found a SNP in *matB* (SLIV_RS22895) in all isolates of TK24 evolution line B that resulted in an A516D substitution in MatB (Table 1). MatAB are an enzyme couple that produces the extracellular polysaccharide poly-β-*N*-acetylglucosamine (PNAG), which acts as a sticky polymer that 'glues' hyphae together, leading to pellet formation in submerged cultures[302,306]. Inactivation of *matAB* in *S. lividans* results in loss of PNAG production and thus fragmented growth, as well as increased growth rate[302,306].

To evaluate the effect of the mutations within the *mat* locus of TK24 on both morphology and resistance to DMdoxo, the evolved isolates were grown in submerged TSB cultures (Figure 7A). All evolved isolates exhibited more fragmented growth with smaller pellets compared to the parental strain. Given the similarity in phenotypes among the evolved strains, we used TK24-EvoA1 as representative strain to investigate the impact of the *mat* mutations on DMdoxo resistance. The impact of the altered morphology of the evolved strains on DMdoxo resistance was studied by microtiter plate (MTP) cultivation in a BioLector system. This automated cultivation device provides non-invasive measurements of biomass concentration based on back-scattered light. For each strain, $1.0 \cdot 10^6$ CFU·mL^{-1} pregerminated spores were inoculated in 1 mL of TSB medium with increasing DMdoxo concentrations. Biomass measurements were taken at a 15-min interval. This method was applied to evaluate the DMdoxo resistance of TK24-EvoA1 and its parent *S. lividans* TK24 in a submerged environment. Additionally, a *matAB* deletion mutant of *S. lividans* 1326[306] and its parent were evaluated using the same method. *S. lividans* 1326 is a closely related strain to TK24 that carries two genomic plasmids. The *matAB* deletion mutant (GAD05) enabled the evaluation of how morphology affects anthracycline resistance, independent of other mutations.

As expected, TK24-EvoA1 demonstrated accelerated growth compared to the parental strain, demonstrated by the steeper growth curve and higher biomass concentration (Figure 7B). *S. lividans* TK24 exhibited growth inhibition at 0.5 µM DMdoxo and complete growth arrest at 2 µM DMdoxo. TK24-EvoA1 demonstrated improved resistance, with growth inhibition only beginning to be observed at 16 µM DMdoxo and growth was still observed at the highest tested concentration of 32 µM DMdoxo (Figure 7B). While *S. lividans* 1326 Δ*matAB* also exhibited faster growth than the parental strain, the mutant did not show higher resistance to DMdoxo, with both parent and mutant being fully inhibited by concentrations as low as 1 µM DMdoxo. These observations collectively suggest that while fragmented morphology is associated with an increased growth rate, it does not directly influence resistance to DMdoxo.

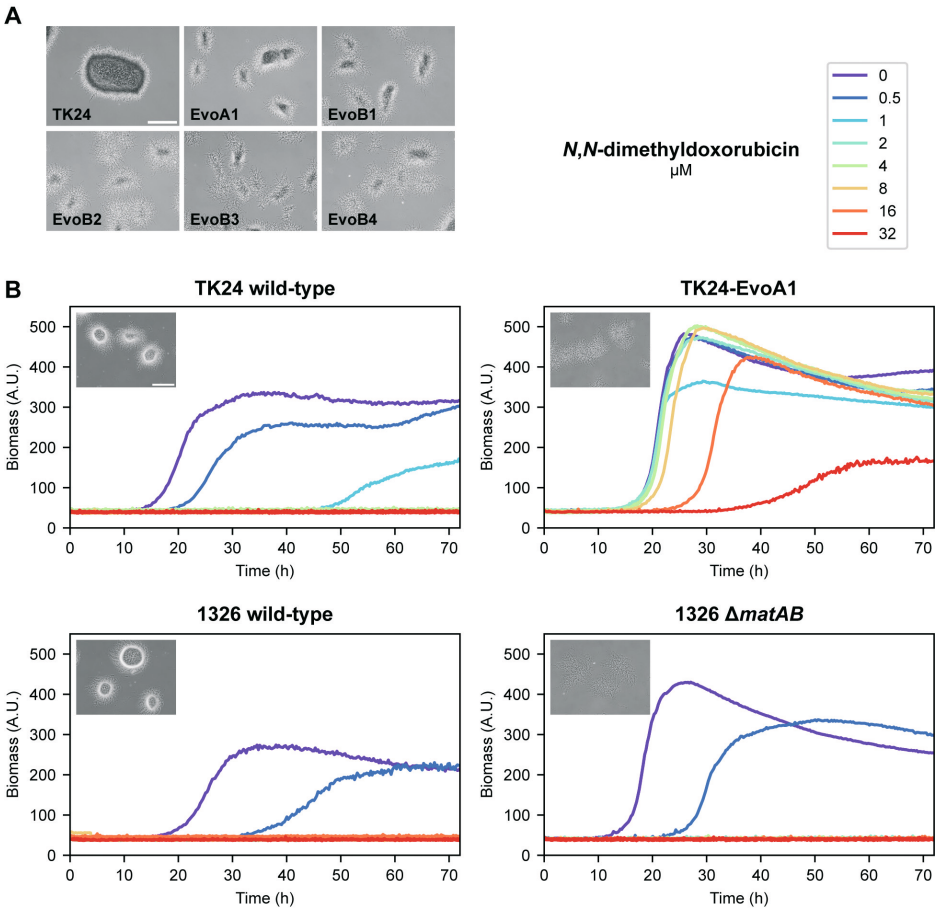


Figure 7. Inactivation of *matAB* does not directly affect DMdoxo resistance. (A) *S. lividans* TK24 and five evolved isolates were cultivated in TSB medium in shake flasks for 24 h. All evolved isolates exhibited a more fragmented morphology compared to the parental strain. Scale bar: 200 µm. **(B)** *S. lividans* strains TK24, TK24-EvoA1, 1326 and 1326 Δ*matAB* were cultivated in 1 mL of TSB medium with 0.5 to 32 µM DMdoxo in the BioLector. TK24-EvoA1 demonstrated uninhibited growth up to 8 µM DMdoxo, while TK24, 1326 and 1326 Δ*matAB* were already significantly inhibited by 0.5 µM DMdoxo. Deletion of *matAB* in *S. lividans* 1326 creased the growth rate but did not directly affect resistance to DMdoxo. Scale bar: 200 µm.

Evolution of *S. peucetius* to *N,N*-dimethyldoxorubicin generates mutations in *fusA*

Next, we explored the evolved isolates of *S. peucetius* with enhanced resistance to Doxo and DMdoxo. For *S. peucetius* we sequenced single colony isolates from two parallel evolution lines, which were designated "*S. peucetius*-EvoAx" and "*S. peucetius*-EvoBx" (Supplementary Table S1). Three single colony isolates were sequenced from evolution line A and four from evolution line B. Whole-genome sequencing and genomic variant detection was performed similarly as for TK24. The genome of the parental strain was used as a reference to filter out all changes relative to the published genome of *S. peucetius* var. *caesius* ATCC 27952 (accession

NZ_CP022438.1). After filtering the data, a total of 16 distinct mutations were identified across all the *S. peucetius* evolved isolates (Table 3). These mutations included single nucleotide polymorphisms (SNPs), as well as insertions, deletions or substitutions of short sequences (up to 13 base pairs).

Table 3. Genomic variants identified in *S. peucetius* isolates from evolution experiments with DMdoxo.

Position*	Locus tag*	Variants	Annotation	Description	Isolate+
Genomic variants detected in evolution line A					
1,524,293	CGZ69_ RS07190	deletion Δ12 bp	ΔPTPV 7–18/1368 nt	MHS family MFS transporter	A1–3
1,535,150	CGZ69_ RS07230	deletion $G_{6\rightarrow5}$	frameshift 248/2262 nt	molybdopterindependent oxidoreductase	A1–3
2,186,646	CGZ69_ RS10020	substitution G→T	Y332* TAC→TAA	Z1 domaincontaining protein	A1–3
2,610,861	CGZ69_ RS12060	insertion $C_{6\rightarrow7}$	intergenic 200	CYTH and CHAD domaincontaining protein	A2–3
4,422,376	CGZ69_ RS20380	deletion Δ13 bp	intergenic 351	sigma70 family RNA polymerase sigma factor	A1–3
4,584,873	CGZ69_ RS21225	insertion $C_{6\rightarrow7}$	frameshift 883/2127 nt	elongation factor G (*fusA*)	A1–3
5,014,608	CGZ69_ RS23245	substitution G→A	intergenic 51	ABC transporter substratebinding protein	A1–3
5,280,211	CGZ69_ RS24490	substitution GT→CC	V422P GTC→CCC	excinuclease ABC subunit UvrA (*drrC*)	A1–3
5,777,792	CGZ69_ RS26780	substitution T→C	L925P CTC→CCC	translation initiation factor IF2 (*infB*)	A1–3
5,915,471	CGZ69_ RS27320	substitution G→A	A3089T GCC→ACC	nonribosomal peptide synthetase	A2–3
7,182,877	CGZ69_ RS32420	substitution C→A	P81H CCT→CAT	DUF4012 domaincontaining protein	A1–3
Genomic variants detected in evolution line B					
1,042,186	CGZ69_ RS04840	substitution G→T	intergenic 1	SDR family NAD(P)dependent oxidoreductase	B1–4
1,992,539	CGZ69_ RS09140	insertion $C_{6\rightarrow5}$	frameshift 923/957 nt	16S rRNA (cytosine(1402) N(4))methyltransferase (*rsmH*)	B1, B4
2,147,743	CGZ69_ RS09835	substitution G→A	T76M ACG→ATG	endonuclease/exonuclease/phosphatase family protein	B1–4
2,184,740	CGZ69_ RS10015	substitution T→G	H38P CAC→CCC	PD(D/E)XK motif protein	B1–4
4,585,095	CGZ69_ RS21225	deletion Δ1 bp)	frameshift 1105/2127 nt	elongation factor G (*fusA*)	B2–3

* The nucleotide positions and locus tags refer to the published reference genome of *S. peucetius* var. *caesius* ATCC 27952 (accession NZ_CP022438.1). Only non-silent mutations in coding sequences and mutations in intergenic sequences are shown.

+ The notation refers to the annotation of *S. peucetius*-Evo strains as specified in Supplementary Table S1.

A few mutations stood out (Table 3). Firstly, only one mutation was identified within the daunorubicin BGC. All isolates from evolution line A harboured a mutation in *drrC* (CGZ69_RS24490), resulting in a V422P amino acid substitution. DrrC is an UvrA-like protein that is involved in DNA repair[68]. Furthermore, two mutations were identified in separate transporter loci. The first SNP was located within the promoter region of an ABC transporter gene (CGZ69_RS23245), and was found in all isolates from evolution line A. Secondly, all isolates from this evolution line also harboured a 12-base pair deletion at the beginning of a major facilitator superfamily (MFS) transporter gene (CGZ69_RS07190). Furthermore, two distinct mutations occurred in parallel in both evolution lines resulting in frameshift mutations in *fusA*, a gene that encodes elongation factor G in *Streptomyces*[307]. This gene is widely conserved and is an essential factor for ribosome translocation and recycling[307]. Fusidic acid is an inhibitor of *fusA*, and inactivation of *fusA* results in fusidic acid resistance.

Anthracycline resistance mechanisms and BGC distribution in streptomycetes

The two cryptic transporters CdtAB and SclAB conferred significant resistance to both Doxo and DMdoxo in TK24. Preliminary findings suggested a specific affinity of these transporters for anthracyclines. This observation prompted the question why TK24 harbours two distinct transporters for this class of compounds, and whether these transporters are present in other streptomycetes. It is plausible that these transporters have evolved due to the abundant presence of anthracyclines in their environment. To date, only 13 anthracycline BGCs have been identified[266], but it is unknown how many streptomycetes can produce anthracyclines. Therefore, we analysed 629 complete genome sequences of Streptomycetaceae for the presence of putative anthracycline BGCs and CdtAB or SclAB homologs.

To explore the prevalence of anthracycline BGCs, we developed a custom detection rule using the antiSMASH 7.0 framework[297] based on two criteria. First, the standard type II polyketide synthase (T2PKS) detection rule of antiSMASH was used to identify clusters that encode aromatic polyketides. This rule checks for the presence of the ketosynthase subunits (KS_α/KS_β) of the minimal PKS, and predicts the product class based on KS_β and cyclases in the cluster[308]. To refine the detection for anthracycline BGCs, we introduced a second criteria based on the glycosyltransferases and P450 auxiliary enzymes of known anthracycline BGCs[266]. We manually searched for genes for DnrS (glycosyltransferase) and DnrQ (auxiliary enzyme) homologs in the thirteen known anthracycline BGCs using pBLAST, and constructed profile hidden Markov models (pHMM). A positive hit was determined when either a DnrS or a DnrQ homolog was predicted by be encoded by a T2PKS cluster. Cut-off values were determined using positive controls (known anthracycline BGCs) and negative controls (angucycline BGCs from the MIBiG database[298]). Of the 629 genomes in our study, 5% harboured a putative anthracycline BGC based on our criteria (Supplementary Table S9). The BGCs were manually curated by comparison to known anthracycline BGCs. Most clusters showed high similarity with known anthracycline BGCs, of which aclarubicin (nine clusters) and Doxo (six clusters) were the most abundant. Five clusters exhibited low similarity to known anthracycline BGCs.

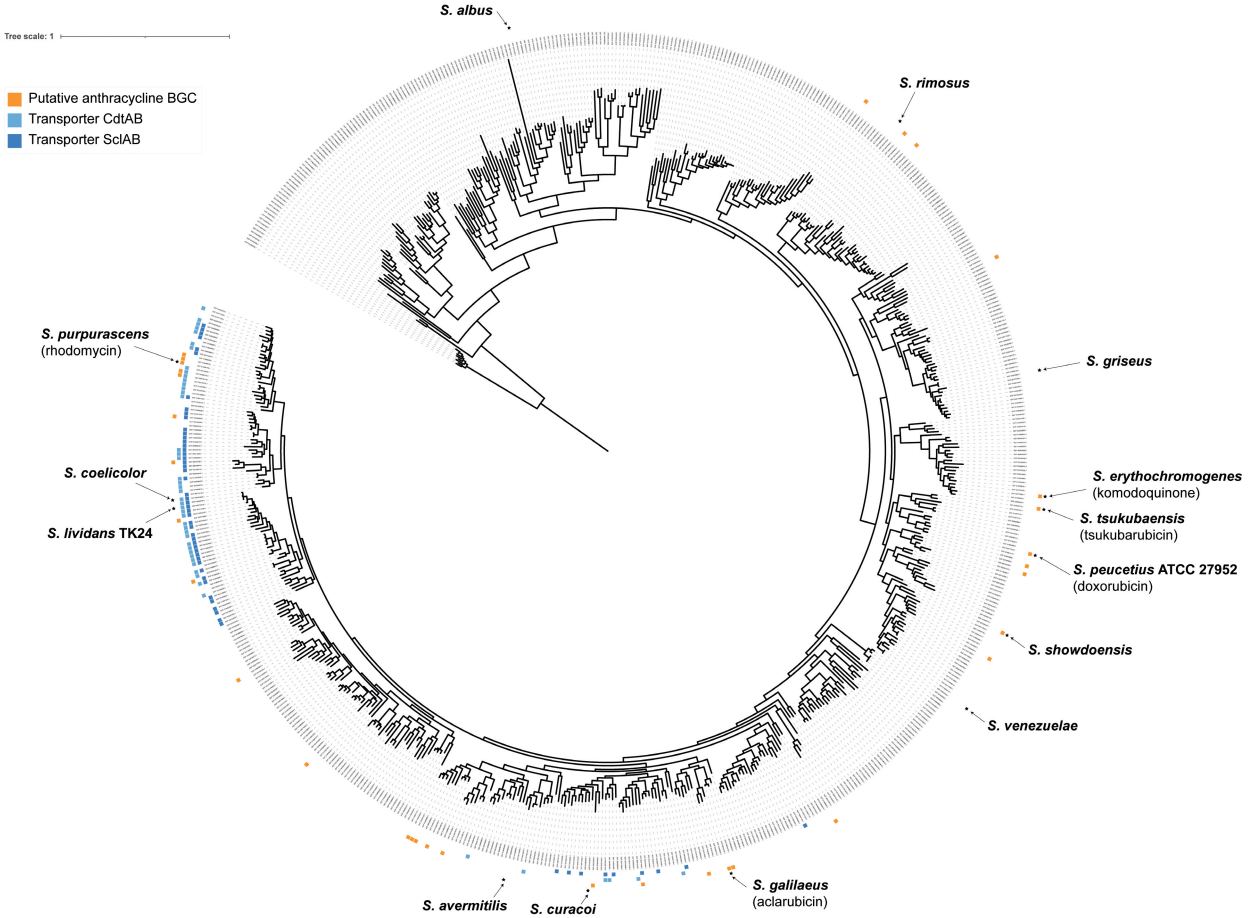


Figure 8. Distribution of CdtAB and SclAB transporters and correlation to putative anthracycline BGCs in actinomycetes. A maximum likelihood phylogenetic tree was generated using 629 *Streptomycetaceae* genomes and eight reference *Oerskovia* species as outgroup obtained from the NCBI RefSeq database. The outer ring indicates strains containing a putative anthracycline BGC (in orange). The middle ring indicates strains that harbour a CdtAB homolog (in light blue), and the inner ring indicates the presence of a SclAB homolog (in dark blue). Known anthracycline producers, *Streptomyces* model strains, and other strains described in this study are indicated.

Subsequently, a detection rule was designed for the presence of transporters encoded by *cdtAB* and *sclAB* using 100 proteins homologous to SCO3417–3418 (orthologs of CdtAB) and SCO4359–4360 (orthologs of SclAB) of *S. coelicolor*. Out of the 629 genomes, 12% yielded a transporter homologous to either CdtAB or SclAB, with 4% of the genomes harbouring both types of transporters. Subsequently, we studied the phylogenetic relationship between the presence of an anthracycline BGC and the CdtAB and SclAB homologs. A maximum likelihood phylogenetic tree was constructed based on the 629 genome sequences. The genomes harbouring a putative anthracycline BGC were scattered across the phylogenetic tree (Figure 8). In contrast, genomes harbouring homologs of CdtAB and SclAB clustered in two distinct groups on the phylogenetic tree. Unsurprisingly, the majority of the transporters were detected in genomes closely related to *S. lividans* (Figure 8). Only six strains were found to simultaneously harbour a putative anthracycline BGC and one of the transporter loci elsewhere in the genome. All putative anthracycline BGCs harboured an ABC or MFS transporter, but these transporters were not closely related to CdtAB or SclAB.

Discussion

Anthracyclines are anticancer drugs that are widely used in the clinic. At the same time, anthracyclines also have antibiotic activity, and exhibit strong toxicity against a wide range of bacteria, including those that produce them. The Doxo-producer *S. peucetius* var. *caesius* is much more sensitive to DMdoxo compared to Doxo (Figure 1). This finding prompted further studies into anthracycline resistance mechanisms within actinomycetes. Screening of our in-house collection of actinomycetes revealed that while the strains exhibited varying sensitivity to Doxo, they were all highly sensitive to DMdoxo. This high sensitivity to DMdoxo was harnessed to conduct adaptive laboratory evolution of *S. lividans* TK24, which resulted in the activation of two cryptic transporters conferred significant resistance to anthracyclines. Constitutive expression of either of these transporters in the parental strain resulted in more than eight-fold increased resistance to both Doxo and DMdoxo.

Analysis of spontaneous mutants of *S. lividans* TK24 with enhanced resistance to DMdoxo revealed the transcriptional activation of two homologous ABC transporters. The expression of *cdtAB* is controlled by the downstream gene encoding a putative PadR-like transcriptional regulator, CdtR. The PadR-family represents a large, diverse, and relatively underexplored protein family among the one-component signal transduction systems. The archetypal PadR acts as a repressor of phenolic acid decarboxylates in Gram-positive bacteria[309]. Various members of the PadR family control the expression of multidrug efflux pumps. For example, LmrR controls the expression of *lmrCD*, encoding a major multidrug ABC transporter in *Lactococcus lactis*[310]. Similarly, LadR controls the expression of *mdrL*, encoding a multidrug MFS efflux pump[311]. Directed inactivation of *cdtR* via the introduction of a stop codon resulted in a phenotype similar to constitutive expression of *cdtAB*, implying that CdtR represses the transcription of *cdtAB*. PadR regulators are generally inactivated via the binding to ligands. In the case of CdtR, the

accumulation of spontaneous mutations activated the transcription of *cdtAB*. Anthracyclines did not elicit anthracycline resistance, and it is yet unknown what the ligand is for CdtR.

The second transporter, SclAB, is controlled by a TetR-like transcriptional regulator, SclR. The TetR family of transcriptional regulators is extensively characterised and is widely associated with antibiotic resistance and the regulation of genes encoding small-molecule transporters[312]. Prior research demonstrated that inactivation of *sclR* in *S. lividans* provides resistance to various compounds, including the macrolide spiramycin, daunorubicin and ethidium bromide[305]. Further studies also revealed a role of SclAB in resistance against the acyldepsipeptides, which are also macrolide antibiotics[313]. *S. coelicolor* harbours three TetR-regulated ABC-family transporters (see Supplemental Table S4)[305]. Deletion of each TetR regulatory gene (SCO1718, SCO4357 and SCO5384) resulted in increased production of actinorhodin and undecylprodigiosin, as well as mild resistance to different classes of antibiotics[305]. Deletion of SCO4358 (an ortholog of *sclR*) in *S. coelicolor* increased daunorubicin resistance from 6 $\mu g \cdot mL^{-1}$ to 10 $\mu g \cdot mL^{-1}$, which is much less than we observed for the *sclR* deletion mutant in TK24.

Our work indicates that both CdtAB and SclAB provide particularly strong resistance to anthracyclines. When we introduced expression cassettes containing *cdtAB* or *sclAB*, or disrupted *cdtR* or *sclR*, a more than eight-fold increase in resistance was observed to both Doxo and the stronger antibiotic DMdoxo. However, only a marginal increase in resistance was seen for the other antibiotics tested. This suggests that the transporters preferentially provide resistance to anthracyclines over other tetracyclic polyketides. This interpretation is further supported by the observation that the enhanced expression of these transporters offers a level of resistance comparable to that of the Doxo transporter, DrrAB. Both CdtAB and SclAB transporters are homologs of DrrAB, with CdtA and SclA share 51.4 and 51.1% sequence identity with DrrA, respectively. The two *S. lividans* transporters CdtA and SclA share 63.0% sequence identity (Table 2). This preliminary data suggests that both two transporters exhibit specificity for anthracyclines, although further studies should be performed to confirm this.

In addition to mutations in the two transporter loci, mutations were identified in the *mat* locus in the two parallel evolution lines of *S. lividans* TK24. These genes are involved in the biosynthesis of the exopolysaccharide PNAG, which forms a layer that covers the vegetative hyphae[302,306]. Originally discovered in a high-dilution rate chemostat evolution experiment, their inactivation might confer growth advantages in our evolution experiment with serial batch cultivation, where strains grow at the maximum growth rate[314]. Our results indicate that the mutations in the *mat* locus did not directly affect Doxo resistance; however, the positive effect of the deletion of *matAB* on the growth rate may have facilitated resistance development.

An important question is why *S. lividans* TK24 harbours two cryptic transporters that provide resistance to anthracyclines. In their natural environments, streptomycetes are confronted with a diverse array of natural products produced by other species[51,315]. To survive in such hostile environments, streptomycetes not only produce a diverse array of natural products,

but also acquire or evolve highly specific resistance elements against exogenous antibiotics[316]. Consequently, many streptomycetes harbour resistance mechanisms against multiple classes of antibiotics[317]. For example, the model organism *S. coelicolor* harbours specific resistance genes against vancomycin and chloramphenicol, which it does not produce itself. Two MFS efflux pumps (SCO7526 and SCO7662) provide chloramphenicol resistance, and the corresponding genes are constitutively expressed even in absence of chloramphenicol[318]. The vancomycin resistance cassette is regulated by a two-component system involving VanR and VanS, and is activated in presence of vancomycin[319,320]. Interestingly, in contrast to the chloramphenicol and vancomycin resistance mechanisms, the *cdtAB* and *sclAB* gene pairs were silent under the tested growth conditions, even in the presence of anthracyclines. The only way to activate the genes was by evolving resistant colonies by challenging *S. lividans* TK24 with high concentrations of DMdoxo. Our results show that apart from cryptic BGCs encoding undiscovered natural products, *Streptomyces* genomes also contain cryptic resistance mechanisms. This suggests that these organisms may hold a reservoir of untapped genetic potential, both in terms of antibiotic production and resistance mechanisms. It is important to note that antibiotic resistance often comes at a cost, with mutants typically showing reduced fitness[321,322], and we cannot rule out that the same holds for anthracycline resistance.

Bioinformatics analysis revealed the presence of genes encoding close homologs of the CdtAB and SclAB transporters in 12% of Streptomycetaceae reference genomes. Considering this high frequency of occurrence, we expect that their silence may be conditional; in other words, in nature these genes may be activated by an environmental signal. Alternatively, activation of the transporters may require random mutations that occur occasionally within a colony, resulting in resistance in a small part of the population. Some 5% of the selected actinomycete genomes contain a putative anthracycline BGC. This finding aligns with prior research that identified daunorubicin-like BGCs in 3.6% of 1110 selected *Streptomyces* genomes[168]. Thus, the existence of anthracycline transporters may be explained by the frequent occurrence of Actinobacteria that produce anthracyclines. The presence of anthracycline BGCs did not correlate with the presence of the transporter genes. Only six genomes were found to simultaneously harbour an anthracycline BGC and one of the transporter loci elsewhere in the genome. This suggests that the CdtAB and SclAB transporters function as a resistance mechanism against anthracyclines in the environment.

Self-resistance mechanisms against toxic natural products such as anthracyclines are typically encoded within the BGCs[57,323]. In the case of the CdtAB and SclAB transporters we failed to detect a direct correlation with anthracycline BGCs, suggesting that anthracycline resistance may be a more general trait of Actinobacteria. In addition, it should be noted that we identified wild-type streptomycetes with high resistance to anthracyclines but which lacked genes for the two transporters and anthracycline BGCs, and that we obtained spontaneous anthracycline-resistant mutants of *S. lividans* (line B) that exhibited strong resistance, but did not show enhanced expression of either of the transporter loci. These results suggest that actinomycetes harbour additional yet unidentified anthracycline resistance mechanisms. *S. venezuelae*

and *S. rimosus* showed surprisingly high resistance to Doxo, but neither strain harboured a putative anthracycline BGC or CdtAB-like and SclAB-like transporters in their genomes. We hypothesised that the jadomycin BGC in *S. venezuelae* may be involved in Doxo resistance, because of their structural similarities. However, deletion of the jadomycin BGC in *S. venezuelae* did not affect resistance to Doxo. Thus, another anthracycline resistance mechanism must be operational. Screening of our MBT collection of Actinobacteria revealed that a substantial number of actinomycetes exhibited resistance to relatively high concentrations of Doxo, whereby a spectrum of resistance levels was observed, with some strains growing at concentrations exceeding 200 µM. Some strains failed to develop in the presence of anthracyclines, while others were unaffected and developed aerial hyphae even at the highest tested concentrations. Els4, Hm84 and MBT74 demonstrated significant resistance to Doxo. Like in *S. venezuelae*, no putative anthracycline BGC or CdtAB-like and SclAB-like transporters were detected in their genomes, again suggesting alternative mechanisms of anthracycline resistance.

In the DMdoxo-evolved *S. peucetius* isolates, two distinct frameshift mutations occurred in the parallel evolution lines in *fusA*. The gene encodes elongation factor G, which is widely conserved and is an essential factor for ribosome translocation and recycling[307]. Elongation factor G is the target of fusidic acid, and mutations in *fusA* occur spontaneously in presence of fusidic acid. We are currently investigating whether these mutations are responsible for the increased anthracycline resistance of the *S. peucetius* isolates.

Interestingly, a DMdoxo-evolved isolate of *S. showdoensis* was exceptionally resistant to both Doxo and DMdoxo, and the mutation did not noticeably alter growth or development of the strain. No CdtAB-like and SclAB-like transporters could be detected within the *S. showdoensis* genome, but we detected a putative anthracycline BGC. The most closely related BGCs are those that encode the biosynthesis of komodoquinone (MiBIG cluster BGC0001815, 65% similarity) and of cinerubin B (MiBIG cluster BGC0000212, 57% similarity)[298]. The BGC contains a putative ABC transporter, which could be responsible for the strong anthracycline resistance of this strain but warrants further investigation.

In conclusion, our findings revealed the presence of anthracycline transporters within actinomycetes that do not produce anthracyclines themselves. Furthermore, our results show that additional resistance mechanisms remain to be identified in other anthracycline resistance strains. These results indicated that cryptic resistance mechanisms can be activated upon prolonged exposure to toxic compounds.

Materials and Methods

Bacterial strains and growth conditions

The bacterial strains used in this work are listed in Supplementary Table S1. *E. coli* strains JM109[281] and ET12567 harbouring pUZ8002[282] were used for routine cloning and conjugation of

plasmids to *Streptomyces*, respectively. *E. coli* strains were cultivated at 37 °C on Luria-Bertani (LB) agar plates or in LB medium supplemented with the appropriate antibiotics.

Strains *S. coelicolor* A3(2), *S. coelicolor* M145, *S. lividans* 1326 and *S. lividans* TK24[1] were obtained from the John Innes Centre strain collection. *Streptomyces* strains *S. peucetius* var. *caesius* ATCC 27952, *S. galilaeus* ATCC 31615, *S. venezuelae* ATCC 10712 and *S. rimosus* ATCC 10970, *S. showdoensis* ATCC 15227 and *S. curacoi* DSM 40107 were obtained from the DSMZ strain collection. Other strains were obtained from the Leiden University strain collection, consisting of strains previously isolated from soil samples of Qinling Mountains, Shanxi province, China from the Himalaya mountain range in Nepal or from Dutch dune soil[294], from a wastewater treatment plant[295] or from sponges[296].

All media and routine *Streptomyces* techniques have been described previously[1]. Soy flour mannitol (SFM) agar plates were used for the collection of spores, conjugation experiments and phenotypical characterisation. Tryptone soy broth (TSB) was used for liquid cultivation of *Streptomyces* strains. The growth media were supplemented with 20 $\mu g \cdot mL^{-1}$ thiostrepton when required. Cultures were grown in a total volume of 20 mL of liquid medium in 100 mL Erlenmeyer flasks equipped with metal coils. Shake flasks were incubated in an orbital shaker with a 2-inch orbit at 200 rpm at 30 °C. In cases of poor sporulation, mycelial stocks were prepared as an alternative to spore stocks. Strains were cultivated in TSB medium for 2 days, the biomass was washed with 10.3% (w/v) sucrose, resuspended in 20% (w/v) glycerol, and stored at -80 °C. To study the morphology of *Streptomyces* strains in liquid environments, strains were cultivated in TSB medium without metal coils, and imaged using a Zeiss Axio Lab A1 upright microscope equipped with an Axiocam MRc camera.

Construction of plasmids and strains

All plasmids described in this work are listed in Supplementary Table S2 and oligonucleotides in Supplementary Table S3. Plasmid maps were generated using SnapGene 6.0 (Supplementary Figure S1).

Constructs for expression of transporter genes

For the expression of biosynthetic genes, the integrative vector pSET152[274] was employed. pSET152 integrates into the attachment sites within the *Streptomyces* genome for bacteriophage φC31 and harbours an apramycin resistance cassette.

To generate a construct for expression of *cdtA* (SLIV_RS20700) and *cdtB* (SLIV_RS20705) from *Streptomyces lividans* TK24 (Supplementary Table S4), the coding sequence (+0/+1782 relative to the start codon of *cdtA*) was amplified by primers MH401/MH402 from genomic DNA and digested using NdeI/XbaI. A DNA fragment containing the *ermE** promoter[273] was digested from pHM10a[324] using EcoRI/NdeI. The two DNA fragments were simultaneously cloned into EcoRI/XbaI-digested pSET152 to generate pGWS1441.

To generate a construct for expression of *sclA* (SLIV_RS16660) and *sclB* (SLIV_RS16655) from *S. lividans* TK24 (Supplementary Table S4), the coding sequence (+0/+1906 relative to the start codon of *sclA*) was amplified by primers MH403/MH404 from genomic DNA. A DNA fragment containing the pSET152 backbone and the *ermE** promoter was excised from pGWS1441 using NdeI/XbaI. The coding sequence of *sclAB* was cloned into linearised *ermE**p::pSET152 via Gibson assembly[277] to generate pGWS1442. To generate a construct for expression of *drrA* and *drrB* from *Streptomyces peucetius* var. *caesius* ATCC 27952 (further referred to as *S. peucetius*, Supplementary Table S4), the coding sequence (+0/+1897 relative to the start codon of *drrA*) was amplified by primers MH405/MH406 from *S. peucetius* genomic DNA and digested using NdeI/XbaI. A DNA fragment containing the pSET152 backbone and the *ermE** promoter was excised from pGWS1441 using NdeI/XbaI. The PCR product containing *drrAB* was cloned into *ermE**p::pSET152 to generate pGWS1443.

Constructs for gene disruption

The CRISPR cytidine deaminase-based base editing system (CRISPR-cBEST) was employed for gene disruption[304]. Firstly, the *tipA* promoter in pCRISPR-cBEST[304] was replaced with the *gapdh* promoter. Therefore, a fragment containing the *ermE** promoter, a sgRNA scaffold and the *gapdh* promoter was digested from the previously published construct pGWS1370[325] using NcoI/NdeI, and subsequently cloned into pCRISPR-cBEST to generate pGWS1384. Consequently, the expression of Cas9 nickase (D10A), APOBEC-1 (cytidine deaminase) and UGI (uracil-DNA glycosylase inhibitor) within pGWS1384 was regulated by the *gapdh* promoter instead of the *tipA* promoter.

Inactivation of *cdtR* (SLIV_RS20695) was achieved by creating a stop codon at nucleotide position 40 (Q14*). A *cdtR*-targeting spacer was introduced into NcoI-linearised pGWS1384 via Gibson assembly[277] using the bridging oligonucleotide MH407, generating pGWS1444. Similarly, to inactivate *cdtA* (SLIV_RS20700) by creating a stop codon at a nucleotide position 526 (W178*), oligonucleotide MH408 was introduced into pGWS1384, generating pGWS1445. Furthermore, to inactivate *sclR* (SLIV_RS16665) by creating a stop codon at a nucleotide position 61 (W21*), oligonucleotide MH409 was introduced into pGWS1384, generating pGWS1446.

Following conjugation, individual exconjugants were randomly picked and streaked on SFM agar plates supplemented with 50 μg·mL^{-1} apramycin. Colonies were then streaked again on SFM plates without antibiotics, after which single colonies were selected. Genomic DNA was then extracted, and the coding sequence of *cdtR*, *cdtA* or *sclR* was PCR-amplified using primers MH410/MH411, MH412/MH413 and MH414/MH415, respectively. The PCR products were sequenced to confirm the mutations. The spacers used to create the mutations were generated using CRISPY-web[326], and are listed in Supplementary Table S3.

Construct for deletion of the jadomycin BGC

The strategy for creating deletion mutants is based on the unstable multicopy vector pWHM3[269], as described previously[271]. In this approach, we used the derivative pWHM3-oriTthat harbours *oriT*

to allow for its conjugative transfer[280]. Briefly, a knock-out construct was generated containing an apramycin resistance cassette that is flanked by the upstream and downstream regions of the targeted genes. The about 1.5 kb flanking regions of the jadomycin BGC (upstream of *jadR3* and downstream of *jadR**[300]) were amplified from *S. venezuelae* ATCC 10712 genomic DNA using primers MH416/MH417 and MH418/MH419. The apramycin resistance gene *aacC4* flanked by two *loxP* recognition sites was amplified using primers MH420/MH421. The three DNA fragments were subsequently cloned into EcoRI/HindIII-linearised pWHM3-oriT using Gibson assembly[277]. The resulting knock-out construct was designated as pGWS1447. Subsequently, the construct was introduced into *Streptomyces venezuelae* ATCC 10712 via conjugation. The desired double-crossover mutant was selected by resistance against apramycin (50 $\mu g \cdot mL^{-1}$) and sensitivity to thiostrepton (20 $\mu g \cdot mL^{-1}$). The successful replacement of the jadomycin BGC by the apramycin resistance cassette was confirmed by Sanger sequencing of the PCR product of primers MH422/MH423.

Microbial inhibition assays

To investigate the resistance to Doxo and DMdoxo in nature, we assessed our laboratory collection of actinomycetes (see section on bacterial strains above). For screening purposes, 2 µL of highly concentrated spore or mycelial stock was spotted onto SFM agar plates supplemented with increasing Doxo (Accord Healthcare Limited, UK) or DMdoxo[16] concentrations. For individual testing of *S. lividans* strains, 5 µL of spore or mycelial stock was spotted at a concentration of $1.0 \cdot 10^4$ colony forming units (CFU) per spot. After 3 to 6 days of incubation at 30 °C, growth was examined visually. Additionally, the assay was conducted using rifampicin (Boehringer Ingelheim, Germany), tetracycline hydrochloride (Duchefa Biochemie BV, Netherlands), and thiostrepton.

Adaptive laboratory evolution

For evolution experiments, strains were inoculated in 20 mL of TSB medium supplemented with a sub-inhibitory concentration of DMdoxo[16]. Once the culture reached stationary growth, an aliquot was streaked on SFM agar plates supplemented with increasing DMdoxo concentrations. Biomass from the highest concentration that supported growth was subsequently inoculated in fresh medium with the corresponding DMdoxo concentration. The process was repeated until the strain sustained growth in TSB medium supplemented with 175 µM DMdoxo. Spore or mycelial stocks were prepared from single colony isolates and the evolved strains were designated by "-Evo" (Supplementary Table S1).

MTP cultivation

Microtiter plate (MTP) cultivation was performed in a 48-well FlowerPlate (MTP-48-BOH2, Beckman Coulter, Brea, CA, USA) covered by a gas-permeable sealing foil for reduced evaporation (F-GPR-10, Beckman Coulter) in an automated cultivation device (BioLector II, Beckman Coulter). For MTP cultivation, 1 mL of TSB medium supplemented with increasing DMdoxo concentrations was inoculated with $1.0 \cdot 10^6$ $CFU \cdot mL^{-1}$ pregerminated spores. Spore stocks were pregerminated in 2xYT medium[1] for 5 hours. The shaking frequency was set to 1200 rpm, temperature was

controlled at 30 °C, and relative humidity was controlled at 85%. Back-scattered light (gain 6), pH and DO were recorded at a 15-min interval. All experiments were performed at least in triplicate.

Whole genome extraction and sequencing

Genomic DNA was extracted using phenol-chloroform extraction as described previously[1]. Sequencing was outsourced to Novogene (Cambridge, UK). PCR-free library preparation was performed to avoid sequencing biases. Sequencing was performed on an Illumina NovaSeq 6000 in paired-end mode with a read length of 150 bp.

Genome annotation of *Streptomyces* sp. Els4 and *Streptomyces* sp. Hm84 was performed using Prokka v.1.14.6[327]. AntiSMASH 7.0[297] was used under the default settings to predict BGCs in the genomic sequences of Els4, Hm84 and MBT74, which were annotated using the MiBIG database[298]. Genomic variant detection of evolved isolates of *S. lividans* TK24 and *S. peucetius* was performed using *breseq* v.0.38.1[301]. The genomes of *S. lividans* TK24 (accession NZ_CP009124.1) and *S. peucetius* var. *caesius* ATCC 27952 (accession NZ_CP022438.1) were downloaded from the NCBI database and used as reference.

RNA extraction and sequencing

TK24 and TK24-EvoA1 were streaked on minimal medium[1] agar plates supplemented with 0.5% mannitol and 1% glycerol (w/v) covered with cellophane disks at 30 °C for 24 h or 64 h. Biomass was harvested and RNA was isolated as described previously using Kirby mix[1]. RNA sequencing was outsourced to Novogene (Cambridge, UK). Ribosomal RNA was first removed from the samples and cDNA was synthesised from the purified RNA samples. Sequencing of the cDNA was performed on an Illumina NovaSeq 6000 in paired-end mode with a read length of 150 bp. Clean reads were mapped to the *S. lividans* TK24 reference sequence (accession NZ_CP009124.1). DESeq2 v.1.34.0[303] was used for differential expression analysis.

Phylogenetic analysis

The reference genomes of 625 members of the family Streptomycetaceae were downloaded from NCBI RefSeq (downloaded April 21st, 2023). The genomes of *Streptomyces coelicolor* M145 (accession GCA_000203835), *S. lividans* TK24 (accession GCF_000739105), *S. peucetius* var. *caesius* ATCC 27952 (accession GCF_002777535) and *S. venezuelae* ATCC 10712 (accession GCF_008639165) were added to the set, creating a total of 629 genomes.

To create a new anthracycline detection rule, we focused our search on four individual marker genes from *S. peucetius* (i.e. *dpsA*, *dpsB*, *dnrS* and *dnrQ*). Both *dpsA* and *dpsB* are captured by antiSMASH's[297] existing type II polyketide synthase (T2PKS) rule. To determine homologs of DnrS and DnrQ, percentage amino acid identity cutoffs were predetermined based on individual BLASTp searches against a library of experimentally verified anthracycline BGCs[266]. For profile hidden Markov model (pHMM) construction, we included homologs that shared at least 80% sequence coverage and met the resulting amino acid identity cutoffs of 47% (DnrS) and 36%

(DnrQ). The retrieved amino acid sequences were aligned with MUSCLE v.3.8.1551[328] and profiles were built using the hmmbuild tool from the HMMER v.3.3.2 suite[329] (http://hmmer.org/). A positive hit was determined when the criteria of antiSMASH's T2PKS rule was met, combined with either a DnrS or a DnrQ homolog encoding gene. Known anthracycline cluster homologs were manually searched using the hmmsearch tool from the HMMR v.3.3.2 suite to determine a bit score cutoff for true and false positive hit delineation. Using the same methodology, a detection rule was determined for the presence of homologs of *cdtAB* or *sclAB* using 100 proteins homologous to SCO3417–3418 (orthologs of CdtAB) and SCO4359–4360 (orthologs of SclAB) of *S. coelicolor*.

A maximum likelihood phylogenetic tree was constructed based on the 629 genome sequences. Eight reference genomes of Oerskovia species were used as outgroup (downloaded from NCBI RefSeq). The phylogenetic tree was generated with PhyloPhlAn v3.0[330], using DIAMOND[331] as mapping tool, MAFFT[332] for the multiple sequence alignment, trimAl[333] for alignment trimming, and RAxML[334] for generating a phylogenetic tree. iTOL[335] was used for visualisation.

Table S1. Strains used in this study.

Strain	Description	References
Escherichia coli JM109	For routine plasmid maintenance and cloning	[281]
Escherichia coli ET12567/pUZ8002	Methylation-deficient strain for conjugating plasmids into *Streptomyces*	[282]
Streptomyces coelicolor A3(2)	Wild-type strain	[1]
Streptomyces coelicolor M145	*S. coelicolor* A3(2) SCP1$^-$ SCP2$^-$	[1]
Streptomyces lividans 1326	Wild-type strain, also known as *S. lividans* 66	[1]
Streptomyces lividans TK24	*S. lividans* 1326 SLP2$^-$ SLP3$^-$	[1]
Streptomyces venezuelae ATCC 10712	Wild-type strain, producer of jadomycin	ATCC
Streptomyces galilaeus ATCC 31615	Wild-type strain, producer of aclacinomycins	ATCC
Streptomyces rimosus ATCC 10970	Wild-type strain, producer of tetracyclines	ATCC
Streptomyces peucetius var. *caesius* ATCC 27952	Wild-type strain, producer of daunorubicin and doxorubicin	[8]
Streptomyces showdoensis ATCC 15227	Wild-type strain	ATCC
Streptomyces curacoi DSM 40107	Wild-type strain	ATCC
Streptomyces sp. Els4	*Streptomyces* isolated from soil sample from Elswout, The Netherlands	Laboratory collection
Streptomyces sp. Els22	*Streptomyces* isolated from soil sample from Elswout, The Netherlands	Laboratory collection
Streptomyces sp. Els46	*Streptomyces* isolated from soil sample from Elswout, The Netherlands	Laboratory collection
Streptomyces sp. Hm84	*Streptomyces* isolated from soil sample from Himalayas, Nepal	[294]
Streptomyces sp. QL25	*Streptomyces* isolated from soil sample from Qinling Mountains, China	[294]
Streptomyces sp. MBT74	*Streptomyces* isolated from soil sample from Qinling Mountains, China	[294]
S. coelicolor-Evo	Evolved from *S. coelicolor* A3(2)*	This work
S. galilaeus-Evo	Evolved from *S. galilaeus**	This work

[continued on next page]

Table S1. *[continued]*

Strain	Description	References
S. showdoensis-Evo	Evolved from *S. showdoensis**	This work
S. curacoi-Evo	Evolved from *S. curacoi**	This work
S. peucetius-Evo	Evolved from *S. peucetius**	This work
TK24-EvoA1	Evolved from TK24*	This work
TK24-EvoB1	Evolved from TK24*	This work
TK24-EvoB2	Evolved from TK24*	This work
TK24-EvoB3	Evolved from TK24*	This work
TK24-EvoB4	Evolved from TK24*	This work
MAG401	TK24 pGWS1441 (*cdtAB*)	This work
MAG402	TK24 pGWS1442 (*sclAB*)	This work
MAG403	TK24 pGWS1443 (*drrAB*)	This work
MAG404	TK24 Δ*cdtR*	This work
MAG405	TK24 Δ*sclR*	This work
MAG406	TK24 Δ*cdtR* Δ*sclR*	This work
MAG407	TK24 Δ*cdtA*	This work
MAG408	TK24-EvoA1 Δ*cdtA*	This work
GAD05	*S. lividans* 1326 Δ*matAB*	[306]
MAG409	*S. venezuelae* ΔjadomycinBGC	This work

* Isolated from evolution experiment with DMdoxo.

Table S2. Plasmids used in this study.

Plasmid	Description	References
pSET152	*E. coli*/*Streptomyces* shuttle vector, harbouring *attP* site and integrase for phage φC31 for stable integration into the chromosomal *attB* site of *Streptomyces*, Apra^R	[274]
pWHM3-oriT	*E. coli*/*Streptomyces* shuttle vector, high copy number in *E. coli*, harbouring *oriT* site for conjugative transfer in the NdeI site, Amp^R, Thio^R	[280]
pCRISPR-cBEST	Empty vector for cytidine deaminase based base editing, Apra^R, Thio^R	[304]
pGWS1370	pSET152-derivative harbouring *tipA* promoter, Apra^R	[325]
pGWS1384	pCRISPR-cBEST-derivative with *gapdh* promoter instead of *tipA* promoter, Apra^R, Thio^R	This work
pGWS1441	pSET152-derivative with *S. lividans cdtA* and *cdtB* under control of the *ermE** promoter, Apra^R	This work
pGWS1442	pSET152-derivative with *S. lividans sclA* and *sclB* under control of the *ermE** promoter, Apra^R	This work
pGWS1443	pSET152-derivative with *S. peucetius drrA* and *drrB* under control of the *ermE** promoter, Apra^R	This work
pGWS1444	pGWS1384-derivative with a spacer targeting *cdtR* Q49, Apra^R, Thio^R	This work
pGWS1445	pGWS1384-derivative with a spacer targeting *cdtA* W178, Apra^R, Thio^R	This work
pGWS1446	pGWS1384-derivative with a spacer targeting *sclR* W21, Apra^R, Thio^R	This work
pGWS1447	pWHM3-oriT-derivative with the flanking regions of the *S. venezuelae* jadomycin BGC interspersed with the Apra^R-*loxP* cassette, Amp^R, Thio^R, Apra^R	This work

Table S3. Oligonucleotides used in this study.

Primer	Sequence (5' to 3')*
MH401	GATCGAATTCCATATGACAGTGGCCGACGCGGCG
MH402	GATCAAGCTTTCTAGAGCAGAGGTGCCCGTCCCTCG
MH403	CCACTCCACAGGAGGACCCATATGAGCGAGCGACACGCGGT
MH404	GCTTGGGCTGCAGGTCGACTCTAGAGTGGAGATCCACCGCTCCCC
MH405	GATCGAATTCCATATGAACACGCAGCCGACACG
MH406	GATCAAGCTTTCTAGACTCACACCCCCTCAACGACG
MH407	CGGTTGGTAGGATCGACGGCCGCCAGCACGGGCGGGCCCAGTTTTAGAGCTAGAAATAGC
MH408	CGGTTGGTAGGATCGACGGCCCGAGTCCCACACCTCGGCGGTTTTAGAGCTAGAAATAGC
MH409	CGGTTGGTAGGATCGACGGCGGTGTCCCACAACAGTTCGAGTTTTAGAGCTAGAAATAGC
MH410	ATGTCAGCGATCCGTCTCCT
MH411	CCGAGTGGACCCAGTAGTTC
MH412	CCGGCAGAACCTGGAGATGT
MH413	CCTTGAGTTCGTCCGCCGTG
MH414	GTCCCCCTTCCGTTCCCTTACTGA
MH415	TGGTTGACCTCCAGCAGCCAG
MH416	GTTGTAAAACGACGGCCAGTGAATTCGTGGATGTCCTCGTCGTTGA
MH417	CATCACCTCTAGACTCAGTGCCACAAGCGTCTA
MH418	CATCTCTAGATGTTCGTACTTCCTGGTGGC
MH419	AGCTATGACCATGATTACGCCAAGCTTGGTAGAAGCCCGACATACCG
MH420	TTGTGGCACTGAGTCTAGAGGTGATGGATAACTTCGTATAGCAT
MH421	AAGTACGAACATCTAGAGATGCGCGATAACTTCGT
MH422	GCCGATACAGGTCGAAGTCC
MH423	GACGCGATCTTCTCGGACC

* Restriction sites used for cloning are presented in bold face: CATATG, NdeI; TCTAGA, XbaI. Spacers used for CRISPR base editing are underlined.

Table S4. Origin and function of genes and enzymes used or discussed in this study.

Gene	Enzyme	Size (nt/aa)	Locus tag*	StrepDB SLI+	StrepDB SCO+	Catalytic function
cdtR	CdtR	642/213	SLIV_RS20695	SLI_3762	SCO3419	PadR-family transcriptional regulator
cdtA	CdtA	942/313	SLIV_RS20700	SLI_3761	SCO3418	DrrA-like ABC transporter (ATP-binding subunit)
cdtB	CdtB	783/260	SLIV_RS20705	SLI_3760	SCO3417	DrrB-like ABC transporter (permease subunit)
sclR	SclR	807/268	SLIV_RS16665	SLI_4593	SCO4358	TetR-family transcriptional regulator
sclA	SclA	1011/336	SLIV_RS16660	SLI_4594	SCO4359	DrrA-like ABC transporter (ATP-binding subunit)
sclB	SclB	843/280	SLIV_RS16655	SLI_4595	SCO4360	DrrB-like ABC transporter (permease subunit)
		705/234	SLIV_RS29140	SLI_2021	SCO1718	TetR-family transcriptional regulator
		999/332	SLIV_RS29135	SLI_2022	SCO1719	DrrA-like ABC transporter (ATP-binding subunit)
		816/271	SLIV_RS29130	SLI_2023	SCO1720	DrrB-like ABC transporter (permease subunit)
		642/213	SLIV_RS11605	SLI_5652	SCO5384	TetR-family transcriptional regulator
		783/260	SLIV_RS11610	SLI_5651	SCO5383	DrrA-like ABC transporter (ATP-binding subunit)
		750/249	SLIV_RS11615	SLI_5650	SCO5382	DrrB-like ABC transporter (permease subunit)
drrA	DrrA	993/330	CGZ69_RS24655	SLI_4076	SCO3824	ABC transporter (ATP-binding subunit)
drrB	DrrB	852/283	CGZ69_RS24650	SLI_4077	SCO3825	ABC transporter (permease subunit)

* Gene locus tags refer to the published reference genome of *S. lividans* TK24 (accession NZ_CP009124.1) and *S. peucetius* var. *caesius* ATCC 27952 (accession NZ_CP022438.1).

\+ Gene annotation in the *S. lividans* 1326 genome (SLI) and closest homologous gene in the *S. coelicolor* genome (SCO) based on the nomenclature of the StrepDB database (http://strepdb.streptomyces.org.uk).

Table S5. Genomic features of *Streptomyces* sp. Els4 and *Streptomyces* sp. Hm84.

	Els4	Hm84
Number of contigs	164	163
Largest contig	319,936	506,368
Total length	8,870,031	9,455,732
N50	125,962	118,908
CDS	7,634	8,242
rRNAs	6	6
tRNAs	89	83

Table S6. BGCs detected in the genome of *Streptomyces* sp. Els4 using antiSMASH 7.0.

Protocluster	Type	Most similar known BGC*
1	RiPP-like	-
2	T2PKS, oligosaccharide, NRPS	warkmycin (97%)
3	T1PKS, NRPS	-
4	NRPS-like, lanthipeptide-class-iv, transAT-PKS	cycloheximide (66%)
5	T1PKS	-
6	terpene, T1PKS, NRPS-like	-
7	NRPS	-
8	NRPS, NRPS-like	-
9	RiPP-like	-
10	melanin	melanin (100%)
11	T3PKS, NRPS	-
12	ectoine, butyrolactone	-
13	arylpolyene	-
14	lanthipeptide-class-iii	-
15	terpene	geosmin (100%)
16	linaridin	-
17	lanthipeptide-class-ii, lanthipeptide-class-iii	-
18	NI-siderophore	desferrioxamin B (80%)
19	terpene	-
20	NRPS	-
21	terpene	hopene (69%)
22	ectoine	ectoine (100%)
23	butyrolactone	-
24	NRPS, arylpolyene, ladderane	skyllamycin (52%)
25	T1PKS, other	-
26	NRP-metallophore, NRPS	coelichelin (90%)
27	NRPS, T1PKS	SGR PTMs (100%)
28	RiPP-like	-

[continued on next page]

Table S6. *[continued]*

Protocluster	Type	Most similar known BGC*
29	NI-siderophore	-
30	terpene	-
31	transAT-PKS, PKS-like	-
32	thiopeptide, LAP	-
33	terpene	isorenieratene (100%)
34	T3PKS	naringenin (100%)
35	NRPS	-
36	melanin	melanin (100%)
37	NRPS, NRP-metallophore	griseobactin (84%)
38	NRPS	-

* The most closely related known BGC is reported when at least 50% of the genes exhibit similarity.

Table S7. BGCs detected in the genome of *Streptomyces* sp. Hm84 using antiSMASH 7.0.

Protocluster	Type	Most similar known BGC*
1	RiPP-like	-
2	terpene	-
3	RiPP-like	-
4	siderophore	-
5	T1PKS	-
6	lanthipeptide-class-iii	-
7	NRPS, T1PKS, NRPS-like	-
8	siderophore	desferrioxamin (83%)
9	NRPS, NAPAA	-
10	siderophore	-
11	hglE-KS, T1PKS	-
12	terpene	geosmin (100%)
13	T2PKS	spore pigment (83%)
14	melanin	-
15	RRE-containing	-
16	nucleoside	-
17	LAP, thiopeptide	-
18	ectoine	ectoine (100%)
19	T3PKS	-
20	NAPAA	-
21	NRPS	-
22	terpene	albaflavenone (100%)
23	NRPS	-
24	RiPP-like	-

[continued on next page]

Table S7. *[continued]*

Protocluster	Type	Most similar known BGC*
25	terpene	carotenoid (63%)
26	T3PKS	alkylresorcinol (100%)
27	melanin	melanin (71%)
28	terpene	hopene (84%)
29	indole	-
30	T1PKS, PKS-like, NRPS-like	-
31	butyrolactone	-
32	T1PKS, ectoine	-
33	T1PKS, butyrolactone	-
34	butyrolactone	-
35	T1PKS	-
36	T1PKS	-
37	T2PKS	jadomycin (85%)

* The most closely related known BGC is reported when at least 50% of the genes exhibit similarity.

Table S8. BGCs detected in the genome of *Streptomyces* sp. MBT74 using antiSMASH 7.0.

Protocluster	Type	Most similar known BGC*
1	T2PKS	spore pigment (83%)
2	RiPP-like	-
3	phenazine	-
4	melanin	-
5	NAPAA	-
6	NI-siderophore	-
7	NRPS	-
8	terpene	albaflavenone (100%)
9	T3PKS	flaviolin (100%)
10	NRPS-like, T1PKS, NRPS	-
11	ectoine	ectoine (100%)
12	RiPP-like	-
13	terpene	geosmin (100%)
14	NI-siderophore	desferrioxamin (83%)
15	T1PKS	-
16	thiopeptide, LAP	-
17	T3PKS	alkylresorcinol (100%)
18	RiPP-like	-
19	NI-siderophore	-
20	terpene	hopene (61%)
21	butyrolactone	-

* The most closely related known BGC is reported when at least 50% of the genes exhibit similarity.

Table S9. Putative anthracycline BGCs detected in the reference genomes of 625 members of the family Streptomycetaceae.

Location	Organism*	Most similar known BGC (similarity)
NZ_AGBF01000013.1 :3475–83811	*S. zinciresistens* K42	cytorhodin (82%)
NZ_BMML01000021.1 :144082–218040	*S. fuscichromogenes* CGMCC 4.7110	aranciamycin (78%)
NZ_BMQK01000002.1 :535976–616788	*S. ruber* JCM 3131	cytorhodin (50%)
NZ_BMSO01000019.1 :12468–93240	*S. bellus* JCM 4292	cosmomycin D (60%)
NZ_BMTM01000017.1 :10575–103634	*S. janthinus* JCM 4387	cytorhodin (84%)
NZ_BMUK01000008.1 :375570–469210	*S. purpurascens* JCM 4509	cytorhodin (84%)
NZ_BMUP01000006.1 :475604–568638	*S. violarus* JCM 4534	cytorhodin (84%)
NZ_BMVC01000018.1 :18422–109983	*S. finlayi* JCM 4637	kosinostatin (77%)
NZ_BMVY01000030.1 :0–66622	*S. tauricus* JCM 4837	cinerubin B (100%)
NZ_BMWA01000001.1 :309989–403064	*S. viridiviolaceus* JCM 4855	cytorhodin (82%)
NZ_BMWD01000002.1 :353044–441234	*S. fructofermentans* JCM 4956	cinerubin B (100%)
NZ_BNBF01000007.1 :191587–279349	*S. capoamus* JCM 4253	cinerubin B (100%)
NZ_CP020700.1 :5211320–5289097	*S. tsukubensis* NRRL 18488	komodoquinone B (97%)
NZ_CP023693.1 :6171688–6259901	*S. cinereoruber* ATCC 19740	cytorhodin (82%)
NZ_CP023694.1 :7072200–7152971	*S. coeruleorubidus* ATCC 13740	cosmomycin D (62%)
NZ_CP023703.1 :6303449–6391243	*S. galilaeus* ATCC 14969	cinerubin B (100%)
NZ_CP029188.1 :6338721–6433635	*S. tirandamycinicus* HNM0039	cosmomycin C (100%)
NZ_FMZK01000002.1 :69913–150677	*S. prasinopilosus* CGMCC 4.3504	cytorhodin (47%)
NZ_JAGPYQ010000001 .1:2767761–2855941	*S.* sp. BH-SS-21	cinerubin B (100%)
NZ_JAIQLH010000037.1 :0–56893	*S. huiliensis* SCA2-4	aranciamycin (78%)

[continued on next page]

Table S9. *[continued]*

Location	Organism*	Most similar known BGC (similarity)
NZ_JAPELN010000001.1 :6826013–6913829	*S. bobili* NBC_00018	cinerubin B (100%)
NZ_JAPEPV010000002.1 :126993–202530	*S. viridodiastaticus* NBC_01548	kosinostatin (35%)
NZ_JNWJ01000033.1 :12534–95124	*S. yerevanensis* NRRL B-16943	griseorhodin A (93%)
NZ_JNZG01000006.1 :170654–255869	*S. erythrochromogenes* NRRL B-2112	komodoquinone B (100%)
NZ_JODM01000005.1 :177751–265519	*S. violaceorubidus* NRRL B-16381	cinerubin B (100%)
NZ_KQ948766.1 :0–76988	*S. griseoruber* DSM 40281	cinerubin B (100%)
NZ_KQ948995.1 :59575–152007	*S. resistomycificus* DSM 40133	steffimycin D (88%)
NZ_KZ679040.1 :471754–560086	*S. dioscori* A217	cinerubin B (100%)
NZ_LAQS01000005.1 :116538–203674	*S. showdoensis* ATCC 15227	komodoquinone B (65%)
NZ_NDXL01000001.1 :1980945–2061737	*S. kasugaensis* BCRC 12349	cytorhodin (49%)
NZ_SUMB01000006.1 :333894–423185	*S. piniterrae* jys28	griseorhodin A (87%)
NZ_VAWE01000001.1 :2640914–2721684	*S. marianii* ICN19	cosmomycin D (62%)

* *Streptomyces* abbreviated to *S.*

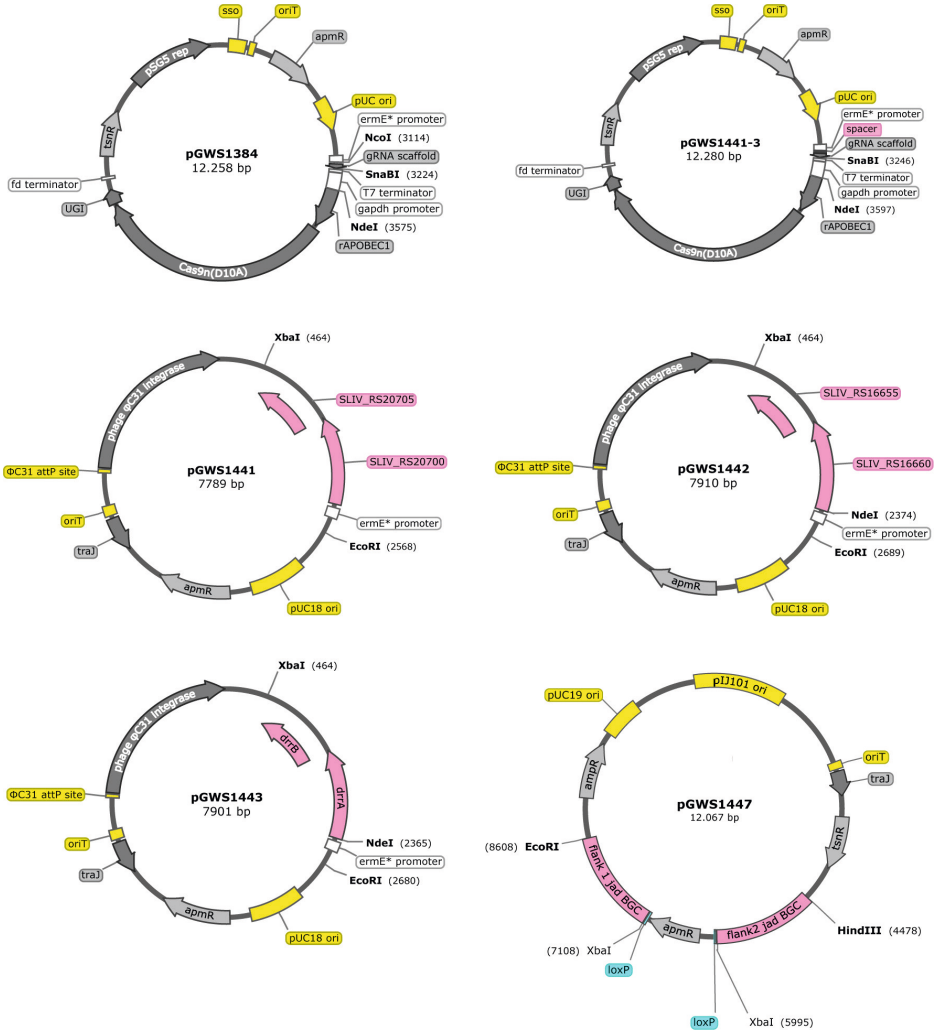


Figure S1. Plasmid maps of constructs used in this study. Restriction sites used for cloning are indicated. Resistance cassettes are abbreviated as: *ampR*, ampicillin; *apmR*, apramycin; *tsnR*, thiostrepton.

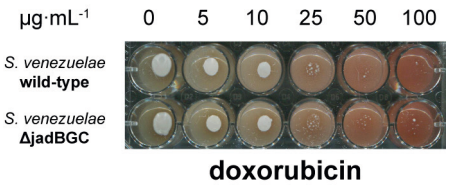


Figure S2. Impact of the jadomycin BGC deletion on doxorubicin resistance in *S. venezuelae*. Wild-type *S. venezuelae* and a mutant strain with the entire jadomycin BGC deleted (MAG409) were spotted on SFM agar plates supplemented with 5 to 100 µg·mL-1 (i.e. 9.2 to 184 µM) Doxo, and incubated at 30 °C for 3 days. Deletion of the jadomycin BCG did not affect resistance to Doxo.

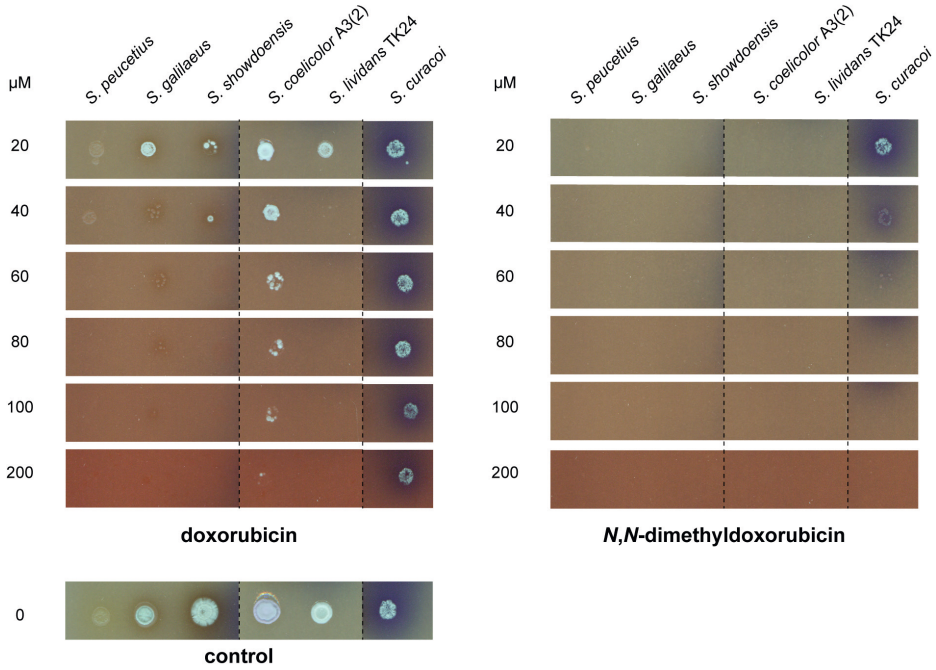


Figure S3. Evaluation of anthracycline resistance of parental strains used in evolution experiment. Parental strains of the evolution experiment were spotted at high density on SFM agar plates supplemented with 20 to 200 μM Doxo or DMdoxo, and incubated at 30 °C for 3 days.



N,N-dimethylated anthracyclines with improved antibiotic activity

Mandy B. Hulst, Michella M. Voet, Tanny J.K. van der Reijden, Dennis P.A. Wander, Peter H. Nibbering, Gilles P. van Wezel[†] and Jacques J.C. Neefjes[†]

[†] Corresponding authors.

Abstract

The sharp increase in infections associated with multi-drug resistant pathogens calls for alternatives for existing clinical antibiotics. A major issue that prevents clinical application of many antibiotic candidates is cytotoxicity. One example are members of the anthracycline polyketides, which are DNA-targeting drugs that while originally discovered as antibiotics, now find widespread clinical use as anticancer agents. Here we show that *N,N*-dimethylated anthracyclines, which have strongly reduced side effects, show improved activities as antibiotics. Screening a collection of structurally diverse anthracyclines against a panel of ESKAPE pathogens showed potent activity against Gram-positive bacteria. *N,N*-dimethylated variants had significantly improved antibacterial activity and also demonstrated moderate activity against Gram-negative *Acinetobacter baumannii*. *N,N*-dimethyldoxorubicin (compound **2**) and an *N,N*-dimethylated doxorubicin trisaccharide derivative (compound **6**) demonstrated the highest antimicrobial activity. These compounds exhibited a two-fold higher activity against methicillin-resistant *Staphylococcus aureus* (MRSA) compared to doxorubicin in phosphate buffered saline, and even 16-fold higher activity in pooled human plasma ($LC_{99.9}$ of 2 μM). A resistance development assay indicated that MRSA failed to develop resistance to *N,N*-dimethyldoxorubicin over 25 passages, indicating robust antimicrobial activity. These findings suggest that *N,N*-dimethylated anthracyclines hold promise as potential last-resort antibiotics in the battle against multi-drug resistant pathogens.

Introduction

The current state of antimicrobial resistance presents a global crisis in public health. The widespread emergence of multi-drug resistant (MDR) pathogens calls for the development of novel antibiotics[336,337]. Ongoing efforts encompass a variety of approaches, including the screening of microbial collections for bioactive natural products and chemical synthesis. However, the discovery of novel antibiotic classes has declined dramatically in recent decades[338,339]. As an alternative strategy, there is a growing interest in revisiting compound classes not conventionally applied as antimicrobial drugs[340,341].

Anthracyclines represent a class of highly potent anticancer compounds[15,266]. They are aromatic type II polyketides featuring a linear tetracyclic 7,8,9,10-tetrahydro-5,12-naphthacenequinone scaffold and are decorated with one or more sugar moieties[30]. Many of these compounds were initially discovered due to their antimicrobial activity[10,30]. However, their potential as antibiotics was constrained by severe side effects, directing their exclusive application as chemotherapeutic agents[13]. The most prominent clinically used natural anthracyclines are daunorubicin (**32**, Figure 1) and doxorubicin (**1**, Figure 1), both isolated from *Streptomyces peucetius*[8–10], and aclarubicin (**12**, Figure 1), a natural product of *Streptomyces galilaeus*[33]. Furthermore, semi-synthetic anthracyclines such as epirubicin (**13**, Figure 1) and idarubicin have gained widespread use in clinical oncology[13].

Anthracyclines intercalate into DNA, which results in two distinct activities[14,15]. Firstly, they induce DNA damage by causing DNA double-strand breaks through the inhibition or poisoning of topoisomerase II, an essential enzyme involved in DNA replication and repair. Secondly, anthracyclines cause chromatin damage by evicting histones, the proteins involved in packaging DNA into a condensed structure. The major side effects associated with anthracycline treatment, including cardiotoxicity, the development of secondary tumours and infertility, result from the combination of these two activities, such as is the case for daunorubicin (**32**) and doxorubicin (**1**)[14,16]. In contrast, anthracyclines that primarily induce chromatin damage, such as aclarubicin (**12**) and *N,N*-dimethyldoxorubicin (**2**, Figure 1), are associated with reduced side effects. These "detoxified" anthracyclines lack cardiotoxicity and do not induce second tumours[14,16], and can be more safely administered to patients in a poor conditions. A comprehensive evaluation of a structurally diverse library of anthracyclines revealed that the presence of a tertiary amine on the first sugar moiety generally results in the loss of DNA-damaging activity while exhibiting improved cytotoxicity[17–19]. This finding offers a promising strategy for the development of improved anthracyclines.

Anthracyclines with limited side effects offer the potential for a therapeutic window as antimicrobial agents, opening up new possibilities in addressing antimicrobial resistance. In recent years, the antimicrobial activity of several anthracyclines against a range of pathogens has been explored in a limited number of studies, primarily through high-throughput screenings of compound libraries. For instance, in a screening of the National Cancer Institute compound

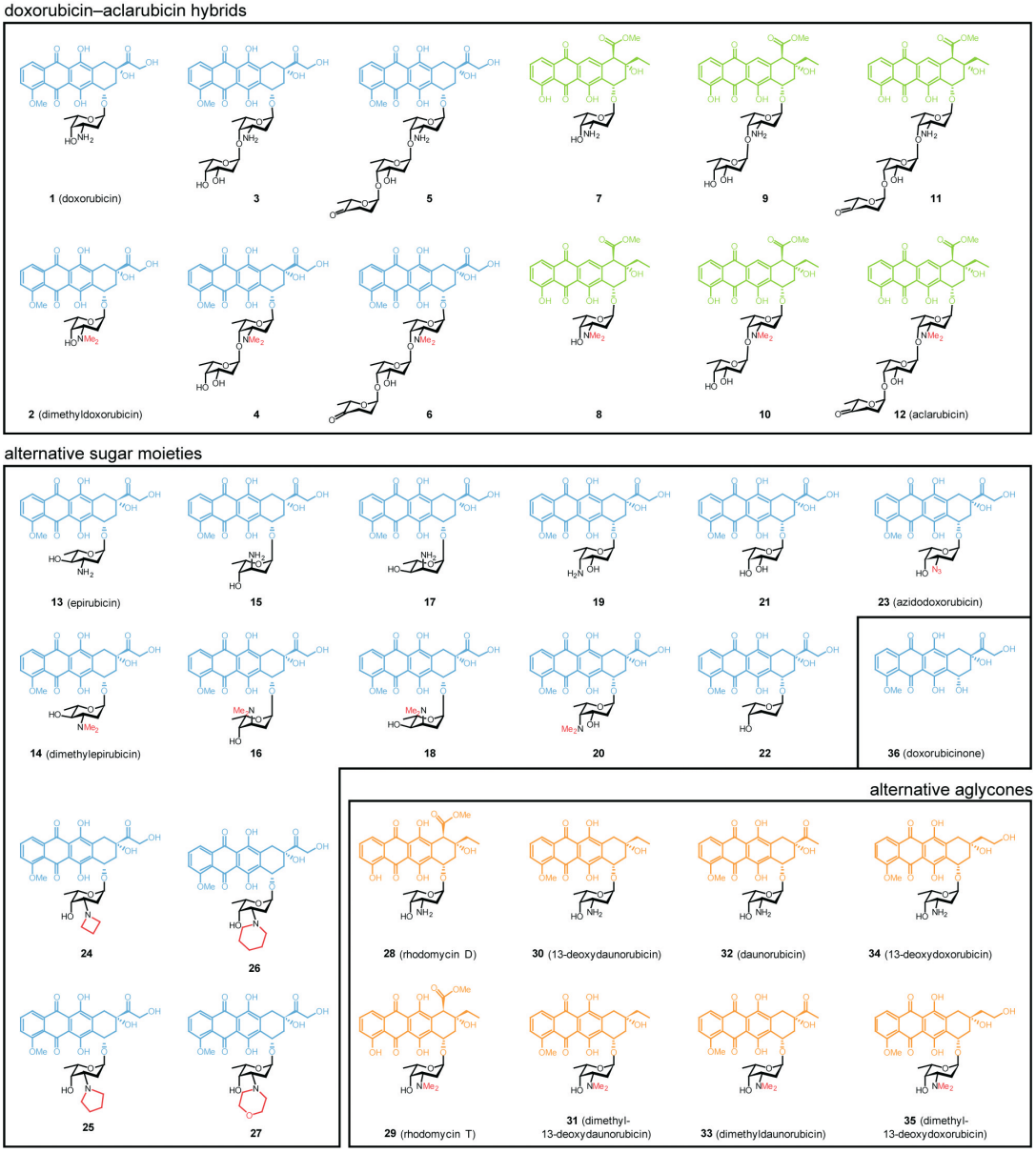


Figure 1. Chemical structures of compounds 1–36, evaluated in this study. Doxorubicin–aclarubicin hybrids (**1**–**12**), (*N,N*-dimethylated) doxorubicin epimers (**13**–**18**), (*N,N*-dimethylated) doxorubicin regio-isomers (**19** and **20**), doxorubicin with replacement of removal of the basic amine group (**21**–**23**), doxorubicin with alternative alkylation (**24**–**27**), (*N,N*-dimethylated) doxorubicin derivatives differing in the aglycone part (**28**–**35**), and doxorubicinone (**36**). The doxorubicin aglycone is depicted in blue, the aclarubicin aglycone in green, and alternative aglycones in yellow. Tertiary amines and the azide group are indicated in red.

library, six anthracyclines were identified as active against *Borrelia burgdorferi*, among which daunorubicin (**32**) and *N,N*-dimethyldaunorubicin (**33**, Figure 1)[342]. In another high-throughput screening of an FDA-approved drugs library, daunorubicin (**32**) exhibited antimicrobial activity against *Staphylococcus aureus* small-colony variants[343]. Additionally, daunorubicin (**32**) demonstrated potent antimicrobial activity against *Mycobacterium absceccus*[344]. Furthermore, idarubicin exhibited bactericidal activity against methicillin-resistant *S. aureus* (MRSA) and methicillin-resistant *Staphylococcus epidermis*[345].

The mechanism underlying the antimicrobial activity was attributed to cell membrane disruption activity[345]. Another potential application of anthracyclines lies in the treatment of sepsis. Epirubicin (**13**) conferred robust protection against sepsis in an experimental mouse model at a low dose regiment[346]. However, a comprehensive comparison of a diverse library of anthracyclines against a wide panel of pathogens has been lacking, underscoring the urgent need or a more in-depth investigation.

The goal of this study was to evaluate the antimicrobial activity of a library of 35 structurally diverse anthracyclines against ESKAPE pathogens. Compounds with potent cytotoxic activity against human cancer cell lines also exhibited enhanced antimicrobial activity, particularly against Gram-positive bacteria. Generally, the *N,N*-dimethylated compounds exhibited increased antimicrobial activity. Among these compounds, *N,N*-dimethyldoxorubicin (**2**) and compound **6**, composed of the doxorubicin aglycone combined with the aclarubicin trisaccharide (Figure 1), exhibited the strongest antimicrobial activity, especially for Gram-positive bacteria including MRSA.

Results

Minimal inhibitory concentration of a 35-compound anthracycline library

Recent advances in the development of less toxic anthracyclines present a promising opportunity to explore their potential as antibiotics. To search for anthracyclines with antibiotic activity, we screened a library consisting of 35 different compounds (Figure 1). The library is composed of a set of structurally diverse anthracyclines, each characterised by variations in the aglycone or the sugar moiety. The anthracyclines are divided into three main groups. The first group consists of doxorubicin and aclarubicin hybrids (**1**–**12**)[18]. The second group consists of (*N,N*-dimethylated) doxorubicin variants featuring alternative sugar moieties: diastereomers (**13**–**18**)[19], regio-isomers (**19**–**20**)[17], replacement or removal of the basic amine (**21**–**23**)[17], and variations in the amine alkylation (**24**–**27**)[17]. The last group consists of (*N,N*-dimethylated) doxorubicin variants with alternative aglycones (**28**–**35**)[17]. The anticancer activities of these anthracyclines have been previously investigated[17–19].

Since anthracyclines are known to exhibit in particular bioactivity against Gram-positive bacteria, while their activity against Gram-negative bacteria is generally low, the antimicrobial assays were initially focused on the Gram-positive *Bacillus subtilis* and methicillin-resistant

Staphylococcus aureus USA300 ($MRSA_{USA300}$). Minimum inhibitory concentrations (MICs) were determined using the antimicrobial broth microdilution susceptibility assay. In this assay, a mid-logarithmic growth-phase culture was exposed to anthracycline concentrations ranging from 0.5 to 64 µM (see Materials and Methods for details).

The anthracyclines had varying antibiotic activity (Table 1). Doxorubicin (**1**) exhibited an MIC of 8 µM against *B. subtilis* and of 16 µM against $MRSA_{USA300}$. Importantly, *N,N*-dimethyldoxorubicin (**2**) exhibited a four-fold lower MIC against both strains. Among the doxorubicin–aclarubicin hybrids, the dimethylated variants consistently demonstrated stronger antimicrobial activity. Notably, the doxorubicin–aclarubicin hybrid with the doxorubicin aglycone and aclarubicin trisaccharide (compound **6**) exhibited the highest activity of the entire library against *B. subtilis* (0.5 µM) and $MRSA_{USA300}$ (1 µM). Similarly, for the diastereomers and regio-isomers, the dimethylated variants consistently demonstrated stronger antimicrobial activity. The non-dimethylated variants generally did not exhibit any antimicrobial activity, with the exception of epirubicin (**13**) that exhibited intermediate bioactivity, with an MIC of 16 µM against both Gram-positive strains. Removal or replacement of the basic amine group had moderate effect on the antimicrobial activity.

Table 1. Minimal inhibitory concentration of anthracyclines 1–35 against Gram-positive bacteria.

#	Group	A*	S*	M*	*B. subtilis* (µM)	$MRSA_{USA300}$ (µM)
1	doxorubicin–aclarubicin hybrids	doxo	1	x	8	16
2	doxorubicin–aclarubicin hybrids	doxo	1	Me_2	2	4
3	doxorubicin–aclarubicin hybrids	doxo	2	x	›64	›64
4	doxorubicin–aclarubicin hybrids	doxo	2	Me_2	4	8
5	doxorubicin–aclarubicin hybrids	doxo	3	x	16	›64
6	doxorubicin–aclarubicin hybrids	doxo	3	Me_2	0.5	1
7	doxorubicin–aclarubicin hybrids	acla	1	x	64	›64
8	doxorubicin–aclarubicin hybrids	acla	1	Me_2	32	32
9	doxorubicin–aclarubicin hybrids	acla	2	x	32	64
10	doxorubicin–aclarubicin hybrids	acla	2	Me_2	2	8
11	doxorubicin–aclarubicin hybrids	acla	3	x	32	›64
12	doxorubicin–aclarubicin hybrids	acla	3	Me_2	2	4
13	diastereomers	doxo	1	x	16	16
14	diastereomers	doxo	1	Me_2	4	8
15	diastereomers	doxo	1	x	›64	›64
16	diastereomers	doxo	1	Me_2	32	16
17	diastereomers	doxo	1	x	›64	64
18	diastereomers	doxo	1	Me_2	16	16

[continued on next page]

Table 1. *[continued]*

#	Group	A*	S*	M*	*B. subtilis* (µM)	$MRSA_{USA300}$ (µM)
19	regio-isomers	doxo	1	x	64	64
20	regio-isomers	doxo	1	Me_2	4	4
21	replacement/removal of amine	doxo	1	OH	16	32
22	replacement/removal of amine	doxo	1	H	8	32
23	replacement/removal of amine	doxo	1	N_3	4	16
24	alternative amine alkylation	doxo	1	cyclic	2	4
25	alternative amine alkylation	doxo	1	cyclic	1	2
26	alternative amine alkylation	doxo	1	cyclic	1	4
27	alternative amine alkylation	doxo	1	cyclic	1	2
28	alternative aglycones	other	1	x	8	8
29	alternative aglycones	other	1	Me_2	8	8
30	alternative aglycones	other	1	x	16	32
31	alternative aglycones	other	1	Me_2	8	16
32	alternative aglycones	other	1	x	4	8
33	alternative aglycones	other	1	Me_2	2	4
34	alternative aglycones	other	1	x	›64	›64
35	alternative aglycones	other	1	Me_2	32	32

* Column A: the aglycone structure is indicated as: acla, aclarubicin aglycone; doxo, doxorubicin aglycone; other, alternative aglycone. Column S: number of sugar moieties. Column M: modification or replacement of the amine group: x, no modification; Me_2, dimethylation; OH, replacement of amine by hydroxyl group; H, removal of amine; N_3, replacement of amine by azide; cyclic, amine alkylation with cyclic group.

However, compounds **24**–**27** exhibited low micromolar MICs (1–4 µM) against both strains, indicating that tertiary alkylation of the amine group resulted in a significantly increased bioactivity. For the compounds with alternative aglycones, dimethylation resulted in a two-fold increase in antimicrobial activity, with the exception of rhodomycin D (**28**), which exhibited the same MICs as its dimethylated derivative rhodomycin T (**29**). Notably, both 13-deoxydoxorubicin (**34**) and its dimethylated derivative (**35**) exhibited poor antimicrobial activity.

Taken together, *N,N*-dimethylation or tertiary alkylation of the amine group resulted in increased antimicrobial activity against Gram-positive bacteria. A subset of the anthracyclines was chosen for further studies of their antimicrobial activity against a broader range of pathogens. For this we selected the following compounds: doxorubicin–aclarubicin hybrids with the doxorubicin aglycone (**1**–**6**), harbouring different numbers of sugar moieties, with or without dimethylation; aclarubicin (**12**), which features an alternative aglycone with a dimethylated trisaccharide; azidodoxorubicin (**23**), which contains an azide group; and the aglycone doxorubicinone (**36**).

Bactericidal activity of anthracyclines against ESKAPE pathogens

The bactericidal activity of compounds **1**–**6**, **12**, **23** and **36** was tested against different clinical isolates from the ESKAPE panel[347], including *Enterococcus faecium* LUH15122, *S. aureus* LUH14616 ($MRSA_{LUH14616}$), *Klebsiella pneumoniae* LUH15104, *Acinetobacter baumannii* RUH875, *Pseudomonas aeruginosa* LUH15103, and *Enterobacter cloacae* LUH15114. The Gram-positive *Staphylococcus epidermidis* LUH15163 and *Streptococcus pyogenes* LUH2762, were also included. Mid-logarithmic growth-phase cultures were exposed to compounds at concentrations ranging from 0.061 to 64 µM (See Materials and Methods for details).

Table 2. Bactericidal activity of anthracyclines against planktonic bacteria. Killing of *E. faecium* LUH15122, *S. aureus* LUH14616, *S. epidermidis* LUH15163, *S. pyogenes* LUH2762, *K. pneumoniae* LUH15104, *A. baumannii* RUH875, *P. aeruginosa* LUH15103, and *E. cloacae* LUH15114 after 24 h exposure to 0.061 to 64 µM of compound **1**–**6**, **12**, **23** or **36** in PBS with or without 50% pooled human plasma. The results are expressed as the 99.9% lethal concentration ($LC_{99.9}$).

			PBS								
Gram	**Species**	**Strain**	**1**	**3**	**5**	**2**	**4**	**6**	**12**	**23**	**36**
+	*E. faecium*	LUH15122	›64	›64	64	2	16	4	8	›64	›64
	S. aureus	LUH14616	8	›64	›64	4	8	4	16	›64	32
	S. epidermidis	LUH15163	8	›64	16	1	4	1	8	64	32
	S. pyogenes	LUH2762	4	16	4	1	2	1	8	8	16
-	*K. pneumoniae*	LUH15104	›64	›64	›64	›64	›64	›64	›64	›64	›64
	A. baumannii	RUH875	64	›64	›64	16	32	16	›64	›64	›64
	P. aeruginosa	LUH15103	›64	›64	›64	›64	›64	›64	›64	›64	›64
	E. cloacae	LUH15114	›64	›64	›64	›64	›64	›64	›64	›64	›64
			PBS with 50% pooled human plasma								
Gram	**Species**	**Strain**	**1**	**3**	**5**	**2**	**4**	**6**	**12**	**23**	**36**
+	*E. faecium*	LUH15122	›64	›64	›64	›64	›64	›64	›64	›64	›64
	S. aureus	LUH14616	32	›64	64	2	8	2	›64	64	›64
	S. epidermidis	LUH15163	›64	›64	64	2	4	1	›64	›64	›64
	S. pyogenes	LUH2762	4	64	16	1	2	1	32	›64	›64
-	*K. pneumoniae*	LUH15104	›64	›64	›64	64	›64	›64	›64	›64	›64
	A. baumannii	RUH875	64	›64	›64	8	32	32	›64	›64	›64
	P. aeruginosa	LUH15103	›64	›64	›64	›64	›64	›64	›64	›64	›64
	E. cloacae	LUH15114	›64	›64	›64	32	›64	›64	›64	›64	›64

The results are shown in Table 2 and Supplementary Figure S1. Doxorubicin (**1**) exhibited activity against $MRSA_{LUH14616}$, *S. epidermis* and *S. pyogenes*. Compound **3**, featuring a non-dimethylated disaccharide, only displayed activity against *S. pyogenes*. The non-dimethylated trisaccharide (compound **5**) was active against *S. epidermis* and *S. pyogenes*. The dimethylated doxorubicin variants (compounds **2**, **4** and **6**) effectively killed all Gram-positive strains at concentrations in the low micromolar range (1–16 µM). *N,N*-dimethyldoxorubicin (**2**) and compound **6**, which

features the doxorubicin aglycone with the aclarubicin trisaccharide, exhibited particularly strong activity against *S. epidermis* (1 µM) and *S. pyogenes* (1 µM). Aclarubicin (**12**) had moderate activity against all Gram-positive strains (8–16 µM). Azidodoxorubicin (**23**) was active only against *S. pyogenes*, while doxorubicinone (**36**) exhibited moderate activity overall. Interestingly, the dimethylated doxorubicin variants (compounds **2**, **4** and **6**) exhibited moderate bactericidal activity against *A. baumannii* (16–32 µM). Finally, none of the compounds inhibited growth of *K. pneumoniae*, *P. aeruginosa* or *E. cloacae*).

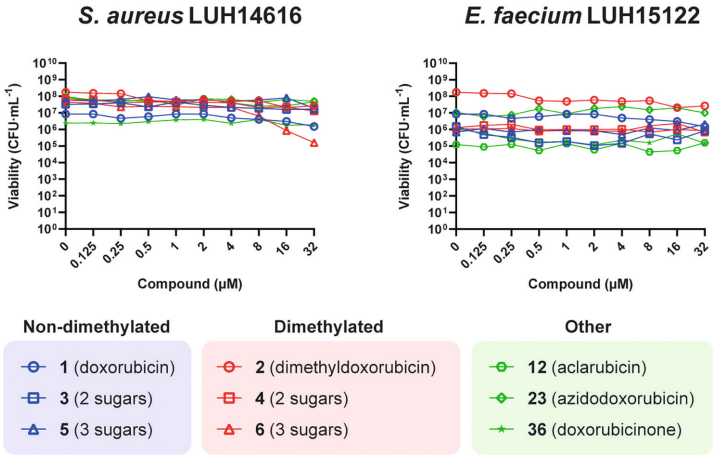


Figure 2. Bactericidal activity of anthracyclines against mature biofilms. Viability of 7-days-mature biofilms of *E. faecium* LUH15122 and *S. aureus* LUH14616 after 24 h exposure to 0.125 to 32 µM of compound **1**–**6**, **12**, **23** or **36**. The results are expressed as the number of viable bacteria in colony forming units (CFU) per mL for each compound concentration. Non-dimethylated doxorubicin variants are represented in blue, dimethylated doxorubicin variants are represented in red, and others in green.

To simulate physiologically relevant conditions, the bactericidal assays were repeated in PBS with 50% pooled human plasma. Under these conditions, the dimethylated doxorubicin derivatives retained their bactericidal activity against $MRSA_{LUH14616}$, *S. epidermis* and *S. pyogenes* (1–8 µM), whereas the non-dimethylated compounds and aclarubicin demonstrated reduced efficacy (Table 2, Supplementary Figure S1). *E. faecium* was resistant to all compounds in 50% plasma. Importantly, the dimethylated compounds also retained their activity against *A. baumannii* in 50% plasma.

We also investigated the effect of shorter treatment time on the bactericidal activity. Therefore, $MRSA_{LUH14616}$ and *A. baumannii* RUH875 were exposed for 1, 2, 3, 4 or 24 h to doxorubicin (**1**) or *N,N*-dimethyldoxorubicin (**2**) in PBS, PBS with 2% TSB and PBS with 50% pooled human plasma (Supplementary Table S2). Both compounds were active against both strains after 1 h, but more efficient killing was shown after 24 h exposure.

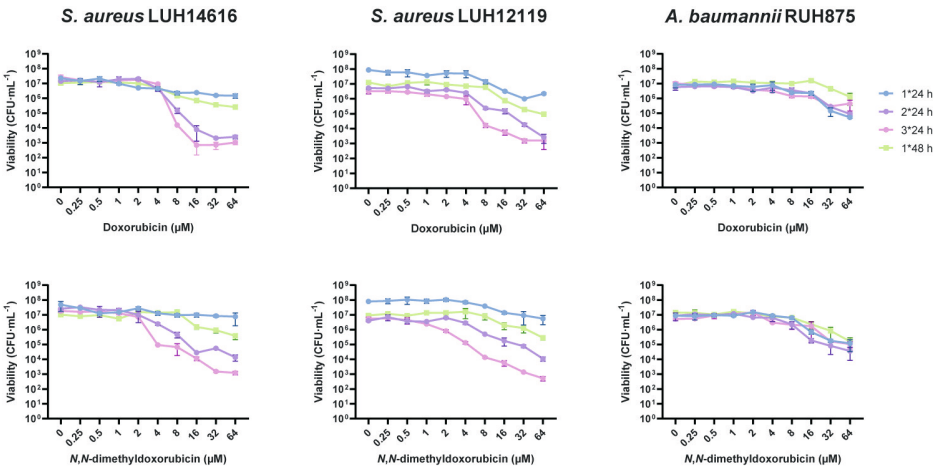


Figure 3. Bactericidal activity of anthracyclines against immature biofilms of MRSA. Viability of 24-h-immature biofilms of *S. aureus* LUH14616, *S. aureus* LUH12119 and *A. baumannii* RUH875 after one, two or three times 24 h or one time 48 h exposure to 0.125 to 32 μM of doxorubicin (**1**) or *N,N*-dimethyldoxorubicin (**2**). The results are expressed as the number of viable bacteria in colony forming units (CFU) per mL for each compound concentration.

Antibiofilm activity of anthracyclines

The efficacy of compounds **1**–**6**, **12**, **23** and **36** in eradicating mature bacterial biofilms of $MRSA_{LUH14616}$ and *E. faecium* LUH15122 after 24-h exposure was evaluated (see Materials and Methods for details). At the highest tested concentration of 32 μM, compounds **1**–**6**, **12**, **23** and **36** did not eradicate mature biofilms of $MRSA_{LUH14616}$ and *E. faecium* (Figure 2). The most notable antibiofilm activity was observed with compound **6**, which killed 99.6% of mature biofilm of $MRSA_{LUH14616}$ at 32 μM.

We further tested the antibiofilm activity of anthracyclines against less mature biofilms of *S. aureus* using a stronger treatment regiment. In this experiment, we included a second *S. aureus* strain ($MRSA_{LUH12119}$). We exposed immature (24-h-old) biofilms of $MRSA_{LUH14616}$ and $MRSA_{LUH12119}$ to doxorubicin (**1**) and *N,N*-dimethyldoxorubicin (**2**) with one, two or three times 24 h or one time 48 h incubation time (see Materials and Methods for details). Multiple treatment of immature biofilms of both MRSA strains improved the efficacy of the anthracyclines, whereas longer treatment time had only moderate effect (Figure 3). Three times 24 h treatment with 32 μM of doxorubicin (**1**) or *N,N*-dimethyldoxorubicin (**2**) killed 99.9% of both $MRSA_{LUH14616}$ and $MRSA_{LUH12119}$.

Resistance development of MRSA to anthracyclines

In light of the growing concern for resistance against antibiotics, we evaluated the potential $MRSA_{LUH14616}$ and $MRSA_{LUH12119}$ to develop resistance to anthracyclines. Serial passaging of the two MRSA strains in the presence of sub-inhibitory concentrations of doxorubicin (**1**) resulted in the selection of isolates with a maximum of 16-fold increase in MIC after 25 passages (Figure 4). Importantly, in the case of *N,N*-dimethyldoxorubicin (**2**), the MIC did not increase more than

two-fold despite of 25 passages. In contrast, exposure to the antibiotic rifampicin resulted in a rapid increase in resistance, with a 256-fold increase in MIC after just eight passages, and reaching an MIC of 2 mg·mL^{-1} after 11 passages (Figure 4).

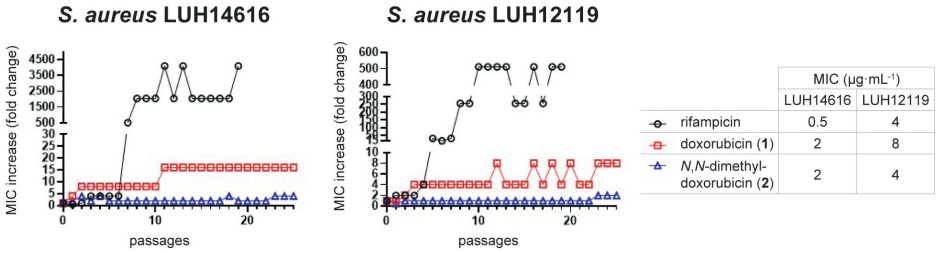


Figure 4. Resistance development of MRSA against doxorubicin and *N,N*-dimethyldoxorubicin. Resistance development of *S. aureus* LUH14616 and LUH12119 to doxorubicin (**1**), *N,N*-dimethyldoxorubicin (**2**) and rifampicin. Values are fold changes in minimal inhibitory concentration (MIC) relative to the MIC of the first passage.

Discussion

The escalating global crisis of antimicrobial resistance, coupled with a concerning stagnation in the discovery of novel antibiotics, underscores the urgent need for innovative strategies in addressing this challenge[337,338]. In this context, we explored the potential application of detoxified anthracyclines, well-known anticancer drugs, as antibiotics. Our findings revealed that dimethylated anthracyclines exhibit robust bactericidal activity against Gram-positive bacteria as well as Gram-negative *A. baumannii*. Considering that dimethylated anthracyclines lack DNA-damaging activity, which is associated with reduced side effects[16], this makes detoxified anthracyclines promising candidates as antibiotics.

Evaluation of a library of anthracyclines indicated that dimethylation consistently increased the activity against *B. subtilis* and MRSA$_{USA300}$. In particular compound **6**, featuring the doxorubicin aglycone with a dimethylated trisaccharide, exhibited a very low MIC of only 1 μM against MRSA$_{USA300}$. Furthermore, the doxorubicin derivatives with cyclic amines (compounds **24**–**27**) exhibited low MICs (2–4 μM) against MRSA$_{USA300}$. Subsequent evaluation of the bactericidal activity of a subset of the library against pathogens of the ESKAPE panel indicated that dimethylated anthracyclines effectively killed mainly Gram-positive bacteria. *N,N*-dimethyldoxorubicin (**2**) and compound **6** exhibited an $LC_{99.9}$ of 4 μM against MRSA$_{LUH14616}$ and of 1 μM against clinical isolates of *S. epidermis* and *S. pyogenes*. The compounds also demonstrated moderate activity against Gram-negative *A. baumannii*, and retained their activity in physiologically relevant conditions (50% human plasma). Importantly, MRSA$_{LUH14616}$ and MRSA$_{LUH12119}$ did not develop resistance to *N,N*-dimethyldoxorubicin (**2**) after 25 passages in sub-inhibitory conditions. However, the anthracyclines were ineffective in eradicating mature biofilms of MRSA$_{LUH14616}$ and *E. faecium*. Immature biofilms of MRSA$_{LUH14616}$ and MRSA$_{LUH12119}$ could be killed for 99.9% by multiple exposures to 32 μM of doxorubicin (**1**) or *N,N*-dimethyldoxorubicin (**2**).

N,N-dimethylation of anthracyclines generally results in the elimination of DNA double-strand break activity in human cancer cell lines, while cytotoxicity remains due to the release of nucleosomes from defined areas in the genome[17–19]. Obviously, histone release will not be a factor relevant for the antimicrobial activities. Still, our results indicate that *N,N*-dimethylation improves the antimicrobial activity of anthracyclines. Additionally, cyclic amines demonstrated low MIC values against *B. subtilis* and $MRSA_{USA300}$. This is in contrast to the anticancer activities, which were unaffected by alternative alkylation of the amine moiety of doxorubicin[17]. Furthermore, changing the position of the amine in the sugar moiety had minor effects on cytotoxicity[17], while this strongly reduced the antimicrobial activity (compounds **15**, **17** and **19**). The cytotoxicity of anthracyclines is associated with histone eviction activity[16], but the antimicrobial mode-of-action of anthracyclines has been poorly studied as the drugs usually have major toxic activities to experimental animals and patients. A recent study reported the antimicrobial activity of the cancer drug idarubicin, another doxorubicin derivative with a modified aglycone structure that is also cardiotoxic, and presented a model for its mode-of-action[345]. Idarubicin was found to target the cell membrane and bacterial topoisomerase II subunits GyrA and GyrB[345]. The increased hydrophobicity of dimethylated anthracyclines may result in better membrane solubility, which could offer an explanation for their improved antimicrobial activity. Additionally, it is possible that DNA gyrase inhibitory activity is improved in the dimethylated anthracyclines, adding another potential factor to their improved efficacy. We are currently investigating the mode-of-action of dimethylated anthracyclines via resistance assays and uptake experiments.

Repurposing of anticancer compounds as antimicrobials has gained increasing attention in recent years. For example, the toxic cancer drug mitomycin C, the antimicrobial properties of the DNA-targeting anticancer compound mitomycin C have been evaluated, revealing promising activity against bacterial persist cells[348] and efficient killing of Gram-negative *A. baumannii*[349]. Additionally, mitoxantrone, another toxic cancer drug that acts via DNA damage and free radical formation, has been proposed as potential antibiotic for the treatment of vancomycin-resistant *Enterococcus faecalis* (VRE)[350]. However, the application of anticancer compounds as antibiotics is limited by their inherent toxicity to human cells. Consequently, their application as antimicrobial agents must be approached strategically, such as through topical treatments or as a last resort in cases involving MDR pathogens. Alternatively, derivatives of anticancer compounds may be found that exhibit reduced toxicity, with detoxified anthracyclines serving as an example. In the context of doxorubicin treatment, cardiotoxicity is the dose limiting side effect, restricting administration to a cumulative dose of 450–550 $mg \cdot m^{-2}$ [351]. Anthracyclines with reduced cardiotoxicity like *N,N*-dimethyldoxorubicin (**2**) could be applied at higher accumulative dosages[15]. The feasibility of employing anthracyclines as antibiotics relies on the specific applications and pharmacodynamics. However, the low bactericidal concentrations observed for both *N,N*-dimethyldoxorubicin (**2**) and compound **6** are a basis for further optimisation of these drugs for *in vivo* application as antibiotics for especially Gram-positive bacteria.

In conclusion, our work provides a beautiful example of how compounds from the antibiotic class of anticancer drugs can be modified to reduce the side effects in patients while enhancing the antibiotic activities. The detoxification of anticancer compounds presents a promising alternative strategy to replenish the antibiotics discovery pipelines and combat antimicrobial resistance.

Materials and Methods

Chemical compounds

The anthracyclines used in this work are presented in Figure 1. The 35-compound anthracycline library consists of doxorubicin and aclarubicin derivatives with variations in the tetracyclic aglycone and the sugar moieties. Doxorubicin (**1**) was purchased from Pharmachemie (the Netherlands). Aclarubicin (**12**, sc-200160) and doxorubicinone (**36**, sc-218273) were purchased from Santa Cruz Biotechnology (USA). Epirubicin (**13**) was purchased from Accord Healthcare Limited (UK). Daunorubicin (**32**) was purchased from Sanofi-Aventis (the Netherlands). All other anthracyclines were synthesised as described previously[16–19].

Bacterial strains and cultivation conditions

The bacterial strains used in this work are listed in Supplementary Table S1. Clinical isolates of *Enterococcus faecium* (LUH15122), *Staphylococcus aureus* (LUH14616, LUH12119 and USA300), *Staphylococcus epidermidis* (LUH15163), *Streptococcus pyogenes* (LUH2762), *Klebsiella pneumoniae* (LUH15104), *Acinetobacter baumannii* (RUH875), *Pseudomonas aeruginosa* (LUH15103), and *Enterobacter cloacae* (LUH15114), and the model strain *Bacillus subtilis* 168 were used. Before each experiment, glycerol stocks were streaked onto blood agar plates, and incubated at 37 °C overnight. Subsequently, approximately five colonies were inoculated into tryptic soy broth (TSB). The bacteria were cultured at 37 °C at 200 rpm to mid-logarithmic growth phase, and diluted to the desired inoculum concentration, based on the optical density at 600 nm (OD_{600}).

Minimum inhibitory concentration

Minimum inhibitory concentrations (MICs) were determined using the antimicrobial broth microdilution susceptibility assay according to the Clinical and Laboratory Standards Institute (CLSI) guidelines. Briefly, a mid-logarithmic growth-phase culture (OD_{600} of 0.5) was exposed to anthracycline concentrations ranging from 0.5 to 64 µM. Cation-adjusted Mueller–Hinton Broth (CAMHB) was prepared by supplementing Mueller–Hinton Broth (MHB) with 0.5 mM $CaCl_2$ and 0.5 mM $MgCl_2$. Anthracyclines were dissolved in DMSO to a concentration of 6.4 mM and subsequently diluted to 128 µM in CAMHB. The compounds solutions were serially diluted two-fold in CAMHB into microtiter plates to a volume of 50 µL per well. The bacterial suspension was 100-fold diluted in CAMHB, and 50 µL was added to each well to achieve a final OD_{600} of 0.0025. Plates were sealed with an adhesive membrane, and incubated at 37 °C overnight. Biomass formation in each well was visually inspected. The MIC was defined as the

lowest anthracycline concentration at which no growth was observed. *N,N*-dimethyldoxorubicin (**2**) was tested at two-fold dilutions of 112 µM or 149 µM instead of 64 µM for *B. subtilis* and USA300, respectively. Compounds **4**–**7**, **11**, **21**, **22** and **26** were tested at two-fold dilutions of 85 µM instead of 64 µM for both strains. In these cases, the MIC values were rounded up to 0.5, 1, 2, 4, 8, 16, 32, 64 or ›64 µM.

Bactericidal activity

Bactericidal activity was determined according to the CLSI guidelines. Briefly, a mid-logarithmic growth-phase culture was centrifuged for 10 min at 3000 rpm and washed with 10 mL of phosphate buffered saline (PBS; pH 7.4, 140 mM NaCl). Anthracyclines were dissolved in PBS to a concentration of 426.7 µM, and subsequently serially diluted two-fold in PBS into microtiter plates to a volume of 30 µL per well to achieve a final concentration in the range of 0.061–64 µM for Gram-positive strains and 4-64 µM for Gram-negative strains. Subsequently, 50 µL of PBS with 4% TSB or 50 µL of pooled human plasma (Sanquin) was added to each well, resulting in a final concentration of 2% TSB or 50% (v/v) plasma. Except in case of *S. pyogenes* LUH2762, where a final concentration of 10% TSB was applied in both PBS and plasma experiments. Finally, the bacterial suspension was diluted in PBS to approximately $5{\cdot}10^6$ CFU·mL^{-1}, and 20 µL was added to each well to achieve a achieve final concentration of approximately $1{\cdot}10^6$ CFU·mL^{-1}. Plates were sealed with an adhesive membrane, and incubated at 37 °C for 24 h. Viability was determined via a colony forming units (CFU) assay. A dilution series of the bacterial suspensions was prepared in PBS and plated on Mueller–Hinton (MH) agar plates. Plates were incubated at 37 °C for 24 h. The bactericidal activity was reported as the 99.9% lethal concentration ($LC_{99.9}$), i.e., the lowest anthracycline concentration that killed ≥99.9% of bacteria. One replicate of *N,N*-dimethyldoxorubicin (**2**) with each strain was tested at two-fold dilutions of 112 µM instead of 64 µM. In this cases, the MIC values were rounded up to 0.5, 1, 2, 4, 8, 16, 32, 64 or ›64 µM. To study shorter treatment times of planktonic bacteria, the plates were incubated for 1, 2, 3 or 4 h instead of 24 h.

Treatment of immature and mature biofilms

A mid-logarithmic growth-phase culture was centrifuged for 10 min at 3400 rpm. The biomass was resuspended in 2 mL of PBS, and subsequently diluted in brain heart infusion (BHI) medium to approximately $1{\cdot}10^7$ CFU·mL^{-1}. Subsequently, 100 µL of the bacterial suspension was added to each well of a microtiter plate. Plates were sealed with an adhesive membrane, and incubated for 24 h (immature) or 7 days (mature) at 37 °C in a humidified atmosphere. For mature biofilm experiments, plates were sealed with a breathable membrane. After incubation, planktonic bacteria were carefully removed from each well. The biofilm was washed twice with 100 µL of PBS. Subsequently, 100 µL of anthracyclines diluted in PBS in the range of 0.125–32 µM was added to each well. As untreated control, bacteria were exposed to PBS without anthracyclines. For immature biofilms anthracyclines were diluted in PBS with 2% TSB. After 24 h incubation at 37 °C in a humidified atmosphere, the biofilm was washed twice with PBS and resuspended in 100 µL PSB by 10 min of sonication. Viability was determined via a CFU assay of MH agar and reported as the $LC_{99.9}$ value. For mature biofilm treatment with *N,N*-dimethyldoxorubicin,

the tested concentrations deviated from the intended range. In this case, the $LC_{99.9}$ value was rounded up to 0.125, 0.25, 0.5, 1, 2, 4, 8, 16, 32 or ›32 µM. For multiple treatment of immature biofilms, after 24 h incubation with anthracyclines, the biofilm was washed twice with PBS. The biofilm was treated with 100 µL of fresh anthracycline solution of the same concentration, and incubated for another 24 h. For prolonged treatment of immature biofilms, the incubation time was extended to 48 h.

Resistance development

Development of resistance to anthracyclines was performed as described by Habets and Brockhurst[352]. For comparison, development of resistance to the clinically relevant antibiotic rifampicin (Sigma-Aldrich) was determined. Briefly, *S. aureus* LUH12119 and LUH14616 were cultured overnight at 37 °C at 200 rpm in modified RPMI-1640 medium (with 20 mM HEPES and L-glutamine, without sodium bicarbonate). Compounds were dissolved in PBS and serially diluted two-fold in modified RPMI-1640 medium into microtiter plates to a volume of 100 µL per well (with a final concentration of 0.5–64 µM for anthracyclines and 0.5–4.1 $mg \cdot mL^{-1}$ for rifampicin). Subsequently, 5 µL of overnight culture was added to each well. Plates were sealed with an adhesive membrane, and incubated at 37 °C at 200 rpm for 24 h. Biomass formation in each well was visually inspected. The MIC was defined as the lowest anthracycline concentration at which no growth was observed. Subsequently, 5 µL of the culture at 0.5-fold MIC was added to 100 µL of fresh medium containing a two-fold dilution range of the compounds. The plates were treated and analysed as described above. This process was repeated for 25 passages.

Supplementary Information

Table S1. Bacterial strains used in this work.

Gram	Species	Strain	Class
+	*Bacillus subtilis*	168	Model strain
	Enterococcus faecium	LUH15122	MDR
	Staphylococcus aureus	LUH14616	MRSA
	Staphylococcus aureus	LUH12119	MRSA
	Staphylococcus aureus	USA300	MRSA
	Staphylococcus epidermidis	LUH15163	MDR
	Streptococcus pyogenes	LUH2762	MDR
-	*Klebsiella pneumoniae*	LUH15104	MDR
	Acinetobacter baumannii	RUH875	MDR
	Pseudomonas aeruginosa	LUH15103	MDR
	Enterobacter cloacae	LUH15114	MDR

Table S2. Short treatment time of anthracyclines against planktonic bacteria. Killing of *S. aureus* LUH14616 and *A. baumannii* RUH875 after 1, 2, 3, 4 or 24 h exposure to 1 to 64 µM of doxorubicin (**1**) or *N,N*-dimethyldoxorubicin (**2**) in PBS, PBS with 2% TSB or PBS with 50% pooled human plasma. The results are expressed as the 99.9% lethal concentration ($LC_{99.9}$).

***S. aureus* LUH14616**										
	doxorubicin (**1**)					*N,N*-dimethyldoxorubicin (**2**)				
Medium	**1h**	**2h**	**3h**	**4h**	**24h**	**1h**	**2h**	**3h**	**4h**	**24h**
PBS	›64	›64	›64	64		›64	›64	32	32	
PBS + 2% TSB	›64	›64	64	64	32	›64	›64	32	16	4
PBS + 50% plasma	›64	›64	›64	64	32	›64	›64	32	16	1
***A. baumannii* RUH875**										
	doxorubicin (**1**)					*N,N*-dimethyldoxorubicin (2)				
Medium	**1h**	**2h**	**3h**	**4h**	**24h**	**1h**	**2h**	**3h**	**4h**	**24h**
PBS	64	64	64	64		›64	64	64	32	
PBS + 2% TSB	›64	›64	64	64	64	32	32	16	16	16
PBS + 50% plasma	›64	64	32	32	64	32	32	16	16	8

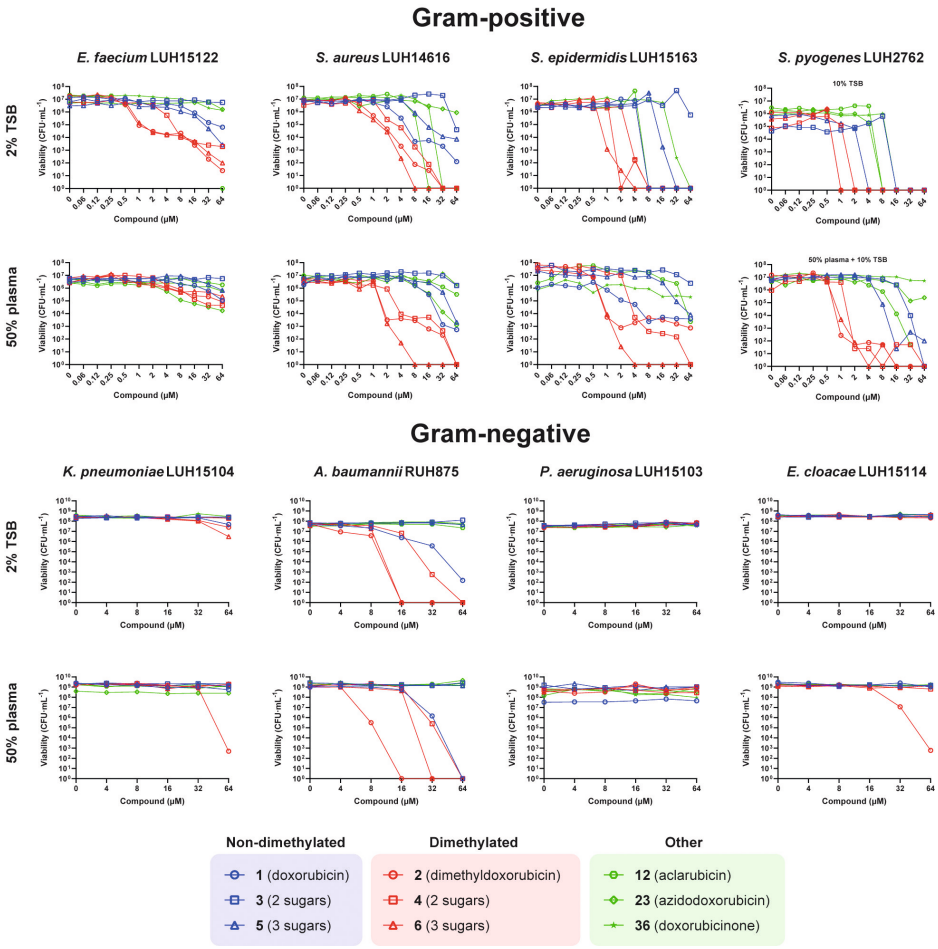


Figure S1. Bactericidal activity of anthracyclines against planktonic bacteria. Viability of *E. faecium* LUH15122, *S. aureus* LUH14616, *S. epidermidis* LUH15163, *S. pyogenes* LUH2762, *K. pneumoniae* LUH15104, *A. baumannii* RUH875, *P. aeruginosa* LUH15103, and *E. cloacae* LUH15114 after 24 h exposure to 0.061 to 64 μM of compound **1**–**6**, **12**, **23** or **36** in PBS with or without 50% pooled human plasma. The results are expressed as the number of viable bacteria in colony forming units (CFU) per mL for each compound concentration. Non-dimethylated doxorubicin variants are represented in blue, dimethylated doxorubicin variants are represented in red, and others in green.



Integrated proteomics and metabolomics analysis of small-scale *Streptomyces peucetius* cultures

Mandy B. Hulst, Lina M. Bayona Maldonado, Chao Du and Gilles P. van Wezel

Abstract

The cultivation and characterisation of *Streptomyces* strains in a high-throughput manner is important to screen for natural products under a range of culturing conditions. However, small-scale cultivation of mycelial microorganisms faces major challenges such as high biological variability and reduced mixing efficiency. Here we present an integrated quantitative proteomics and metabolomics workflow to analyse natural product biosynthesis in small-scale *Streptomyces* cultures. Wild-type *Streptomyces peucetius* and an industrial production strain were cultivated in 1 mL complex media in a microbioreactor (BioLector) with continuous non-invasive monitoring of growth data, pH and dissolved oxygen concentrations. Cultures were subjected to paired omics data analysis, with protein expression analysed by quantitative proteomics on the biomass, and metabolomics analysis on the spent media. Despite the inherent challenges of reproducibility of growing *Streptomyces* pellets in submerged cultures, the technical reproducibility of the paired omics data was sufficiently high to allow proper interpretation of the data. This shows that our methodology holds promise for automated high-throughput multi-omics analysis of *Streptomyces* strains. This approach will aid scientists in the study of biosynthetic gene cluster expression in combination with metabolite analysis.

Introduction

Streptomycetes are prolific producers of bioactive natural products with various activities including antibacterial, antifungal, insecticidal, antiviral and anticancer[2–4]. This industrially important genus of Gram-positive bacteria exhibits a distinctive multicellular lifestyle[21]. The life cycle of *Streptomyces* starts with the formation of spores, which disperse for survival in challenging environments. Following germination, the spores develop into a complex network of vegetative hyphae[43,44]. In response to nutrient depletion or environmental stresses, a programmed cell death process is activated within the vegetative hyphae[57,353]. This process releases essential nutrients for the formation of aerial hyphae, which ultimately develop into spore chains[21]. The autolytic degradation of the vegetative hyphae is temporally correlated with the production of natural products, which is tightly regulated by a complex signalling system[5,45,354]. The genes involved in the production of these bioactive metabolites are typically clustered on the genome in so-called biosynthetic gene clusters (BGCs). Recent advances in genome mining have revealed the presence of numerous and highly diverse BGCs in the genomes of *Streptomyces* bacteria[46,168,355]. This discovery holds promising implications for addressing the current antibiotic crisis[338,339].

Systematic screening efforts are required to active and annotate the BGCs that often remain silent under standard laboratory conditions. Identification of the corresponding metabolites can be accelerated through the application of various omics techniques, such as metabolomics, transcriptomics and proteomics analysis. The combination of multiple omics techniques presents a particularly promising strategy, providing insights into the correlation of BGC expression and metabolite production[52,356–358]. For screening purposes, small-scale cultivation in submerged environments is favoured over solid cultures, because it provides a more rapid and economically feasible approach to study extensive strain collections under diverse experimental conditions[359]. Microbioreactor (MBR) systems are of particular interest in this context. These systems not only provide extensive bioprocess monitoring, but present opportunities for integration into liquid handling robots[360]. Achieving reproducible small-scale cultivation of *Streptomyces* is challenging, yet it is feasible with tightly controlled inoculation strategies and well-characterised cultivation methods[361,362]. In submerged environments, *Streptomyces* grows as mycelial networks, typically forming dense pellets or mycelial mats[363]. This leads to diffusion gradients of nutrients within the pellets, which results in increased culture heterogeneity[363]. Previous work from our laboratory indicates that the model strains *Streptomyces lividans* and *Streptomyces coelicolor* can be cultured in low volumes of 100 µL in microtiter plates while maintaining enzyme and antibiotic production by optimising the agitation rate[362]. In another study, *S. lividans* was successfully cultivated in a 1 mL volume by optimising the preculturing strategy[361]. Their workflow involved the BioLector, an automated cultivation device that allows for non-invasive measurement of biomass formation, pH and dissolved oxygen (DO) concentration and fluorescence in a 48-well format. A recent study developed an automated workflow for multi-omics screening of microbial model organisms[364]. Their work focused on *Escherichia coli*, *Saccharomyces cerevisiae* and *Pseudomonas putida*, which are all unicellular organisms without complex morphologies.

In this study, we present a workflow for integrated quantitative proteomics and metabolomics analysis of 1 mL MBR cultures of *Streptomyces peucetius*, producer of the anticancer compounds daunorubicin and doxorubicin. Our results indicate that the technical reproducibility highly depends on the quality of the biological replicates. We show that it is feasible to analyse both the metabolome and proteome of small-scale *Streptomyces* cultures in a high-throughput manner, although further development of the method is required to reduce biological variance.

Results

Inoculum strategy for microbioreactor cultivation

Streptomyces strains are typically cultivated in shake flasks or on agar plates to generate proteomics and metabolomics datasets. In this study, we aimed to assess the feasibility of generating such datasets from microbioreactor (MBR) cultures. To achieve this, we used the BioLector, which has the advantage of non-invasive monitoring of growth, pH and dissolved oxygen (DO) concentration in real time. The device makes use of 48-wells plates with a working volume of 800 to 2400 µL. In this study, we used a wild-type and an industrial strain of *S. peucetius*. *S. peucetius* var. *caesius* ATCC 27952 (further referred to as WT) produces the anticancer compounds daunorubicin and doxorubicin[8,266]. The industrial strain *S. peucetius* G001 produces more than 100-fold more daunorubicin in production media[268]. Strictly controlled inoculation procedures are key to generate reliable growth data from complex mycelial cultures. We applied a relatively simple inoculation method that involves the fragmentation of mycelium into small fragments for direct inoculation of microtiter plates (Figure 1A).

WT and G001 were grown on SFM agar plates, and subsequently transferred to shake flasks containing TSB. The shake flasks were equipped with metal coils to facilitate dispersion of the mycelium. The submerged cultures were homogenised using an IKA tube drive. Small mycelial fragments were collected using a sterile syringe filled with cotton wool, and stocked in glycerol. The colony forming unit (CFU) concentration of the fragmented mycelial stocks was determined (see Materials and Methods for details). The optimal homogenising parameters were determined based on the morphology of the strains. For 48 h TSB cultures of both strains, homogenising for 2 min at 6000 rpm was sufficient to obtain small mycelial fragments at a high CFU concentration. Using this method, 20 mL of TSB culture would typically generate 5 mL glycerol stock of approximately $1{\cdot}10^{8}$ CFU·mL^{-1}.

Microbioreactor cultivation of *S. peucetius*

MBR cultivation was performed in a 48-well FlowerPlate with 1 mL working volume in a BioLector device with non-invasive measurement of growth, pH and DO concentration (Figure 1B). The flower-shaped wells provide a baffle-like structure, promoting dispersed mycelial growth. Modified R5 medium (R5*) was used as the cultivation medium, consisting of 50% diluted liquid R5 medium supplemented with TES buffer of pH 7.2 to a final concentration of 20 mM. Fragmented mycelial stocks of WT and G001 were inoculated into 1 mL R5* media, achieving

a concentration of $1{\cdot}10^6$ CFU·mL^{-1} with ten replicates. The cultures were agitated at 1200 rpm and online measurements were recorded at a 15 min interval. After 68 h, five replicate cultures were sacrificed for proteomics and metabolomics analysis (t_1, n=5). The remaining five replicates cultures were sampled after 115 h (t_2, n=5).

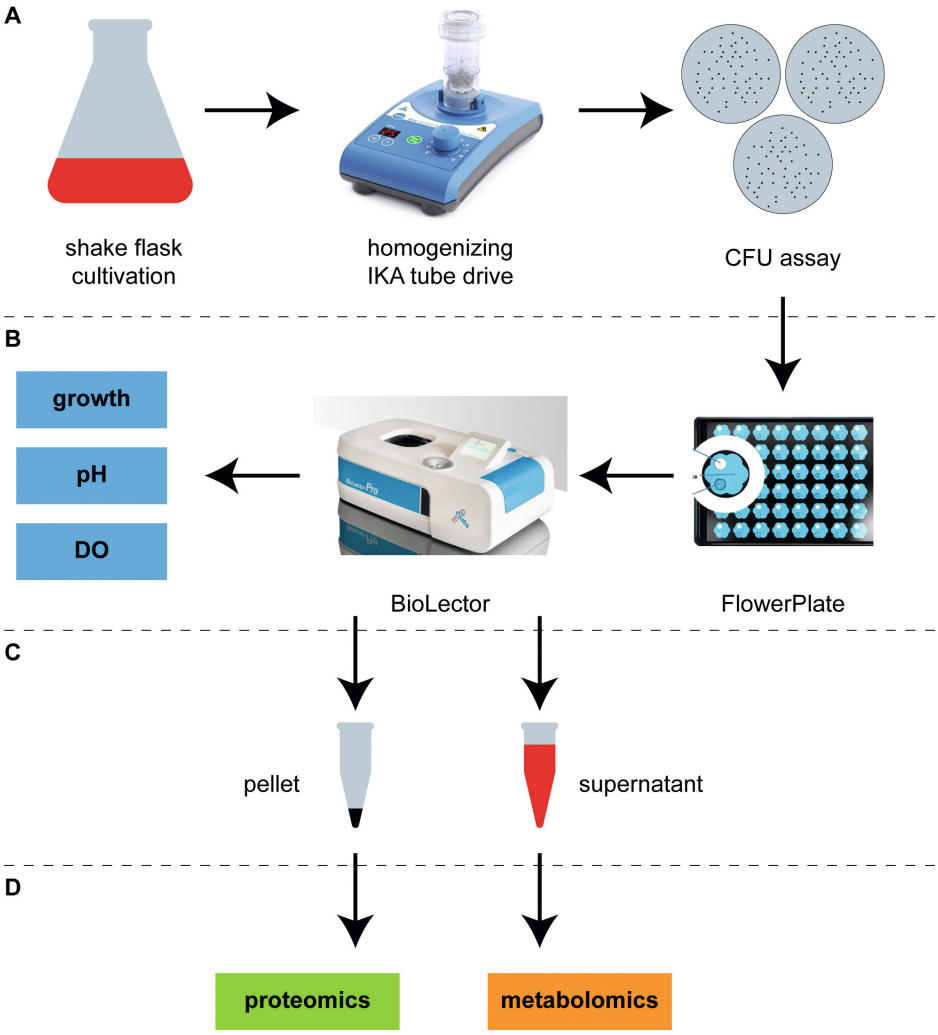


Figure 1. Workflow for integrated proteomics and metabolomics analysis of microbioreactor cultures. **(A)** To prepare the inoculi, precultures were homogenised and the CFU of the mycelial fragments were determined. **(B)** FlowerPlates were filled with 1 mL media and inoculated with fragmented mycelial stock. The plates were incubated in a BioLector with online measurement of growth, pH and dissolved oxygen (DO) concentration. **(C)** Sample preparation involved separation of pellet and supernatant via centrifugation. **(D)** The samples were processed for quantitative proteomics and metabolomics analysis, resulting in a paired dataset for each culture. Images: https://www.ika.com, https://www.m2p-labs.com/.

The growth profiles of the replicate cultures overlapped consistently during both the lag (about 0–15 h) and the growth phase (about 15–30 h) for both strains (Figure 2A). However, the values were more different following the onset of the stationary phase at about 30 h (Figure 2A).

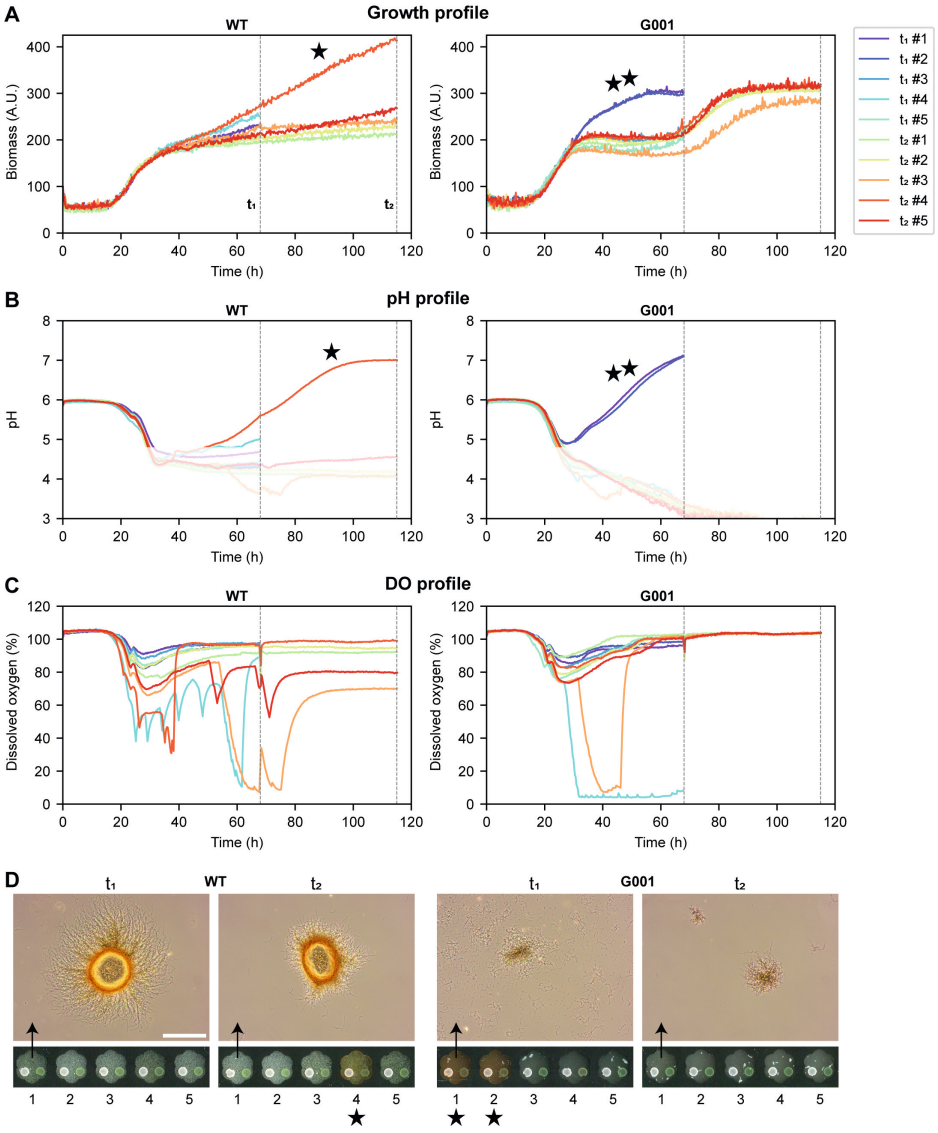


Figure 2. Online monitoring of growth, pH and dissolved oxygen (DO) of *S. peucetius* microbioreactor (MBR) cultures. *S. peucetius* WT and G001 were cultivated in 1 mL modified R5 medium (R5*) in an MBR for 68 h (t_1, n=5) or 115 h (t_2, n=5). **(A)** Growth profile based on scattered light measurements. **(B)** pH based on optical sensor data. The accurate measurement range lies between pH 4.8–7.2. **(C)** DO based on optical sensor data. **(D)** Morphology of WT and G001 at t_1 and t_2 (culture 1 for both strains). Outliers in growth, pH and phenotype are indicated by a star and were discarded for proteomics and metabolomics analyses. Scale bar: 200 µm.

The average biomass-specific growth rate during mid-growth phase (20–25 h) was 0.098±0.006 h^{-1} for WT and 0.082±0.008 h^{-1} for G001. The pH profiles overlapped consistently until the values dropped below the measurement range after about 30 h (Figure 2B). The DO concentration indicated that the stationary phase occurred at about 30 h when the DO concentration increased back to 100% saturation (Figure 2C). In six out of twenty wells, the DO data demonstrated irregular patterns, suggesting erroneous measurements in those particular wells. In terms of morphology, while WT formed mycelial pellets, G001 had a more fragmented morphology with a smaller pellet size (Figure 2D). WT sample 4 at t_2 and G001 samples 1 and 2 at t_1 exhibited increased red pigment production compared to the other cultures (Figure 2D, indicated with a star). The growth and pH data of these cultures also differed from the remaining replicates. The pH of the cultures turned basic during the stationary phase, and the growth measurements had higher final values (Figure 2A and 2B, indicated with a star). Based on the phenotype and cultivation data, we decided to omit these three cultures from the proteomics and metabolomics analyses.

In parallel to the MBR cultivations, the fragmented mycelial stocks of WT and G001 were inoculated in triplicate to the same CFU concentration in 10 mL R5* media in shake flasks. After 68 h (t_1) and 115 h (t_2), 950 µL of culture was collected from both the MBR plates (n=5) and the shake flasks (n=3). For MBR cultures, a single well was sacrificed for each sample, whereas each shake flask was sampled at both timepoints. The samples were centrifuged (Figure 1C), the pellets were used for proteomics analysis, and the supernatants for metabolomics analysis (Figure 1D).

Quantitative proteomics analysis of *S. peucetius* microbioreactor cultures

The biomass samples of *S. peucetius* WT and G001 MBR and shake flask cultures were processed for quantitative proteomics. As describe above, we discarded three MBR samples because of their highly divergent phenotypes as compared to all other samples, resulting in five samples of WT at t_1 (n=5), four samples of WT at t_2 (n=4), and five samples of G001 at t_2 (n=5), and three samples of G001 at t_1 (n=3). Additionally, three shake flasks cultures of each strain were sampled at both timepoints (n=3). The proteins were extracted and analysed using liquid chromatography-mass spectrometry (LC-MS) analysis (see Materials and Methods for details). The data were normalised and filtered using MaxQuant software (v2.2.0.0)[289].

In total, 3135 proteins were detected across all samples, and at least 2432 proteins were detected in each individual sample. The *S. peucetius* genome contains 6592 putative coding sequences, so we could detect 48% of the proteins in at least one sample. Venn diagrams were created using the web-based tool InteractiVenn[365]. Most proteins (89%) were detected in both strains under all experimental conditions (Supplementary Figure S1A). Principle component analysis (PCA) was used to visualise the similarities between the individual samples. The samples separated by strain and cultivation method in the PCA score plot, indicating that the two cultivation methods resulted in strong differences in the proteomes of the two strains (Figure 3A). Furthermore, the two strains showed strongly different proteomes, which may be

expected when comparing a wild-type and industrial strain. The MBR samples of WT showed more variability between the individual samples than the G001 samples. Proteins with a minimum two-fold difference in abundance and a *p*-value ‹0.05 in a two-sample *t*-test were considered differentially expressed.

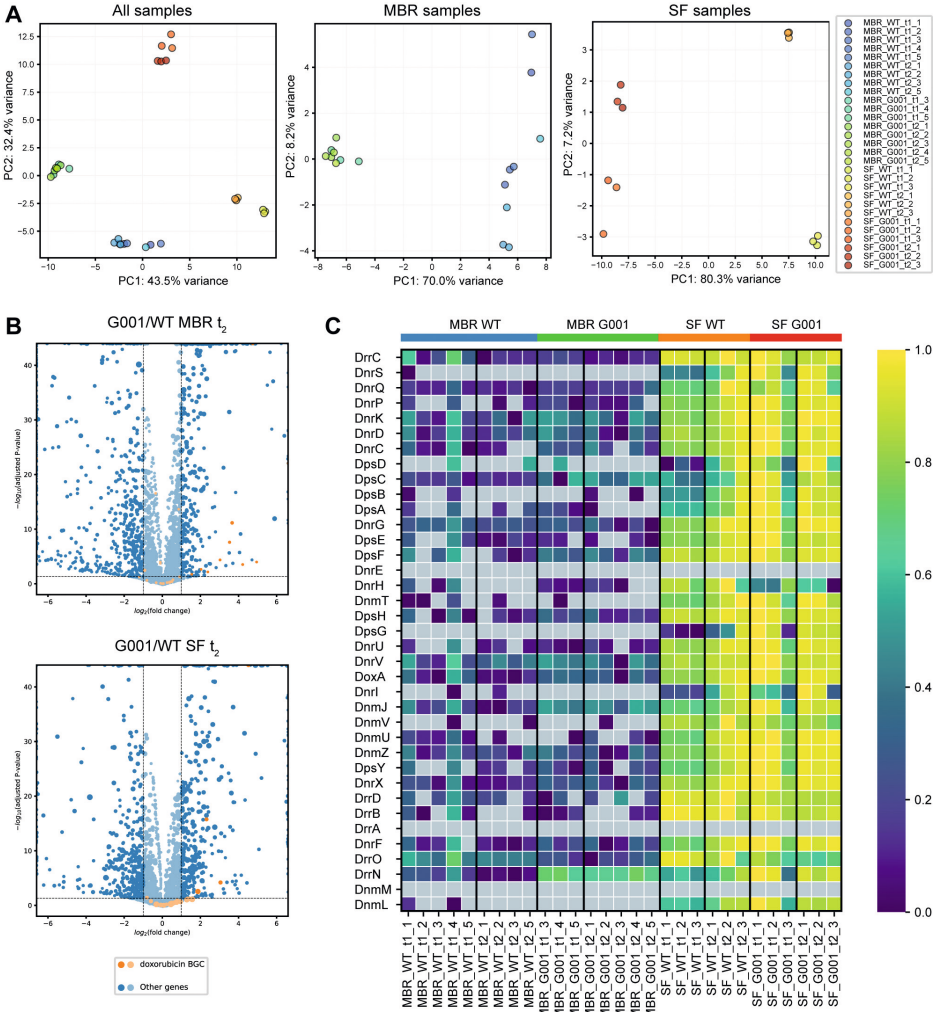


Figure 3. Proteomics analysis of *S. peucetius* grown in a microbioreactor (MBR) and in shake flasks (SF). **(A)** PCA score plots of proteomics data of G001 and WT grown in R5* in a MBR or in shake flasks for 68 h (t_1) or 115 h (t_2). Left panel: all samples, middle panel: only MBR samples, right panel: only shake flask samples. **(B)** Volcano plots of proteomics data of MBR (upper panel) and shake flask (lower panel) cultivation of G001 and WT at t_2. Proteins with an FDR-adjusted *p*-value ›0.05 and fold change ‹2 are represented in a lighter shade. Positive $\log_2$ fold change values represent overexpression in G001. Proteins derived from the doxorubicin BGC are indicated in orange. **(C)** Heatmap showing the relative abundance of the proteins encoded by the doxorubicin BGC in each sample. Grey tiles indicate that the protein was not detected.

Volcano plots were generated to compare the protein expression in the two strains at the second timepoint in each cultivation method. Differentially expressed proteins are visualised in darker shade, and proteins that belong to the doxorubicin BGC were indicated in orange. For both MBR and shake flask cultures, several proteins encoded by the doxorubicin BGC were upregulated in G001 as compared to WT (Figure 3B). A heatmap was generated of the relative abundance that shows the detected proteins that belong to the doxorubicin BGC. This revealed that the expression of the doxorubicin BGC was relatively high in the shake flask cultures as compared to the MBR cultures (Figure 3C). In the MBR cultures, not all proteins encoded by the doxorubicin BGC could be detected.

Taken together, we could detect about half of the proteins encoded by the genome of *S. peucetius* in both shake flask and MBR cultures using this integrated workflow. PCA analysis indicated a strong correlation among individual samples from the same strain, and distinct separation between samples from the different strains.

Metabolomics analysis of *S. peucetius* microbioreactor cultures

The supernatants of *S. peucetius* WT and G001 cultures grown in R5* in either MBR or shake flasks were processed for metabolomics analysis (see Materials and Methods for details). As describe above, we discarded three MBR samples with differing phenotype. Metabolites were extracted using LC-18 SPE tubes, eluted using methanol, and analysed using LC-MS. The LC-MS data was processed using MZmine 3[366], resulting in a list containing all the mass features and their peak areas detected in each crude extract.

Venn diagrams were created using the web-based tool InteractiVenn[365]. Of all detected metabolites, 20% were detected only in MBR extracts, and 28% only in shake flask extracts (Supplementary Figure S1B). Furthermore, 22% of the metabolites were only detected in WT extracts and 8.6% only in G001 extracts (Supplementary Figure S1B). PCA analysis was performed using MetaboAnalyst 6.0 with log transformation and pareto scaling[367]. The samples separated by strain and cultivation method, but the timepoints were not clearly separated in PC1 and PC2 (Figure 4A). To study the abundance of the individual metabolites, a heatmap with hierarchical clustering was generated using MetaboAnalyst 6.0[367]. The anthracyclines doxorubicin, daunorubicin and 13-dihydrodaunorubicin were annotated using a previously described method[293]. The anthracyclines were highly abundant in the extracts of G001 grown in shake flasks (Figure 4B). In contrast, the anthracyclines could not be detected in the extracts of MBR-grown cultures. This is in accordance with the protein levels that relate to the doxorubicin BGC, which were relatively low in the MBR samples. Interestingly, the heatmap indicated that different metabolite groups were detected in MBR and shake flask cultures. The processed data obtained from MZMine 3 were exported to the Feature-Based Molecular Networking (FBMN) workflow[368] on GNPS[369] to create a molecular network (see Materials and Methods for details). Interestingly, the spectral families were distinctly separated between the two cultivation methods (Figure 5). Spectral families 5, 6 and 9 were only detected in the MBR-derived extracts (in blue and green). Other spectral families were overrepresented in the shake

flask-derived extracts (in red and orange). Spectral family 8 comprised the anthracyclines 13-dihydrodaunorubicin, daunorubicin and doxorubicin. Three features in spectral family 1 were annotated as dehydrorabelomycin, a non-glycosylated angucycline polyketide, by comparison of MS/MS data against GNPS spectral libraries[369,370]. No compounds could be dereplicated in the spectral families that were overrepresented in the MBR cultures.

Taken together, we detected differences in the chemical space between MBR and shake flask cultures. The MBR cultures provided consistent and reproducible metabolome profiles. High expression of doxorubicin biosynthetic proteins corresponded to high abundance of anthracyclines in the crude extracts.

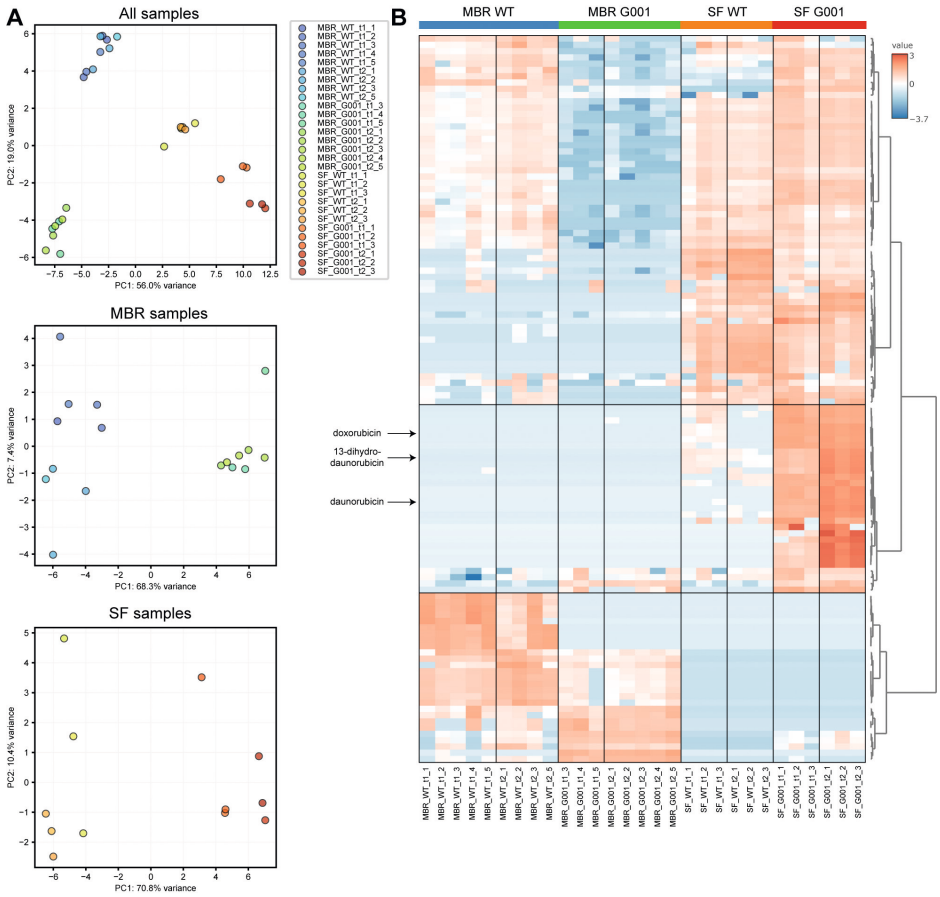


Figure 4. Metabolomics analysis of *S. peucetius* grown in a microbioreactor (MBR) and in shake flasks (SF). **(A)** PCA score plots of metabolomics data of G001 and WT grown in R5* in a MBR or in shake flasks for 68 h (t_1) or 115 h (t_2). **(C)** Heatmap with hierarchical clustering showing the relative abundance of the mass features detected in each sample. Mass features with relatively high peak areas are presented in red. The anthracyclines doxorubicin, daunorubicin and 13-dihydrodaunorubicin are indicated.

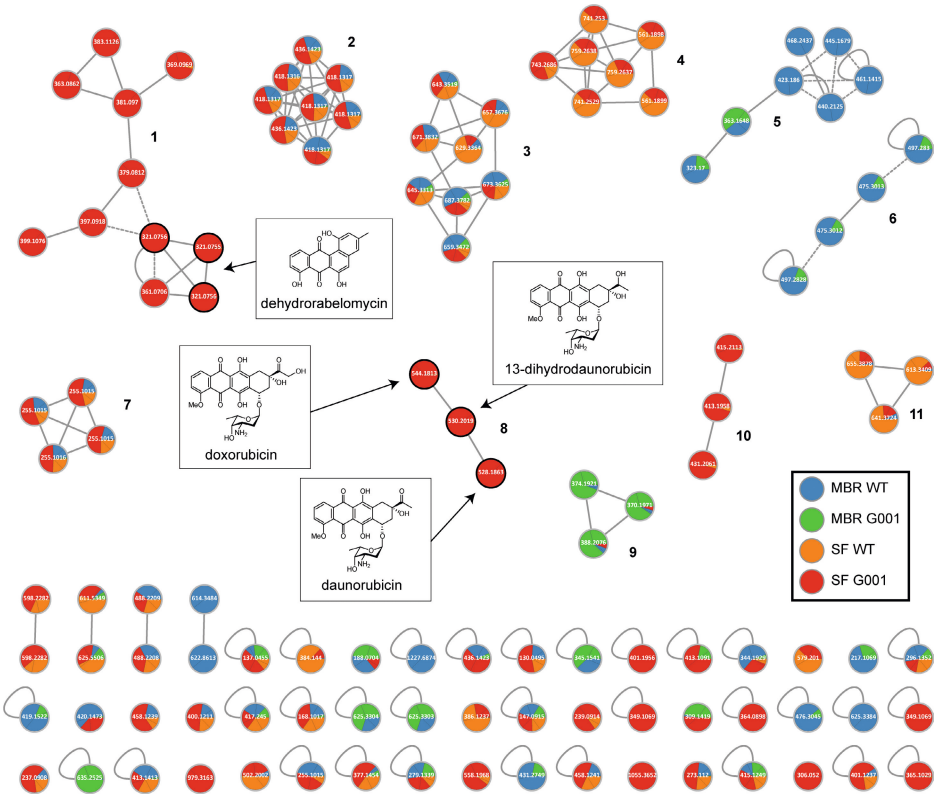


Figure 5. Molecular network of the ions detected in the crude extracts of *S. peucetius* grown in a microbioreactor (MBR) and in shake flasks (SF). A pie chart was mapped to the nodes which represents the relative intensities of the ion in the MBR extracts of WT (blue) and G001 (green), and in the shake flask extracts of WT (orange) and G001 (red). The nodes are labelled by the precursor mass of their ions. The dashed edges connect different ions of the same molecule and solid edges connect nodes based on their MS/MS similarity. Nodes highlighted with a black stroke represent annotated compounds: 13-dihydrodaunorubicin, daunorubicin, doxorubicin and dehydrorabelomycin.

Discussion

Streptomycetes harbour a wealth of BGCs with yet unidentified natural products[2,371]. As a promising strategy to accelerate the discovery of these potentially bioactive metabolites, we developed a high-throughput multi-omics workflow for characterisation of *Streptomyces* strain collections at diverse experimental conditions. To achieve this, a workflow was developed for integrated quantitative proteomics and metabolomics analysis of small-scale *Streptomyces* cultures. As test strains for the system, *S. peucetius* WT and its industrial variant G001 were selected and grown in 1 mL volume, followed by proteomics and metabolomics analyses. The results of these paired omics experiments indicated that reproducible data with high sensitivity can be obtained from *S. peucetius* grown in small culture volumes.

Optimisation of the cultivation method is required to reduce biological variability. MBR cultures of *S. peucetius* WT and G001 showed high biological variability, with two of the ten G001 cultures and one of the ten WT cultures showing a significantly different phenotype with increased red pigmentation. These samples had to be removed from further analysis via metabolomics and proteomics. Optimisation of the inoculum procedure may reduce the biological variability between the replicate cultures. For instance, the reproducibility of MBR cultures of *S. lividans* was optimised by applying two pre-cultures in shake flasks and subsequently inoculating a MBR based on optical density[361]. When disregarding the three cultures with increased red pigmentation, the remaining replicates were of good quality in terms of growth and pH data. However, the DO concentration measurements did not consistently align across all replicate samples. The measurement of DO concentration relies on fluorescence measurement conducted via an optical sensor positioned inside the cultivation chamber. Consequently, the production of fluorescent metabolites, such as anthracyclines, could potentially interfere with the DO measurements[372]. Alternatively, the irregularity of the DO curves may also have resulted from a technical error with the sensor. The consistent growth and pH profiles observed between the replicate cultures confirm that this cultivation method is suitable for process control applications with *Streptomyces*. Integrating the BioLector device with the corresponding liquid robot handling system (RoboLector) provides opportunities for more complex cultivation strategies[373]. For instance, elicitors may be added to the cultures at a specific timepoints or growth phase to study the effect on natural product biosynthesis, or a pH control strategy may be considered, by the addition of acid or base solutions based on online measurements.

Proteomics and metabolomics analysis of the MBR cultures yielded promising results. PCA analysis of both datasets indicated distinct separation among samples based on strain, and strong correlation among samples of the same strain. The shake flask samples demonstrated better separation between the two timepoints as compared to the MBR-derived samples. These results indicate that the metabolic state between the timepoints varies more in shake flask-grown cultures than in well-controlled MBR-grown cultures. Furthermore, the expression of the proteins encoded by the doxorubicin BGC was relatively high in shake flask cultures, which corresponded to a higher abundance of anthracyclines in the associated crude extracts. Molecular networking of the mass features identified in each extract indicated that the metabolite profiles in the shake flask and MBR cultures were very different. These results indicate that the metabolite extraction method has good sensitivity to detect differences in the chemical space, and that MBR cultivation can result in the detection of different (and hence probably also new) metabolites than what is produced in shake flasks. It would be of interest to expand this study to other streptomycetes, and analyse more replicate cultures for better statistical analysis. Additionally, the proteomics and metabolomics sample preparation could be automated using liquid handling robotics. Both methods are highly dependent on sample preparation procedures and quenching of biochemical reactions at the time of sampling, posing challenges for automation. To study the extracellular metabolome, we used solid-phase extraction with methanol, which is a fast method but reduced sensitivity[374]. Recent developments the proteomics field have provided sensitive label-free quantitative mass-

spectrometry methods that we applied in this workflow[52]. In the future, new developments in mass spectrometry-based analytical procedures may provide more sensitive multi-omics data from small sample sizes.

In conclusion, we developed a workflow for integrated quantitative proteomics and metabolomics analysis of small-scale *Streptomyces* cultures. The workflow provided good quality data from a technical perspective, although biological reproducibility should be optimised in future work.

Materials and Methods

Bacterial strains and culture media

Two *Streptomyces peucetius* strains were used in this study. *S. peucetius* var. *caesius* ATCC 27952[8] is a wild-type strain that produces daunorubicin and doxorubicin (designated WT). *S. peucetius* G001[268] is derived from ATCC 27952 by *N*-methyl-*N'*-nitro-*N*-nitrosoguanidine mutagenesis and has increased production of daunorubicin. All media and routine *Streptomyces* techniques have been described previously[1]. Soy flour mannitol (SFM) agar plates were used for phenotypical characterisation. Luria-Bertani (LB) agar plates were used for viability assays. Tryptone soy broth (TSB) was used for preparation of mycelial stocks. Modified R5 medium (R5*) was used for shake flask and microbioreactor (MBR) cultivation. R5 liquid medium was prepared following the agar recipe[1] without the addition of agar. R5* was prepared by diluting the R5 liquid medium to 50% in a TES buffer of pH 7.2 to a final concentration of 20 mM TES.

Preparation of mycelial stocks

Strains were streaked on SFM agar plates and incubated at 30 °C for 7 days. Five single colonies were inoculated in 20 mL of TSB medium in 100 mL Erlenmeyer flasks equipped with metal coils. The cultures were incubated in an orbital shaker at 200 rpm (1 inch orbit) at 30 °C for 48 h. Cultures were centrifuged (10 min, 3000 rpm), resuspended with 15 mL of 10.3% (w/v) sucrose and centrifuged again (10 min, 3000 rpm). For preparation of mycelial stocks, the washed biomass was resuspended in 2–5 mL of 20% (w/v) glycerol and stored in aliquots of 1 mL at -80 °C. For preparation of fragmented mycelial stocks, the washed biomass was resuspended in 15 mL of 10.3% (w/v) sucrose. The mycelial suspensions were homogenised using a ULTRA-TURRAX Tube Drive (IKA, Germany) in a 15 mL dispersing tube (DT-20 eco, IKA, Germany). The mycelium suspensions were homogenised at 6000 rpm for 1 min, cooled down on ice for 1 min, and homogenised again at 6000 rpm for 1 min. The mycelium suspensions were collected from the dispersing tube using two volumes of 10.3% (w/v) sucrose. The large mycelial fragments were filtered out using a sterile syringe filled with cotton wool. The mycelium suspensions were centrifuged (10 min, 3000 rpm) and resuspended in 2–5 mL 20% glycerol. Fragmented mycelial stocks were stored in aliquots of 1 mL at -80 °C. The concentration of viable mycelial fragments was determined using a colony forming units (CFU) assay. A dilution series was prepared in 10.3% (w/v) sucrose and plated on LB agar plates. CFUs were counted after 2 days incubation at 30 °C.

Shake flask cultivation

Shake flask cultivations were performed in 50 mL Erlenmeyer shake flasks without metal coils. Fragmented mycelial stocks were centrifuged (2 min, 6000 rpm), and resuspended in R5* medium to $1{\cdot}10^8$ CFU·mL^{-1}. Subsequently, 9.9 mL of R5* medium was inoculated with 1 mL of mycelium suspension to a final concentration of $1{\cdot}10^6$ CFU·mL^{-1}. Shake flasks were incubated in an orbital shaker at 200 rpm (1 inch orbit) at 30 °C for 5 days. All experiments were performed in triplicate.

Microbioreactor cultivation

MBR cultivation was performed in an automated cultivation device (BioLector II, Beckman Coulter). Strains were cultivated in 1 mL working volume in a 48-well FlowerPlate (MTP-48-BOH2, Beckman Coulter, USA) covered with an adhesive gas-permeable membrane for reduced evaporation (F-GPR48-10, Beckman Coulter). Fragmented mycelial stocks were centrifuged (2 min, 6000 rpm), and resuspended in R5* medium to $1{\cdot}10^8$ CFU·mL^{-1}. Subsequently, 990 µL of R5* medium was inoculated with 10 µL of mycelium suspension to a final concentration of $1{\cdot}10^6$ CFU·mL^{-1}. The shaking frequency was set to 1200 rpm (3 mm orbit), temperature was controlled at 30 °C, and relative humidity was controlled at 85%. Online measurements were recorded at a 15 min interval. Growth was measured using the scattered light filter module at gain 6 (E-OP-401). The pH and dissolved oxygen (DO) concentration were measured using the corresponding optical sensors (optodes) integrated in the microtiter plates. The data was obtained using the LG1 (E-OP-421) and RF (E-OP-428) filter modules, for pH and DO respectively. All experiments were performed with five replicates.

Sample collection

After 68 h and 115 h incubation, 950 µL samples were obtained from shake flask (n=3) or MBR cultures (n=5). For MBR cultures, a single well was sacrificed for each sample, whereas each shake flask was sampled at both timepoints. Samples were cooled down on ice and centrifuged (10 min, 13,000 rpm, 4 °C). The supernatant was transferred to a fresh tube. Biomass and supernatant samples were snap-frozen in liquid nitrogen and stored at -80 °C until analysis.

Proteomics sample preparation and LC-MS/MS analysis

Frozen biomass samples were washed using washing buffer [100 mM Tris-HCl (pH 7.5), 150 mM KCl, 10 mM $MgCl_2$]. Subsequently, the biomass was lysed using a Bioruptor Plus (Diagenode SA) and proteins were extracted using lysis buffer [4% SDS, 100 mM Tris-HCl (pH 7.6), 50 mM EDTA]. Sample preparation for LC-MS/MS measurement was performed as described previously[286]. Briefly, total protein was precipitated using the chloroform-methanol method[287] and dissolved in 0.1% RapiGest surfactant (Waters Crop.) at 95 °C. The protein concentration was determined using the BCA method. Protein samples were reduced by adding 5 mM DTT and incubated in the dark at 60 °C for 30 min, followed by thiol group protection using 21.6 mM iodoacetamide and incubation in the dark at room temperature for 30 min. Subsequently, 0.1 µg of trypsin (recombinant, proteomics grade, Roche) per 10 µg of protein was added, and samples were digested overnight at 37 °C. After digestion, trifluoroacetic acid was added to a concentration of 0.5%. The samples were incubated at 37 °C for 30 min, followed by centrifugation to degrade

and remove the RapiGest surfactant. 4 µg of peptides was cleaned and desalted using the StageTips method[288]. Briefly, 4 µg of peptides was loaded onto a conditioned StageTip (premade SPE tips, cat No. C18.T1.10.960, Affinisep), washed twice using a 0.5% formic acid solution, and eluted with elution solution (80% acetonitrile and 0.5% formic acid). Acetonitrile was evaporated using a SpeedVac. The final peptide concentration was adjusted to 40 ng·µL^{-1} using sample solution (3% acetonitrile and 0.5% formic acid) for analysis.

Quantitative proteomics was performed as described previously[286]. Briefly, the desalted peptide solution was separated using an UltiMate 3000 RSLCnano system (Thermo Scientific) set in a trap-elute configuration, coupled with a QExactive HF mass spectrometer (Thermo Scientific). The liquid chromatography system used a Waters nanoEase M/Z Symmetry C_{18} trap column (5 µm, 100 Å, 180 µm × 20 mm) for peptide loading and retention, and a Waters nanoEase M/Z HSS T3 C_{18} analytical column (1.8 µm, 100 Å, 75 µm × 250 mm) for peptide separation. The mass spectrometer was operated in positive mode with data-dependent acquisition.

Proteomics data analysis

Raw LC-MS/MS files were analysed using MaxQuant software v2.2.0.0[289] using the label-free quantification (LFQ) method. Only proteins that were detected in at least 30% of the replicates of one treatment group were included in the analysis. LFQ data was imported to DESeq2 v1.38[303] and differential expression analysis was performed with the function logarithmic fold change shrinkage[375]. PCA plots were generated from the variance stabilising transformed data in Python (v3.10) with matplotlib (v3.7.1). Volcano plots were generated from the differential expression analysis data. LFQ data was log-transformed and normalised by protein to the value of 1 using scikit-learn (v1.3.0), and heatmaps were generated using seaborn (v0.12.2).

Metabolomics sample preparation and LC-MS/MS analysis

For metabolite extraction, supernatant was loaded onto LC-18 SPE tubes (Supelco, 100 mg), previously conditioned with 1 mL of methanol and 1 mL of water. The resin was then washed with 1 mL of water to remove salts and polar media components, and the metabolites were eluted using 1 mL of methanol.

LC-MS/MS acquisition was performed using Shimadzu Nexera X2 UHPLC system, with attached photodiode array detector (PDA), coupled to Shimadzu 9030 QTOF mass spectrometer (MS), equipped with a standard electrospray ionisation (ESI) source unit, in which a calibrant delivery system (CDS) was installed. A total of 2 µL were injected into a Waters Acquity HSS C_{18} column (1.8 µm, 100 Å, 2.1 × 100 mm). The column was maintained at 30 °C, and run at a flow rate of 0.5 mL·min^{-1}, using 0.1% formic acid in H_2O as solvent A, and 0.1% formic acid in acetonitrile as solvent B. A gradient was employed for chromatographic separation starting at 15% B for 1 min, then 15–60% B for 9 min, 60–100% B for 1 min, and finally held at 100% B for 3 min. The column was re-equilibrated to 5% B for 3 min before the next run was started. The PDA acquisition was performed in the range 200–600 nm, at 4.2 Hz, with 1.2 nm slit width. The flow cell was maintained at 40 °C.

All the samples were analysed in positive polarity, using data dependent acquisition mode. In this regard, full scan MS spectra (*m/z* 100–2000, scan rate 20 Hz, ID disabled) were followed by three data dependent MS/MS spectra (*m/z* 100–2000, scan rate 20 Hz, ID disabled) for the three most intense ions per scan. The ions were selected when they reach an intensity threshold of 1500, isolated at the tuning file Q1 resolution, fragmented using collision induced dissociation at fixed collision energy of 20 eV, and excluded for 0.01 s before being re-selected for fragmentation. The parameters used for the ESI source were: interface voltage 4 kV, interface temperature 300 °C, nebulising gas flow 3 $L \cdot min^{-1}$, and drying gas flow 10 $L \cdot min^{-1}$. Samples were randomised before injection and pooled QC were injected.

Metabolomics data analysis

LC-MS raw data files were converted to mzXML centroid files using Shimadzu LabSolutions Postrun Analysis. The files were then imported into MZmine 3 (v3.9.0) for data processing[366]. For all the modules unless stated differently, *m/z* tolerance was set to 0.002 *m/z* or 10.0 ppm, RT tolerance was set to 0.05 min and minimum scans were set to 6. For mass detection in positive polarity and when using the algorithm centroid the noise was set to 1000 for MS1 and 10 for MS2, the option of detecting isotopes signals below noise level was selected. For the module ADAP chromatogram builder to minimum intensity for consecutive scans was set to 3000 and the minimum absolute height to 10000. For peak deconvolution the local minimum resolver algorithm was used with a chromatographic threshold of 90%, a minimum search range RT of 0.05, a minimum absolute hight of 1000, and a minimum ratio peak top/edge of 1.80. The 13C isotope filter module was used with RT tolerance of 0.03 min, and maximum charge of 3. The isotopic peaks finder module was set using the chemical elements C, H, N, O, and S, and a maximum charge isotope *m/z* of 3. To align the peak lists, the weight of *m/z* was set at 4 and the weight of RT was set at 1. The aligned feature list was filtered using the duplicate filter module in the filter mode new average, and the feature list row filter features present in at least 2 samples. The peak finder module was used, the intensity tolerance was set at 10% and the RT tolerance at 0.1 min. In order to build the ion identity network, the correlation group module was used with a minimum feature height of 10000 and an intensity threshold for correlation of 1000. For the ion identity network module, the ion identity library parameters were a maximum charge of 3, maximum molecules per cluster of 3, and adducts $[M+H]^+$, $[M+Na]^+$, $[M+K]^+$, $[M+NH_4]^+$, modifications $[M-H_2O]^+$, $[M-2H_2O]^+$, and $[M-3H_2O]^+$. The resulted feature list was exported to be used for GNPS feature based molecular networking analysis. In addition, the quantitative table was filtered to remove features from the media or with low technical repeatability by removing features which average intensity in the media samples was more than 30% of the average in the samples, or the relative standard deviation (RSD) in the pooled QC was higher than 30%. PCA analysis was performed using MetaboAnalyst 6.0[367]. Log transformation with pareto scaling was applied to the data. PCA plots were generated in Python (v3.10) with matplotlib (v3.7.1). Venn diagrams were created using the web-based tool InteractiVenn[365].

The processed data obtained from MZMine 3 were exported to the Feature-Based Molecular Networking (FBMN) workflow[368] on GNPS[369] to create a molecular network. In addition, the MS/

MS data was filtered and all fragment ions within +/- 17 Da of the precursor *m/z* were removed. MS/MS spectra were window filtered by choosing only the top 6 fragment ions in the +/- 50 Da window throughout the spectrum. The tolerance for precursor ion mass and MS/MS fragment ion were set to 0.01 Da. To generate the network, only edges with cosine values above 0.7 and more than 6 matched fragment peaks were taken into account. Moreover, to keep the edges between two nodes they must be in each other's top 10 most similar nodes. Lastly, the maximum size of a molecular family was set to 100. The MS/MS spectra were compared against GNPS spectral libraries[369,370]. The library spectra were filtered in the same manner as the input data. All matches kept between network spectra and library spectra were required to have a score above 0.7 and at least 6 matched peaks. Additional edges obtained from the ion identity network analysis in MZmine3 were also included in the network[376]. For visualisation of the molecular network Cytoscape (v3.10.1) was used[377]. Edges were coloured according to the edge type, cosine edges were coloured grey and MS1 IIMN edges were coloured red. A heatmap was generated from the doxorubicin related nodes using MetaboAnalyst 6.0[367] using with settings.

Supplemental Information

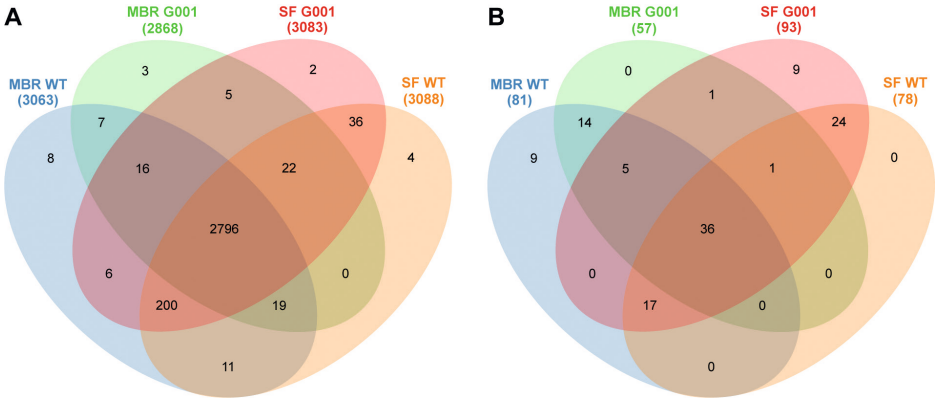


Figure S1. Venn diagrams of *S. peucetius* proteins and metabolites detected in microbioreactor (MBR) and in shake flask (SF) cultures. (A) Total number of proteins detected across all samples of WT from MBR (blue), G001 from MBR (green), G001 from shake flask (red) and WT from shake flask (orange). Most proteins (89%) were detected in both strains under all experimental conditions. **(B)** Total number of mass features detected across all samples of WT from MBR (blue), G001 from MBR (green), G001 from shake flask (red) and WT from shake flask (orange). Of the 116 detected mass features, 20% were detected only in MBR cultures, and 28% only in shake flask cultures.



General discussion

Anthracyclines are important anticancer drugs, despite severe dose-limiting side effects. Since their discovery in the 1950s[28], many efforts have been directed toward developing detoxified anthracyclines with better efficacy. More than 500 naturally occurring anthracyclines have been isolated from Actinobacteria[172,173,266], yet only daunorubicin (Dauno, Figure 1), doxorubicin (Doxo, Figure 1) and aclarubicin (Acla, Figure 1) are used in the clinic for cancer treatment[13]. Metabolic engineering strategies have yielded numerous derivatives mostly via combinatorial biosynthesis[216] and glycodiversification[105]. Moreover, comprehensive structural libraries of anthracyclines have been prepared through organic synthesis[17–19,378]. Despite these efforts, only semi-synthetic epirubicin, idarubicin, pirarubicin and valrubicin have been successfully introduced into the clinic[87].

Recent insights into the mode-of-action of anthracyclines have prompted renewed interest into this important class of anticancer compounds (**Chapter 2**). One of the most promising compounds is *N,N*-dimethyldoxorubicin (DMdoxo, Figure 1), a hybrid structure that combines the aglycone of Doxo with the amino sugar moiety of Acla, generated through semi-synthesis[16]. DMdoxo has potent cytotoxic activity but does not induce cardiotoxicity, the most acute and treatment-limiting side effect of Doxo[16]. Evaluation of anthracycline structural libraries indicated that the presence of a tertiary amine on the first sugar moiety of anthracyclines generally corresponds to the loss of DNA-damaging activity combined with improved cytotoxicity[17–19]. These results are promising for the development of detoxified anthracyclines.

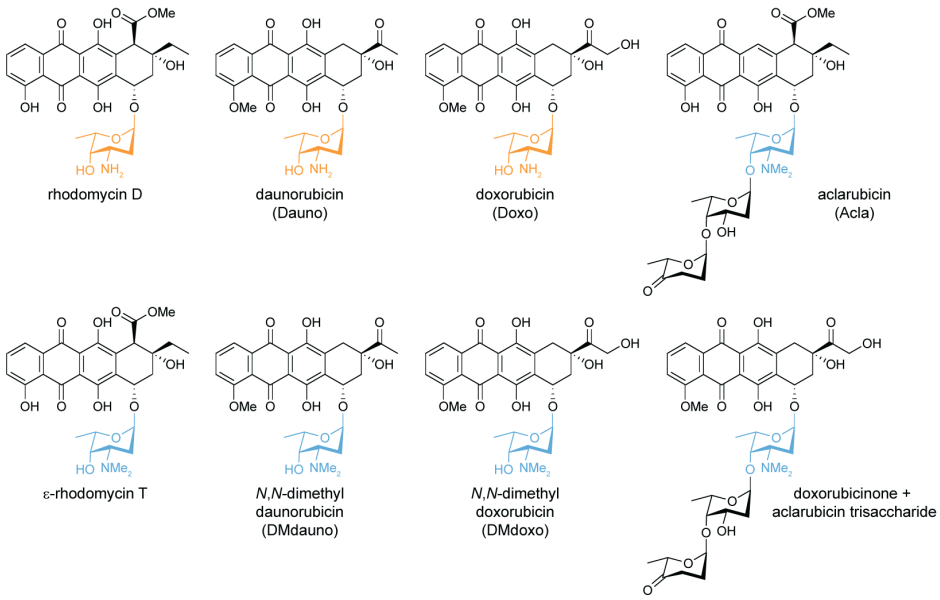


Figure 1. Chemical structures of relevant anthracyclines. The amino sugar L-daunosamine is represented in orange and the *N,N*-dimethylated derivative L-rhodosamine is represented in blue.

For clinical applications, Doxo is currently produced via a combination of fermentation and organic chemistry. In the first step, Dauno is obtained biosynthetically via fermentation of an industrial *Streptomyces peucetius* strain. Subsequently, biosynthetic Dauno is converted to Doxo via chemical 14-hydroxylation. Doxo can be obtained fully biosynthetically, but the final tailoring enzymatic reaction catalysed by the cytochrome P450 monooxygenase DoxA is notoriously inefficient[153], resulting in low yields. To date, DMdoxo has not been isolated from natural sources, but biosynthesis would be an attractive option for scaling up production of this promising compound.

For this reason, we aimed to engineer the Doxo biosynthetic pathway in *S. peucetius* for the production of biosynthetic *N,N*-dimethylated anthracyclines (**Chapter 3**). The challenges that we encountered instigated the study of anthracycline resistance mechanisms in *Streptomyces* (**Chapter 4**), and potential applications of detoxified anthracyclines as antibiotics (**Chapter 5**). Finally, to facilitate future screening and strain engineering efforts of *Streptomyces* producer strains, we developed a workflow for integrated quantitative proteomics and metabolomics from small-scale *Streptomyces* cultures (**Chapter 6**).

Challenges in engineering anthracycline biosynthesis

Combinatorial biosynthesis of anthracyclines has been widely applied for the generation of anthracycline hybrids in *Streptomyces*[216,266]. Especially the Acla-producer *Streptomyces galilaeus* has been focus of many studies, mainly via the introduction of tailoring enzymes from other anthracycline biosynthetic pathways[115,217–222,224]. Alternatively, anthracycline biosynthetic genes have been expressed in heterologous hosts, such as *Streptomyces venezuelae*[231,232], *Streptomyces coelicolor*[109] and *Streptomyces lividans*[109,117], that do not naturally produce anthracyclines.

Our approach to achieve biosynthesis of DMdauno and DMdoxo involved modifying the Doxo biosynthetic pathway in the industrial *S. peucetius* strain G001 (**Chapter 3**). We introduced the methyltransferase genes essential for TDP-L-rhodosamine biosynthesis, along with the corresponding glycosyltransferase genes from *S. galilaeus*, in G001. To abolish the production of non-dimethylated anthracyclines, we deleted *dnrS* encoding the Doxo glycosyltransferase. Subsequently, expression of the rhodomycin methyltransferase gene *rdmC* resulted in the successful production of DMdauno, although with limited productivity.

Our data showed that the presence of the rhodosamine moiety inhibits the three consecutive hydroxylation reactions required to form the Doxo aglycone structure. These reactions are catalysed by the cytochrome P450 monooxygenase DoxA, an enzyme unique to the Doxo pathway[266]. It has long been known that the final reaction in the biosynthetic pathway from Dauno to Doxo is extremely inefficient[153,254]. In fact, this is the reason why Doxo is currently produced semi-synthetically from daunorubicin in industry. Enzymatic assays of DoxA with *N,N*-dimethylated compounds showed significantly lower activity than with its natural substrates, indicating that this enzyme is the bottleneck for biosynthetic production of

DMdoxo. One potential solution could involve engineering of DoxA for improved activity. However, attempts to determine the structure of DoxA have thus far been unsuccessful, complicating rational engineering approaches. Alternatively, high-throughput methods using random or model-guided mutagenesis may prove successful in identifying DoxA variants with improved activity[379]. Another potentially limiting factor for DMdoxo biosynthesis is the significantly stronger toxicity of *N,N*-dimethylated anthracyclines to *S. peucetius* compared to the non-dimethylated variants. This finding motivated us to delve into anthracycline resistance in *Streptomyces*.

Cryptic anthracycline resistance genes in *Streptomyces*

Self-resistance mechanisms against toxic natural products are often encoded within biosynthetic gene clusters (BGCs)[57,323]. Anthracycline BGCs typically harbour ATP-binding cassette (ABC) transporter genes to support the efflux of the toxic metabolites[266]. Besides that, the presence of antibiotics in the environment resulted in the evolution or acquisition of highly specific resistance mechanisms against exogenous antibiotics[316,317]. In **Chapter 4**, we explored resistance against anthracyclines in actinomycetes via screening of our in-house strain collection and adaptive laboratory evolution experiments.

Screening of our in-house MBT collection of Actinobacteria revealed that while Doxo resistance was relatively common, all strains were highly sensitive to DMdoxo. Selected streptomycetes were challenged with DMdoxo in an adaptive laboratory evolution experiment, which resulted in strongly increased anthracycline resistance within five generations. Transcriptomics analysis of a DMdoxo-resistant *S. lividans* TK24 isolate revealed upregulation of two ATP-binding cassette (ABC) transporter gene pairs, *cdtAB* and *sclAB*. CdtAB and SclAB are homologous to the DrrAB transporter in the Dauno BGC that facilitates the efflux of Dauno and Doxo[64]. We detected SNPs in the promotor regions of *cdtAB* and *sclAB*, and within the coding regions of the corresponding regulatory genes *cdtR* and *sclR*. SclAB has been previously identified in a similar evolution experiment where *S. lividans* was challenged with the macrolide antibiotic spiramycin[305]. Deletion of the downstream TetR-family regulatory gene, *sclR*, or overexpression of *sclAB* provided mild resistance to various antibiotics, including daunorubicin[305,313]. Our work indicates that both CdtAB and SclAB provide particularly strong resistance to anthracyclines. Introducing expression cassettes containing *cdtAB* or *sclAB*, or disrupting *cdtR* or *sclR* in the parental strain, resulted in more than eight-fold increase in resistance to both Doxo and the stronger antibiotic DMdoxo. Homologs of the CdtAB and SclAB transporters occur frequently within the family of Streptomycetaceae, and their presence is not correlated to the occurrence of putative anthracycline BGCs.

Interestingly, in *S. lividans* the expression of the transporters was not directly activated during challenge with anthracyclines, but only via the accumulation of spontaneous mutations after prolonged exposure to the toxic compound DMdoxo. These findings show that apart from cryptic BGCs encoding undiscovered natural products, *Streptomyces* genomes also contain cryptic resistance mechanisms.

Potential antimicrobial applications of detoxified anthracyclines

Although anthracyclines were originally discovered through their antimicrobial activity, severe side effects prevented their development as antibiotics[10,13,30]. However, recent insights into the development of detoxified anthracyclines with limited side effects may open up a potential therapeutic window for their application as antibiotics. Interestingly, actinomycetes were highly sensitive to DMdoxo (Chapter 4), a promising detoxified anthracycline[15,16]. This further evoked our interest in exploring the potential antimicrobial applications of detoxified anthracyclines.

In **Chapter 5**, we evaluated the antimicrobial activity of a structurally diverse library of anthracyclines[16–19] against ESKAPE pathogens. *N,N*-dimethylated anthracyclines exhibited robust bactericidal activity against Gram-positive bacteria as well as Gram-negative *A. baumannii*. In particular, DMdoxo and an *N,N*-dimethylated Doxo trisaccharide derivative (Figure 1, compound **6** in Chapter 5) demonstrated the strongest antimicrobial activity. Importantly, although streptomycetes activated anthracycline resistance within a few generations upon exposure to subinhibitory concentrations (Chapter 4), we did not observe the development of resistance against Doxo and DMdoxo in methicillin-resistant *Staphylococcus aureus* (MRSA).

The presence of a tertiary amine on the first sugar moiety of anthracycline typically leads to the loss of DNA-damaging activity, which is associated with cardiotoxicity, the most treatment-limiting side effect of anthracyclines[17–19]. Our findings indicate that this is also correlated with improved antibiotic activity. The antimicrobial mode-of-action of anthracyclines remains poorly understood, although recently idarubicin was shown to target the cell membrane and bacterial topoisomerase II[345]. It would be of interest to further elucidate the antimicrobial mode-of-action of anthracyclines, and in particular the factors contributing to the improved activity of dimethylated anthracyclines. Although dimethylated anthracyclines have reduced toxicity, their limited side effects will still prevent their application as first-line antibiotics. Instead, we envision their potential application as in life-threatening situations, such as combating sepsis[346].

Toward high-throughput characterisation of *Streptomyces*

Streptomycetes remain an important source of new bioactive natural products[2–4]. To accelerate the discovery of these metabolites, high-throughput methods to characterise large strain collections under many experimental conditions are needed[52,356,357,359]. The mycelial morphology of streptomycetes in submerged cultures can cause significant biological variability[363]. Nonetheless, achieving reproducible small-scale cultivation of *Streptomyces* is feasible with tightly controlled inoculation strategies and well-characterised cultivation methods[361,362].

In **Chapter 6**, we present a workflow for integrated quantitative proteomics and metabolomics from microbioreactor (MBR) *Streptomyces* cultures. Our results indicate that reproducible and sensitive data can be obtained from small-culture volumes. However, further optimisation of the cultivation method is required to reduce biological variability. This methodology could complement existing approaches for natural product discovery, such as co-culture experiments, screenings with small-molecule elicitors, or computational methods[49,284].

Outlook

Anthracyclines have been cornerstones in oncology treatment for decades. Further understanding of biosynthesis and bioactivities of anthracyclines is important for anticancer and antimicrobial applications of these compounds.

Combinatorial biosynthesis is an effective approach for generating hybrid anthracyclines. In this work, expression of aclarubicin and rhodomycin biosynthetic genes in *S. peucetius* led to the biosynthesis of *N,N*-dimethylated anthracyclines. A similar approach could be applied for the biosynthesis of other detoxified anthracyclines, such as the *N,N*-dimethylated Doxo trisaccharide derivative, which demonstrated potent antimicrobial activity toward ESKAPE pathogens. Additionally, it would be of interest to explore the putative anthracycline BGCs that were detected in Streptomycetaceae to identify their cognate products and potentially discover new tailoring enzymes.

N,N-dimethylated anthracyclines demonstrated strong toxicity to Gram-positive bacteria, including actinomycetes. Although this finding presents promising prospects for their application as antibiotics, an important question that remains is the antimicrobial mode-of-action of anthracyclines. Uptake experiments utilising the fluorescent nature of anthracyclines via microscopy could offer valuable insights. Additionally, structure-activity relationship experiments may provide a better understanding of the factors contributing to the stronger antimicrobial activity of dimethylated anthracyclines. Finally, these insights may guide the engineering of anthracyclines for effective anticancer and antimicrobial applications.



Nederlandse samenvatting

Actinomyceten vormen een diverse fylum van meercellige Gram-positieve bacteriën. Deze bacteriën zijn bekend omdat ze veel bioactieve metabolieten produceren, die veelal worden gebruikt als medicijnen voor mensen, dieren en planten. Een belangrijke groep van metabolieten die worden geproduceerd door actinomyceten zijn de anthracyclines. Anthracyclines zijn belangrijke antikankermedicijnen, ondanks dat ze ernstige bijwerkingen hebben. Sinds hun ontdekking in de jaren 1950 is er veel werk gedaan aan het ontwikkelen van anthracyclines met nog betere antikanker activiteit en minder bijwerkingen. Sindsdien zijn er meer dan 500 anthracyclines geïsoleerd uit actinomyceten, waarvan alleen daunorubicine (Dauno), doxorubicine (Doxo) en aclarubicine (Acla) momenteel in de kliniek worden gebruikt. Daarnaast zijn er enkele semisynthetische varianten gemaakt die ook met succes zijn geïntroduceerd in de kliniek.

Recentelijke nieuwe inzichten in de werkingswijze van anthracyclines hebben hernieuwde interesse gewekt in deze belangrijke groep van antikankermedicijnen (**Hoofdstuk 2**). Eén van de meest veelbelovende verbindingen is *N,N*-dimethyldoxorubicine (DMdoxo), een hybride structuur van de aglycon van Doxo met de aminosuiker van Acla die is gemaakt via semi-synthese. DMdoxo heeft sterke cytotoxische activiteit maar veroorzaakt geen cardiotoxiciteit, wat de meest acute en behandeling beperkende bijwerking van Doxo is. Een evaluatie van een grote collectie van anthracyclines wees uit dat de aanwezigheid van een tertiaire amine op de eerste suikergroep van een anthracycline over het algemeen leidt tot minder DNA-beschadigende activiteit, wat geassocieerd is met cardiotoxiciteit, de meest beperkende bijwerking van anthracyclines. Tegelijkertijd is de cytotoxische activiteit juist sterker bij deze moleculen. Deze resultaten zijn veelbelovend voor de ontwikkeling van nog meer anthracyclines met sterke antikanker activiteit en beperkte bijwerkingen.

Op dit moment wordt Doxo geproduceerd via een combinatie van microbiële fermentatie en organische chemie. In de eerste stap wordt Dauno biosynthetisch gemaakt via fermentatie van een *Streptomyces peucetius*. Vervolgens wordt het biosynthetische Dauno omgezet in Doxo via chemische 14-hydroxylering. In principe kan Doxo ook volledig biosynthetisch worden verkregen, maar de laatste enzymatische stap in het proces is erg inefficiënt, wat resulteert in lage opbrengsten.

Voor de productie van DMdoxo als antikankermedicijn zou biosynthese een aantrekkelijke optie zijn, maar het wordt niet door bacteriën geproduceerd. Daarom was het eerste doel van deze studie om de biosyntheseroute van Doxo in *S. peucetius* zo aan te passen dat er *N,N*-gedimethyleerde anthracyclines kunnen worden gemaakt (**Hoofdstuk 3**). Tijdens dit proces kwamen er verschillende uitdagingen naar voren, die leidden tot vervolgstudies naar resistentiemechanismen tegen anthracyclines in *Streptomyces* (**Hoofdstuk 4**) en potentiële toepassingen van anthracyclines met beperkte bijwerkingen als antibiotica (**Hoofdstuk 5**). Tenslotte is er een methode ontwikkeld voor gecombineerde proteoom- en metaboloomanalyse van kleinschalige *Streptomyces* culturen om toekomstig onderzoek van streptomyceten als productiestammen te versnellen (**Hoofdstuk 6**).

Uitdagingen voor de biosynthese van *N,N*-gedimethyleerde anthracyclines

Het combineren van anthracycline biosyntheseroutes uit verschillende streptomyceten is veel toegepast om hybride anthracyclines te genereren. Met name de Acla-producerende bacterie *Streptomyces galilaeus* is veel bestudeerd, waarbij voornamelijk enzymen zijn geïntroduceerd die de latere stappen in de anthracycline biosyntheseroutes katalyseren. Daarnaast zijn genen die betrokken zijn bij anthracycline biosynthese tot expressie gebracht in heterologe gastheren, zoals *Streptomyces venezuelae*, *Streptomyces coelicolor* en *Streptomyces lividans*, die van nature zelf geen anthracyclines produceren.

Om de biosynthese van DMdauno en DMdoxo te realiseren hebben we de biosyntheseroute voor Doxo in de industriële *S. peucetius* stam G001 aangepast (**Hoofdstuk 3**). Allereerst hebben we de methyltransferasegenen die nodig zijn voor de productie van TDP-L-rhodosamine en de glycosyltransferasegenen van *S. galilaeus* geïntroduceerd in G001. Vervolgens hebben we het Doxo glycosyltransferasegen *dnrS* verwijderd om de productie van niet-gemethyleerde anthracyclines te stoppen. Daarna hebben we het rhodomycine methyltransferasegen *rdmC* geïntroduceerd, wat resulteerde in de succesvolle productie van DMdauno, zij dat de stam slechts beperkte hoeveelheden produceerde.

De resultaten toonden aan dat de aanwezigheid van de gedimethyleerde suikergroep de drie opeenvolgende hydroxylatiereacties remt die nodig zijn om de aglycon van Doxo te vormen. Deze reacties worden gekatalyseerd door de cytochroom P450-monooxygenase DoxA, een enzym dat uniek is voor Doxo biosynthese. Het is al lang bekend dat de uiteindelijke reactie in de biosyntheseroute van Dauno naar Doxo zeer inefficiënt is, wat ook de reden is waarom Doxo in de industrie semisynthetisch wordt geproduceerd vanuit Dauno. Het blijkt dat de gedimethyleerde verbindingen nog slechter worden omgezet door DoxA dan de natuurlijke substraten. Het is dus duidelijk dat DoxA een bottleneck is als we DMdoxo willen maken via biosynthese. Een mogelijke oplossing zou kunnen zijn om DoxA te modificeren voor verbeterde activiteit. Aangezien de structuur van DoxA niet bekend is, is het moeilijk om te voorspellen welke mutaties een verbeterde activiteit zouden kunnen opleveren. Anderzijds zouden high-throughput methoden met willekeurige of modelgeleide mutagenese succesvol kunnen zijn bij het identificeren van DoxA-varianten met verbeterde activiteit. Een ander mogelijk beperkende factor voor DMdoxo biosynthese is de sterkere toxiciteit van *N,N*-gedimethyleerde anthracyclines voor *S. peucetius* in vergelijking met de niet-gedimethyleerde varianten. Dit motiveerde ons om resistentiemechanismen tegen anthracyclines in *Streptomyces* te onderzoeken.

Cryptische anthracycline resistentiegenen in *Streptomyces*

Biosynthetische genclusters (BGC's) voor toxische metabolieten coderen vaak ook zelf-resistentie. Anthracycline BGC's bevatten meestal ATP-bindende cassette (ABC) transportergenen die zorgen voor de export van deze toxische metabolieten. Over het algemeen bevatten actinomyceten ook zeer specifieke resistentiemechanismen tegen antibiotica die ze tegenkomen in het milieu. In **Hoofdstuk 4** hebben we resistentie tegen anthracyclines in actinomyceten bestudeerd door middel van een screening van onze stammencollectie en met behulp van evolutie experimenten.

De screening van onze MBT-collectie van actinomyceten liet zien dat resistentiemechanismen tegen anthracyclines relatief vaak voorkomt, maar dat alle stammen zeer gevoelig zijn voor DMdoxo. Vervolgens werden een aantal streptomyceten blootgesteld aan steeds hogere concentraties DMdoxo in een evolutie-experiment, wat resulteerde in sterk verhoogde anthracycline resistentie al na vijf generaties. Transcriptoomanalyse van een DMdoxo-resistente *S. lividans* TK24 stam toonde aan dat de expressie van twee paren van ABC-transportergenen, *cdtAB* en *sclAB*, sterk was verhoogd. CdtAB en SclAB zijn homoloog aan de DrrAB-transporter in het Dauno BGC die zorgt voor export van Dauno en Doxo. Daarnaast vonden we mutaties in de promotorregio's van *cdtAB* en *sclAB*, en ook in de coderende regio's van de corresponderende regulatiegenen *cdtR* en *sclR*. SclAB is eerder geïdentificeerd in een evolutie-experiment waar *S. lividans* werd blootgesteld aan het macrolide antibioticum spiramycine. Het verwijderen van het corresponderende TetR-familie regulatiegen, *sclR*, of overexpressie van *sclAB* zorgde voor milde resistentie tegen verschillende antibiotica, waaronder Dauno. Onze studie laat zien dat zowel CdtAB als SclAB bijzonder sterke resistentie bieden tegen anthracyclines. Het introduceren van expressiecassettes met *cdtAB* of *sclAB*, of het uitschakelen van *cdtR* of *sclR* in de originele stam, resulteerde in een meer dan achtvoudige toename van resistentie tegen zowel Doxo als het sterkere antibioticum DMdoxo. Homologen van de CdtAB- en SclAB-transporters komen vaak voor binnen de familie van *Streptomycetaceae*, en de aanwezigheid is niet gecorreleerd met het voorkomen van mogelijke anthracycline BGC's.

Interessant genoeg werd in *S. lividans* de expressie van de transporters niet direct geactiveerd tijdens blootstelling aan anthracyclines, maar alleen via de accumulatie van spontane mutaties na langdurige blootstelling aan de toxische verbinding DMdoxo. Deze bevindingen tonen aan dat *Streptomyces* genomen niet alleen cryptische BGC's bevatten die nog onbekende bioactieve metabolieten kunnen coderen, maar ook cryptische resistentiemechanismen.

Potentiële antimicrobiële toepassingen van anthracyclines met beperkte bijwerkingen

Hoewel anthracyclines oorspronkelijk zijn ontdekt vanwege hun antimicrobiële activiteit, worden ze niet gebruikt als antibiotica doordat ze ernstige bijwerkingen hebben. Recentelijk verkregen inzichten in de ontwikkeling van anthracyclines met beperkte bijwerkingen kunnen ervoor zorgen dat er wel een mogelijkheid is om anthracyclines als antibiotica te gaan gebruiken. Aangezien actinomyceten zeer gevoelig zijn voor DMdoxo, een veelbelovende anthracycline met beperkte bijwerkingen, besloten we om de antimicrobiële activiteit van anthracyclines verder te onderzoeken.

In **Hoofdstuk 5** is een collectie van anthracyclines getest op mogelijke bioactiviteit tegen ESKAPE pathogenen. *N,N*-gedimethyleerde anthracyclines vertoonden bactericide activiteit tegen Gram-positieve bacteriën en de Gram-negatieve A. *baumannii*. Met name DMdoxo en een *N,N*-gedimethyleerde Doxo variant met drie suikergroepen lieten de sterkste antimicrobiële activiteit zien. Het is belangrijk om te vermelden dat we geen ontwikkeling van resistentie tegen Doxo en DMdoxo observeerden in methicilline resistente *Staphylococcus aureus* (MRSA).

De aanwezigheid van een tertiaire amine op de eerste suikergroep van anthracyclines leidt over het algemeen tot het verlies van DNA-beschadigende activiteit, wat geassocieerd is met cardiotoxiciteit, een ernstige bijwerking van anthracyclines die de toepassing beperkt. Onze resultaten laten zien dat dit ook correleert aan verbeterde antibioticum activiteit. Het mechanisme dat zorgt voor de antimicrobiële activiteit van anthracyclines is nog steeds niet erg duidelijk, al is recentelijk aangetoond dat idarubicine zich richt op het celmembraan en de bacteriële topoisomerase II. Het zou interessant zijn om het antimicrobiële werkingsmechanisme van anthracyclines beter te begrijpen en met name de factoren die bijdragen aan de verbeterde activiteit van gedimethyleerde anthracyclines. Hoewel gedimethyleerde anthracyclines verminderde toxiciteit hebben, zullen ook de beperkte bijwerkingen ervoor zorgen dat ze niet als eerstelijnsantibiotica worden gebruikt. In plaats daarvan zien we vooral een toepassing in levensbedreigende situaties, zoals bij de bestrijding van sepsis.

High-throughput analyse van *Streptomyces* culturen

Streptomyceten blijven een belangrijke bron van nieuwe bioactieve metabolieten. Om de ontdekking van deze metabolieten te versnellen, zijn high-throughput methoden nodig om grote stammencollecties onder veel verschillende experimentele omstandigheden te onderzoeken. De morfologie van streptomyceten in vloeibare culturen zorgt vaak voor een sterke heterogeniteit in experimentele waarden. Het is belangrijk om reproduceerbare kleinschalige culturen van *Streptomyces* te bereiken. Dit kan bijvoorbeeld door goed na te denken welk inoculum wort gebruikt, alsmede over de experimentele omstandigheden.

In **Hoofdstuk 6** wordt een methode beschreven waarbij kwantitatieve proteoom- en metaboloomanalyse van *Streptomyces* worden gecombineerd. Deze zijn uitgevoerd in goed gecontroleerde microbioreactor (MBR) culturen. Onze resultaten laten zien dat er uit dergelijke kleinschalige culture betrouwbare en sensitieve data kan worden verkregen. Verdere optimalisatie van de methode is echter vereist om biologische variatie verder te verminderen. Deze methode kan worden toegepast in de zoektocht naar nieuwe bioactieve metabolieten die door streptomyceten worden geproduceerd.

Vooruitzicht

Anthracyclines vormen al decennia een belangrijke basis voor medicijnen die worden toegepast in de oncologie. Het is belangrijk om meer te weten te komen over de biosynthese en bioactiviteiten van anthracyclines voor de ontwikkeling van nieuwe antikankermedicijnen en antibiotica.

Het combineren van biosyntheseroutes voor anthracyclines zoals die in verschillende streptomyceten is een effectieve aanpak gebleken voor het genereren van hybride moleculen. Expressie van genen uit de biosynthese routes voor aclarubicine en rhodomycine in *S. peucetius* leidde tot de biosynthese van *N*,*N*-gedimethyleerde anthracyclines en met name DMdauno. Een vergelijkbare aanpak zou kunnen worden toegepast voor de biosynthese van andere interessante anthracyclines, zoals de *N*,*N*-gedimethyleerde Doxo variant met drie suikergroepen die krachtige antimicrobiële activiteit vertoonde tegen ESKAPE pathogenen. Bovendien zou

het interessant zijn om de mogelijke anthracycline BGC's te bestuderen die aanwezig zijn in verschillende *Streptomycetaceae*.

N,*N*-gedimethyleerde anthracyclines vertonen sterke bioactiviteit tegen Gram-positieve bacteriën, waaronder actinomyceten. Hoewel deze ontdekking een veelbelovend perspectief is voor de mogelijke toepassingen van anthracyclines als antibiotica, blijft een belangrijke vraag wat de het mechanisme erachter precies is. Het bestuderen van de opnamen van anthracyclines via microscopie zou waardevolle inzichten kunnen opleveren, waarbij gebruik kan worden gemaakt van het feit dat anthracyclines van zichzelf fluorescent zijn.. Bovendien kan het bestuderen van de structuur-activiteit relatie nieuwe inzichten verschaffen in de factoren die bijdragen aan de antimicrobiële activiteit van gedimethyleerde anthracyclines. Ten slotte kunnen deze inzichten helpen bij de rationele engineering van anthracyclines voor effectievere antikanker-medicijnen en antibiotica.



References

1. Kieser, T., Bibb, M.J., Buttner, M.J., Chater, K.F., and Hopwood, D.A. (2000). Practical *Streptomyces* genetics (John Innes Foundation).
2. Baltz, R.H. (2007). Antimicrobials from actinomycetes: back to the future. *Microbe* **2**, 125–131.
3. Bérdy, J. (2005). Bioactive microbial metabolites. *J. Antibiot.* **58**, 1–26.
4. Hopwood, D.A. (2007). *Streptomyces* in nature and medicine: the antibiotic makers (Oxford University Press).
5. Bibb, M.J. (2005). Regulation of secondary metabolism in streptomycetes. *Curr. Opin. Microbiol.* **8**, 208–215.
6. van Wezel, G.P., and McDowall, K.J. (2011). The regulation of the secondary metabolism of *Streptomyces*: new links and experimental advances. *Nat. Prod. Rep.* **28**, 1311–1333.
7. Mak, S., Xu, Y., and Nodwell, J.R. (2014). The expression of antibiotic resistance genes in antibiotic-producing bacteria. *Mol. Microbiol.* **93**, 391–402.
8. Arcamone, F., Cassinelli, G., Fantini, G., Grein, A., Orezzi, P., Pol, C., and Spalla, C. (1969). Adriamycin, 14-hydroxydaunomycin, a new antitumor antibiotic from *S. peucetius* var. *caesius*. *Biotechnol. Bioeng.* **11**, 1101–1110.
9. Camerino, B., and Palamidessi, G. (1960). Derivati della parazina II. Sulfonamdopir. *Gazz. Chim. Ital.* **90**, 1802–1815.
10. Di Marco, A., Cassinelli, G., and Arcamone, F. (1981). The discovery of daunorubicin. *Cancer Treat. Rep.* **65**, 3–8.
11. Lown, W.J. (1993). Discovery and development of anthracycline antitumour antibiotics. *Chem. Soc. Rev.* **22**, 165–176.
12. Tan, C., Tasaka, H., Yu, K.-P., Murphy, M.L., and Karnofsky, D.A. (1967). Daunomycin, an antitumor antibiotic, in the treatment of neoplastic disease. Clinical evaluation with special reference to childhood leukemia. *Cancer* **20**, 333–353.
13. Weiss, R.B. (1992). The anthracyclines: will we ever find a better doxorubicin. *Semin. Oncol.* **19**, 670–686.
14. Pang, B., Qiao, X., Janssen, L., Velds, A., Groothuis, T., Kerkhoven, R., Nieuwland, M., Ovaa, H., Rottenberg, S., van Tellingen, O., et al. (2013). Drug-induced histone eviction from open chromatin contributes to the chemotherapeutic effects of doxorubicin. *Nat. Commun.* **4**, 1908.
15. van der Zanden, S.Y., Qiao, X., and Neefjes, J. (2021). New insights into the activities and toxicities of the old anticancer drug doxorubicin. *FEBS J.* **288**, 6095–6111.
16. Qiao, X., van der Zanden, S.Y., Wander, D.P.A., Borràs, D.M., Song, J.-Y.Y., Li, X., van Duikeren, S., van Gils, N., Rutten, A., van Herwaarden, T., et al. (2020). Uncoupling DNA damage from chromatin damage to detoxify doxorubicin. *Proc. Natl. Acad. Sci. U.S.A.* **117**, 15182–15192.
17. van Gelder, M.A., van der Zanden, S.Y., Vriends, M.B.L., Wagensveld, R.A., van der Marel, G.A., Codée, J.D.C., Overkleeft, H.S., Wander, D.P.A., and Neefjes, J.J.C. (2023). Re-exploring the anthracycline chemical space for better anti-cancer compounds. *J. Med. Chem.* **66**, 11390–11398.
18. Wander, D.P.A., van der Zanden, S.Y., van der Marel, G.A., Overkleeft, H.S., Neefjes, J., and Codée, J.D.C. (2020). Doxorubicin and aclarubicin: shuffling anthracycline glycans for improved anti-cancer agents. *J. Med. Chem.* **63**, 12814–12829.
19. Wander, D.P.A., van der Zanden, S.Y., Vriends, M.B.L., van Veen, B.C., Vlaming, J.G.C., Bruyning, T., Hansen, T., van der Marel, G.A., Overkleeft, H.S., Neefjes, J.J.C., et al. (2021). Synthetic (*N*,*N*-dimethyl)doxorubicin glycosyl diastereomers to dissect modes of action of anthracycline anticancer drugs. *J. Org. Chem.* **86**, 5757–5770.
20. Newman, D.J., and Cragg, G.M. (2020). Natural products as sources of new drugs over the nearly four decades from 01/1981 to 09/2019. *J. Nat. Prod.* **83**, 770–803.
21. Barka, E.A., Vatsa, P., Sanchez, L., Gaveau-Vaillant, N., Jacquard, C., Klenk, H.-P., Clément, C., Ouhdouch, Y., and van Wezel, G.P. (2016). Taxonomy, physiology, and natural products of Actinobacteria. *Microbiol. Mol. Biol. Rev.* **80**, 1–43.
22. Bérdy, J. (2005). Bioactive microbial metabolites. *J. Antibiot.* **58**, 1–26.
23. Hertweck, C. (2009). The biosynthetic logic of polyketide diversity. *Angew. Chem. Int. Ed.* **48**, 4688–4716.
24. Olano, C., Méndez, C., and Salas, J.A. (2010). Post-PKS tailoring steps in natural product-producing actinomycetes from the perspective of combinatorial biosynthesis. *Nat. Prod. Rep.* **27**, 571–616.
25. Duggar, B.M. (1948). Aureomycin: a product of the continuing search for new antibiotics. *Ann. N. Y. Acad. Sci.* **51**, 177–181.

26. Griffin, M.O., Fricovsky, E., Ceballos, G., and Villarreal, F. (2010). Tetracyclines: a pleitropic family of compounds with promising therapeutic properties. Review of the literature. *Am. J. Physiol. Cell Physiol.* **299**, C539–C548.

27. Grossman, T.H. (2016). Tetracycline antibiotics and resistance. *Cold Spring Harb. Perspect. Med.* **6**, a025387.

28. Brockmann, H., and Bauer, K. (1950). Rhodomycin, ein rotes antibioticum aus actinomyceten. *Naturwissenschaften* **37**, 492–493.

29. Minotti, G., Menna, P., Salvatorelli, E., Cairo, G., and Gianni, L. (2004). Anthracyclines: molecular advances and pharmacologic developments in antitumor activity and cardiotoxicity. *Pharmacol. Rev.* **56**, 185–229.

30. Brockmann, H. (1963). Anthracyclinones and anthracyclines. Rhodomycinone, pyrromycinone and their glycosides. *Fortschr. Chem. Org. Naturst.* **21**, 121–182.

31. Arcamone, F.M. (2009). Fifty years of chemical research at Farmitalia. *Chem. Eur. J.* **15**, 7774–7791.

32. Wiley, P.F., MacKellar, F.A., Caron, E.L., Company, T.U., and Kelly, R.B. (1968). Isolation, characterization and degradation of nogalamycin. *Tetrahedron Lett.* **6**, 663–668.

33. Oki, T., Matsuzawa, Y., Yoshimoto, A., Numata, K., Kitamura, I., Hori, S., Takamatsu, A., Umezawa, H., Ishizuka, M., Naganawa, H., et al. (1975). New antitumor antibiotic, aclacinomycins A and B. *J. Antibiot.* **28**, 830–834.

34. Kelly, R.C., Schletter, I., Koert, J.M., MacKellar, F.A., and Wiley, P.F. (1977). Structures of Steffimycin and Steffimycin B. *J. Org. Chem.* **42**, 3591–3596.

35. Li, L.H., and Krueger, W.C. (1991). The biochemical pharmacology of nogalamycin and its derivatives. *Pharmacol. Ther.* **51**, 239–255.

36. Olano, C., Méndez, C., Salas, J.A., Mendez, C., and Salas, J.A. (2009). Antitumor compounds from actinomycetes: from gene clusters to new derivatives by combinatorial biosynthesis. *Nat. Prod. Rep.* **26**, 628–660.

37. Goodfellow, M. (2012). Phylum XXVI. Actinobacteria phyl. nov. In Bergey's Manual of Systematic Bacteriology, M. Goodfellow, P. Kämpfer, H.-J. Busse, M. E. Trujillo, K.-I. Suzuki, W. Ludwig, and W. B. Whitman, eds. (Springer), pp. 1–2083.

38. Claessen, D., Rozen, D.E., Kuipers, O.P., and Søgaard-Andersen, L. (2014). Bacterial solutions to multicellularity: a tale of biofilms, filaments and fruiting bodies. *Nat. Rev. Microbiol.* **12**, 115–124.

39. Flärdh, K., Richards, D.M., Hempel, A.M., Howard, M., and Buttner, M.J. (2012). Regulation of apical growth and hyphal branching in *Streptomyces*. *Curr. Opin. Microbiol.* **15**, 737–743.

40. Jakimowicz, D., and van Wezel, G.P. (2012). Cell division and DNA segregation in *Streptomyces*: how to build a septum in the middle of nowhere? *Mol. Microbiol.* **85**, 393–404.

41. Chater, K.F., Biró, S., Lee, K.J., Palmer, T., and Schrempf, H. (2010). The complex extracellular biology of *Streptomyces*: review article. *FEMS Microbiol. Rev.* **34**, 171–198.

42. Chater, K.F. (2011). Differentiation in *Streptomyces*: the properties and programming of diverse cell-types. In *Streptomyces*: Molecular Biology and Biotechnology, P. Dyson, ed. (Caister Academic Press), pp. 43–86.

43. Chater, K.F., and Losick, R. (1997). Mycelial life-style of *Streptomyces coelicolor* A3(2) and its relatives. In Bacteria as Multicellular Organisms (Oxford University Press), pp. 149–182.

44. Flärdh, K., and Buttner, M.J. (2009). *Streptomyces* morphogenetics: dissecting differentiation in a filamentous bacterium. *Nat. Rev. Microbiol.* **7**, 36–49.

45. van der Heul, H.U., Bilyk, B.L., McDowall, K.J., Seipke, R.F., and van Wezel, G.P. (2018). Regulation of antibiotic production in Actinobacteria: new perspectives from the post-genomic era. *Nat. Prod. Rep.* **35**, 575–604.

46. Bentley, S.D., Chater, K.F., Cerdeño-Tárraga, A.-M., Challis, G.L., Thomson, N.R., James, K.D., Harris, D.E., Quail, M.A., Kieser, H., Harper, D., et al. (2002). Complete genome sequence of the model actinomycete *Streptomyces coelicolor* A3(2). *Nature* **417**, 141–147.

47. Zhu, H., Sandiford, S.K., and van Wezel, G.P. (2014). Triggers and cues that activate antibiotic production by actinomycetes. *J. Ind. Microbiol. Biotechnol.* **41**, 371–386.

48. Baral, B., Akhgari, A., and Metsä-Ketelä, M. (2018). Activation of microbial secondary metabolic pathways: avenues and challenges. *Synth. Syst. Biotechnol.* **3**, 163–178.

49. Rutledge, P.J., and Challis, G.L. (2015). Discovery of microbial natural products by activation of silent biosynthetic gene clusters. *Nat. Rev. Microbiol.* **13**, 509–523.

50. van Bergeijk, D.A., Terlouw, B.R., Medema, M.H., and van Wezel, G.P. (2020). Ecology and genomics of Actinobacteria: new concepts for natural product discovery. *Nat. Rev. Microbiol.* **18**, 546–558.

51. van der Meij, A., Worsley, S.F., Hutchings, M.I., and van Wezel, G.P. (2017). Chemical ecology of antibiotic production by actinomycetes. *FEMS Microbiol. Rev.* **41**, 392–416.

52. Du, C., and van Wezel, G.P. (2018). Mining for microbial gems: integrating proteomics in the postgenomic natural product discovery pipeline. *Proteomics* **18**, 1700332.

53. Manteca, A., Mäder, U., Connolly, B.A., Sanchez, J., Mader, U., Connolly, B.A., and Sanchez, J. (2006). A proteomic analysis of *Streptomyces coelicolor* programmed cell death. *Proteomics* **6**, 6008–6022.

54. Cox, G., Koteva, K., and Wright, G.D. (2014). An unusual class of anthracyclines potentiate Gram-positive antibiotics in intrinsically resistant Gram-negative bacteria. *J. Antimicrob. Chemother.* **69**, 1844–1855.

55. Kronheim, S., Daniel-Ivad, M., Duan, Z., Hwang, S., Wong, A.I., Mantel, I., Nodwell, J.R., and Maxwell, K.L. (2018). A chemical defence against phage infection. *Nature* **564**, 283–286.

56. Tenconi, E., Traxler, M., Tellatin, D., van Wezel, G.P., Rigali, S., Wezel, G.P.V., van Wezel, G.P., and Rigali, S. (2020). Prodiginines postpone the onset of sporulation in *Streptomyces coelicolor*. *Antibiotics* **9**, 1–14.

57. Tenconi, E., and Rigali, S. (2018). Self-resistance mechanisms to DNA-damaging antitumor antibiotics in Actinobacteria. *Curr. Opin. Microbiol.* **45**, 100–108.

58. Challis, G.L., and Hopwood, D.A. (2003). Synergy and contingency as driving forces for the evolution of multiple secondary metabolite production by *Streptomyces* species. *Proc. Natl. Acad. Sci. U.S.A.* **100**, 14555–14561.

59. Fewer, D.P., and Metsä-Ketelä, M. (2020). A pharmaceutical model for the molecular evolution of microbial natural products. *FEBS J.* **287**, 1429–1449.

60. Firn, R.D., and Jones, C.G. (2003). Natural products - a simple model to explain chemical diversity. *Nat. Prod. Rep.* **20**, 382–391.

61. Borst, P., Schinkel, A.H., and Others (2013). P-glycoprotein ABCB1: a major player in drug handling by mammals. *Eur. J. Clin. Invest.* **123**, 4131–4133.

62. Dhakal, D., Lim, S.-K., Kim, D.H., Kim, B.-G., Yamaguchi, T., and Sohng, J.K. (2018). Complete genome sequence of *Streptomyces peucetius* ATCC 27952, the producer of anticancer anthracyclines and diverse secondary metabolites. *J. Biotechnol.* **267**, 50–54.

63. Lomovskaya, N., Otten, S.L., Doi-Katayama, Y., Fonstein, L., Liu, X.-C., Takatsu, T., Inventi-Solari, A., Filippini, S., Torti, F., Colombo, A.L., et al. (1999). Doxorubicin overproduction in *Streptomyces peucetius*: cloning and characterization of the *dnrU* ketoreductase and *dnrV* genes and the *doxA* cytochrome P-450 hydroxylase gene. *J. Bacteriol.* **181**, 305–318.

64. Guilfoile, P.G., and Hutchinson, C.R. (1991). A bacterial analog of the *mdr* gene of mammalian tumor cells is present in *Streptomyces peucetius*, the producer of daunorubicin and doxorubicin. *Proc. Natl. Acad. Sci. U.S.A.* **88**, 8553–8557.

65. Malla, S., Niraula, N.P., Liou, K., and Sohng, J.K. (2010). Improvement in doxorubicin productivity by overexpression of regulatory genes in *Streptomyces peucetius*. *Res. Microbiol.* **161**, 109–117.

66. Karuppasamy, K., Srinivasan, P., Ashokkumar, B., Tiwari, R., Kanagarajadurai, K., and Prasad, R. (2015). Partial loss of self-resistance to daunorubicin in *drrD* mutant of *Streptomyces peucetius*. *Biochem. Eng. J.* **102**, 98–107.

67. Furuya, K., Richard Hutchinson, C., and Hutchinson, C.R. (1998). The DrrC protein of *Streptomyces peucetius*, a UvrA-like protein, is a DNA-binding protein whose gene is induced by daunorubicin. *FEMS Microbiol. Lett.* **168**, 243–249.

68. Lomovskaya, N., Hong, S.K., Kim, S.U., Fonstein, L., Furuya, K., and Hutchinson, R.C. (1996). The *Streptomyces peucetius drrC* gene encodes a UvrA-like protein involved in daunorubicin resistance and production. *J. Bacteriol.* **178**, 3238–3245.

69. Prija, F., and Prasad, R. (2017). DrrC protein of *Streptomyces peucetius* removes daunorubicin from intercalated *dnrI* promoter. *Microbiol. Res.* **202**, 30–35.

70. Dubey, R., Kattusamy, K., Dharmalingam, K., and Prasad, R. (2014). Daunorubicin forms a specific complex with a secreted serine protease of *Streptomyces peucetius*. *World J. Microbiol. Biotechnol.* **30**, 253–261.

71. Hoskisson, P.A., and van Wezel, G.P. (2019). *Streptomyces coelicolor*. *Trends Microbiol.* **27**, 468–469.

72. Hopwood, D.A. (2006). Soil to genomics: the *Streptomyces* chromosome. *Annu. Rev. Genet.* **40**, 1–23.

73. van Keulen, G., and Dyson, P.J. (2014). Production of specialized metabolites by *Streptomyces coelicolor* A3(2). *Adv. Appl. Microbiol.* **89**, 217–266.

74. Wietzorrek, A., and Bibb, M. (1997). A novel family of proteins that regulates antibiotic production in streptomycetes appears to contain an OmpR-like DNA-binding fold. *Mol. Microbiol.* **25**, 1181–1184.

75. Fernández-Moreno, M.A., Caballero, J.L., Hopwood, D.A., Malpartida, F., Fernandez-Moreno, M.A., Caballero, J.L., Hopwood, D.A., and Malpartida, F. (1991). The *act* cluster contains regulatory and antibiotic export genes, direct targets for translational control by the *bldA* tRNA gene of *Streptomyces*. *Cell* **66**, 769–780.

76. Lawlor, E.J., Baylis, H.A., and Chater, K.F. (1987). Pleiotropic morphological and antibiotic deficiencies result from mutations in a gene encoding a tRNA-like product in *Streptomyces coelicolor* A3(2). *Genes Dev.* **1**, 1305–1310.

77. Narva, K.E., and Feitelson, J.S. (1990). Nucleotide sequence and transcriptional analysis of the *redD* locus of *Streptomyces coelicolor* A3(2). *J. Bacteriol.* **172**, 326–333.

78. Takano, E., Gramajo, H.C., Strauch, E., Andres, N., White, J., and Bibb, M.J. (1992). Transcriptional regulation of the *redD* transcriptional activator gene accounts for growth-phase-dependent production of the antibiotic undecylprodigiosin in *Streptomyces coelicolor* A3(2). *Mol. Microbiol.* **6**, 2797–2804.

79. White, J., and Bibb, M. (1997). *bldA* dependence of undecylprodigiosin production in *Streptomyces coelicolor* A3(2) involves a pathway-specific regulatory cascade. *J. Bacteriol.* **179**, 627–633.

80. Tang, L., Grimm, A., Zhang, Y.X., and Hutchinson, C.R. (1996). Purification and characterization of the DNA-binding protein Dnrl, a transcriptional factor of daunorubicin biosynthesis in *Streptomyces peucetius*. *Mol. Microbiol.* **22**, 801–813.

81. Furuya, K., and Hutchinson, C.R. (1996). The DnrN protein of *Streptomyces peucetius*, a pseudo-response regulator, is a DNA-binding protein involved in the regulation of daunorubicin biosynthesis. *J. Bacteriol.* **178**, 6310–6318.

82. Jiang, H., and Hutchinson, C.R. (2006). Feedback regulation of doxorubicin biosynthesis in *Streptomyces peucetius*. *Res. Microbiol.* **157**, 666–674.

83. Wang, L., and Vining, L.C. (2003). Control of growth, secondary metabolism and sporulation in ‹i›Streptomyces venezuelae‹i› ISP5230 by *jadW1*, a member of the *afsA* family of gamma-butyrolactone regulatory genes. *Microbiology* **149**, 1991–2004.

84. Yang, K.Q., Han, L., and Vining, L.C. (1995). Regulation of jadomycin B production in *Streptomyces venezuelae* ISP5230: involvement of a repressor protein *jadR2*. *J. Bacteriol.* **177**, 6111–6117.

85. Yang, K.Q., Han, L., He, J.Y., Wang, L.R., and Vining, L.C. (2001). A repressor-response regulator gene pair controlling jadomycin B production in *Streptomyces venezuelae* ISP5230. *Gene* **279**, 165–173.

86. Wang, L.Q., Tian, X.Y., Wang, J., Yang, H.H., Fan, K.Q., Xu, G.M., Yang, K.Q., and Tan, H.R. (2009). Autoregulation of antibiotic biosynthesis by binding of the end product to an atypical response regulator. *Proc. Natl. Acad. Sci. U.S.A.* **106**, 8617–8622.

87. Martins-Teixeira, M.B., and Carvalho, I. (2020). Antitumour anthracyclines: progress and perspectives. *ChemMedChem* **15**, 933–948.

88. Kurata, T., Okamoto, I., Tamura, K., and Fukuoka, M. (2007). Amrubicin for non-small-cell lung cancer and small-cell lung cancer. *Invest. New Drugs* **25**, 499–504.

89. Mortensen, S.A. (1987). Aclarubicin: preclinical and clinical data suggesting less chronic cardiotoxicity compared with conventional anthracyclines. *Eur. J. Haematol. Suppl.* **47**, 21–31.

90. Staib, P., Lathan, B., Knöppel-Schwark, S., Tesch, H., Voliotis, D., Steinmetz, H.T., Schwonzen, M., Wickramanayake, P.D., and Dieh, V. (1998). Cytosine arabinoside, etoposide and aclarubicin (AVA) for the treatment of acute myeloid leukemia (AML) in elderly patients. *Ann. Oncol.* **9**, 221–223.

91. Wei, G., Ni, W., Chiao, J.W., Cai, Z., Huang, H., and Liu, D. (2011). A meta-analysis of CAG (cytarabine, aclarubicin, G-CSF) regimen for the treatment of 1029 patients with acute myeloid leukemia and myelodysplastic syndrome. *J. Hematol. Oncol.* **4**, 46.

92. Frederick, C.A., Williams, L.D., Ughetto, G., van der Marel, G.A., van Boom, J.H., Rich, A., and Wang, A.H.J. (1990). Structural comparison of anticancer drug-DNA complexes: adriamycin and daunomycin. *Biochemistry* **29**, 2538–2549.

93. Pommier, Y., Sun, Y., Huang, S.Y.N., and Nitiss, J.L. (2016). Roles of eukaryotic topoisomerases in transcription, replication and genomic stability. *Nat. Rev. Mol. Cell Biol.* **17**, 703–721.

94. Dong, K.C., and Berger, J.M. (2007). Structural basis for gate-DNA recognition and bending by type IIA topoisomerases. *Nature* **450**, 1201–1205.

95. Wu, C.C., Li, T.K., Farh, L., Lin, L.Y., Lin, T.S., Yu, Y.J., Yen, T.J., Chiang, C.W., and Chan, N.L. (2011). Structural basis of type II topoisomerase inhibition by the anticancer drug etoposide. *Science* **333**, 459–462.

96. Yang, F., Kemp, C.J., and Henikoff, S. (2013). Doxorubicin enhances nucleosome turnover around promoters. *Curr. Biol.* **23**, 782–787.

97. Pang, B., de Jong, J., Qiao, X., Wessels, L.F.A., and Neefjes, J. (2015). Chemical profiling of the genome with anti-cancer drugs defines target specificities. *Nat. Chem. Biol.* **11**, 472–480.

98. Weiss, R.B., Sarosy, G., Clagett-Carr, K., Russo, M., and Leyland-Jones, B. (1986). Anthracycline analogs: the past, present, and future. *Cancer Chemother. Pharmacol.* **18**, 185–197.

99. Spigel, D.R., Shah, C., Lorigan, P., McNally, R., Renschler, M., and Oliver, J. (2009). Amrubicin (AMR) and cardiotoxicity in second-line treatment of small cell lung cancer (SCLC): A pooled analysis of left ventricular ejection fraction (LVEF) in two phase II trials. *J. Clin. Oncol.* **27**, e19019.

100. Berthiaume, J.M., and Wallace, K.B. (2007). Adriamycin-induced oxidative mitochondrial cardiotoxicity. *Cell Biol. Toxicol.* **23**, 15–25.

101. Ladas, E.J., Jacobson, J.S., Kennedy, D.D., Teel, K., Fleischauer, A., and Kelly, K.M. (2004). Antioxidants and cancer therapy: a systematic review. *J. Clin. Oncol.* **22**, 517–528.

102. Luger, K., Mäder, A.W., Richmond, R.K., Sargent, D.F., and Richmond, T.J. (1997). Crystal structure of the nucleosome core particle at 2.8 Å resolution. *Nature* **389**, 251–260.

103. Felix, C.A. (1998). Secondary leukemias induced by topoisomerase-targeted drugs. *Biochim. Biophys. Acta - Gene Struct. Expression* **1400**, 233–255.

104. Metsä-Ketelä, M., Niemi, J., Mäntsälä, P., and Schneider, G. (2008). Anthracycline biosynthesis: genes, enzymes and mechanisms. In Anthracycline Chemistry and Biology I: Biological Occurence and Biosynthesis, Synthesis and Chemistry Topics in Current Chemistry., K. Krohn, ed. (Springer), pp. 101–140.

105. Brown, K.V., Wandi, B.N., Metsä-Ketelä, M., and Nybo, S.E. (2020). Pathway engineering of anthracyclines: blazing trails in natural product glycodiversification. *J. Org. Chem.* **85**, 12012–12023.

106. Hertweck, C., Luzhetskyy, A., Rebets, Y., and Bechthold, A. (2007). Type II polyketide synthases: gaining a deeper insight into enzymatic teamwork. *Nat. Prod. Rep.* **24**, 162–190.

107. Bao, W., Sheldon, P.J., and Hutchinson, C.R. (1999). Purification and properties of the *Streptomyces peucetius* DpsC $β$- ketoacyl:acyl carrier protein synthase III that specifies the propionate-starter unit for type II polyketide biosynthesis. *Biochemistry* **38**, 9752–9757.

108. Jackson, D.R., Shakya, G., Patel, A.B., Mohammed, L.Y., Vasilakis, K., Wattana-Amorn, P., Valentic, T.R., Milligan, J.C., Crump, M.P., Crosby, J., et al. (2018). Structural and functional studies of the daunorubicin priming ketosynthase DpsC. *ACS Chem. Biol.* **13**, 141–151.

109. Räty, K., Kantola, J., Hautala, A., Hakala, J., Ylihonko, K., and Mäntsälä, P. (2002). Cloning and characterization of *Streptomyces galilaeus* aclacinomycins polyketide synthase (PKS) cluster. *Gene* **293**, 115–122.

110. Grimm, A., Madduri, K., Ali, A., Hutchinsonb, C.R., and Hutchinson, C.R. (1994). Characterization of the *Streptomyces peucetius* ATCC 29050 genes encoding doxorubicin polyketide synthase. *Gene* **151**, 1–10.

111. Rajgarhia, V.B., and Strohl, W.R. (1997). Minimal *Streptomyces* sp. strain C5 daunorubicin polyketide biosynthesis genes required for aklanonic acid biosynthesis. *J. Bacteriol.* **179**, 2690–2696.

112. Ylihonko, K., Tuikkanen, J., Jussila, S., Cong, L., and Mäntsälä, P. (1996). A gene cluster involved in nogalamycin biosynthesis from *Streptomyces nogalater*: sequence analysis and complementation of early-block mutations in the anthracycline pathway. *Mol. Gen. Genet.* **251**, 113–120.

113. Bräuer, A., Zhou, Q., Grammbitter, G.L.C., Schmalhofer, M., Rühl, M., Kaila, V.R.I., Bode, H.B., and Groll, M. (2020). Structural snapshots of the minimal PKS system responsible for octaketide biosynthesis. *Nat. Chem.* **12**, 755–763.

114. Keatinge-Clay, A.T., Maltby, D.A., Medzihradszky, K.F., Khosla, C., and Stroud, R.M. (2004). An antibiotic factory caught in action. *Nat. Struct. Mol. Biol.* **11**, 888–893.

115. Torkkell, S., Kunnari, T., Palmu, K., Hakala, J., Mäntsälä, P., and Ylihonko, K. (2000). Identification of a cyclase gene dictating the C-9 stereochemistry of anthracyclines from *Streptomyces nogalater*. *Antimicrob. Agents Chemother.* **44**, 396–399.

116. Hautala, A., Torkkell, S., Räty, K., Kunnari, T., Kantola, J., Mäntsälä, P., Hakala, J., and Ylihonko, K. (2003). Studies on a second and third ring cyclization in anthracycline biosynthesis. *J. Antibiot.* **56**, 143–153.

117. Kantola, J., Kunnari, T., Hautala, A., Hakala, J., Ylihonko, K., and Mäntsälä, P. (2000). Elucidation of anthracyclinone biosynthesis by stepwise cloning of genes for anthracyclines from three different *Streptomyces* spp. *Microbiology* **146**, 155–163.

118. Grocholski, T., Koskiniemi, H., Lindqvist, Y., Mäntsälä, P., Niemi, J., and Schneider, G. (2010). Crystal structure of the cofactor-independent monooxygenase SnoaB from *Streptomyces nogalater*: implications for the reaction mechanism. *Biochemistry* **49**, 934–944.

119. Machovina, M.M., Ellis, E.S., Carney, T.J., Brushett, F.R., and DuBois, J.L. (2019). How a cofactor-free protein environment lowers the barrier to O2 reactivity. *J. Biol. Chem.* **294**, 3661–3669.

120. Chung, J., Fujii, I., Harada, S., Sankawa, U., Ebizuka, Y., Chung, J. young, Fujii, I., Harada, S., Sankawa, U., and Ebizuka, Y. (2002). Expression, purification, and characterization of AknX anthrone oxygenase, which is involved in aklavinone biosynthesis in *Streptomyces galilaeus*. *J. Bacteriol.* **184**, 6115–6122.

121. Jansson, A., Koskiniemi, H., Mäntsälä, P., Niemi, J., and Schneider, G. (2004). Crystal structure of a ternary complex of DnrK, a methyltransferase in daunorubicin biosynthesis, with bound products. *J. Biol. Chem.* **279**, 41149–41156.

122. Kallio, P., Sultana, A., Niemi, J., Mäntsälä, P., and Schneider, G. (2006). Crystal structure of the polyketide cyclase AknH with bound substrate and product analogue: Implications for catalytic mechanism and product stereoselectivity. *J. Mol. Biol.* **357**, 210–220.

123. Sultana, A., Kallio, P., Jansson, A., Wang, J.S., Niemi, J., Mäntsälä, P., and Schneider, G. (2004). Structure of the polyketide cyclase SnoaL reveals a novel mechanism for enzymatic aldol condensation. *EMBO J.* **23**, 1911–1921.

124. Dickens, M.L., Ye, J., and Strohl, W.R. (1996). Cloning, sequencing, and analysis of aklaviketone reductase from *Streptomyces* sp. strain C5. *J. Bacteriol.* **178**, 3384–3388.

125. Gullón, S., Olano, C., Abdelfattah, M.S., Braña, A.F., Rohr, J., Méndez, C., and Salas, J.A. (2006). Isolation, characterization, and heterologous expression of the biosynthesis gene cluster for the antitumor anthracycline steffimycin. *Appl. Environ. Microbiol.* **72**, 4172–4183.

126. Wang, G., Chen, J., Zhu, H., and Rohr, J. (2017). One-pot enzymatic total synthesis of presteffimycinone, an early intermediate of the anthracycline antibiotic steffimycin biosynthesis. *Org. Lett.* **19**, 540–543.

127. Singh, S., Phillips, G.N., and Thorson, J.S. (2012). The structural biology of enzymes involved in natural product glycosylation. *Nat. Prod. Rep.* **29**, 1201–1237.

128. White-Phillip, J., Thibodeaux, C.J., and Hung-wen, L. (2009). Enzymatic synthesis of TDP-deoxysugars. *Methods Enzymol.* **459**, 521–544.

129. Olano, C., Lomovskaya, N., Fonstein, L., Roll, J.T., and Hutchinson, C.R. (1999). A two-plasmid system for the glycosylation of polyketide antibiotics: bioconversion of ε-rhodomycinone to rhodomycin D. *Chem. Biol.* **6**, 845–855.

130. Räty, K., Kunnari, T., Hakala, J., Mäntsälä, P., and Ylihonko, K. (2000). A gene cluster from *Streptomyces galilaeus* involved in glycosylation of aclarubicin. *Mol. Gen. Genet.* **264**, 164–172.

131. Siitonen, V., Nji Wandi, B., Törmänen, A.-P., and Metsä-Ketelä, M. (2018). Enzymatic synthesis of the *C*-glycosidic moiety of nogalamycin R. *ACS Chem. Biol.* **13**, 2433–2437.

132. Kang, H.-S.S., and Brady, S.F. (2013). Arimetamycin A: improving clinically relevant families of natural products through sequence-guided screening of soil metagenomes. *Angew. Chem. Int. Ed.* **52**, 11063–11067.

133. Adnani, N., Chevrette, M.G., Adibhatla, S.N., Zhang, F., Yu, Q., Braun, D.R., Nelson, J., Simpkins, S.W., McDonald, B.R., Myers, C.L., et al. (2017). Coculture of marine invertebrate-associated bacteria and interdisciplinary technologies enable biosynthesis and discovery of a new antibiotic, keyicin. *ACS Chem. Biol.* **12**, 3093–3102.

134. Ma, H.M., Zhou, Q., Tang, Y.M., Zhang, Z., Chen, Y.S., He, H.Y., Pan, H.X., Tang, M.C., Gao, J.F., Zhao, S.Y., et al. (2013). Unconventional origin and hybrid system for construction of pyrrolopyrrole moiety in kosinostatin biosynthesis. *Chem. Biol.* **20**, 796–805.

135. Barton, W.A., Lesniak, J., Biggins, J.B., Jeffrey, P.D., Jiang, J., Rajashankar, K.R., Thorson, J.S., and Nikolov, D.B. (2001). Structure, mechanism and engineering of a nucleotidylyltransferase as a first step toward glycorandomization. *Nat. Struct. Biol.* **8**, 545–551.

136. Blankenfeldt, W., Asuncion, M., Lam, J.S., and Naismith, J.H. (2000). The structural basis of the catalytic mechanism and regulation of glucose-1-phosphate thymidylyltransferase (RmlA). *EMBO J.* **19**, 6652–6663.

137. Allard, S.T.M., Beis, K., Giraud, M.F., Hegeman, A.D., Gross, J.W., Wilmouth, R.C., Whitfield, C., Graninger, M., Messner, P., Allen, A.G., et al. (2002). Toward a structural understanding of the dehydratase mechanism. *Structure* **10**, 81–92.

138. Kubiak, R.L., Thoden, J.B., and Holden, H.M. (2013). Structure of EvaA: a paradigm for sugar 2,3-dehydratases. *Biochemistry* **52**, 2078–2088.

139. Burgie, E.S., Thoden, J.B., and Holden, H.M. (2007). Molecular architecture of DesV from *Streptomyces venezuelae*: a PLP-dependent transaminase involved in the biosynthesis of the unusual sugar desosamine. *Protein Sci.* **16**, 887–896.

140. Merkel, A.B., Major, L.L., Errey, J.C., Burkart, M.D., Field, R.A., Walsh, C.T., and Naismith, J.H. (2004). The position of a key tyrosine in dTDP-4-keto-6-deoxy-D-glucose-5-epimerase (EvaD) alters the substrate profile for this RmlC-like enzyme. *J. Biol. Chem.* **279**, 32684–32691.

141. Thibodeaux, C.J., Melançon, C.E., and Liu, H.W. (2007). Unusual sugar biosynthesis and natural product glycodiversification. *Nature* **446**, 1008–1016.

142. Schmidt, R., Ulanova, D., Wick, L.Y., Bode, H.B., and Garbeva, P. (2019). Microbe-driven chemical ecology: past, present and future. *ISME J.* **13**, 2656–2663.

143. Liang, D.M., Liu, J.H., Wu, H., Wang, B.B., Zhu, H.J., and Qiao, J.J. (2015). Glycosyltransferases: mechanisms and applications in natural product development. *Chem. Soc. Rev.* **44**, 8350–8374.

144. Claesson, M., Siitonen, V., Dobritzsch, D., Metsä-Ketelä, M., and Schneider, G. (2012). Crystal structure of the glycosyltransferase SnogD from the biosynthetic pathway of nogalamycin in *Streptomyces nogalater*. *FEBS J.* **279**, 3251–3263.

145. Gui, C., Mo, X., Gu, Y.C., and Ju, J. (2017). Elucidating the sugar tailoring steps in the cytorhodin biosynthetic pathway. *Org. Lett.* **19**, 5617–5620.

146. Leimkuhler, C., Fridman, M., Lupoli, T., Walker, S., Walsh, C.T., and Kahne, D. (2007). Characterization of rhodosaminyl transfer by the AknS/AknT glycosylation complex and its use in reconstituting the biosynthetic pathway of aclacinomycin A. *J. Am. Chem. Soc.* **129**, 10546–10550.

147. Lu, W., Leimkuhler, C., Gatto, G.J., Kruger, R.G., Oberthür, M., Kahne, D., and Walsh, C.T. (2005). AknT is an activating protein for the glycosyltransferase AknS in L-aminodeoxysugar transfer to the aglycone of aclacinomycin A. *Chem. Biol.* **12**, 527–534.

148. Garrido, L.M., Lombó, F., Baig, I., Nur-E-Alam, M., Furlan, R.L.A.A., Borda, C.C., Braña, A., Méndez, C., Salas, J.A., Rohr, J., et al. (2006). Insights in the glycosylation steps during biosynthesis of the antitumor anthracycline cosmomycin: characterization of two glycosyltransferase genes. *Appl. Microbiol. Biotechnol.* **73**, 122–131.

149. Moncrieffe, M.C., Fernandez, M.J., Spiteller, D., Matsumura, H., Gay, N.J., Luisi, B.F., and Leadlay, P.F. (2012). Structure of the glycosyltransferase EryCIII in complex with its activating P450 homologue EryCII. *J. Mol. Biol.* **415**, 92–101.

150. Hong, Y.-S., Hwang, C.K., Hong, S.-K., Kim, Y.H., and Lee, J.J. (1994). Molecular cloning and characterization of the aklavinone 11-hydroxylase gene of *Streptomyces peucetius* subsp. *caesius* ATCC 27952. *J. Bacteriol.* **176**, 7096–7101.

151. Grocholski, T., Yamada, K., Sinkkonen, J., Tirkkonen, H., Niemi, J., and Metsä-Ketelä, M. (2019). Evolutionary trajectories for the functional diversification of anthracycline methyltransferases. *ACS Chem. Biol.* **14**, 850–856.

152. Madduri, K., and Hutchinson, C.R. (1995). Functional characterization and transcriptional analysis of a gene cluster governing early and late steps in daunorubicin biosynthesis in *Streptomyces peucetius*. *J. Bacteriol.* **177**, 3879–3884.

153. Walczak, R.J., Dickens, M.L., Priestley, N.D., and Strohl, W.R. (1999). Purification, properties, and characterization of recombinant *Streptomyces* sp. strain C5 DoxA, a cytochrome P-450 catalyzing multiple steps in doxorubicin biosynthesis. *J. Bacteriol.* **181**, 298–304.

154. Al-Mestarihi, A., Romo, A., Liu, H.W., and Bachmann, B.O. (2013). Nitrososynthase-triggered oxidative carbon-carbon bond cleavage in baumycin biosynthesis. *J. Am. Chem. Soc.* **135**, 11457–11460.

155. Lindqvist, Y., Koskiniemi, H., Jansson, A., Sandalova, T., Schnell, R., Liu, Z., Mäntsälä, P., Niemi, J., and Schneider, G. (2009). Structural basis for substrate recognition and specificity in aklavinone-11-hydroxylase from rhodomycin biosynthesis. *J. Mol. Biol.* **393**, 966–977.

156. Niemi, J., and Mäntsälä, P. (1995). Nucleotide sequences and expression of genes from *Streptomyces purpurascens* that cause the production of new anthracyclines in *Streptomyces galilaeus*. *J. Bacteriol.* **177**, 2942–2945.

157. Jansson, A., Niemi, J., Mäntsälä, P., and Schneider, G. (2003). Crystal structure of aclacinomycin methylesterase with bound product analogues: implications for anthracycline recognition and mechanism. *J. Biol. Chem.* **278**, 39006–39013.

158. Wang, Y., Niemi, J., Airas, K., Ylihonko, K., Hakala, J., and Mäntsälä, P. (2000). Modifications of aclacinomycin T by aclacinomycin methyl esterase (RdmC) and aclacinomycin-10-hydroxylase (RdmB) from *Streptomyces purpurascens*. *Biochim. Biophys. Acta - Protein Struct. Mol. Enzymol.* **1480**, 191–200.

159. Jansson, A., Koskiniemi, H., Erola, A., Wang, J., Mäntsälä, P., Schneider, G., and Niemi, J. (2005). Aclacinomycin 10-hydroxylase is a novel substrate-assisted hydroxylase requiring *S*-adenosyl-L-methionine as cofactor. *J. Biol. Chem.* **280**, 3636–3644.

160. Grocholski, T., Dinis, P., Niiranen, L., Niemi, J., and Metsä-Ketelä, M. (2015). Divergent evolution of an atypical *S*-adenosyl-L-methionine–dependent monooxygenase involved in anthracycline biosynthesis. *Proc. Natl. Acad. Sci. U.S.A.* **112**, 9866–9871.

161. Siitonen, V., Blauenburg, B., Kallio, P., Mäntsälä, P., and Metsä-Ketelä, M. (2012). Discovery of a two-component monooxygenase SnoaW/SnoaL2 involved in nogalamycin biosynthesis. *Chem. Biol.* **19**, 638–646.

162. Beinker, P., Lohkamp, B., Peltonen, T., Niemi, J., Mäntsälä, P., and Schneider, G. (2006). Crystal structures of SnoaL2 and AclR: two putative hydroxylases in the niosynthesis of aromatic polyketide antibiotics. *J. Mol. Biol.* **359**, 728–740.

163. Zhang, Z., Gong, Y.K., Zhou, Q., Hu, Y., Ma, H.M., Chen, Y.S., Igarashi, Y., Pan, L., and Tang, G.L. (2017). Hydroxyl regioisomerization of anthracycline catalyzed by a four-enzyme cascade. *Proc. Natl. Acad. Sci. U.S.A.* **114**, 1554–1559.

164. Nji Wandi, B., Siitonen, V., Palmu, K., and Metsä-Ketelä, M. (2020). The Rieske oxygenase SnoT catalyzes 2”-hydroxylation of L-rhodosamine in nogalamycin biosynthesis. *ChemBioChem* **21**, 3062–3066.

165. Siitonen, V., Selvaraj, B., Niiranen, L., Lindqvist, Y., Schneider, G., and Metsä-Ketelä, M. (2016). Divergent non-heme iron enzymes in the nogalamycin biosynthetic pathway. *Proc. Natl. Acad. Sci. U.S.A.* **113**, 5251–5256.

166. Nji Wandi, B., Siitonen, V., Dinis, P., Vukic, V., Salminen, T.A., and Metsä-Ketelä, M. (2020). Evolution-guided engineering of non-heme iron enzymes involved in nogalamycin biosynthesis. *FEBS J.* **287**, 2998–3011.

167. Alexeev, I., Sultana, A., Mäntsälä, P., Niemi, J., and Schneider, G. (2007). Aclacinomycin oxidoreductase (AknOx) from the biosynthetic pathway of the antibiotic aclacinomycin is an unusual flavoenzyme with a dual active site. *Proc. Natl. Acad. Sci. U.S.A.* **104**, 6170–6175.

168. Belknap, K.C., Park, C.J., Barth, B.M., and Andam, C.P. (2020). Genome mining of biosynthetic and chemotherapeutic gene clusters in *Streptomyces* bacteria. *Sci. Rep.* **10**, 2003.

169. Imbert, M., Bechet, M., Blondeau, R., Béchet, M., and Blondeau, R. (1995). Comparison of the main siderophores produced by some species of *Streptomyces*. *Curr. Microbiol.* **31**, 129–133.

170. Martín-Sánchez, L., Singh, K.S., Avalos, M., van Wezel, G.P., Dickschat, J.S., and Garbeva, P. (2019). Phylogenomic analyses and distribution of terpene synthases among *Streptomyces*. *Beilstein J. Org. Chem.* **15**, 1181–1193.

171. Baltz, R.H. (2008). Renaissance in antibacterial discovery from actinomycetes. *Curr. Opin. Pharmacol.* **8**, 557–563.

172. Elshahawi, S.I., Shaaban, K.A., Kharel, M.K., and Thorson, J.S. (2015). A comprehensive review of glycosylated bacterial natural products. *Chem. Soc. Rev.* **44**, 7591–7697.

173. Laatsch, H., and Fotso, S. (2008). Naturally occurring anthracyclines. In Anthracycline Chemistry and Biology I: Biological Occurence and Biosynthesis, Synthesis and Chemistry Topics in Current Chemistry., K. Krohn, ed. (Springer), pp. 3–74.

174. Kim, H.S., Kim, Y.H., Yoo, O.J., and Lee, J.J. (1996). Aclacinomycin X, a novel anthracycline antibiotic produced by *Streptomyces galilaeus* ATCC 31133. *Biosci. Biotechnol. Biochem.* **60**, 906–908.

175. Li, W., Yang, X., Yang, Y., Zhao, L., Xu, L., and Ding, Z. (2015). A new anthracycline from endophytic *Streptomyces* sp. YIM66403. *J. Antibiot.* **68**, 216–219.

176. Saito, S., Katsuda, Y., Johdo, O., and Yoshimoto, A. (1995). New rhodomycin analogs, SS-288A and SS-288B, produced by a *Streptomyces violaceus* A262 mutant. *Biosci. Biotechnol. Biochem.* **59**, 135–137.

177. Phipps, R.K., Blunt, J.W., Cole, A.L.J., and Munro, M.H.G. (2004). Anthracycline derivatives from a marine-derived New Zealand streptomycete. *Arkivoc* **10**, 94–100.

178. Chun-ling, X., Shu-yi, S., and Yue-qin, Z. (2001). The structure of new anthracycline antibiotics, G0041-3c. *Chin. J. Antibiotics* **26**, 85–88.

179. Johdo, O., Yoshioko, T., Takeuchi, T., and Yoshimoto, A. (1997). Isolation of new anthracyclines 10-*O*-rhodosaminyl β-rhodomycinone and β-isorhodomycinone from mild-acid treated culture of obelmycin-producing *Streptomyces violaceus*. *J. Antibiot.* **50**, 522–525.

180. Komatsu, Y., Takahashi, O., and Hayashi, H. (1998). Identification of the anthracycline antibiotic 4-*O*-(β-D-glucopyranuronosyl)-ε-rhodomycinone, produced by *Streptomyces ruber* JCM3131, as an up-regulator of MHC class-I molecules in B16/BL6 cells. *J. Antibiot.* **51**, 85–88.

181. Kawauchi, T., Sasaki, T., Yoshida, K., Matsumoto, H., Chen, R.-X., Huang, M.-Y., and Otani, T. (1997). A new anthracycline antibiotic, IT-62-B, converts the morphology of ras-transformed cells back to normal: taxonomy, fermentation, isolation, structure elucidation and biological characterization. *J. Antibiot.* **50**, 297–303.

182. Ishii, K., Kondo, S., Nishimura, Y., Hamada, M., Takeuchi, T., and Umezawa, H. (1983). Decilorubicin, a new anthracycline antibiotic. *J. Antibiot.* **36**, 451–453.

183. Wu, Q.-B., Chen, X.-A., Lv, Z.-Y., Zhang, X.-Y., Liu, Y., and Li, Y.-Q. (2021). Activation and discovery of tsukubarubicin from *Streptomyces tsukubaensis* through overexpressing SARPs. *Appl. Microbiol. Biotechnol.* **105**, 4731–4741.

184. Wang, Q., Zhou, B., yuan Ji, Y., jian Zhang, H., jun Ma, Z., Shen, L., and jing Ding, W. (2019). Bioactive constituents from marine-derived *Streptomyces* sp. NB-A13. *Phytochem. Lett.* **30**, 154–159.

185. Yang, S.W., Chan, T.M., Terracciano, J., Patel, R., Loebenberg, D., Chen, G., Patel, M., Gullo, V., Pramanik, B., and Chu, M. (2004). A new anthracycline antibiotic micromonomycin from *Micromonospora* sp. *J. Antibiot.* **57**, 601–604.

186. Zitouni, A., Mathieu, F., Coppel, Y., Pont, F., Sabaou, N., and Lebrihi, A. (2004). Mutactimycin PR, a new anthracycline antibiotic from *Saccharothrix* sp. SA 103 II. Physico-chemical properties and structure elucidation. *J. Antibiot.* **57**, 373–378.

187. Speitling, M., Nattewan, P., Yazawa, K., Mikami, Y., Grün-Wollny, I., Ritzau, M., Laatsch, H., and Gräfe, U. (1998). Demethyl mutactimycins, new anthracycline antibiotics from *Nocardia* and *Streptomyces* strains. *J. Antibiot.* **51**, 693–698.

188. Itoh, T., Kinoshita, M., Aoki, S., and Kobayashi, M. (2003). Komodoquinone A, a novel neuritogenic anthracycline, from marine *Streptomyces* sp. KS3. *J. Nat. Prod.* **66**, 1373–1377.

189. Intaraudom, C., Bunbamrung, N., Dramae, A., Danwisetkanjana, K., Rachtawee, P., and Pittayakhajonwut, P. (2015). Antimalarial and antimycobacterial agents from *Streptomyces* sp. BCC27095. *Tetrahedron Lett.* **56**, 6875–6877.

190. Koyama, N., Shigeno, S., Kanamoto, A., and Tomoda, H. (2020). Steffimycin E, a new anti-mycobacterial agent against *Mycobacterium avium* complex, produced by *Streptomyces* sp. OPMA02852. *J. Antibiot.* **73**, 581–584.

191. Liu, C.Y., Li, Y.L., Lu, J.H., Qian, L.L., Xu, K., Wang, N.N., Chang, W.Q., and Lou, H.X. (2021). Steffimycin F, a new steffimycin-type derivative from the lichen-derived actinomycetes *Streptomyces* sp. *J. Mol. Struct.* **1227**, 129352.

192. Khalil, Z.G., Raju, R., Piggott, A.M., Salim, A.A., Blumenthal, A., and Capon, R.J. (2015). Aranciamycins I and J, antimycobacterial anthracyclines from an Australian marine-derived *Streptomyces* sp. *J. Nat. Prod.* **78**, 949–952.

193. Nachtigall, J., Schulz, D., Beil, W., Süssmuth, R.D., and Fiedler, H.P. (2010). Aranciamycin anhydride, a new anthracycline-type antibiotic isolated from *Streptomyces* sp. Tü 6384. *J. Antibiot.* **63**, 397–399.

194. Motohashi, K., Takagi, M., and Shin-Ya, K. (2010). Tetracenoquinocin and 5-iminoaranciamycin from a sponge-derived *Streptomyces* sp. Sp080513GE-26. *J. Nat. Prod.* **73**, 755–758.

195. Hopp, D.C., Rabenstein, J., Rhea, J., Smith, C., Romari, K., Clarke, M., Francis, L., Irigoyen, M., Milanowski, D., Luche, M., et al. (2008). Mutactimycin E, a new anthracycline antibiotic with Gram-positive activity. *J. Antibiot.* **61**, 675–679.

196. Tanaka, Y., Gräfe, U.D.O., Yazawa, K., Mikami, Y., and Ritzau, M. (1997). Nocardicyclins A and B: new anthracycline antibiotics produced by *Nocardia pseudobrasiliensis*. *J. Antibiot.* **50**, 822–827.

197. Wan, X., Ren, H.J., Du, M.N., Qi, H., Zhang, H., Chen, A.L., and Wang, J.D. (2017). A new cyano-substituted anthracycline metabolite from *Streptomyces* sp. HS-NF-1006. *J. Antibiot.* **70**, 219–221.

198. Lu, C., Zhao, Y., Jia, W.Q., Zhang, H., Qi, H., Xiang, W.S., Wang, J.D., and Wang, X.J. (2017). A new anthracycline-type metabolite from *Streptomyces* sp. NEAU-L3. *J. Antibiot.* **70**, 1026–1028.

199. Furumai, T., Igarashi, Y., Higuchi, H., Saito, N., and Oki, T. (2002). Kosinostatin, a quinocycline antibiotic with antitumor activity from *Micromonospora* sp. TP-A0468. *J. Antibiot.* **55**, 128–133.

200. Rodríguez-Hernández, D., Melo, W.G.P., Menegatti, C., Lourenzon, V.B., do Nascimento, F.S., and Pupo, M.T. (2019). Actinobacteria associated with stingless bees biosynthesize bioactive polyketides against bacterial pathogens. *New J. Chem.* **43**, 10109–10117.

201. El-Naggar, M.Y. (2007). Kosinostatin, a major secondary metabolite isolated from the culture filtrate of *Streptomyces violaceusniger* strain HAL64. *J. Microbiol.* **45**, 262–267.

202. Cong, Z., Huang, X., Liu, Y., Liu, Y., Wang, P., Liao, S., Yang, B., Zhou, X., Huang, D., and Wang, J. (2019). Cytotoxic anthracycline and antibacterial tirandamycin analogues from a marine-derived *Streptomyces* sp. SCSIO 41399. *J. Antibiot.* **72**, 45–49.

203. Sousa, T.D.S., Jimenez, P.C., Ferreira, E.G., Silveira, E.R., Braz-Filho, R., Pessoa, O.D.L.L., and Costa-Lotufo, L.V. (2012). Anthracyclinones from *Micromonospora* sp. *J. Nat. Prod.* **75**, 489–493.

204. Shaaban, K.A., Shaaban, M., Meiners, M., Schüffler, A., Kelter, G., Fiebig, H.H., and Laatsch, H. (2021). Boshramycinones A-C: new anthracyclinones produced by a marine-derived *Streptomyces sp.*: isolation, structure elucidation and biological activities. *Nat. Prod. Res.* **35**, 1281–1291.

205. Abdelfattah, M.S., Elmallah, M.I.Y., Mohamed, A.A., and Ishibashi, M. (2017). Sharkquinone, a new *ana*-quinonoid tetracene derivative from marine-derived *Streptomyces* sp. EGY1 with TRAIL resistance-overcoming activity. *J. Nat. Med.* **71**, 564–569.

206. Supong, K., Sripreechasak, P., Phongsopitanun, W., Tanasupawat, S., Danwisetkanjana, K., Bunbamrung, N., and Pittayakhajonwut, P. (2019). Antimicrobial substances from the rare actinomycete *Nonomuraea rhodomycinica* NR4-ASC07T. *Nat. Prod. Res.* **33**, 2285–2291.

207. Pullen, C., Schmitz, P., Meurer, K., Bamberg, D.D.V., Lohmann, S., De Castro França, S., Groth, I., Schlegel, B., Möllmann, U., Gollmick, F., et al. (2002). New and bioactive compounds from *Streptomyces* strains residing in the wood of Celastraceae. *Planta* **216**, 162–167.

208. Maskey, R.P., Grün-Wollny, I., and Laatsch, H. (2003). Resomycins A-C: new anthracyclinone antibiotics formed by a terrestrial *Streptomyces* sp. *J. Antibiot.* **56**, 795–800.

209. Tsukamoto, N., Fujii, I., Ebizuka, Y., and Sankawa, U. (1992). Cloning of aklavinone biosynthesis genes from *Streptomyces galilaeus*. *J. Antibiot.* **45**, 1286–1294.

210. Ye, J., Dickens, M.L., Plater, R., Li, Y., Lawrence, J., and Strohl, W.R. (1994). Isolation and sequence analysis of polyketide synthase genes from the daunomycin-producing *Streptomyces* sp. strain C5. *J. Bacteriol.* **176**, 6270–6280.

211. Luzhetskyy, A., Mayer, A., Hoffmann, J., Pelzer, S., Holzenkämper, M., Schmitt, B., Wohlert, S.E., Vente, A., and Bechthold, A. (2007). Cloning and heterologous expression of the aranciamycin biosynthetic gene cluster revealed a new flexible glycosyltransferase. *ChemBioChem* **8**, 599–602.

212. Medema, M.H., Takano, E., and Breitling, R. (2013). Detecting sequence homology at the gene cluster level with MultiGeneBlast. *Mol. Biol. Evol.* **30**, 1218–1223.

213. Hillenmeyer, M.E., Vandova, G.A., Berlew, E.E., and Charkoudian, L.K. (2015). Evolution of chemical diversity by coordinated gene swaps in type II polyketide gene clusters. *Proc. Natl. Acad. Sci. U.S.A.* **112**, 13952–13957.

214. Metsä-Ketelä, M., Salo, V., Halo, L., Hautala, A., Hakala, J., Mäntsälä, P., and Ylihonko, K. (1999). An efficient approach for screening minimal PKS genes from *Streptomyces*. *FEMS Microbiol. Lett.* **180**, 1–6.

215. Metsä-Ketelä, M., Halo, L., Munukka, E., Hakala, J., Mäntsäla, P., and Ylihonko, K. (2002). Molecular evolution of aromatic polyketides and comparative sequence analysis of polyketide ketosynthase and 16S ribosomal DNA genes from various *Streptomyces* species. *Appl. Environ. Microbiol.* **68**, 4472–4479.

216. Niemi, J., Metsä-Ketelä, M., Schneider, G., and Mäntsälä, P. (2008). Biosynthetic anthracycline variants. In Anthracycline Chemistry and Biology I: Biological Occurence and Biosynthesis, Synthesis and Chemistry Topics in Current Chemistry., K. Krohn, ed. (Springer), pp. 75–99.

217. Niemi, J., Ylihonko, K., Hakala, J., Pärssinen, R., Kopio, A., and Mäntsälä, P. (1994). Hybrid anthracycline antibiotics: production of new anthracyclines by cloned genes from *Streptomyces purpurascens* in *Streptomyces galilaeus*. *Microbiology* **140**, 1351–1358.

218. Kunnari, T., Niemi, J., Ylihonko, K., Mäntsälä, P., and Hakala, J. (1997). Hybrid anthracyclines by a genetically engineered *Streptomyces galilaeus* mutant. *Bioorg. Med. Chem. Lett.* **7**, 725–726.

219. Torkkell, S., Kunnari, T., Palmu, K., Mäntsälä, P., Hakala, J., and Ylihonko, K. (2001). The entire nogalamycin biosynthetic gene cluster of *Streptomyces nogalater*: characterization of a 20-kb DNA region and generation of hybrid structures. *Mol. Genet. Genomics* **266**, 276–288.

220. Ylihonko, K., Hakala, J., Kunnari, T., and Mantsälä, P. (1996). Production of hybrid anthracycline antibiotics by heterologous expression of *Streptomyces nogalater* nogalamycin biosynthesis genes. *Microbiology* **142**, 1965–1972.

221. Cheol Kyu Hwang, Hang Sub Kim, Young Soo Hong, Young Ho Kim, Hong, S.K., Kim, S.J., and Jung Joon Lee (1995). Expression of *Streptomyces peucetius* genes for doxorubicin resistance and aklavinone 11-hydroxylase in *Streptomyces galilaeus* ATCC 31133 and production of a hybrid aclacinomycin. *Antimicrob. Agents Chemother.* **39**, 1616–1620.

222. Kim, H.S., Hong, Y.S., Kim, Y.H., Yoo, O.J., and Lee, J.J. (1996). New anthracycline metabolites produced by the aklavinone 11-hydroxylase gene in *Streptomyces galilaeus* ATCC 31133. *J. Antibiot.* **49**, 355–360.

223. Miyamoto, Y., Ohta, S., Johdoc, O., Nagamatsu, Y., and Yoshimoto, A. (2000). Production of a new hybrid anthracycline 4-*O*-methylepelmycin by heterologous expression of *dnrK* in epelmycin-producing *Streptomyces violaceus* genes. *J. Antibiot.* **53**, 828–836.

224. Hu, Y., Zhang, Z., Yin, Y., and Tang, G.L. (2020). Directed biosynthesis of iso-aclacinomycins with improved anticancer activity. *Org. Lett.* **22**, 150–154.

225. Räty, K., Hautala, A., Torkkell, S., Kantola, J., Mäntsälä, P., Hakala, J., and Ylihonko, K. (2002). Characterization of mutations in aclacinomycin A-non-producing *Streptomyces galilaeus* strains with altered glycosylation patterns. *Microbiology* **148**, 3375–3384.

226. Siitonen, V., Räty, K., and Metsä-Ketelä, M. (2016). Laboratory course on *Streptomyces* genetics and secondary metabolism. *Biochem. Mol. Biol. Educ.* **44**, 492–499.

227. Kunnari, T., Tuikkanen, J., Hautala, A., Hakala, J., Ylihonko, K., and Mäntsälä, P. (1997). Isolation and characterization of and 8-demethoxy steffimycins and generation of 2,8-demethoxy steffimycins in *Streptomyces steffisburgensis* by the nogalamycin biosynthesis genes. *J. Antibiot.* **50**, 496–501.

228. Madduri, K., Kennedy, J., Rivola, G., Inventi-Solari, A., Filippini, S., Zanuso, G., Colombo, A.L., Gewain, K.M., Occi, J.L., MacNeil, D.J., et al. (1998). Production of the antitumor drug epirubicin (4'-epidoxorubicin) and its precursor by a genetically engineered strain of *Streptomyces peucetius*. *Nat. Biotechnol.* **16**, 69–74.

229. Luzhetskyy, A., Hoffmann, J., Pelzer, S., Wohlert, S.E., Vente, A., and Bechthold, A. (2008). Aranciamycin analogs generated by combinatorial biosynthesis show improved antitumor activity. *Appl. Microbiol. Biotechnol.* **80**, 15–19.

230. Olano, C., Abdelfattah, M.S., Gullón, S., Braña, A.F., Rohr, J., Méndez, C., and Salas, J.A. (2008). Glycosylated derivatives of steffimycin: insights into the role of the sugar moieties for the biological activity. *ChemBioChem* **9**, 624–633.

231. Han, A.R., Park, J.W., Lee, M.K., Ban, Y.H., Yoo, Y.J., Kim, E.J., Kim, E., Kim, B.-G., Sohng, J.K., and Yoon, Y.J. (2011). Development of a *Streptomyces venezuelae*-based combinatorial biosynthetic system for the production of glycosylated derivatives of doxorubicin and its biosynthetic intermediates. *Appl. Environ. Microbiol.* **77**, 4912–4923.

232. Kim, E., Song, M.C., Kim, M.S., Beom, J.Y., Jung, J.A., Cho, H.S., and Yoon, Y.J. (2017). One-pot combinatorial biosynthesis of glycosylated anthracyclines by cocultivation of *Streptomyces* strains producing aglycones and nucleotide deoxysugars. *ACS Comb. Sci.* **19**, 262–270.

233. Huo, L., Hug, J.J., Fu, C., Bian, X., Zhang, Y., Muller, R., and Müller, R. (2019). Heterologous expression of bacterial natural product biosynthetic pathways. *Nat. Prod. Rep.* **36**, 1412–1436.

234. Myronovskyi, M., and Luzhetskyy, A. (2019). Heterologous production of small molecules in the optimized: *Streptomyces* hosts. *Nat. Prod. Rep.* **36**, 1281–1294.

235. Gomez-Escribano, J.P., and Bibb, M.J. (2011). Engineering *Streptomyces coelicolor* for heterologous expression of secondary metabolite gene clusters. *Microb. Biotechnol.* **4**, 207–215.

236. Baltz, R.H. (2016). Genetic manipulation of secondary metabolite biosynthesis for improved production in *Streptomyces* and other actinomycetes. *J. Ind. Microbiol. Biotechnol.* **43**, 343–370.

237. Malla, S., Niraula, N.P., Liou, K., and Sohng, J.K. (2009). Enhancement of doxorubicin production by expression of structural sugar biosynthesis and glycosyltransferase genes in *Streptomyces peucetius*. *J. Biosci. Bioeng.* **108**, 92–98.

238. Rokem, J.S., Lantz, A.E., and Nielsen, J. (2007). Systems biology of antibiotic production by microorganisms. *Nat. Prod. Rep.* **24**, 1262–1287.

239. Bilyk, O., and Luzhetskyy, A. (2016). Metabolic engineering of natural product biosynthesis in Actinobacteria. *Curr. Opin. Biotechnol.* **42**, 98–107.

240. Robertsen, H.L., Weber, T., Kim, H.U., and Lee, S.Y. (2018). Toward systems metabolic rngineering of *Streptomycetes* for secondary metabolites production. *Biotechnol. J.* **13**, 1–12.

241. Stutzman-Engwall, K.J., Otten, S.L., and Hutchinson, C.R. (1992). Regulation of secondary metabolism in *Streptomyces* spp. and overproduction of daunorubicin in *Streptomyces peucetius*. *J. Bacteriol.* **174**, 144–154.

242. Parajuli, N., Hung, T.V., Ishida, K., Hang, T.T., Hei, C.L., Liou, K., Jae, K.S., Viet, H.T., Ishida, K., Tong, H.T., et al. (2005). Identification and characterization of the *afsR* homologue regulatory gene from *Streptomyces peucetius* ATCC 27952. *Res. Microbiol.* **156**, 707–712.

243. Kang, S.H., Huang, J., Lee, H.N., Hur, Y.A., Cohen, S.N., and Kim, E.S. (2007). Interspecies DNA microarray analysis identifies WblA as a pleiotropic down-regulator of antibiotic biosynthesis in *Streptomyces*. *J. Bacteriol.* **189**, 4315–4319.

244. Chaudhary, A.K., Singh, B., Maharjan, S., Jha, A.K., Kim, B.G., and Sohng, J.K. (2014). Switching antibiotics production on and off in actinomycetes by an IclR family transcriptional regulator from *Streptomyces peucetius* ATCC 27952. *J. Microbiol.* **24**, 1065–1072.

245. Zabala, D., Braña, A.F., Flórez, A.B., Salas, J.A., Méndez, C., Brana, A.F., Florez, A.B., Salas, J.A., Mendez, C., Braña, A.F., et al. (2013). Engineering precursor metabolite pools for increasing production of antitumor mithramycins in *Streptomyces argillaceus*. *Metab. Eng.* **20**, 187–197.

246. Zabala, D., Branã, A.F., Salas, J.A., Méndez, C., Brana, A.F., Salas, J.A., and Mendez, C. (2016). Increasing antibiotic production yields by favoring the biosynthesis of precursor metabolites glucose-1-phosphate and/or malonyl-CoA in *Streptomyces* producer strains. *J. Antibiot.* **69**, 179–182.

247. Wang, W., Li, S., Li, Z., Zhang, J., Fan, K., Tan, G., Ai, G., Lam, S.M., Shui, G., Yang, Z., et al. (2020). Harnessing the intracellular triacylglycerols for titer improvement of polyketides in *Streptomyces*. *Nat. Biotechnol.* **38**, 76–83.

248. Lee, N.R., Rimal, H., Lee, J.H., and Oh, T.J. (2014). Characterization of dephosphocoenzyme a kinase from *Streptomyces peucetius* ATCC27952, and its application for doxorubicin overproduction. *J. Microbiol.* **24**, 1238–1244.

249. Li, S., Li, Z., Pang, S., Xiang, W., and Wang, W. (2021). Coordinating precursor supply for pharmaceutical polyketide production in *Streptomyces*. *Curr. Opin. Biotechnol.* **69**, 26–34.

250. Hutchinson, C.R., and Colombo, A.L. (1999). Genetic engineering of doxorubicin production in *Streptomyces peucetius*: a review. *J. Ind. Microbiol. Biotechnol.* **23**, 647–652.

251. Fierro, F., Barredo, J.L., Diez, B., Gutierrez, S., Fernandez, F.J., and Martin, J.F. (1995). The penicillin gene cluster is amplified in tandem repeats linked by conserved hexanucleotide sequences. *Proc. Natl. Acad. Sci. U.S.A.* **92**, 6200–6204.

252. Yanai, K., Murakami, T., and Bibb, M. (2006). Amplification of the entire kanamycin biosynthetic gene cluster during empirical strain improvement of *Streptomyces kanamyceticus*. *Proc. Natl. Acad. Sci. U.S.A.* **103**, 9661–9666.

253. Nah, H.J., Pyeon, H.R., Kang, S.H., Choi, S.S., and Kim, E.S. (2017). Cloning and heterologous expression of a large-sized natural product biosynthetic gene cluster in *Streptomyces* species. *Front. Microbiol.* **8**, 394.

254. Malla, S., Prasad Niraula, N., Singh, B., Liou, K., and Kyung Sohng, J. (2010). Limitations in doxorubicin production from *Streptomyces peucetius*. *Microbiol. Res.* **165**, 427–435.

255. Singh, B., Lee, C.B., and Sohng, J.K. (2009). Precursor for biosynthesis of sugar moiety of doxorubicin depends on rhamnose biosynthetic pathway in *Streptomyces peucetius* ATCC 27952. *Appl. Microbiol. Biotechnol.* **85**, 1565–1574.

256. Lomovskaya, N., Doi-Katayama, Y., Filippini, S., Nastro, C., Fonstein, L., Gallo, M., Colombo, A.L., and Hutchinson, C.R. (1998). The *Streptomyces peucetius dpsY* and *dnrX* genes govern early and late steps of daunorubicin and doxorubicin biosynthesis. *J. Bacteriol.* **180**, 2379–2386.

257. Scotti, C., and Hutchinson, C.R. (1996). Enhanced antibiotic production by manipulation of the *Streptomyces peucetius dnrH* and *dnmT* genes involved in doxorubicin (adriamycin) biosynthesis. *J. Bacteriol.* **178**, 7316–7321.

258. Sanchez, S., Chavez, A., Forero, A., Garcia-Huante, Y., Romero, A., Sanchez, M., Rocha, D., Sanchez, B., Avalos, M., Guzman-Trampe, S., et al. (2010). Carbon source regulation of antibiotic production. *J. Antibiot.* **63**, 442–459.

259. Escalante, L., Ramos, I., Imriskova, I., Langley, E., and Sanchez, S. (1999). Glucose repression of anthracycline formation in *Streptomyces peucetius* var. *caesius*. *Appl. Microbiol. Biotechnol.* **52**, 572–578.

260. Dekleva, M.L., Titus, J.E.A., and Strohl, W.R. (1985). Nutrient effects on anthracycline production by *Streptomyces peucetius* in a defined medium. *Can. J. Microbiol.* **31**, 287–294.

261. Martin, J.F., Sola-Landa, A., Santos-Beneit, F., Fernandez-Martinez, L.T., Prieto, C., Rodriguez-Garcia, A., Martín, J.F., Sola-Landa, A., Santos-Beneit, F., Fernández-Martínez, L.T., et al. (2011). Cross-talk of global nutritional regulators in the control of primary and secondary metabolism in *Streptomyces*. *Microb. Biotechnol.* **4**, 165–174.

262. Wang, X., Tian, X., Wu, Y., Shen, X., Yang, S., and Chen, S. (2018). Enhanced doxorubicin production by *Streptomyces peucetius* using a combination of classical strain mutation and medium optimization. *Prep. Biochem. Biotechnol.* **48**, 514–521.

263. Simón-Gracia, L., Sidorenko, V., Uustare, A., Ogibalov, I., Tasa, A., Tshubrik, O., and Teesalu, T. (2021). Novel anthracycline utorubicin for cancer therapy. *Angew. Chem. Int. Ed.* **60**, 17018–17027.

264. Staunton, J., and Weissman, K.J. (2001). Polyketide biosynthesis: a millennium review. *Nat. Prod. Rep.* **18**, 380–416.

265. Shen, B. (2003). Polyketide biosynthesis beyond the type I, II and III polyketide synthase paradigms. *Curr. Opin. Chem. Biol.* **7**, 285–295.

266. Hulst, M.B., Grocholski, T., Neefjes, J.J.C., van Wezel, G.P., and Metsä-Ketelä, M. (2022). Anthracyclines: biosynthesis, engineering and clinical applications. *Nat. Prod. Rep.* **39**, 814–841.

267. Dickens, M.L., Priestley, N.D., and Strohl, W.R. (1997). *In vivo* and *in vitro* bioconversion of epsilon-rhodomycinone glycoside to doxorubicin: functions of DauP, DauK, and DoxA. *J. Bacteriol.* **179**, 2641–2650.

268. Lambert, M., and Ylihonko, K. (2008). Genetically modified strains producing anthracycline metabolites useful as cancer drugs.

269. Vara, J., Lewandowska-Skarbek, M., Wang, Y.G., Donadio, S., and Hutchinson, C.R. (1989). Cloning of genes governing the deoxysugar portion of the erythromycin biosynthesis pathway in *Saccharopolyspora erythraea* (*Streptomyces erythreus*). *J. Bacteriol.* **171**, 5872–5881.

270. Ylihonko, K., Hakala, J., Niemi, J., Lundell, J., and Mantsala, P. (1994). Isolation and characterization of aclacinomycin A-non-producing *Streptomyces galilaeus* (ATCC 31615) mutants. *Microbiology* **140**, 1359–1365.

271. Świątek, M.A., Tenconi, E., Rigali, S., and van Wezel, G.P. (2012). Functional analysis of the *N*-acetylglucosamine metabolic genes of *Streptomyces coelicolor* and role in control of development and antibiotic production. *J. Bacteriol.* **194**, 1136–1144.

272. Fedoryshyn, M., Welle, E., Bechthold, A., and Luzhetskyy, A. (2008). Functional expression of the Cre recombinase in actinomycetes. *Appl. Microbiol. Biotechnol.* **78**, 1065–1070.

273. Bibb, M.J., Janssen, G.R., and Ward, J.M. (1985). Cloning and analysis of the promoter region of the erythromycin gene (*ermE*) of *Streptomyces erythraeus*. *Gene* **38**, 215–226.

274. Bierman, M., Logan, R., O'Brien, K., Seno, E.T., Nagaraja Rao, R., and Schoner, B.E. (1992). Plasmid cloning vectors for the conjugal transfer of DNA from *Escherichia coli* to *Streptomyces* spp. *Gene* **116**, 43–49.

275. Bai, C., Zhang, Y., Zhao, X., Hu, Y., Xiang, S., Miao, J., Lou, C., and Zhang, L. (2015). Exploiting a precise design of universal synthetic modular regulatory elements to unlock the microbial natural products in *Streptomyces*. *Proc. Natl. Acad. Sci. U.S.A.* **112**, 12181–12186.

276. Chen, Y.-J., Liu, P., Nielsen, A.A.K., Brophy, J.A.N., Clancy, K., Peterson, T., and Voigt, C.A. (2013). Characterization of 582 natural and synthetic terminators and quantification of their design constraints. *Nat. Methods* **10**, 659–664.

277. Gibson, D.G., Young, L., Chuang, R.-Y., Venter, J.C., Hutchison, C.A., and Smith, H.O. (2009). Enzymatic assembly of DNA molecules up to several hundred kilobases. *Nat. Methods* **6**, 343–345.

278. Pulido, D., and Jiménez, A. (1987). Optimization of gene expression in *Streptomyces lividans* by a transcription terminator. *Nucleic Acids Res.* **15**, 4227–4240.

279. Gregory, M.A., Till, R., and Smith, M.C.M. (2003). Integration site for *Streptomyces* phage φBT1 and development of site-specific integrating vectors. *J. Bacteriol.* **185**, 5320–5323.

280. Wu, C., van der Heul, H.U., Melnik, A.V., Lubben, J., Dorrestein, P.C., Minnaard, A.J., Choi, Y.H., van Wezel, G.P., Lübben, J., Dorrestein, P.C., et al. (2019). Lugdunomycin, an angucycline-derived molecule with unprecedented chemical architecture. *Angew. Chem. Int. Ed.* **58**, 2809–2814.

281. Yanisch-Perron, C., Vieira, J., and Messing, J. (1985). Improved M13 phage cloning vectors and host strains: nucleotide sequences of the M13mp18 and pUC19 vectors. *Gene* **33**, 103–119.

282. MacNeil, D.J., Gewain, K.M., Ruby, C.L., Dezeny, G., Gibbons, P.H., and MacNeil, T. (1992). Analysis of *Streptomyces avermitilis* genes required for avermectin biosynthesis utilizing a novel integration vector. *Gene* **111**, 61–68.

283. Pluskal, T., Castillo, S., Villar-Briones, A., and Orešič, M. (2010). MZmine 2: Modular framework for processing, visualizing, and analyzing mass spectrometry-based molecular profile data. *BMC Bioinform.* **11**, 395.

284. van Bergeijk, D.A., Elsayed, S.S., Du, C., Santiago, I.N., Roseboom, A.M., Zhang, L., Carrión, V.J., Spaink, H.P., and van Wezel, G.P. (2022). The ubiquitous catechol moiety elicits siderophore and angucycline production in *Streptomyces*. *Commun. Chem.* **5**, 14.

285. Myers, O.D., Sumner, S.J., Li, S., Barnes, S., and Du, X. (2017). One step forward for reducing false positive and false negative compound identifications from mass spectrometry metabolomics data: new algorithms for constructing extracted ion chromatograms and detecting chromatographic peaks. *Anal. Chem.* **89**, 8696–8703.

286. Zhang, Z., Du, C., de Barsy, F., Liem, M., Liakopoulos, A., van Wezel, G.P., Choi, Y.H., Claessen, D., and Rozen, D.E. (2020). Antibiotic production in *Streptomyces* is organized by a division of labor through terminal genomic differentiation. *Sci. Adv.* **6**, eaay5781.

287. Wessel, D., and Flügge, U.I. (1984). A method for the quantitative recovery of protein in dilute solution in the presence of detergents and lipids. *Anal. Biochem.* **138**, 141–143.

288. Rappsilber, J., Mann, M., and Ishihama, Y. (2007). Protocol for micro-purification, enrichment, pre-fractionation and storage of peptides for proteomics using StageTips. *Nat. Protoc.* **2**, 1896–1906.

289. Cox, J., and Mann, M. (2008). MaxQuant enables high peptide identification rates, individualized p.p.b.-range mass accuracies and proteome-wide protein quantification. *Nat. Biotechnol.* **26**, 1367–1372.

290. Gilchrist, C.L.M., and Chooi, Y.-H. (2021). clinker & clustermap.js: automatic generation of gene cluster comparison figures. *Bioinformatics* **37**, 2473–2475.

291. Madeira, F., Pearce, M., Tivey, A.R.N., Basutkar, P., Lee, J., Edbali, O., Madhusoodanan, N., Kolesnikov, A., and Lopez, R. (2022). Search and sequence analysis tools services from EMBL-EBI in 2022. *Nucleic Acids Res.* **50**, W276–W279.

292. Koroleva, A., Artukka, E., Yamada, K., Ilomäki, M., Kannisto, M., Wander, D.P.A., Hulst, M.B., Niemi, J., van Wezel, G.P., Neefjes, J.J.C., et al. Metabolic engineering for production of biosynthetic doxorubicin (manuscript in preparation).

293. Hulst, M.B., Zhang, L., van der Heul, H.U., Du, C., Elsayed, S.S., Koroleva, A., Grocholski, T., Wander, D.P.A., Metsä-Ketelä, M., Neefjes, J., et al. (2024). Metabolic engineering of *Streptomyces peucetius* for biosynthesis of *N*,*N*-dimethylated anthracyclines. *Front. Bioeng. Biotechnol.* **12**, 1363803.

294. Zhu, H., Swierstra, J., Wu, C., Girard, G., Choi, Y.H., van Wamel, W., Sandiford, S.K., and van Wezel, G.P. (2014). Eliciting antibiotics active against the ESKAPE pathogens in a collection of actinomycetes isolated from mountain soils. *Microbiology* **160**, 1714–1726.

295. Kapteijn, R. (2024). Mechanisms and consequences of horizontal gene transfer in cell wall-deficient cells of *Kitasatospora viridifaciens*.

296. Kennedy, J., Baker, P., Piper, C., Cotter, P.D., Walsh, M., Mooij, M.J., Bourke, M.B., Rea, M.C., O'Connor, P.M., Ross, R.P., et al. (2009). Isolation and analysis of bacteria with antimicrobial activities from the marine sponge *Haliclona simulans* collected from Irish waters. *Mar. Biotechnol.* **11**, 384–396.

297. Blin, K., Shaw, S., Augustijn, H.E., Reitz, Z.L., Biermann, F., Alanjary, M., Fetter, A., Terlouw, B.R., Metcalf, W.W., Helfrich, E.J.N., et al. (2023). antiSMASH 7.0: new and improved predictions for detection, regulation, chemical structures and visualisation. *Nucleic Acids Res.* **51**, W46–W50.

298. Terlouw, B.R., Blin, K., Navarro-Muñoz, J.C., Avalon, N.E., Chevrette, M.G., Egbert, S., Lee, S., Meijer, D., Recchia, M.J.J., Reitz, Z.L., et al. (2023). MIBiG 3.0: a community-driven effort to annotate experimentally validated biosynthetic gene clusters. *Nucleic Acids Res.* **51**, D603–D610.

299. Malmierca, M.G., González-Montes, L., Pérez-Victoria, I., Sialer, C., Braña, A.F., García Salcedo, R., Martín, J., Reyes, F., Méndez, C., Olano, C., et al. (2018). Searching for glycosylated natural products in actinomycetes and identification of novel macrolactams and angucyclines. *Front. Microbiol.* **9**, 39.

300. Kim, W., Lee, N., Hwang, S., Lee, Y., Kim, J., Cho, S., Palsson, B., and Cho, B.-K. (2020). Comparative genomics determines strain-dependent secondary metabolite production in *Streptomyces venezuelae* strains. *Biomolecules* **10**, 864.

301. Deatherage, D.E., and Barrick, J.E. (2014). Identification of mutations in laboratory-evolved microbes from next-generation sequencing data using *breseq*. In Engineering and Analyzing Multicellular Systems: Methods and Protocols Methods in Molecular Biology., L. Sun and W. Shou, eds. (Springer), pp. 165–188.

302. van Dissel, D., Willemse, J., Zacchetti, B., Claessen, D., Pier, G.B., and van Wezel, G.P. (2018). Production of poly-β-1,6-*N*-acetylglucosamine by MatAB is required for hyphal aggregation and hydrophilic surface adhesion by *Streptomyces*. *Microb. Cell* **5**, 269–279.

303. Love, M.I., Huber, W., and Anders, S. (2014). Moderated estimation of fold change and dispersion for RNA-seq data with DESeq2. *Genome Biol.* **15**, 550.

304. Tong, Y., Whitford, C.M., Robertsen, H.L., Blin, K., Jørgensen, T.S., Klitgaard, A.K., Gren, T., Jiang, X., Weber, T., and Lee, S.Y. (2019). Highly efficient DSB-free base editing for streptomycetes with CRISPR-BEST. *Proc. Natl. Acad. Sci. U.S.A.* **116**, 20366–20375.

305. Lei, Y., Asamizu, S., Ishizuka, T., and Onaka, H. (2023). Regulation of multidrug efflux pumps by TetR family transcriptional repressor negatively affects secondary metabolism in *Streptomyces coelicolor* A3(2). *Appl. Environ. Microbiol.* **89**, e01822-22.

306. van Dissel, D., Claessen, D., Roth, M., and Van Wezel, G.P. (2015). A novel locus for mycelial aggregation forms a gateway to improved *Streptomyces* cell factories. *Microb. Cell Factories* **14**, 44.

307. Yamamoto, H., Qin, Y., Achenbach, J., Li, C., Kijek, J., Spahn, C.M.T., and Nierhaus, K.H. (2014). EF-G and EF4: translocation and back-translocation on the bacterial ribosome. *Nat. Rev. Microbiol.* **12**, 89–100.

308. Villebro, R., Shaw, S., Blin, K., and Weber, T. (2019). Sequence-based classification of type II polyketide synthase biosynthetic gene clusters for antiSMASH. *Journal of Industrial Microbiology and Biotechnology* **46**, 469–475.

309. Barthelmebs, L., Lecomte, B., Divies, C., and Cavin, J.-F. (2000). Inducible metabolism of phenolic acids in *Pediococcus pentosaceus* is encoded by an autoregulated operon which involves a new class of negative transcriptional regulator. *J. Bacteriol.* **182**, 6724–6731.

310. Agustiandari, H., Lubelski, J., van den Berg van Saparoea, H.B., Kuipers, O.P., and Driessen, A.J.M. (2008). LmrR is a transcriptional repressor of expression of the multidrug ABC transporter LmrCD in *Lactococcus lactis*. *J. Bacteriol.* **190**, 759–763.

311. Huillet, E., Velge, P., Vallaeys, T., and Pardon, P. (2006). LadR, a new PadR-related transcriptional regulator from *Listeria monocytogenes*, negatively regulates the expression of the multidrug efflux pump MdrL. *FEMS Microbiol. Lett.* **254**, 87–94.

312. Cuthbertson, L., and Nodwell, J.R. (2013). The TetR family of regulators. *Microbiol. Mol. Biol. Rev.* **77**, 440–475.

313. Gominet, M., Seghezzi, N., and Mazodier, P. (2011). Acyl depsipeptide (ADEP) resistance in *Streptomyces*. *Microbiology* **157**, 2226–2234.

314. Dragosits, M., and Mattanovich, D. (2013). Adaptive laboratory evolution – principles and applications for biotechnology. *Microb. Cell Factories* **12**, 64.

315. Brown, E.D., and Wright, G.D. (2016). Antibacterial drug discovery in the resistance era. *Nature* **529**, 336–343.

316. Hobson, C., Chan, A.N., and Wright, G.D. (2021). The antibiotic resistome: a guide for the discovery of natural products as antimicrobial agents. *Chem. Rev.* **121**, 3464–3494.

317. D'Costa, V.M., McGrann, K.M., Hughes, D.W., and Wright, G.D. (2006). Sampling the antibiotic resistome. *Science* **311**, 374–377.

318. Vecchione, J.J., Alexander, B., and Sello, J.K. (2009). Two distinct major facilitator superfamily drug efflux pumps mediate chloramphenicol resistance in *Streptomyces coelicolor*. *Antimicrob. Agents Chemother.* **53**, 4673–4677.

319. Hong, H.-J., Hutchings, M.I., Neu, J.M., Wright, G.D., Paget, M.S.B., and Buttner, M.J. (2004). Characterization of an inducible vancomycin resistance system in *Streptomyces coelicolor* reveals a novel gene (*vanK*) required for drug resistance. *Mol. Microbiol.* **52**, 1107–1121.

320. Hutchings, M.I., Hong, H.-J., and Buttner, M.J. (2006). The vancomycin resistance VanRS two-component signal transduction system of *Streptomyces coelicolor*. *Mol. Microbiol.* **59**, 923–935.

321. Abrudan, M.I., Smakman, F., Grimbergen, A.J., Westhoff, S., Miller, E.L., van Wezel, G.P., and Rozen, D.E. (2015). Socially mediated induction and suppression of antibiosis during bacterial coexistence. *Proc. Natl. Acad. Sci. U.S.A.* **112**, 11054–11059.

322. Westhoff, S., Kloosterman, A.M., van Hoesel, S.F.A., van Wezel, G.P., and Rozen, D.E. (2021). Competition sensing changes antibiotic production in *Streptomyces*. *mBio* **12**, e02729-20.

323. Mungan, M.D., Alanjary, M., Blin, K., Weber, T., Medema, M.H., and Ziemert, N. (2020). ARTS 2.0: feature updates and expansion of the Antibiotic Resistant Target Seeker for comparative genome mining. *Nucleic Acids Res.* **48**, W546–W552.

324. Motamedi, H., Shafiee, A., and Cai, S.-J. (1995). Integrative vectors for heterologous gene expression in *Streptomyces* spp. *Gene* **160**, 25–31.

325. Zhang, L., Ramijan, K., Carrión, V.J., van der Aart, L.T., Willemse, J., van Wezel, G.P., and Claessen, D. (2021). An alternative and conserved cell wall enzyme that can substitute for the lipid II synthase MurG. *mBio* **12**, e03381-20.

326. Blin, K., Pedersen, L.E., Weber, T., and Lee, S.Y. (2016). CRISPy-web: an online resource to design sgRNAs for CRISPR applications. *Synth. Syst. Biotechnol.* **1**, 118–121.

327. Seemann, T. (2014). Prokka: rapid prokaryotic genome annotation. *Bioinformatics* **30**, 2068–2069.

328. Edgar, R.C. (2004). MUSCLE: a multiple sequence alignment method with reduced time and space complexity. *BMC Bioinform.* **5**, 113.

329. Finn, R.D., Clements, J., and Eddy, S.R. (2011). HMMER web server: interactive sequence similarity searching. *Nucleic Acids Res.* **39**, W29–W37.

330. Asnicar, F., Thomas, A.M., Beghini, F., Mengoni, C., Manara, S., Manghi, P., Zhu, Q., Bolzan, M., Cumbo, F., May, U., et al. (2020). Precise phylogenetic analysis of microbial isolates and genomes from metagenomes using PhyloPhlAn 3.0. *Nat. Commun.* **11**, 2500.

331. Buchfink, B., Xie, C., and Huson, D.H. (2015). Fast and sensitive protein alignment using DIAMOND. *Nat. Methods* **12**, 59–60.

332. Katoh, K., and Standley, D.M. (2013). MAFFT multiple sequence alignment software version 7: improvements in performance and usability. *Mol. Biol. Evol.* **30**, 772–780.

333. Capella-Gutiérrez, S., Silla-Martínez, J.M., and Gabaldón, T. (2009). trimAl: a tool for automated alignment trimming in large-scale phylogenetic analyses. *Bioinformatics* **25**, 1972–1973.

334. Stamatakis, A. (2014). RAxML version 8: a tool for phylogenetic analysis and post-analysis of large phylogenies. *Bioinformatics* **30**, 1312–1313.

335. Letunic, I., and Bork, P. (2021). Interactive Tree Of Life (iTOL) v5: an online tool for phylogenetic tree display and annotation. *Nucleic Acids Res.* **49**, W293–W296.

336. Davies, J., and Davies, D. (2010). Origins and evolution of antibiotic resistance. *Microbiol. Mol. Biol. Rev.* **74**, 417–433.

337. Murray, C.J.L., Ikuta, K.S., Sharara, F., Swetschinski, L., Aguilar, G.R., Gray, A., Han, C., Bisignano, C., Rao, P., Wool, E., et al. (2022). Global burden of bacterial antimicrobial resistance in 2019: a systematic analysis. *Lancet* **399**, 629–655.

338. Cook, M.A., and Wright, G.D. (2022). The past, present, and future of antibiotics. *Sci. Transl. Med.* **14**, eabo7793.

339. Hutchings, M.I., Truman, A.W., and Wilkinson, B. (2019). Antibiotics: past, present and future. *Curr. Opin. Microbiol.* **51**, 72–80.

340. Boyd, N.K., Teng, C., and Frei, C.R. (2021). Brief overview of approaches and challenges in new antibiotic development: a focus on drug repurposing. *Front. Cell. Infect. Microbiol.* **11**, 684515.

341. Farha, M.A., and Brown, E.D. (2019). Drug repurposing for antimicrobial discovery. *Nat. Microbiol.* **4**, 565–577.

342. Feng, J., Shi, W., Zhang, S., and Zhang, Y. (2015). Identification of new compounds with high activity against stationary phase *Borrelia burgdorferi* from the NCI compound collection. *Emerg. Microbes Infect.* **4**, 1–15.

343. Trombetta, R.P., Dunman, P.M., Schwarz, E.M., Kates, S.L., and Awad, H.A. (2018). A high-throughput screening approach to repurpose FDA-approved drugs for bactericidal applications against *Staphylococcus aureus* small-colony variants. *mSphere* **3**, 10–128.

344. Gumbo, T., Cirrincione, K., and Srivastava, S. (2020). Repurposing drugs for treatment of *Mycobacterium abscessus*: a view to a kill. *J. Antimicrob. Chemother.* **75**, 1212–1217.

345. She, P., Li, S., Zhou, L., Luo, Z., Liao, J., Xu, L., Zeng, X., Chen, T., Liu, Y., and Wu, Y. (2020). Insights into idarubicin antimicrobial activity against methicillin-resistant *Staphylococcus aureus*. *Virulence* **11**, 636–651.

346. Figueiredo, N., Chora, A., Raquel, H., Pejanovic, N., Pereira, P., Hartleben, B., Neves-Costa, A., Moita, C., Pedroso, D., Pinto, A., et al. (2013). Anthracyclines induce DNA damage response-mediated protection against severe sepsis. *Immunity* **39**, 874–884.

347. Rice, L.B. (2008). Federal funding for the study of antimicrobial resistance in nosocomial pathogens: no ESKAPE. *J. Infect. Dis.* **197**, 1079–1081.

348. Kwan, B.W., Chowdhury, N., and Wood, T.K. (2015). Combatting bacterial infections by killing persister cells with mitomycin C. *Environ. Microbiol.* **17**, 4406–4414.

349. Cruz-Muñiz, M.Y., López-Jacome, L.E., Hernández-Durán, M., Franco-Cendejas, R., Licona-Limón, P., Ramos-Balderas, J.L., Martinéz-Vázquez, M., Belmont-Díaz, J.A., Wood, T.K., and García-Contreras, R. (2017). Repurposing the anticancer drug mitomycin C for the treatment of persistent *Acinetobacter baumannii* infections. *Int. J. Antimicrob. Agents* **49**, 88–92.

350. da Silva, R.A.G., Wong, J.J., Antypas, H., Choo, P.Y., Goh, K., Jolly, S., Liang, C., Tay Kwan Sing, L., Veleba, M., Hu, G., et al. (2023). Mitoxantrone targets both host and bacteria to overcome vancomycin resistance in *Enterococcus faecalis*. *Sci. Adv.* **9**, eadd9280.

351. Jones, R.L., Swanton, C., and Ewer, M.S. (2006). Anthracycline cardiotoxicity. *Expert Opin. Drug Saf.* **5**, 791–809.

352. Habets, M.G.J.L., and Brockhurst, M.A. (2012). Therapeutic antimicrobial peptides may compromise natural immunity. *Biol. Lett.* **8**, 416–418.

353. Manteca, A., Fernandez, M., and Sanchez, J. (2006). Cytological and biochemical evidence for an early cell dismantling event in surface cultures of *Streptomyces antibioticus*. *Res. Microbiol.* **157**, 143–152.

354. Liu, G., Chater, K.F., Chandra, G., Niu, G., and Tan, H. (2013). Molecular regulation of antibiotic biosynthesis in *Streptomyces*. *Microbiol. Mol. Biol. Rev.* **77**, 112–143.

355. Ziemert, N., Alanjary, M., and Weber, T. (2016). The evolution of genome mining in microbes – a review. *Nat. Prod. Rep.* **33**, 988–1005.

356. Gubbens, J., Zhu, H., Girard, G., Song, L., Florea, B.I., Aston, P., Ichinose, K., Filippov, D.V., Choi, Y.H., Overkleeft, H.S., et al. (2014). Natural product proteomining, a quantitative proteomics platform, allows rapid discovery of biosynthetic gene clusters for different classes of natural products. *Chem. Biol.* **21**, 707–718.

357. Palazzotto, E., and Weber, T. (2018). Omics and multi-omics approaches to study the biosynthesis of secondary metabolites in microorganisms. *Curr. Opin. Microbiol.* **45**, 109–116.

358. Schorn, M.A., Verhoeven, S., Ridder, L., Huber, F., Acharya, D.D., Aksenov, A.A., Aleti, G., Moghaddam, J.A., Aron, A.T., Aziz, S., et al. (2021). A community resource for paired genomic and metabolomic data mining. *Nat. Chem. Biol.* **17**, 363–368.

359. Long, Q., Liu, X., Yang, Y., Li, L., Harvey, L., McNeil, B., and Bai, Z. (2014). The development and application of high throughput cultivation technology in bioprocess development. *J. Biotechnol.* **192**, 323–338.

360. Hemmerich, J., Noack, S., Wiechert, W., and Oldiges, M. (2018). Microbioreactor systems for accelerated bioprocess development. *Biotechnol. J.* **13**, 1700141.

361. Koepff, J., Keller, M., Tsolis, K.C., Busche, T., Rückert, C., Hamed, M.B., Anné, J., Kalinowski, J., Wiechert, W., Economou, A., et al. (2017). Fast and reliable strain characterization of *Streptomyces lividans* through micro-scale cultivation. *Biotechnol. Bioeng.* **114**, 2011–2022.

362. van Dissel, D., and van Wezel, G.P. (2018). Morphology-driven downscaling of *Streptomyces lividans* to micro-cultivation. *Antonie van Leeuwenhoek* **111**, 457–469.

363. van Dissel, D., Claessen, D., and van Wezel, G.P. (2014). Morphogenesis of *Streptomyces* in submerged cultures. *Adv. Appl. Microbiol.* **89**, 1–45.

364. Donati, S., Mattanovich, M., Hjort, P., Jacobsen, S.A.B., Blomquist, S.D., Mangaard, D., Gurdo, N., Pastor, F.P., Maury, J., Hanke, R., et al. (2023). An automated workflow for multi-omics screening of microbial model organisms. *NPJ Syst. Biol. Appl.* **9**, 1–12.

365. Heberle, H., Meirelles, G.V., da Silva, F.R., Telles, G.P., and Minghim, R. (2015). InteractiVenn: a web-based tool for the analysis of sets through Venn diagrams. *BMC Bioinform.* **16**, 169.

366. Schmid, R., Heuckeroth, S., Korf, A., Smirnov, A., Myers, O., Dyrlund, T.S., Bushuiev, R., Murray, K.J., Hoffmann, N., Lu, M., et al. (2023). Integrative analysis of multimodal mass spectrometry data in MZmine 3. *Nat. Biotechnol.* **41**, 447–449.

367. Xia, J., Psychogios, N., Young, N., and Wishart, D.S. (2009). MetaboAnalyst: a web server for metabolomic data analysis and interpretation. *Nucleic Acids Res.* **37**, W652–W660.

368. Nothias, L.-F., Petras, D., Schmid, R., Dührkop, K., Rainer, J., Sarvepalli, A., Protsyuk, I., Ernst, M., Tsugawa, H., Fleischauer, M., et al. (2020). Feature-based molecular networking in the GNPS analysis environment. *Nat. Methods* **17**, 905–908.

369. Wang, M., Carver, J.J., Phelan, V.V., Sanchez, L.M., Garg, N., Peng, Y., Nguyen, D.D., Watrous, J., Kapono, C.A., Luzzatto-Knaan, T., et al. (2016). Sharing and community curation of mass spectrometry data with Global Natural Products Social Molecular Networking. *Nat. Biotechnol.* **34**, 828–837.

370. Horai, H., Arita, M., Kanaya, S., Nihei, Y., Ikeda, T., Suwa, K., Ojima, Y., Tanaka, K., Tanaka, S., Aoshima, K., et al. (2010). MassBank: a public repository for sharing mass spectral data for life sciences. *J. Mass Spectrom.* **45**, 703–714.

371. Katz, L., and Baltz, R.H. (2016). Natural product discovery: past, present, and future. *J. Ind. Microbiol. Biotechnol.* **43**, 155–176.

372. Kunze, M., Roth, S., Gartz, E., and Büchs, J. (2014). Pitfalls in optical on-line monitoring for high-throughput screening of microbial systems. *Microb. Cell Fact.* **13**, 53.

373. Huber, R., Ritter, D., Hering, T., Hillmer, A.-K., Kensy, F., Müller, C., Wang, L., and Büchs, J. (2009). Robo-Lector – a novel platform for automated high-throughput cultivations in microtiter plates with high information content. *Microb. Cell Factories* **8**, 42.

374. Pinu, F.R., and Villas-Boas, S.G. (2017). Extracellular microbial metabolomics: the state of the art. *Metabolites* **7**, 43.

375. Zhu, A., Ibrahim, J.G., and Love, M.I. (2019). Heavy-tailed prior distributions for sequence count data: removing the noise and preserving large differences. *Bioinformatics* **35**, 2084–2092.

376. Schmid, R., Petras, D., Nothias, L.-F., Wang, M., Aron, A.T., Jagels, A., Tsugawa, H., Rainer, J., Garcia-Aloy, M., Dührkop, K., et al. (2021). Ion identity molecular networking for mass spectrometry-based metabolomics in the GNPS environment. *Nat. Commun.* **12**, 3832.

377. Shannon, P., Markiel, A., Ozier, O., Baliga, N.S., Wang, J.T., Ramage, D., Amin, N., Schwikowski, B., and Ideker, T. (2003). Cytoscape: a software environment for integrated models of biomolecular interaction networks. *Genome Res.* **13**, 2498–2504.

378. Krohn, K. ed. (2008). Anthracycline Chemistry and Biology I (Springer).

379. Markel, U., D. Essani, K., Besirlioglu, V., Schiffels, J., R. Streit, W., and Schwaneberg, U. (2020). Advances in ultrahigh-throughput screening for directed enzyme evolution. *Chem. Soc. Rev.* **49**, 233–262.



Curriculum vitae

Mandy Beatrix Hulst was born in Rotterdam, The Netherlands on the 9th of March, 1994. After attending high school at the Comenius College in Capelle aan den IJssel and graduating in 2011, she decided to take a gap year to participate in a high school exchange program to Idaho, USA.

In 2012, she started the BSc Life Science & Technology, a shared program of Delft University of Technology (TU Delft) and Leiden University. During her BSc studies, she performed an internship in the Industrial Microbiology group at TU Delft, focusing on free energy conservation in yeast under the supervision of dr. Robert Mans and prof. Ton van Maris. After obtaining her BSc degree in June 2015, she continued her studies with the MSc Life Science & Technology at TU Delft, specialising in Cell Factory and Biochemical Engineering. She completed an extracurricular exchange semester to the University of New South Wales (Sydney, Australia). During a second internship in the Industrial Microbiology group at TU Delft, she studied the physiology of yeast through chemostat bioreactor cultivations, supervised by dr. Xavier Hakkaart and prof. Pascal Daran-Lapujade. She concluded her MSc studies with an industrial internship at Chr. Hansen (Hørsholm, Denmark), focusing on extending the shelf-life of yogurt. She obtained her MSc degree in February 2018 with the distinction *cum laude*.

In August 2018, she joined the research group of prof. Gilles van Wezel at the Institute of Biology at Leiden University as a research analyst, where she studied heterologous antibiotic production in *Streptomyces coelicolor*. During this period, she spent two months at the research institute SINTEF (Trondheim, Norway) working on (micro)bioreactor cultivation of streptomycetes under the supervision of dr. Alexander Wentzel and dr. Dino van Dissel. In July 2019, Mandy started her PhD project, focusing on anthracycline biosynthesis in *Streptomyces* under the joint supervision of prof. Gilles van Wezel and prof. Sjaak Neefjes (Leiden University Medical Center). The work on this topic is presented in this thesis. As from May 2024, Mandy works as Fermentation Engineer at Twig Bio Limited in London, UK.



Publications

Hulst, M.B., Zhang, L., van der Heul, H.U., Du, C., Elsayed, S.S., Koroleva, A., Grocholski, T., Wander, D.P.A., Metsä-Ketelä, M., Neefjes, J.J.C., & van Wezel, G.P. (2024). Metabolic engineering of *Streptomyces peucetius* for biosynthesis of *N*,*N*-dimethylated anthracyclines. *Front. Bioeng. Biotechnol.*, 12, 1363803.

Hulst, M.B.*, Grocholski, T.*, Neefjes, J.J.C., van Wezel, G.P., & Metsä-Ketelä, M. (2022). Anthracyclines: Biosynthesis, engineering and clinical applications. *Nat. Prod. Rep.*, 39(4), 814–841.

Hakkaart, X.D.V.*, Liu, Y*., **Hulst, M.B.**, el Masoudi, A., Peuscher, E.J., Pronk, J.T., van Gulik, W.M. & Daran-Lapujade, P. (2020). Physiological responses of *Saccharomyces cerevisiae* to industrially relevant conditions: Slow growth, low pH and high CO_2 levels. *Biotechnol. Bioeng.*, 117(3), 721–735.

* These authors contributed equally.